

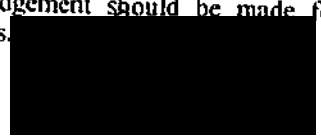
H24/3422

**MONASH UNIVERSITY**  
**THESIS ACCEPTED IN SATISFACTION OF THE**  
**REQUIREMENTS FOR THE DEGREE OF**  
**DOCTOR OF PHILOSOPHY**

ON..... 18 March 2003 .....

.....  
Sec. Research Graduate School Committee

Under the Copyright Act 1968, this thesis must be used only under the normal conditions of scholarly fair dealing for the purposes of research, criticism or review. In particular no results or conclusions should be extracted from it, nor should it be copied or closely paraphrased in whole or in part without the written consent of the author. Proper written acknowledgement should be made for any assistance obtained from this thesis.



### ***List of Publications***

The following publications have arisen from this and related work.

#### **Refereed Publications**

K. Dean, W. D. Cook, M. D. Zipper and P. Burchill

**Curing behaviour of IPNs formed from model VERs and epoxy systems I amine cured epoxy:** *Polymer*, Volume 42, Issue 4, February 2001, Pages 1345-1359

K. Dean, W. D. Cook, M. D. Zipper and P. Burchill

**Curing behaviour of IPNs formed from model VERs and epoxy systems II imidazole cured epoxy:** *Polymer*, Volume 42, Issue 8, April 2001, Pages 3589-3601

Katherine Dean, Wayne D. Cook, Laurent Rey, Jocelyne Galy and Henry Sautereau

**Near Infra-red and Rheological Investigations of Epoxy-Vinyl Ester Interpenetrating Polymer Networks:** *Macromolecules*, Volume 34, 2001, Pages 6623-6630.

Wayne D. Cook, Katherine Dean and John S. Forsythe

**Cure, rheology and properties of IPN thermosets for composite applications:** *Materials Forum*, Volume 25, 2001, Pages 30-59

I. Merdas, A. Tcharkhtchi, F. ThomINETTE, J. Verdu, K. Dean and W. Cook

**Water Absorption by uncrosslinked polymers, networks and IPNs having medium to high Polarity** *Polymer*, Volume 43, Issue 17, August 2002, Pages 4619-4625

Katherine Dean and Wayne Cook

**The effect of curing sequence on the photopolymerization and thermal curing kinetics of dimethacrylate-epoxy Interpenetrating Polymer Networks**

Accepted for publication *Macromolecules* 2002

Katherine Dean and Wayne Cook

**Azo initiator selection to control the curing order in epoxy/dimethacrylate IPNs** submitted to *Polymer* 2002

# **Epoxy-Dimethacrylate Interpenetrating Polymer Networks**

**A thesis submitted to Monash University in partial fulfillment of the  
degree of Doctor of Philosophy**

**Katherine Dean B.Sc. (Hons)**

**School of Physics and Materials Engineering**

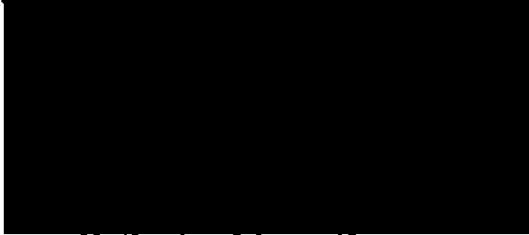
**Monash University**

**Victoria 3800**

**2002**

***Declaration***

This thesis contains no material which has been accepted for the award of any degree or diploma in any university or institution, and to the best of the knowledge of the author and supervisor contains no material previously published or written by any other person except where due reference is made in the text.



Katherine Maree Dean

## *Acknowledgements*

Firstly I would like to thank my principal supervisor Associate Professor Wayne Cook. I would also like to thank my co-supervisor Dr. Peter Burchill and Dr Marcus Zipper for his supervisory role in the earlier years of my PhD studies.

The support of the Co-operative Research Centre for Polymers and the School of Physics and Materials Engineering is greatly appreciated.

I would like to thank my postgraduate colleagues Mark Forrest, Anthony Mayr, Kerryn Wilson, Karen Roberts, Ole Becker, Tim Scott, Christopher Wise, Henry Beh, Chamini Mendis, Laurent Rey, Samira Benali, Alexandra Shekhter, Sally Malony and Soo Ooi for providing not only advice and assistance but for making the whole experience most enjoyable.

I would like to acknowledge Dr Min Lin and Dr Howard Hanley of the National Institute of Science and Technology, Gaithersburg, USA for performing Small Angle Neutron Scattering. I would also like to thank Dr Ilhame Merdas for completing the water absorption experiments, and also Dr Aabbas Tcharkhtchi and Dr Jacque Verdu for the discussions in this area.

Finally I would like to thank Professor Henry Sautereau, Dr Jocelyne Galy, and Professor Jean-Pierre Pascault for the opportunity to complete the rheological component of my thesis at their laboratory in Lyon, which was made possible by the financial support of the CNRS and DIST.

Dedicated to Ken Thomas (1949-2002)

## Table of Contents

Declaration.....	i
Acknowledgements.....	ii
Table of Contents.....	iii
List of Figures.....	vii
List of Tables.....	xiii
List of Publications.....	xv
Abbreviations.....	xviii
Symbols.....	xix
Abstract.....	xxii
<b>Chapter 1</b>	<b>Introductory Remarks..... 1</b>
1.1	INTRODUCTION..... 1
1.2	LAYOUT OF THE DISSERTATION..... 2
<b>Chapter 2</b>	<b>Literature Review..... 3</b>
2.1	POLYMER NETWORKS..... 3
2.1.1	<i>Network Formation</i> ..... 3
2.1.2	<i>Step Growth Polymerization</i> ..... 6
2.1.3	<i>Chain Growth Polymerization</i> ..... 7
2.1.4	<i>Rheological behaviour during network formation</i> ..... 11
2.2	EPOXY RESINS..... 15
2.2.1	<i>Structures</i> ..... 15
2.2.2	<i>1<sup>o</sup> Amine Cure of Epoxies</i> ..... 16
2.2.3	<i>Anhydride cure of Epoxies</i> ..... 20
2.2.4	<i>Imidazole cure of Epoxies</i> ..... 21
2.2.5	<i>Properties and Uses of Epoxy Resins</i> ..... 22
2.3	VINYL ESTERS..... 23
2.3.1	<i>Structure and properties</i> ..... 23
2.3.2	<i>Curing mechanisms</i> ..... 24
2.3.3	<i>Properties and Uses of Vinyl ester Resins</i> ..... 28
2.4	POLYMER BLENDS..... 28
2.4.1	<i>Interpenetrating Polymer Networks</i> ..... 29
2.4.2	<i>Kinetics of Formation of IPNs</i> ..... 30
2.4.3	<i>Methods for determining phase separation in IPNs</i> ..... 35
2.4.4	<i>Phase Separation and morphology of simultaneous IPNs</i> ..... 37
2.5	PHYSICAL PROPERTIES OF CURED THERMOSETS..... 39

2.5.1	<i>Yielding and Fracture</i> .....	39
2.5.2	<i>Mechanical Properties of IPNs</i> .....	41
2.5.3	<i>Polymer Degradation</i> .....	43
2.5.4	<i>Effect of Swelling and Corrosion on Properties</i> .....	46
2.5.5	<i>Applications of IPNs</i> .....	47
<b>Chapter 3</b>	<b>Materials and IPN preparation</b> .....	<b>48</b>
3.1	MATERIALS.....	48
3.2	RESIN CHARACTERIZATION.....	53
3.3	IPN PREPARATION AND CURE .....	54
3.3.1	<i>Model VER, neat dimethacrylate and neat epoxy systems</i> .....	54
3.3.2	<i>IPNs and partial IPN systems</i> .....	55
<b>Chapter 4</b>	<b>Experimental Techniques</b> .....	<b>56</b>
4.1	FOURIER TRANSFORM INFRARED SPECTROSCOPY (FTIR) .....	56
4.1.1	<i>Mid-FTIR</i> .....	56
4.1.2	<i>near FTIR band</i> .....	60
4.2	DIFFERENTIAL SCANNING CALORIMETRY (DSC) .....	62
4.3	SOXHLET EXTRACTIONS .....	64
4.4	RHEOLOGY .....	65
4.5	DENSITY MEASUREMENTS.....	67
4.6	SMALL ANGLE NEUTRON SCATTERING (SANS).....	67
4.7	WATER UPTAKE OF CURED RESINS .....	67
4.8	MECHANICAL PROPERTIES OF CURED RESINS .....	68
4.8.1	<i>Compression Testing</i> .....	68
4.8.2	<i>Flexural Testing</i> .....	69
4.8.3	<i>Error Analysis</i> .....	70
<b>Chapter 5</b>	<b>Kinetics of Formation of networks</b> .....	<b>71</b>
5.1	ALIPHATIC AND AROMATIC AMINES BASED IPNS .....	71
5.1.1	<i>Introduction</i> .....	71
5.1.2	<i>Differential scanning calorimetry of IPN cure and extraction studies</i> .....	71
5.1.3	<i>Fourier transform infra-red spectroscopy of IPN cure</i> .....	89
5.1.4	<i>Conclusions</i> .....	94
5.2	IMIDAZOLE BASED IPNS .....	95
5.2.1	<i>Introduction</i> .....	95
5.2.2	<i>Differential scanning calorimetry of IPN cure</i> .....	95
5.2.3	<i>Fourier transform infra-red spectroscopy of IPN cure</i> .....	108
5.2.4	<i>Conclusions</i> .....	117

5.3	ANHYDRIDE BASED IPNS.....	118
5.3.1	Introduction.....	118
5.3.2	Differential scanning calorimetry of IPN cure.....	118
5.3.3	Conclusions.....	120
<b>Chapter 6</b>	<b>Chemorheology of IPNs and correlation with near FTIR.....</b>	<b>121</b>
6.1	INTRODUCTION.....	121
6.2	CURING KINETICS.....	121
6.3	GELATION.....	126
6.4	VITRIFICATION.....	130
6.5	CONCLUSION.....	134
<b>Chapter 7</b>	<b>Azo initiator selection to control the curing order in epoxy/dimethacrylate IPNs.....</b>	<b>136</b>
7.1	INTRODUCTION.....	136
7.2	CURING KINETICS.....	137
7.3	CONCLUSIONS.....	147
<b>Chapter 8</b>	<b>DMTA and SANS of cured systems.....</b>	<b>149</b>
8.1	INTRODUCTION.....	149
8.2	DYNAMICAL MECHANICAL THERMAL ANALYSIS (DMTA).....	149
8.3	SMALL ANGLE NEUTRON SCATTERING (SANS).....	161
8.4	CONCLUSIONS.....	168
<b>Chapter 9</b>	<b>Dual Photopolymerization and thermal curing kinetics of dimethacrylate-epoxy IPNs.....</b>	<b>171</b>
9.1	INTRODUCTION.....	171
9.2	CURE KINETICS AND DMTA.....	172
9.3	CONCLUSION.....	193
<b>Chapter 10</b>	<b>Properties of cured IPNs.....</b>	<b>195</b>
10.1	INTRODUCTION.....	195
10.2	WATER ABSORPTION.....	196
10.3	COMPRESSIVE MODULUS AND YIELD.....	199
10.4	FLEXURAL TESTING.....	203

---

10.5	CONCLUSIONS.....	204
<b>Chapter 11</b>	<b>Conclusions and Suggestions for Further Studies...</b>	<b>205</b>
11.1	CONCLUSIONS.....	205
11.2	SUGGESTIONS FOR FUTURE WORK.....	215
	Appendix I .....	217
	References:.....	218

## List of Figures

Figure 2.1 Time-temperature-transformation cure diagram for a thermosetting system (after Gillham <sup>20</sup> ).	5
Figure 2.2 A schematic of step growth polymerization initially with the unreacted tetrafunctional monomer (a), in the early stages of polymerization ( $p \approx 5\%$ in 3D) (b), and at gelation ( $p = 33\%$ ) showing 3D connectivity (c).	6
Figure 2.3 Chain growth polymerization prior to any reaction (a) and at gelation ( $p < 5\%$ in 3D) (b).	8
Figure 2.4 Evolution of steady-shear viscosity and equilibrium modulus at the gel point <sup>46</sup> .	11
Figure 2.5 Logarithm of the relaxation modulus versus relaxation time near the gel point.	12
Figure 2.6 Logarithm of the real modulus versus logarithm of the frequency near the gel point.	14
Figure 2.7 Diglycidyl ether of bisphenol-A (DGEBA).	15
Figure 2.8 The reaction mechanism for epoxy using an amine curing agent.	17
Figure 2.9 The structure of DAO.	19
Figure 2.10 The structure of DDM.	19
Figure 2.11 Reaction mechanisms for polymerization process of epoxies using anhydrides <sup>25,80</sup> .	20
Figure 2.12 Reaction mechanisms for polymerization process of epoxies using imidazoles <sup>84</sup> .	22
Figure 2.13 The structure of bisphenol-A epoxy methacrylate <sup>17,86,87</sup> .	23
Figure 2.14 The Novolac epoxy acrylate structure <sup>86</sup> .	23
Figure 2.15 Schematic of the radical initiated polymerization of vinyl ester.	24
Figure 2.16 The photoinitiation mechanism for the ketone/amine system <sup>97,99</sup> .	25
Figure 2.17 The living radical polymerization mechanism for XDT <sup>102</sup> .	26
Figure 2.18. a) Idealized structure of an IPN; b) semi-IPN; c) grafted IPN; d) phase separated IPN.	29
Figure 2.19. Simultaneous IPN formation (adapted from Sperling et al. <sup>6</sup> ).	30
Figure 2.20 Schematic of the theoretical tensile stress as a function of distance from the crack tip for materials with low ( $\sigma_{y1}$ ) and high ( $\sigma_{y2}$ ) yield stress (after Mayr, Cook and Edvard) <sup>181</sup> .	41
Figure 2.21 The energy barrier between two molecular sites, under an applied shear stress ( $\tau$ ) <sup>179,180</sup> .	41
Figure 2.22 Schematic of the potential synergistic properties of IPNs.	47
Figure 3.1 Structure of bisGMA ( $n \approx 0.99$ see Section 3.2).	49
Figure 3.2 Structure of styrene monomer.	49
Figure 3.3 Structure of DEBPADM.	49
Figure 3.4 Structure of PGEMA.	49
Figure 3.5 Structure of DGEBA ( $n = 0.15$ -see Section 3.2).	52
Figure 3.6 Structure of PGE.	52
Figure 3.7 Structures of monofunctional amines and corresponding diamines.	52
Figure 3.8 Structure of I-Mel.	52
Figure 3.9 Structures of DDSA, CHDCA and DMBA.	53
Figure 4.1 mid-FTIR spectra of the pure styrene monomer.	57
Figure 4.2 mid FTIR spectra of DGEBA/BA:VER/AIBN unreacted system as an example of all the peaks on interest used in this work.	58
Figure 4.3 A representative exotherm produced from scanning DSC.	62

Figure 4.4 A representative exotherm produced by photopolymerization of DEBPADMA/CQ/TMA with visible light.....	64
Figure 4.5 Schematic of the Soxhlet extraction.....	65
Figure 4.6 Dual Cantilever Bending test frame with sample.....	66
Figure 4.7 Loading nose and support diagram for 3 point bending test setup.....	70
Figure 5.1 DSC scans of the 50:50 VER/AIBN:DGEBA/An semi-IPN, the 50:50 VER/AIBN:DGEBA/DDM full-IPN and the parent resin systems.....	73
Figure 5.2 DSC scans of 50:50 VER/AIBN:DGEBA/BA, semi-IPN, 50:50 VER/AIBN.....	75
Figure 5.3 Mid-FTIR methacrylate conversion (measured from the decrease in methacrylate absorption at $1645\text{cm}^{-1}$ ) versus time for the VER/AIBN, bisGMA/BA and bisGMA/An at $70^\circ\text{C}$ .....	77
Figure 5.4 Schematic of the Michaels addition of an amine across the methacrylate unsaturation leading to grafting of the epoxy and dimethacrylate networks.....	77
Figure 5.5 DSC scans of the CHP-initiated VER, the An-cured DGEBA and the 50:50 VER/CHP:DGEBA/An semi-IPN.....	79
Figure 5.6 DSC scans of the VER/CHP:DGEBA/BA semi-IPN, the parent resins, the thermal cure of VER and the system VER:DGEBA/BA (without radical initiator).....	80
Figure 5.7 DSC scans of the 50:50 VER/BPO:DGEBA/An and VER/BPO:DGEBA/BA semi-IPNs and the parent resins.....	82
Figure 5.8 DSC scans of the 50:50 VER/MEKP:DGEBA/An semi-IPN and the parent resins.....	83
Figure 5.9 DSC scans of VER/MEKP:DGEBA/BA and the parent resins.....	84
Figure 5.10 Variations of the VER/MEKP:DGEBA/BA semi-IPN system - DSC thermograms of VER/MEKP:BA and VER/MEKP:DGEBA.....	85
Figure 5.11 The effects of cobalt octoate accelerator on the scanning DSC cure of VER/MEKP/Co:DGEBA/An and VER/MEKP/Co:DGEBA/BA.....	86
Figure 5.12. FTIR spectra for the cure of 50:50 VER/AIBN:DGEBA/An at $70^\circ\text{C}$ illustrating the epoxy (E), methacrylate (M) and styrene (S) characteristic peaks.....	89
Figure 5.13 Conversion versus time for the epoxy, methacrylate and styrene in the 50:50 VER/AIBN:DGEBA/An and the parent resins at a cure temperature of $70^\circ\text{C}$ .....	90
Figure 5.14 Conversion versus time for the epoxy, methacrylate and styrene in the 50:50 VER/AIBN:DGEBA/BA semi-IPN and the parent resins at a cure temperature of $70^\circ\text{C}$ .....	91
Figure 5.15 FTIR conversion versus time for the 50:50 VER/CHP:DGEBA/An and the parent resins at $70^\circ\text{C}$ .....	92
Figure 5.16 FTIR conversion versus time for 50:50 VER/CHP:DGEBA/BA and the parent resins at $70^\circ\text{C}$ .....	93
Figure 5.17 DSC scans of VER/AIBN, DGEBA/I-Mel (5 wt%) and their IPNs.....	96
Figure 5.18 DSC scans of bisGMA/AIBN, PGEMA/AIBN, DGEBA/I-Mel (5 wt%), PGE/I-Mel (5 wt%) and their IPNs.....	101
Figure 5.19 DSC scans of VER/CHP, DGEBA/I-Mel (5 wt%) and their IPNs.....	102
Figure 5.20 DSC scans of VER/MEKP, DGEBA/I-Mel (5 wt%) and their 50:50 IPN.....	105
Figure 5.21 DSC scans of the VER/BPO and DGEBA/I-Mel (5 wt%) resins and their 50:50 IPN.....	107

Figure 5.22 FTIR spectra in the region from $1660\text{ cm}^{-1}$ to $1600\text{ cm}^{-1}$ and from $1000\text{ cm}^{-1}$ to $600\text{ cm}^{-1}$ of the 50:50 VER/AIBN:DGEBA/I-MeI (5 wt%) IPN cured at $70^\circ\text{C}$ for varying times and after post-cure at $150^\circ\text{C}$ for 3 hours.....	108
Figure 5.23 Dimethacrylate and styrene conversion versus time in the pure VER/AIBN system and in the 50:50 blend of VER/AIBN:DGEBA/I-MeI at $70^\circ\text{C}$ . The dashed lines show the cure behaviour of the IPN formed with VER/AIBN:DGEBA/aniline (see also Figure 5.13).....	109
Figure 5.24 Dimethacrylate and styrene conversion versus time in the pure VER/AIBN system and in the 50:50 blend of VER/AIBN:DGEBA/I-MeI at $110^\circ\text{C}$ .....	111
Figure 5.25 Epoxy conversion versus time for the neat DGEBA/I-MeI (5 wt%) resin and in the 50:50 blend of the model VER/AIBN:DGEBA/I-MeI (5 wt%).....	112
Figure 5.26 Dimethacrylate and styrene conversion versus time in the pure VER/CHP system and in the 50:50 blend of VER/CHP:DGEBA/I-MeI at $70^\circ\text{C}$ .....	114
Figure 5.27 Epoxy conversion versus time for both the neat DGEBA/I-MeI resin and in the 50:50 blend of VER/CHP:DGEBA/I-MeI.....	115
Figure 5.28 Dimethacrylate and styrene conversion versus time in the VER/MEKP system and in the 50:50 blend of VER/MEKP:DGEBA/I-MeI (5 wt%) at $70^\circ\text{C}$ .....	116
Figure 5.29 Epoxy conversion versus time for both the neat system of DGEBA/I-MeI and in the 50:50 blend of VER/MEKP:DGEBA/I-MeI at 70 and $110^\circ\text{C}$ .....	117
Figure 5.30 DSC scans of VER/AIBN, DGEBA/CHDCA/DMBA and the 50:50 IPN.....	119
Figure 6.1 Near infra-red spectra during cure of the 50:50 VER/AIBN:DGEBA/I-MeI IPN at $70^\circ\text{C}$ ....	122
Figure 6.2 Comparison of the total vinyl conversion in the neat VER/AIBN system, the 50:50 VER/AIBN:DGEBA/I-MeI and VER/AIBN:DGEBA/DDM IPNs at $70^\circ\text{C}$ .....	123
Figure 6.3 Comparison of epoxy conversion in the neat DGEBA systems, the 50:50 wt% VER/AIBN:DGEBA/I-MeI and VER/AIBN:DGEBA/DDM IPNs at $70^\circ\text{C}$ .....	124
Figure 6.4 Steady shear viscosity versus time for the pure components and respective blends at $70^\circ\text{C}$ .	126
Figure 6.5 Frequency dependence of $\tan\delta$ as a function of reaction time for neat DGEBA/I-MeI at $70^\circ\text{C}$ .....	127
Figure 6.6 Frequency dependence of $\tan\delta$ as a function of reaction time for VER/AIBN:DGEBA/I-MeI at $70^\circ\text{C}$ .....	128
Figure 6.7 Frequency dependence of $\tan\delta$ as a function of reaction time for VER/AIBN:DGEBA/DDM at $70^\circ\text{C}$ .....	129
Figure 6.8 Real modulus ( $G'$ ) at 22 rad/s as a function of reaction time for the neat resins and the 50:50 IPNs and for a 50:50 mixture of VER and xylene at $70^\circ\text{C}$ , near the gelation point.....	130
Figure 6.9 Real modulus ( $G'$ ) at 22 rad/s as a function of time for the 50:50 VER/AIBN:DGEBA/I-MeI IPN and the parent resins in the vitrification region at $70^\circ\text{C}$ .....	131
Figure 6.10 Real modulus ( $G'$ ) at 22 rad/s as a function of time for the 50:50 wt% VER/AIBN:DGEBA/DDM IPN and the parent resins in the vitrification region at $70^\circ\text{C}$ .....	132
Figure 7.1 DSC scans of bisGMA/AIBN64, DGEBA/I-MeI and their IPNs.....	139
Figure 7.2 DSC scans of DEBADM/AIBN64, DGEBA/I-MeI and their IPNs.....	140
Figure 7.3 DSC scans of DEBPADM/AIBN64, DEBADM/VAZO88, DGEBA/I-MeI and their IPNs. (D= dimethacrylate peak; E = epoxy peak).....	142

Figure 7.4 DSC scans of DEBPADM/VR110, DEBADM/AZO168 and DGEBA/1-MeI and the 50:50 IPN. (D = dimethacrylate peak; E = epoxy peak) .....	143
Figure 7.5 FTIR spectra in the region from 1660 cm <sup>-1</sup> to 1600 cm <sup>-1</sup> and from 1000cm <sup>-1</sup> to 900cm <sup>-1</sup> for the 50:50 DEBADM/AIBN64:DGEBA/1-MeI IPN cured at 70°C for varying times and after post- cure at 160°C for 3 hours.....	144
Figure 7.6 Epoxy and methacrylate conversion versus time for the neat resins and in the 50:50 blend of DEBADM/AIBN64:DGEBA/1-MeI at 70 °C. ....	145
Figure 7.7 Epoxy and methacrylate conversion versus time for the neat resins and in the 50:50 blend of DEBADM/VR110:DGEBA/1-MeI at 110°C. ....	146
Figure 7.8 Epoxy and methacrylate conversion versus time for the neat resins and in the 50:50 blend of DEBADM/AZO168 (2 wt%):DGEBA/1-MeI at 160°C. ....	147
Figure 8.1 DMTA scans of DGEBA/2wt% 1-MeI, VER/AIBN and the corresponding 50:50 IPN. ....	153
Figure 8.2 DMTA scans of DGEBA/BA, DGEBA/DAO, VER/AIBN and corresponding 50:50 IPNs. ....	154
Figure 8.3 DMTA scans of DGEBA/An, DGEBA/DDM, VER/AIBN and corresponding 50:50 IPNs.....	154
Figure 8.4 DMTA scans of DGEBA/CHDCA/DMBA, VER/AIBN and corresponding 50:50 IPN. ....	155
Figure 8.5 DMTA scans of DEBPADM/AIBN64, DGEBA/2wt% 1-MeI and the corresponding 50:50 IPN .....	157
Figure 8.6 DMTA scans of DEBPADM/VR110, DGEBA/2wt% 1-MeI and the corresponding 50:50 IPN .....	157
Figure 8.7 DMTA scans of DEBPADM/AZO168AIBN, DGEBA/2wt% 1-MeI and the corresponding 50:50 IPN.....	158
Figure 8.8 DMTA scans of DGEBA/Me-I (2 wt%), bisGMA/AIBN, and corresponding 50:50 IPN.....	159
Figure 8.9 DMTA scans of DGEBA/1-MeI (2 wt%), bisGMA/AIBN, and the 50:50 semi-IPNs of PGEM/AIBN:DGEBA/1-MeI (5 wt%) semi-IPN and bisGMA/AIBN:PGE/1-MeI (5 wt%). ....	160
Figure 8.10 Scattering intensity I(Q) versus scattering vector Q for DGEBA/1-MeI, VER/AIBN and the 50:50 IPN. ....	164
Figure 8.11 Scattering intensity I(Q) versus scattering vector Q for DGEBA/DAO, VER/AIBN and the 50:50 IPN. ....	165
Figure 8.12 Scattering intensity I(Q) versus scattering vector Q for DGEBA/DDM, VER/AIBN and the 50:50 IPN. ....	165
Figure 8.13 Scattering intensity I(Q) versus scattering vector Q for DGEBA/CHDCA/DMBA, VER/AIBN and the 50:50 IPN. ....	166
Figure 8.14 Deybe-Bueche fitting of 50:50 VER/AIBN:DGEBA:BA and 50:50 VER/AIBN:DGEBA:DAO scattering data.....	167
Figure 8.15 Deybe-Bueche fitting of 50:50 VER/AIBN:DGEBA:An and 50:50 VER/AIBN:DGEBA:DDM scattering data.....	168
Figure 9.1 Scanning cure of DEBPADM/AIBN:DGEBA/DDSA/CHDCA/DMBA.....	173
Figure 9.2 Photocuring of DEBPADM/CQ/TMA at 50°C with visible light using neutral density filters of differing optical densities (ODs); all systems exposed for 10 min. ....	174
Figure 9.3 Photocuring of DEBPADM/CQ/TMA at 50°C with visible light for varying exposure times using the standard neutral density filter with an optical density of 1.3.....	175

Figure 9.4 Photocuring of DEBPADM/XDT at 50 °C with UV radiation (with no neutral density filter) for varying exposure times.....	175
Figure 9.5 Effect of initiator components on the cure of DGEBA: a) temperature ramping DSC of DGEBA/DDSA/CHDCA/DMBA; b) temperature ramping DSC of DGEBA/DDSA/CHDCA/DMBA/TMA; c) temperature ramping DSC of DGEBA/CQ/TMA; d) temperature ramping DSC of DGEBA/XDT; e) temperature ramping DSC of the 50:50 DEBPADM:DGEBA/DDSA/CHDCA/DMBA .....	176
Figure 9.6 Effect of initiator components on the thermal cure of DEBPADM/CQ/TMA: a) temperature ramping DSC of DEBPADM alone; b) temperature ramping DSC of DEBPADM/CQ/TMA; c) temperature ramping DSC of DEBPADM/CQ/TMA:DGEBA; d) temperature ramping DSC of DEBPADM/CQ/TMA after photocuring for 24s to 20% conversion.....	179
Figure 9.7 Effect of initiator components on the thermal cure of DEBPADM/XDT: a) temperature ramping DSC of DEBPADM alone; b) temperature ramping DSC of DEBPADM/XDT; c) temperature ramping DSC of DEBPADM/XDT (after photocuring for 14s to 20% conversion of methacrylate); d) temperature ramping DSC of DEBPADM/XDT:DGEBA (after photocuring for 25s to 27% conversion of methacrylate); e) DEBPADM/XDT: DDSA/CHDCA (containing the normal amount of ingredients – see Chapter 3).....	180
Figure 9.8 Photocuring behaviour of the 50:50 IPN DEBPADM/CQ/TMA: DGEBA/DDSA/CHDCA/DMBA at 50°C for varying irradiation times with visible light and the effect on the subsequent temperature-ramping exotherm behaviour.....	181
Figure 9.9 Photocure behaviour of 50:50 DEBPADM/XDT: DGEBA/DDSA/CHDCA/DMBA at 50°C for varying times, followed by scanning DSC cure from 50-300°C.....	182
Figure 9.10 Partial scan-cure of the epoxy component followed by photocuring of the dimethacrylate in DEBPADM/XDT:DGEBA/DDSA/CHDCA/DMBA at 50°C.....	184
Figure 9.11 Partial scan-cure of the epoxy component followed by photocuring of dimethacrylate component in DEBPADM/XDT:DGEBA/DDSA/CHDCA/DMBA at 100°C .....	185
Figure 9.12 NIR spectra (path length 1mm) of the IPN based on the 50:50 DEBPADM/XDT: DGEBA/DDSA/CHDCA/DMBA components: a)uncured IPN; b) UV cure of IPN (without DMBA) at 100°C for 40 min; c) UV cure of IPN at 100°C/40 min and then isothermal cure at 100°C/12 h; d) isothermal cure of IPN at 100°C/12 h; e) isothermal cure of IPN at 100°C/12 h and then UV cure at 100°C/40 min; f) 4 <sup>th</sup> order polynomial fit to spectra c to estimate the background spectra. ....	187
Figure 9.13 $\tan \delta$ versus temperature for the thermally cured DGEBA/DDSA/CHDCA/DMBA, photocured DEBPADM/XDT and 50:50 IPN after photocuring/thermally curing.....	188
Figure 9.14 Real modulus ( $E'$ ) versus temperature for the thermally cured DGEBA/DDSA/CHDCA/DMBA, photocured DEBPADM/XDT and 50:50 IPN after photocuring/thermally curing.....	188
Figure 9.15 DMTA scans of DGEBA/CHDCA/DDSA/DMBA, DEBPADM/AIBN and the corresponding 50:50 wt% IPN.....	192
Figure 9.16 DMTA scans of DGEBA/CHDCA/DDSA/DMBA, VER/AIBN and the corresponding 50:50 wt% IPN.....	192

---

<i>Figure 10.1 Typical water sorption curves for VER/AIBN, DGEBA/I-Mel and the corresponding 50:50 IPN at 90°C.....</i>	<i>196</i>
<i>Figure 10.2 Compressive stress-strain curves for DGEBA/I-Mel at 0.1, 1.0 and 10 mm/min.....</i>	<i>201</i>
<i>Figure 10.3 Compressive stress-strain curves for VER/AIBN at 0.1, 1.0 and 10 mm/min.....</i>	<i>201</i>
<i>Figure 10.4 Compressive stress-strain curves for the 50:50 IPN of VER/AIBN:DGEBA/I-Mel at 0.1, 1.0 and 10 mm/min.....</i>	<i>202</i>
<i>Figure 10.5 Compressive yield (MPa)/2kT versus logarithmic strain rate for VER/AIBN, DGEBA/I-Mel and the 50:50 IPN of VER/AIBN:DGEBA/I-Mel.....</i>	<i>202</i>
<i>Figure 10.6 Typical stress-strain results for the DGEBA/I-Mel, VER/AIBN and resulting 50:50 IPN in 3 point bend.....</i>	<i>203</i>

## List of Tables

Table 2.1 Commerical IPN materials (adapted from Cook et al. <sup>201</sup> ) .....	47
Table 3.1 The structures of the peroxide radical initiators utilized and their 10 hour half life temperatures <sup>204</sup> .....	50
Table 3.2 Structures of the azo initiators used and their 10 hour half life temperatures.....	50
Table 3.3 Structures of visible light (470nm) and UV light photoinitiating systems.....	51
Table 3.4 Melting points of epoxy curatives as measured by scanning DSC at 5°C/min.....	55
Table 4.1 Band assignment for chemical groups from mid-FTIR absorption spectra <sup>77,116,310</sup> .....	60
Table 4.2 Band assignments for chemical groups from near-FTIR absorption spectra <sup>212,213</sup> .....	61
Table 5.1 Heat of polymerization and peak temperatures for individual peaks for IPNs involving aromatic amine-cured epoxies.....	87
Table 5.2 Heat of polymerization and peak temperatures for individual peaks for IPNs involving aliphatic amine-cured epoxies.....	88
Table 5.3 Summary of the DSC analysis of the VER cured with various radical initiators, DGEBA cured with I-Mel and the IPNs formed from these resins. ....	98
Table 5.4 Summary of the DSC analysis of the bisGMA/AIBN, PGEMA/AIBN, DGEBA/I-Mel, PGE/I-Mel and the IPNs formed from these resins. ....	100
Table 6.1 Summary of rheology and kinetics at the gel point at 70°C.....	133
Table 6.2 Summary of rheology and kinetics at the onset of vitrification (at $G' = 10^7$ Pa) at 70°C.....	133
Table 7.1 Summary of the DSC analysis of the bisGMA/AIBN64, DEBPADM/AIBN64, DEBPADM/VAZO88, DEBPADM/VR110, DEBPADM/AZO168, DGEBA/I-Mel and the IPNs formed from these resins .....	138
Table 8.1. DMTA results for parent resins and their IPNs .....	150
Table 8.2. DMTA results for parent resins and their IPNs .....	156
Table 8.3 DMTA results for parent resins and their IPNs with PGE and PGEM.....	159
Table 8.4 Scattering length and atomic weight associated with particular atoms <sup>163</sup> .....	161
Table 8.5 Composition and scattering length associated with the repeat unit.....	162
Table 8.6 Summary of scattering length, MW of repeat unit, density and scattering length density for all the neat resins.....	163
Table 8.7 Deybe-Bueche fitting results for 50:50 VER/AIBN:DGEBA:BA and 50:50 VER/AIBN:DGEBA:DAO.....	167
Table 8.8 Deybe-Bueche fitting results for 50:50 VER/AIBN:DGEBA:An and 50:50 VER/AIBN:DGEBA:DDM.....	168
Table 8.9 Summary of phase morphology and curing order of IPNs.....	169
Table 9.1 Glass transition temperatures and conversions for the isothermally cured and photocured DEBPADM/XDT:DGEBA/DDSA/CHDCA/DMBA IPN and its parent resins using various cure schedules. ....	189
Table 10.1 Values of equilibrium mass fraction of water, $m_{\infty}$ at various temperatures for the systems under study. ....	197

---

<i>Table 10.2 Values of heat of dissolution, <math>H_s</math>, and pre-exponential factor, <math>S_0</math>, for the systems under study.</i>	198
<i>Table 10.3 Summary of results from compression experiments</i>	200
<i>Table 10.4 Summary of results from flexural experiments</i>	204
<i>Table 11.1 Summary of the effect of curing order and component miscibility, and a comparison of semi- and full- amine type IPNs.</i>	212
<i>Table 11.2 A summary of the effect of curing order and comparison of semi- and full-IPN formation on the component miscibility.</i>	213

## ***List of Publications***

The following publications have arisen from this and related work.

### **Refereed Publications**

K. Dean, W. D. Cook, M. D. Zipper and P. Burchill

**Curing behaviour of IPNs formed from model VERs and epoxy systems I amine cured epoxy:** *Polymer*, Volume 42, Issue 4, February 2001, Pages 1345-1359

K. Dean, W. D. Cook, M. D. Zipper and P. Burchill

**Curing behaviour of IPNs formed from model VERs and epoxy systems II imidazole cured epoxy:** *Polymer*, Volume 42, Issue 8, April 2001, Pages 3589-3601

Katherine Dean, Wayne D. Cook, Laurent Rey, Jocelyne Galy and Henry Sautereau

**Near Infra-red and Rheological Investigations of Epoxy-Vinyl Ester Interpenetrating Polymer Networks:** *Macromolecules*, Volume 34, 2001, Pages 6623-6630.

Wayne D. Cook, Katherine Dean and John S. Forsythe

**Cure, rheology and properties of IPN thermosets for composite applications:** *Materials Forum*, Volume 25, 2001, Pages 30-59

I. Merdas, A. Tcharkhtchi, F. ThomINETTE, J. Verdu, K. Dean and W. Cook

**Water Absorption by uncrosslinked polymers, networks and IPNs having medium to high Polarity** *Polymer*, Volume 43, Issue 17, August 2002, Pages 4619-4625

Katherine Dean and Wayne Cook

**The effect of curing sequence on the photopolymerization and thermal curing kinetics of dimethacrylate-epoxy Interpenetrating Polymer Networks**  
*Macromolecules* Volume 35, 2002, Pages 7942-7954

Katherine Dean and Wayne Cook

**Azo initiator selection to control the curing order in epoxy/dimethacrylate IPNs**  
submitted to *Polymer* 2002

**Conference Publications**

K. Dean, W. Cook, M. Zipper and P. Burchill

**Curing kinetics of thermosetting resins: vinyl esters**, Preprints of the 37<sup>th</sup> IUPAC International Symposium on Macromolecules, p521, Gold Coast, Australia July 1988

W. D. Cook, K. Dean, P. Burchill, M. D. Zipper, J. Galy, L. Rey, H. Sautereau and J. P. Pascault

**Curing and rheology of IPN thermoset blends**, Proceedings of the 6th European Polymer Blends Conference, PD93, Mainz, Germany, May 17, 1999

K. Dean, W. Cook, L. Rey, J. Galy and H. Sautereau

**Rheological investigations of new IPNs for composite applications**, Preprints of the 1<sup>st</sup> ACUN International Composites Meeting, P243, Sydney, 1999

W. Cook, J. Forsythe, A. Kootsookos, K. Dean and M. Zipper

**New IPN thermosets for composite applications**, Preprints of the 1<sup>st</sup> ACUN International Composites Meeting, P126, Sydney, 1998

K. Dean, W. Cook, M. Zipper and P. Burchill

**Curing behaviour of IPNs formed from model VEPs and epoxy systems**, Proceedings of the 23<sup>rd</sup> Australasian Polymer Symposium, p C2/2, Geelong, Victoria, Dec 1999

W.D. Cook, K. Dean, L. Rey, J. Galy, H. Sautereau and J.P. Pascault

**Curing kinetics of new IPNs for composite applications**, Proceedings of the 23<sup>rd</sup> Australasian Polymer Symposium, p J2/6, Geelong, Victoria, Dec 1999

W. Cook, K. Dean, J. Galy, L. Rey, H. Sautereau and J.P. Pascault

**Cure kinetics and properties of IPNs** Proceedings of the Pacific Polymer Conference, p 333, Guangzhou, December 6-11, 1999.

W.Cook, K. Dean, J. Galy, L. Rey, H. Sautereau, J-P Pascault, S. Ooi, G. Simon and C. Such

**Rheology of bulk and latex IPNs IUPAC Polymer Networks 2000, Krakow Poland, July 2000.**

K. Dean, W. Cook and P. Burchill

**DSC and FTIR investigations of the cure of epoxy-dimethacrylate IPNs IUPAC Polymer Networks 2000, Krakow Poland, July 2000.**

K. Dean, W. Cook and P. Burchill

**Rheology during Cure of Interpenetrating Polymer Networks 24<sup>th</sup> Australasian Polymer Symposium, pA2/4, Beechworth, Victoria, 2001**

W. Cook, K. Dean and S.K. Ooi

**Thermoset Blends - from latex IPNs to IPNs for composite applications 24<sup>th</sup> Australasian Polymer Symposium, A6/1, Beechworth, Victoria, 2001**

K. Dean and W. Cook

**Photopolymerization of dimethacrylate-epoxy Interpenetrating Polymer Networks 25<sup>th</sup> Australasian Polymer Symposium, A 5/2, Armidale, N.S.W., 2002**

Wayne D Cook, Katherine Dean and Soo Ooi

**Control of phase separation of dimethacrylate-epoxy interpenetrating polymer networks by photo-polymerization, 7th European Polymer Blends Conference, Lyon, May 30, 2002**

Wayne D Cook and Katherine Dean

**The use of photo-polymerization in studying the curing kinetics and phase separation of dimethacrylate-epoxy Interpenetrating Polymer Networks 7<sup>th</sup> European Polymer Blends Conference, Lyon, May 29, 2002**

Wayne D Cook, Katherine Dean and Soo Ooi

**The use of photo-polymerization in the study of cure kinetics and phase separation of dimethacrylate-epoxy Interpenetrating Polymer Networks Photopolymerization Fundamentals, Breckenridge, Colorado, USA, June 11, 2002**

**Abbreviations**

AIBN64 or AIBN	azobisisobutyronitrile
An	aniline
bisGMA	bisphenol-A diglycidyl ether dimethacrylate
BA	butylamine
BPO	benzoyl peroxide
CHDCA	cis-1,2-cyclohexanedicarboxylic anhydride
CHP	cumene hydroperoxide
Co	cobalt octoate
CQ	camphorquinone
DAO	1,8-diamino octane
DEBPADM	diethoxylated bisphenol-A dimethacrylate
DGEBA	diglycidyl ether of bisphenol-A
DDM	4,4'-diamino-diphenyl methane
DDSA	n-dodecyl succinic anhydride
DMBA	dimethylbenzylamine
1-MeI	1-methyl imidazole
MEKP	methyl ethyl ketone peroxide
PGE	phenyl glycidyl ether
PGEMA	phenyl glycidyl ether methacrylate
TMA	N,N, 3,5-tetramethyl aniline
VAZO88	1,1'-azobis(cyclohexanenitrile)
VR110	1,1'-azobis(2,4,4-trimethylpentane)
VAZO168	2,2-azobis(2-methylpropane)
VER	model vinyl ester resin based on 70wt% bisphenol-A diglycidyl ether dimethacrylate with 30wt% styrene monomer
XDT	p-xylylenebis(N,N-diethyl dithiocarbamate)

**Symbols**

$A_0$	FTIR peak area of a reactive group at zero time
$A_t$	FTIR peak area of a reactive group at time t
$A_\infty$	FTIR peak area of fully cured reactive group
b	neutron scattering length density
$b_v$	neutron scattering phase contrast factor
$C_\infty$	equilibrium water concentration
D	diffusivity
d	thickness of sample for solvent uptake
E	modulus
$E'$	in-phase storage (elastic) component of modulus from dynamical mechanical analysis
$E''$	out of phase (viscous) component of modulus from dynamical mechanical analysis
f	functionality of branch units
$f_a$	functionality of reactive groups a
$f_b$	functionality of reactive groups b
$G_e$	equilibrium modulus
$G(t)$	relaxation modulus
$G'$	real (storage) shear modulus
$G''$	loss shear modulus
$\Delta G_M$	free energy of mixing
$\Delta H$	enthalpy
$\Delta H_M$	enthalpy of mixing
$H_w$	enthalpy of water vaporization
$H_s$	heat of dissolution
$I(Q)$	absolute neutron scattering intensity
k	Boltzman's constant
$M_n$	number average molecular weight
$M_t$	weight at time t
$M_w$	weight average molecular weight
MW	molecular weight
$m_\infty$	equilibrium mass fraction of water

$N_1$	number of molecules of species 1
$N_2$	number of molecules of species 2
$N$	relaxation exponent
$N_s$	number of neutron scattering centers for a given volume illuminated by the neutron beam
$p$	water vapour pressure
$p_a$	extent of reaction for A groups
$p_b$	extent of reaction for B groups
$p_{gel}$	conversion at gel point
$Q$	neutron scattering vector
$r_1$ and $r_2$	distance from the crack tip
$r$	stoichiometric ratio of 2 reactive groups
$R$	gas constant
$S_n$	strength of the network at the gel point
$S$	coefficient of solubility
$S_0$	water solubility pre-exponential factor
$\Delta S_M$	entropy of mixing
$S(Q)$	neutron scattering structure factor
$P(Q)$	neutron scattering form factor
$T_g$	glass transition temperature
$T_{cure}$	temperature of cure
$T_{g\infty}$	ultimate $T_g$ of the cured system
$T_{g0}$	$T_g$ of the prepolymer
$T_{g(gel)}$	$T_g$ of the gel
$V_1$	molar volume of component 1
$V_2$	molar volume of component 2
$V_M$	total volume of mixture
$V_s$	volume of sample illuminated by the neutron beam
$V_{flow}$	activation volume
$w_s$	fraction of sol
$\bar{x}_n$	number average degree of polymerization
$\bar{x}_w$	weight average degree of polymerization
$\alpha_1$	conversion of reactive groups
$\chi$	binary thermodynamic interaction parameter

---

$\varepsilon$	strain
$\dot{\varepsilon}$	strain rate
$\dot{\varepsilon}_0$	strain rate proportionality
$\dot{\gamma}$	deformation rate tensor
$\gamma$	ratio of A groups on branch units to all A groups in the mixture
$\eta$	steady shear viscosity
$\lambda$	wavelength
$\nu$	moles of elastically active network strands per mass of polymer
$\rho$	moles of crosslinks per mass of polymer
$\rho_w$	density in the wet state
$\sigma_y$	yield strength
$\tau$	shear stress
$\phi_1$	volume fraction of component 1
$\phi_2$	volume fraction of component 2
$\omega$	frequency
$\xi$	correlation length

## *Abstract*

Interpenetrating polymer networks (IPNs) are a combination of two or more crosslinked polymers that are held together by permanent entanglements. IPNs are unique in that the chemical crosslinking of components can hinder thermodynamic phase separation and thus miscible blends can be produced from immiscible polymers. IPNs allow the formation of unique combinations of polymers, which can potentially result in synergistic properties. In this work the polymerization behaviour of a series of epoxy/dimethacrylate simultaneous IPNs based on an epoxy monomer (diglycidyl ether of bisphenol-A, DGEBA) cured with a range of amines or anhydrides and a radically initiated dimethacrylate (diethoxylated bisphenol-A dimethacrylate, DEBPADM or bisphenol-A diglycidyl dimethacrylate, bisGMA), or a model vinyl ester (VER, composed of bisGMA in 30 wt% styrene) has been investigated. The different combinations of curing components, the interactions that occur between components and the order of cure, each affect the overall cure kinetics, resulting morphology and properties of epoxy/dimethacrylate IPNs.

Chemical interactions between components in these IPNs include the Michael addition between the amine curative of the epoxy and the methacrylate unsaturation (leading to grafting between the networks); a redox interaction between the amine and the peroxide initiating system which causes acceleration of the peroxide decomposition and in some cases depletion of the peroxide initiating system of the dimethacrylate; retardation of the propagation reaction by formation of less reactive amine radicals and catalysis of the epoxy-amine reaction by the hydroxy groups in the bisGMA molecule or in the peroxide diluent. Dilution effects were observed by one component on the other, and the cure rate of one component was affected by the level of cure of the second component. In some cases, the presence of unreacted species of one component plasticized the IPN and enabled a higher level of reaction of the other component before vitrification occurred. In addition, when one of the components attained a high level of cure in the early stages of IPN formation, the high level of crosslinking contributed to premature vitrification, which limited the extent of cure of the other component. Although IPNs are ideally a combination of two or more network forming polymers held together exclusively by their permanent mutual entanglements, phase separation was observed in some cases.

The chemorheology of two 50:50 IPNs based on the VER and either imidazole-cured or aromatic amine-cured epoxy resin was monitored via near infrared spectroscopy (NIR) and rheometry. The gel points of the IPNs (as measured by a crossover in  $\tan\delta$  and other criteria) were similar to the VER (which reacted first in both cases) indicating that it was the gelation of the component which reacted first (rather than the gelation of the component which reacted last) that had the dominant effect on the overall gel point of the IPN, as expected. The IPNs showed a delay in gelation (compared with the VER) that was due, in part, to a dilutional effect (confirmed by the study of a diluted VER) and in part due to amine-radical interactions. Both the imidazole and aromatic amine based IPNs and their corresponding parent resins vitrified in the latter stages of the reaction because the isothermal cure temperature was well below the glass transition temperature of the resin components. Compared with the parent resins, the real modulus for both the IPNs rose more slowly to the glassy region and this was consistent with the NIR results.

The effect of curing order in a range of IPNs prepared from an imidazole-cured epoxy resin and a dimethacrylate resin was investigated by the use of azo-initiators, with differing reactivities, for the dimethacrylates. By appropriate azo-initiator selection, it was possible to interchange the order of cure of the components within the IPN so that either the dimethacrylate or epoxy cured first, without the complications due to interactions previously observed between peroxides and aliphatic and aromatic amine curatives. Although the variable azo-selection study did not clearly show changes in phase morphology (all IPNs exhibited single  $T_g$ s), the kinetic studies did clearly show the cure order had been changed.

In the final curing study, a combination of thermal and photochemical initiation was used to study the effect of either photocuring the dimethacrylate followed by thermal cure of the epoxy/anhydride or by thermally curing the epoxy/anhydride first followed by photocuring of the dimethacrylate. When the epoxy component was thermally-cured before isothermal photopolymerization of the dimethacrylate, the final conversion of the dimethacrylate was limited by vitrification or topological restraint of the IPN. When the order of cure was reversed, the thermal cure of the epoxy was reduced, due to topological restraint or due to partitioning of the reactive components into separate phases. NIR studies of the cure of the dimethacrylate and epoxy components confirmed that the cure order affected the final conversion. Dynamic

mechanical thermal analysis (DMTA) studies of the NIR samples revealed a single glass transition and thus a miscible IPN when the epoxy component was cured first, but two glass transitions were observed when the dimethacrylate component was photocured prior to the epoxy/anhydride cure, confirming that phase separation had occurred.

Small angle neutron scattering and DMTA was used to examine the resulting structures of a selection of the IPNs investigated. A range of morphologies resulted, varying from those IPNs which were clearly phase separated (showing two  $T_g$ s and excess small angle neutron scattering) to those that appeared to be a single phase (showing a single  $T_g$  and no small angle neutron scattering). These results indicate the phase structure of IPNs is strongly dependent not only on the miscibility of the components constituting the IPN, but also the polymerization kinetics of those components. The backbone monomers chosen in this work (DEBPADM, bisGMA and DGEBA) were chosen to be similar in structure to increase the miscibility of the polymers, however it may be noted that small changes in structure can have a significant effect on the resulting IPN miscibility. In IPNs containing 1° aliphatic and aromatic amine curing agents for the epoxy, these curatives appear to be responsible for a decrease in miscibility resulting in a two-phase morphology and changing the curing order had little effect on their miscibility. However, in IPNs of dimethacrylate and anhydride-cured DGEBA where there appears to be more miscibility between components, changing the curing order results in either a one or two phase IPN. In addition, the H-bonding between the crosslinking bisGMA (and uncrosslinked poly phenyl glycidyl ether methacrylate) and DGEBA appeared to promote the formation of single phase IPNs. It may be concluded that grafting between components within an IPN (such as occurs in IPNs containing 1° amines) does not necessarily force the formation of a single phase system; in fact it appears that the IPN phase separates prior to any grafting between components and thus the miscibility of the unreacted components within the IPN has the dominant effect on the formation of a single phase material.

The water absorption characteristics of the neat VER and DGEBA cured with either an imidazole or aromatic amines (linear and crosslinking) and their corresponding 50:50 IPNs were studied. The VER was less hydrophilic than the epoxy due to the presence of the non-polar styrene. The IPNs were generally more hydrophilic than their parent resins and this may be explained by the pre-exponential factor varying smoothly

with composition while the enthalpy of dissolution  $H_s$  was close to the value of the most hydrophilic component.

The 50:50 IPN of the VER with an imidazole cured DGEBA, chosen for the mechanical property study exhibited a modulus and yield strength that were close to the average of the parent resins, but the percentage strain at yield in the IPN was higher than the average expected from the neat resins.

In this study of epoxy-dimethacrylate based IPNs, numerous interactions (both chemical and physical) have been systematically identified and interpreted, thus enabling the development of an IPN in which the phase morphology can be precisely controlled by the choice of an appropriate curing regime. The combination of thermal and photoinitiation was one of the most exciting aspects of this work, because it allowed for the complete control of cure order of components within epoxy/dimethacrylate IPNs. To prove it was possible to change the miscibility by changing the cure schedule, the IPNs in this study were either fully photocured followed by thermal cure or vice versa, however, it may also be possible to control the level of phase separation and the type of morphology by intermittent photocuring. This work gave an indication of the variation in miscibility and morphologies (and thus properties) that are possible in these IPN systems. It is only through further research of the structure/property relationships of these systems that the potential applications of these materials can be found. In conclusion, this work has developed some of the key components of the intellectual framework that will allow the formulation of IPNs with the desired level of miscibility and the appropriate phase morphology to provide the required properties for a range of new applications.

# Chapter 1 Introductory Remarks

---

## 1.1 Introduction

Crosslinked (or network) polymers have many advantages over thermoplastics polymers – they can be formed *in situ*, are solvent resistant, do not flow under stress and can be produced as rubbery materials with high extensibility or as glassy materials with high rigidity and thermal resistance. The properties of polymer networks have been varied conventionally by copolymerization. A more recent method of network modification is the production of an interpenetrating polymer network (IPN).<sup>1</sup> Ideally, IPNs are a combination of two or more polymers in network form, with at least one of the polymers crosslinked in the presence of the other which causes interlocking of the networks. A number of different IPNs have been developed; these include semi-IPNs, sequential IPNs, latex IPNs and gradient IPNs<sup>1</sup>, however this study will focus on simultaneous IPNs. For simultaneous IPN formation, all monomers/ or prepolymers plus crosslinking agents and initiators are combined together followed ideally by simultaneous non-interfering polymerization reactions. To ensure non-interfering polymerization, different reaction modes are generally chosen such as chain growth and step growth polymerization, however despite this precaution, grafting between the two networks is not uncommon<sup>2-4</sup>. Three other important factors in the curing of IPNs include chemical interactions<sup>3,5</sup> that may occur between the network components, the occurrence of phase separation<sup>6-8</sup>, and the possibility of vitrification of either one of the networks that may hinder full cure of the other network<sup>5</sup>. An understanding of these factors is essential to the optimum design of an IPN.

## **1.2      Layout of the Dissertation**

This dissertation is predominantly a study of the cure kinetics, chemorheology, morphology and properties of epoxy/dimethacrylate and epoxy/vinyl ester simultaneous IPNs cured with a range of additives for the epoxy and radical initiators for the dimethacrylate. Chapter 2 is an in-depth review of the literature on network polymers, epoxy resins, vinyl ester and dimethacrylates, followed by an overview of IPNs including kinetics and morphology during curing, and structure property relationships. Chapters 3 and 4 outline the materials and the experimental techniques used in this study. The results and discussion are presented in Chapters 5 to 10. Chapter 5 presents the curing kinetics and interactions between components in a range of the IPN systems. After this survey, a smaller number of IPNs were chosen for further investigation. Chapter 6 investigates the chemorheology of a select number of IPN systems. Chapters 7 and 9 investigate the effects of cure order in IPNs on cure kinetics and the resulting morphology. Chapter 8 offers an explanation of the phase morphology of these IPN materials via dynamic mechanical testing and neutron scattering. Chapter 10 contains some properties of cured IPNs including compression and flexural mechanical testing and water sorption studies, and Chapter 11 summarizes the thesis with conclusions and suggestions for future work.

# *Chapter 2*

## *Literature Review*

---

### **2.1 Polymer Networks**

#### **2.1.1 Network Formation**

Network polymers are formed from the crosslinking of multifunctional monomers via either step growth polymerization (see Section 2.1.2) or chain growth polymerization (see Section 2.1.3). Lightly crosslinked polymers generally exhibit good elastic properties whilst highly crosslinked polymers have good thermal and dimensional stability. The build up of a three-dimensional network structure via step growth polymerization is quite well understood and can be explained by classical gelation theory (see Section 2.1.2). However, the formation of three-dimensional polymer networks via chain growth polymerization is a more complicated and less well understood process<sup>9</sup>. Complexities arise from variations in mobility and reactivity of functional groups throughout the course of the chain growth reaction. For example in the free radical polymerization of undiluted multifunctional monomers, the gel effect (Trommsdorff effect, see Section 2.1.3) occurs almost immediately, causing autoacceleration of the reaction. Inhomogeneities within the developing network can also cause complications in free radical polymerization<sup>10</sup>. As polymerization proceeds, the chains increase in size and level of branching. Gelation occurs when a molecule of infinite size is formed<sup>11</sup>. At the gel point, the conversion is not complete and unreacted functional groups are still present in the gel at dangling chain ends or in the chain backbone. A number of species that are not bonded to the network structure are also

present. These molecules are soluble and are described as the *sol* species. Past the gel point the amount of gel increases at the expense of the sol and the mixture transforms from a viscous liquid to an elastic material of infinite viscosity. Further network formation may reduce the mobility of functional groups attached to the network to such an extent that they may become completely isolated from other reactive groups. In general, the structure of network polymers formed either via step growth or chain growth polymerization can be characterized by the presence of gel and sol species, unreacted groups in the sol and gel, network strands, dangling chain ends, entanglements and crosslink points.

As the crosslink density rises in the network and the fraction of sol decreases, the glass transition temperature ( $T_g$ ) is raised<sup>12-14</sup>:

$$T_g = T_{g0} + k'\rho - k''w_s \quad \text{Equation 2.1}$$

where  $\rho$  is the moles of crosslinks per mass of polymer,  $w_s$  is the fraction of sol,  $T_{g0}$  is the  $T_g$  of the uncrosslinked polymer and  $k'$  and  $k''$  are constants dependent on the particular system under consideration<sup>15</sup> but since  $\rho$  and  $w_s$  are not proportional to the conversion, the  $T_g$  is a non-linear function of conversion<sup>13,15</sup>.

It should be noted that since the crosslinking reaction essentially stops if the network polymer approaches a glassy state, the glass transition temperature ( $T_g$ ) of the network, will not, in theory, exceed the temperature of cure ( $T_{cure}$ )\*. The reaction will become diffusion controlled as the  $T_g$  approaches  $T_{cure}$  because the chain mobility is reduced by the rise in  $T_g$ . At this stage the material begins to vitrify (harden), and the overall polymerization rate is reduced resulting in incomplete conversion. In this situation, complete cure can only be obtained if the system is cured at a temperature higher than the ultimate  $T_g$  of the cured system ( $T_{g\infty}$ ).

Isothermal time-temperature-transformation (TTT) diagrams<sup>19,20</sup> can be used to explain the different stages of cure in network polymers. Figure 2.1 shows a typical TTT diagram for a thermosetting system, illustrating the three characteristic

---

\* In practice the  $T_g$  determined by DSC<sup>16,17</sup> or DMTA is often found to be ca. 10°C above the curing temperature, but if the glass transition region is very broad this can approach 70°C<sup>18</sup>.

temperatures corresponding to  $T_{g0}$  (the  $T_g$  of the monomer or the prepolymer),  $T_{g\infty}$  (the  $T_g$  of the fully crosslinked material) and  $T_{g(\text{gel})}$  ( $T_g$  of the gel), and gelation and vitrification curves separate the regions of non-gelled (sol) material, gel and vitrified resin. Figure 2.1 also shows a region illustrating the onset of phase separation of one of the components of an IPN that can occur when the components have poor enthalpic interactions. In Figure 2.1 an intersection of the gelation and vitrification curves can be seen, this intersection occurs at  $T_{g(\text{gel})}$ , hence if  $T_{\text{cure}} = T_{g(\text{gel})}$  gelation and vitrification would occur simultaneously. At low curing temperatures where  $T_{\text{cure}} < T_{g(\text{gel})}$ , vitrification occurs before the gel point is reached so that the polymer solidifies as a low molecular weight linear polymer and not as a crosslinked network. If  $T_{g\infty} > T_{\text{cure}} > T_{g(\text{gel})}$ , which is typical in isothermal curing, the polymer will pass through the gel point, and later enter the vitrification region, where polymerization slows and eventually ceases due to limited mobility in the polymer so that the full conversion is not attained. If  $T_{\text{cure}} > T_{g\infty}$  the polymer can reach full conversion, and will not vitrify during the curing process.

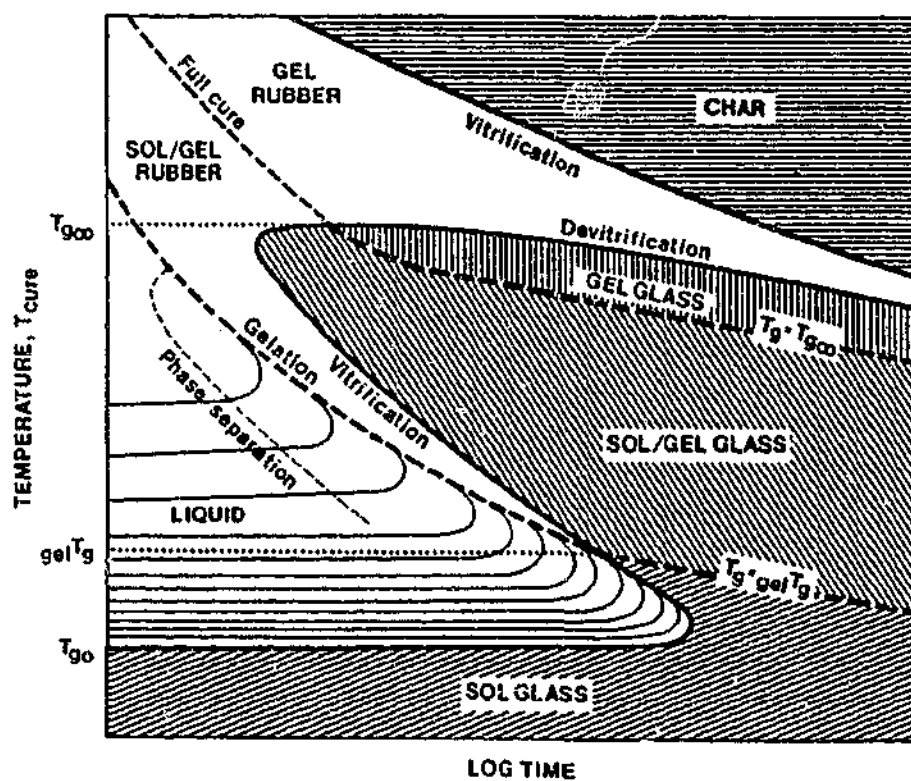
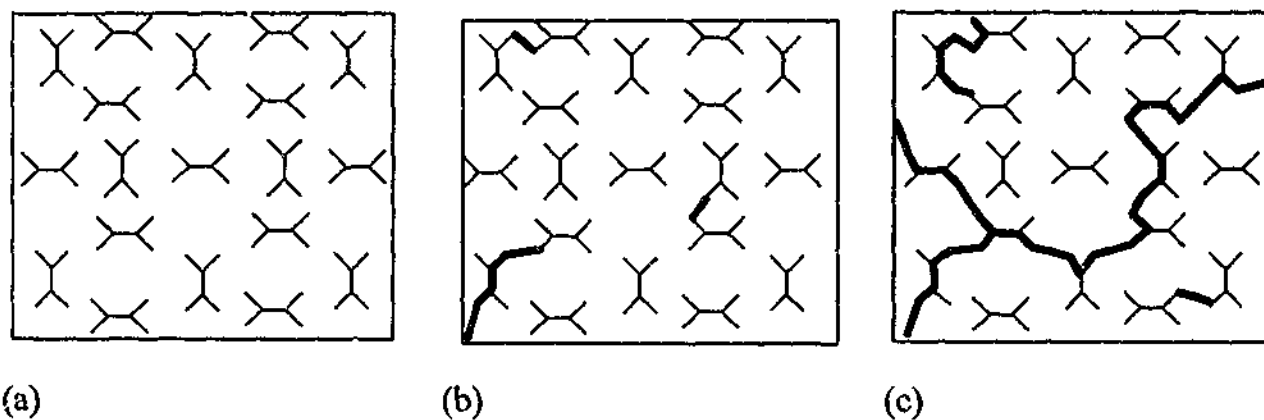


Figure 2.1 Time-temperature-transformation cure diagram for a thermosetting system (after Gillham<sup>20</sup>).

Consequently the cured polymer will be rubbery at the curing temperature but will vitrify to a hard material when cooled to room temperature. Curing at such high temperatures can cause complications such as depolymerization<sup>21</sup> and other degradative processes such as oxidation<sup>22</sup> (identified as charring in Figure 2.1) which can compete with the crosslinking reaction.

### 2.1.2 Step Growth Polymerization

For the formation of a network polymer by the step growth process, the reaction mixture must contain trifunctional or higher functionality species (see Figure 2.2a). If the functionality of the species within the mixture is increased, the conversion required for the formation of polymer network is decreased. Initially only linear and branched polymer molecules are present (see Figure 2.2b), but as more molecules link up, a point is reached when the mixture contains a molecule of essentially infinite molecular weight, i.e. gelation occurs (see Figure 2.2c)<sup>11,23,24</sup>. Further reactions result in the formation of crosslinks so that the network structure develops, and high molecular weight is only achieved at very high conversions<sup>25</sup>.



**Figure 2.2** A schematic of step growth polymerization initially with the unreacted tetrafunctional monomer (a), in the early stages of polymerization ( $p \approx 5\%$  in 3D) (b), and at gelation ( $p = 33\%$ ) showing 3D connectivity (c).

Within the polymer industry, knowledge of the expected conversion at the gel point is invaluable as the change from a viscous liquid to a gel occurs quite suddenly. This has led to a number of theories of gelation, ranging from the simple statistical approach based on the Flory-Stockmayer<sup>26-28</sup> tree-like model to describe the branching of a polymer during curing (assuming that all functional groups have the same reactivity), to the more complex which attempt to take a number of other factors into account including unequal reactivities, substitution effects and intramolecular cyclizations<sup>11,23-25</sup>.

Flory's<sup>23,26,29,30</sup> statistical approach to gelation is based on the weight average degree of polymerization,  $\bar{x}_w$ , approaching infinity at the gel point. However, the

number average degree of polymerization,  $\bar{x}_n$ , is finite at the gel point because the small sol species are of a similar weight fraction as the gel. In this statistical approach it is assumed that all functional groups are of equal reactivity and that no cyclization occurs before gelation. A branching coefficient ( $\alpha$ ) is defined as the probability that a given functional group on a branch unit (having a functionality greater than 2) is connected to another. For the homopolymerization of a monomer with  $f$  reactive functional groups (an  $A_f$  monomer), gelation will occur when  $\alpha(f-1)$  exceeds unity, therefore the critical value of  $\alpha_c$  at gelation is:

$$\alpha_c = \frac{1}{(f-1)} \quad \text{Equation 2.2}$$

Further augmentation of Flory's<sup>23,26,29,30</sup> theory of gelation by Stockmayer<sup>27,28</sup> involving a complicated analysis of distribution functions led to the development of the gelation criterion for the stepwise copolymerization of an  $A_f$  monomer with a  $B_g$  monomer:

$$(p_a p_b)_{gel} = r p_{gel}^2 = \frac{1}{(f_c - 1)(g_c - 1)} \quad \text{Equation 2.3}$$

where  $f_c$  and  $g_c$  are the functionality of the respective reactive groups,  $r$  is the stoichiometric ratio of the two reactive groups and  $p_{gel}$  is the conversion at the gel point.

Macosko and Miller have derived the same equations using a more direct statistical treatment and have obtained more general equations which cover nearly all non-linear stepwise polymerizations<sup>31,32</sup>.

### 2.1.3 Chain Growth Polymerization

Network polymers can also be formed by chain growth polymerization, which involve initiation, propagation and termination steps. Unlike step polymerization with its gradual buildup of oligomeric species (dimers, trimers etc), there are very few reactive species present at any one time in chain growth polymerization and each of these can grow to very high molecular weight very quickly. Due to the high kinetic chain length<sup>33</sup>, in free radical polymerization, gelation occurs at relatively low conversions (generally < 5%) (see Figure 2.3). Inhomogeneities, caused by cyclization

and variations in crosslink density throughout the developing network have been described by Dusek<sup>10</sup> and further complicate gelation in chain growth polymers.

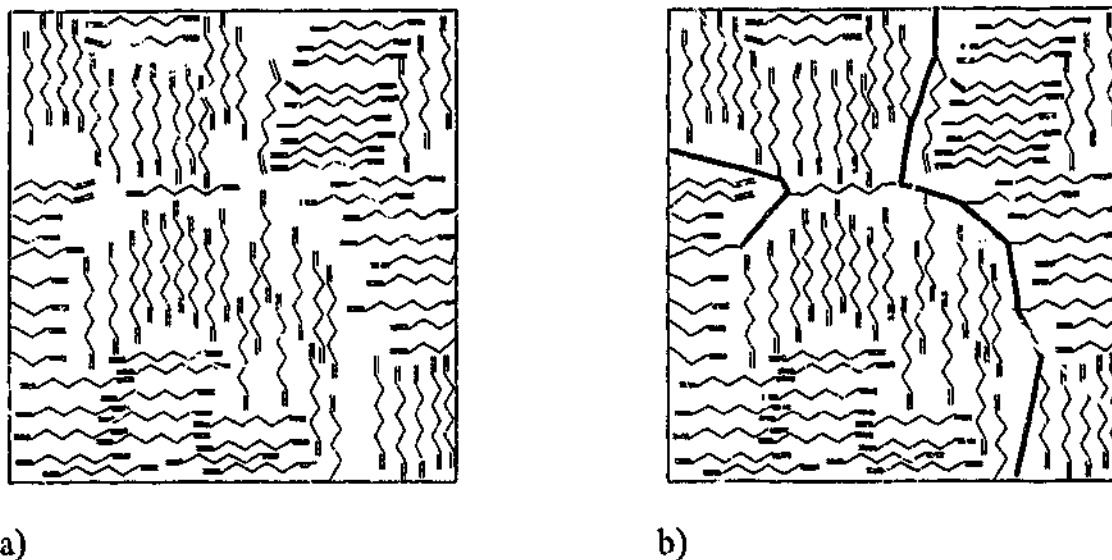
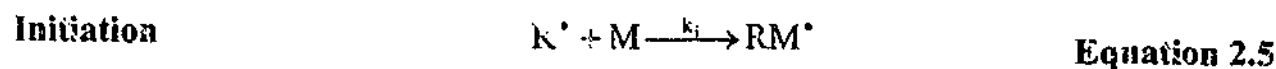
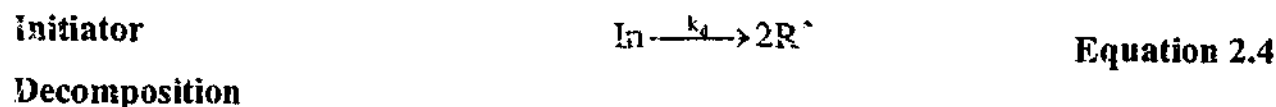


**Figure 2.3** Chain growth polymerization prior to any reaction (a) and at gelation ( $p < 5\%$  in 3D) (b)

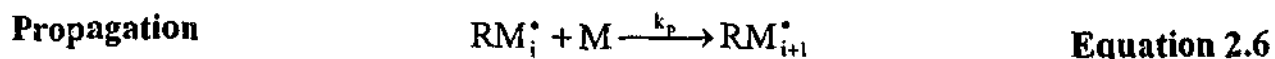
Chain growth polymerization can occur via radical, anionic (see Section 2.2.4) or cationic initiation, but radical polymerization is the most common. For radical polymerization, a reaction scheme is outlined below in Equation 2.4 to Equation 2.8. Radical chain polymerization consists of a progression of initiator decomposition, initiation, propagation and termination steps<sup>34,35</sup>. Several different thermal and photochemical mechanisms can generate free radicals. As shown in Equation 2.4, the general case is the homolytic dissociation of the initiator species (In) to yield a pair of primary radicals ( $R^{\bullet}$ ), where  $k_d$  is the rate constant for the initiator dissociation<sup>34</sup>. The addition of this radical to a monomer molecule then produces the chain initiating species ( $RM^{\bullet}$ ) as shown in Equation 2.5, where M represents a monomer molecule and  $k_i$  is the rate constant of the initiating step<sup>34</sup>.



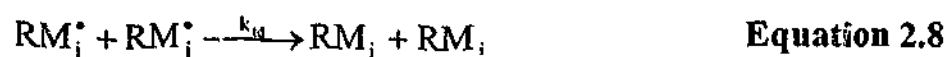
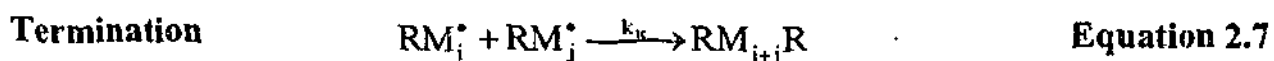
The formation of primary radicals from the initiator (Equation 2.4) proceeds significantly slower than the reaction of these radicals with a monomer molecule

(Equation 2.5), hence it is this first step which is rate-determining and controls the rate  $R_i$  of formation of active centres.

Propagation occurs from the addition of large numbers of monomer molecules to the chain initiating species ( $RM^*$ ). The successive reactions can be represented in general by Equation 2.6, where  $k_p$  is the rate constant for propagation<sup>34</sup>.



After a time, the propagating polymer chain terminates with the annihilation of the radical centres by bimolecular reaction<sup>36</sup> or by trapping of the radical in the matrix<sup>35</sup>. Bimolecular termination can occur by combination (Equation 2.7) or by disproportionation (Equation 2.8 where a hydrogen atom, beta to one radical centre, is transferred to the other radical) which results in the formation of a saturated and an unsaturated chain end<sup>34</sup>. The radical centres of propagating species must come into close proximity for termination and it is generally accepted<sup>37</sup> that bimolecular termination is a diffusion-controlled process, so that the rate constant for termination is dependent on the nature of the medium and the chain length of the two propagating species and as a result decreases dramatically during the polymerization process<sup>37-39</sup>. When the rate of diffusion of radicals is severely restricted by loss of segmental and translational mobility, the termination process can only occur by the successive movement of the radical ends to one another by propagation steps. This diffusion process for termination is called reaction diffusion<sup>37</sup> and causes the termination rate constant to become almost independent of conversion until high conversions or until vitrification is observed.



At the start of the polymerization sequence, the rate of formation of radicals greatly exceeds the rate at which they are lost by termination and so the total concentration of radical species  $[M^*]$  increases rapidly. As a consequence the loss of radicals by termination also increases, so that an equilibrium is quickly attained where

the rate formation of radicals equals the rate of radical termination. The general expression for the rate of monomer consumption, more commonly known as the rate of polymerization ( $R_p$ )<sup>34</sup> is given by:

$$R_p = -\frac{d[M]}{dt} = k_p [M] \left( \frac{R_i}{2k_t} \right)^{\frac{1}{2}} \quad \text{Equation 2.9}$$

As mentioned briefly in Section 2.1.1 there are a number of complications involved in network free radical polymerization. Complexities arise because the mobility and reactivity of the radicals and functional groups vary significantly during the course of the reaction. Early in the polymerization (particularly for a multifunctional monomer), the gel effect or Trommsdorff effect sets in, causing autoacceleration due to a dramatic reduction in translational and segmental mobility of the radicals<sup>35</sup>. At a later stage in the reaction, termination is limited to reaction diffusion<sup>17</sup> in which the movement of radical ends occurs by a succession of propagation steps - when this occurs, the termination rate constant decreases more slowly.

As polymerization proceeds, the mobility of the monomer may become restricted and the rate of propagation will decrease, particularly as the glassy state is approached<sup>17</sup>. For the free radical polymerization of multi-vinyl monomers, the pendant double bond may exhibit enhanced reactivity compared to the free monomer in the initial stages of the reaction but at higher conversions a reversal of relative reactivities may occur due to trapping of the pendant groups in the network structure<sup>35</sup>.

Chain transfer reactions<sup>37,40</sup> are another source of complication in free radical polymerization. These reactions can terminate the growth of a radical chain and are responsible for the reduction in the degree of polymerization. This process generally involves molecules containing an abstractable hydrogen or halogen atom which can combine with the chain radical to yield a dead polymer molecule and a new radical which can then react with another monomer to re-initiate the growth of a new chain<sup>40</sup>.

Inhibitors and retarders are also important to free radical polymerizations since they react with the free radical active centers to produce species that are incapable or very poor at re-initiating polymerization, examples of these include substituted phenolic

derivatives such as hydroquinone and benzoquinone<sup>41,42</sup> and quaternary ammonium salts such as trimethyl benzylammonium chloride<sup>43</sup>. Inhibitors are very efficient and polymerization can be halted completely. Retarders are not as efficient and yield species which slowly re-initiate polymerization, however both are useful in the polymer industry<sup>41,43</sup>.

### 2.1.4 Rheological behaviour during network formation

Thermosetting polymers exhibit profound rheological changes during polymerization - in particular, the steady shear viscosity increases steadily and then diverges at the gel point, where-upon the equilibrium modulus becomes finite<sup>23,44</sup>. The classic evolution of equilibrium properties during gelation is illustrated in Figure 2.4.

In the early stages of the reaction, the steady shear viscosity grows with reaction time as the average molecular weight increases, but as the system approaches the gel point the steady shear viscosity tends to infinity. On approach to the gel point, the equilibrium modulus is zero as the only stresses introduced into this pre-gel material can relax completely in time. The material will still exhibit time-dependent behaviour due to the presence of entanglements. Beyond the critical gel point the crosslinks resist stress relaxation and the equilibrium modulus rises until the reaction is complete<sup>45</sup>.

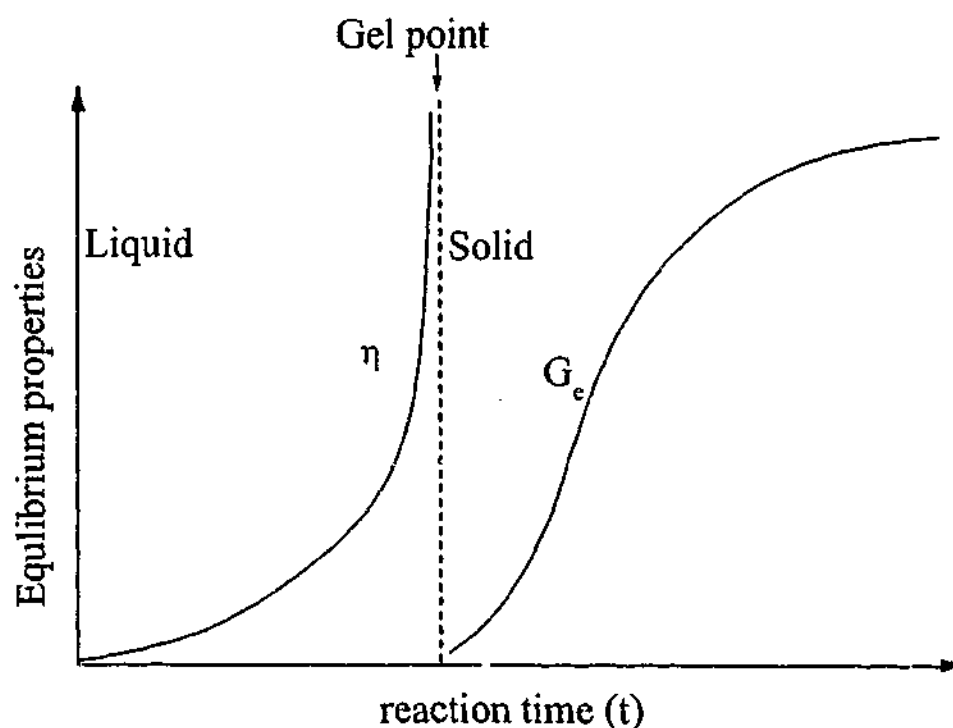


Figure 2.4 Evolution of steady-shear viscosity and equilibrium modulus at the gel point<sup>46</sup>

Scaling concepts developed by de Gennes<sup>24</sup> have recently been applied to the gelation singularity and it has been found<sup>11</sup> that close to gelation, a power-law expression relates the viscosity ( $\eta$ ) and equilibrium modulus to the relative distance from the gel point. In addition, the time dependence of the rheological parameters starts to exhibit universal behaviour. Thus at the gel point, the time-dependent linear viscoelastic behaviour can be described by the 'Gel Equation'<sup>46,47</sup>:

$$\tau(t) = S_n \int_{\infty}^t (t-t')^n \dot{\gamma}(t') dt' \quad \text{Equation 2.10}$$

where  $\tau$  is the stress,  $\dot{\gamma}$  is the deformation rate,  $S_n$  is the strength of the network at the gel point,  $n$  is the relaxation exponent,  $t$  is time and  $t'$  is a dummy variable. The gel equation predicts a power law relationship between the relaxation modulus  $G(t)$  and relaxation time at the gel point and can be expressed as<sup>46-48</sup>:

$$G(t) = S_n t^{-n} \quad \text{Equation 2.11}$$

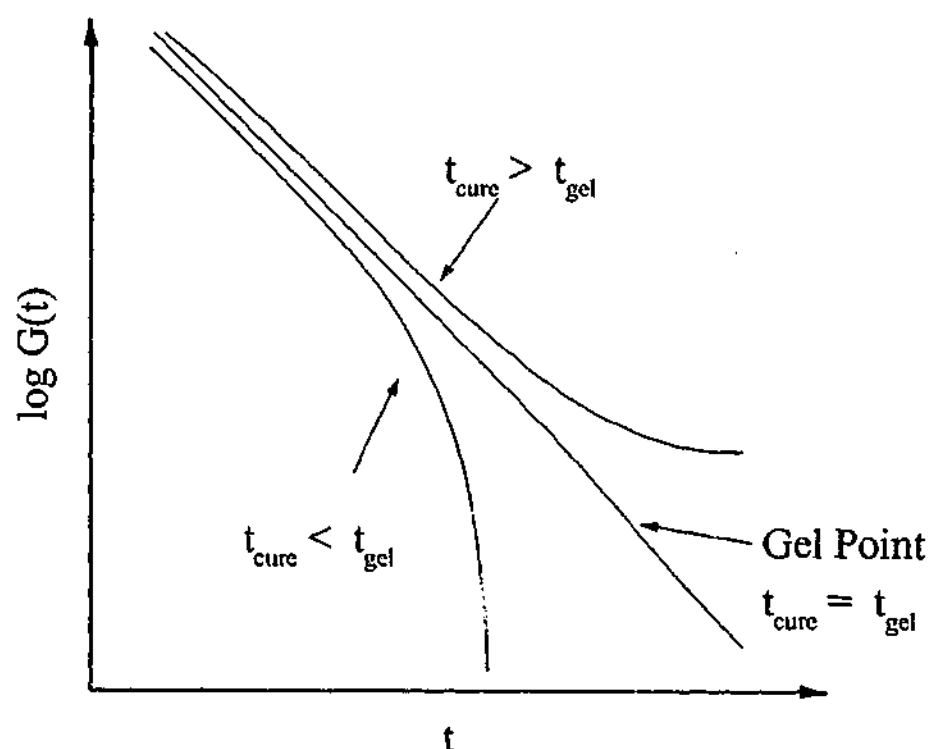


Figure 2.5 Logarithm of the relaxation modulus versus relaxation time near the gel point

Preceding the gel point ( $t_{\text{cure}} < t_{\text{gel}}$ ), the system may be considered a liquid; hence the relaxation modulus can only have a finite value at short relaxation times. At the gel

point ( $t_{\text{cure}}=t_{\text{gel}}$ ) a power law relationship between relaxation modulus ( $G(t)$ ) and relaxation time  $t$  is observed as described by Equation 2.11. After the gel point ( $t_{\text{cure}}>t_{\text{gel}}$ ) the system acts as an elastic solid and the relaxation modulus only approaches a steady value after very long times because the system takes an infinitely long time to relax<sup>46-48</sup>.

Power-law behaviour is also observed in dynamic mechanical experiments at the gel point, where the real ( $G'$ ) and the loss ( $G''$ ) shear moduli scale with a power of the frequency<sup>49-53</sup> as given by Equation 2.12:

$$G' \propto \omega^n; G'' \propto \omega^n \quad \text{Equation 2.12}$$

Also the  $\tan \delta$  becomes frequency independent at the gel point<sup>50,54</sup>:

$$\tan \delta = \frac{G''}{G'} = \tan\left(\frac{n\pi}{2}\right) \quad \text{Equation 2.13}$$

These power law behaviours of the viscoelastic properties are an expression of mechanical self-similarity and are a consequence of structural self-similarity, which evolves as the system approaches the gel point<sup>55</sup>. Thus just prior to the gel point ( $t_{\text{cure}}<t_{\text{gel}}$ ), power law behaviour is approached at higher frequencies, since the structure is highly branched, but at lower frequencies, liquid behaviour is still observed because there is no 3D connectivity. Just after the gel point, power law behaviour is seen at high frequencies because the structure is still lightly branched at high magnification but at lower frequencies rubber-like behaviour is observed because the structure contains network cycles. At the gel point ( $t_{\text{cure}}=t_{\text{gel}}$ ), power law behaviour should be observed over the whole frequency range<sup>50</sup>, shown as a straight line in Figure 2.6 with slope  $n$ . The exponent  $n$  has values ranging from 0.33-1.0 predicted from various gelation theories<sup>54</sup>. After gelation, the polymer may vitrify if the glass transition temperature ( $T_g$ ) approaches the curing temperature ( $T_{\text{cure}}$ )<sup>56</sup> - if this occurs, then the real modulus ( $G'$ ) increases to the value for the glassy state and the loss modulus is often seen to pass through a maximum<sup>14,51</sup> with cure time. Eloundou *et al.*<sup>53</sup> investigated epoxy/amine systems in this region via dynamic rheological experiments and observed a disturbance

of the gelation singularity when the  $T_{\text{cure}}$  was in close proximity to  $T_{\text{g(gel)}}$  because the system was approaching vitrification.

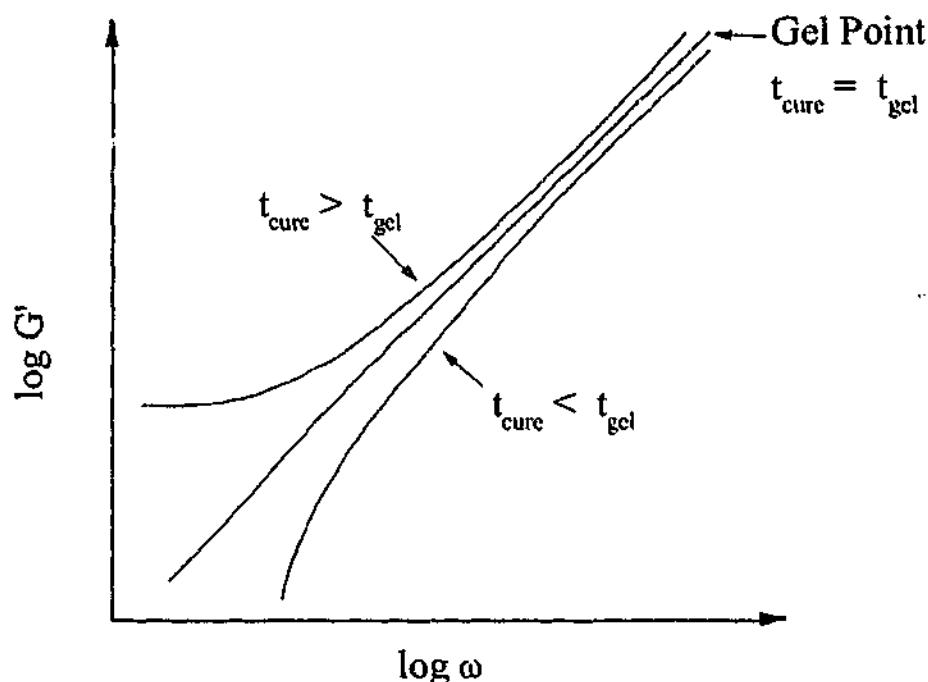


**Figure 2.6** Logarithm of the real modulus versus logarithm of the frequency near the gel point.

After gelation, the modulus in the rubbery region rises due to the increase in the number of elastically active strands. The rubber elasticity equation is<sup>57</sup>:

$$E = 3 \left[ \frac{f-2}{f} \right] v d \rho \quad \text{Equation 2.14}$$

where  $f$  is the functionality of the junctions,  $v$  is the moles of elastically active network strands per mass of polymer (number of  $f$ -functional junctions per unit mass) (mol/kg),  $d$  is the density ( $\text{kg/m}^3$ ),  $R$  is the gas constant and  $T$  is the temperature of measurement (in the rubbery region). For a network with trifunctional network junction points (for example  $N$  in amine/epoxy system), the rubbery modulus,  $E$  (Pa) can be related crosslink density ( $\rho$ ), by the relationship:

$$E = \frac{3}{2} \rho d R T \quad \text{Equation 2.15}$$

## 2.2 Epoxy resins

### 2.2.1 Structures

Some of the earliest epoxy resins marketed were the reaction products of bisphenol-A and epichlorohydrin and this is still the major synthetic route for epoxy resins on the market today<sup>58</sup>. A typical a bisphenol-A based diepoxy resin is shown below in Figure 2.7.

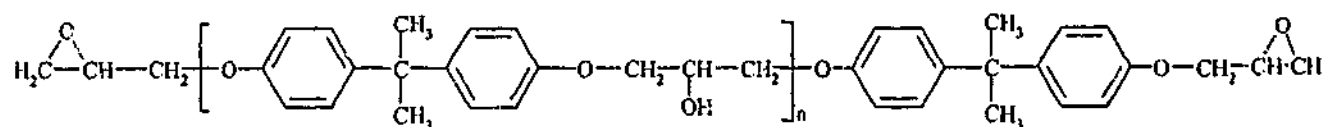


Figure 2.7 Diglycidyl ether of bisphenol-A (DGEBA)

Advances in epoxy technology have led to the production of resins with excellent characteristics for broad-range use, as well as very specific applications. Epoxy resins are used today as protective coatings, electrical applications, reinforced resins, bonding and adhesives, tooling and casting and many more. Epoxy resins are very important in industry for use in specialist applications in which other resins cannot perform to required standards of mechanical properties or chemical resistance. Many applications that utilize epoxy resins involve high added value products - for example epoxy/carbon composites used in the aerospace industry<sup>59</sup>.

The final properties of cured epoxy resins depend on a number of factors, namely the structure of the epoxy prepolymer and the curing agents and their content as well as the conditions employed during the course of the curing process<sup>60</sup>.

### 2.2.2 Curing mechanisms

The cure of epoxies to produce three dimensional networks can occur by either *step growth copolymerization* reaction with a multifunctional curing agent or by a *homopolymerization* reaction initiated by a catalytic curing agent<sup>61</sup>.

### Step Growth Polymerization

The cure of epoxies to form a rigid three-dimensional network by reaction with hardeners requires components which have two or more reactive functional groups, i.e. functionality is  $f > 2$ , depending on the effective functionality of the epoxy group<sup>62</sup>. Anhydride hardeners have a functionality of two but amine curatives often have  $f \geq 4$ . Bisphenol-A diepoxide resins generally have a functionality of two when cured with amines, but are four for anhydride cured systems or when the cure temperature is high enough for reaction of the secondary hydroxy groups formed in the first stage<sup>62</sup>. The cure of epoxy resins initially involves a reaction between epoxy and hardener reactive groups so that relatively small molecules are formed. As the cure continues, larger and larger molecules are formed although the number average molecule weight of these molecules is still small even when many of the reactive groups have reacted. There are many types of hardeners (or crosslinking agents) for epoxy resins including amines (aliphatic and aromatic), anhydrides, polyamides, phenol- and amino-formaldehyde resins<sup>62</sup>.

### Homopolymerization of Epoxies

Epoxy resins may be cured by a chain polymerization mechanism. Both Lewis acids and Lewis bases catalyze the *homopolymerization* of epoxies. Catalytic curing agents include boron trifluoride and tertiary amines that can be used by themselves or combined with hardeners. Examples of tertiary amines and related compounds which can be used as catalytic curing agents include triethylamine, N,N-dimethylbenzylamine and substituted imidazoles<sup>63</sup>.

#### 2.2.2 1° Amine Cure of Epoxies.

Aliphatic and aromatic amines are some of the more common hardeners used to cure epoxy resins via a step growth polymerization. The viscosity increases as the reaction proceeds until an elastic gel is formed. If the cure temperature is less than the final glass transition temperature, the system will vitrify causing a significant limitation in the total cure<sup>19,20</sup>. To counteract the effects of vitrification, the system must be



independent of one another. However, in the reaction of N,N,N'N'-tetraglycidyl-4,4'-diaminodiphenylmethane (TGDDM) with aniline, the reactivity of the epoxy groups depend on the state of reaction of the neighbouring groups, due to H-bonding effects.

The amino groups can also display a substitution effect. From Figure 2.8 the ratios of rate constants can be expressed as  $k_2/k_1$ , where  $k_1$  is the rate constant of the reaction of the primary amine with the epoxy and  $k_2$  is the rate constant of the reaction of the secondary amine with the epoxy. If the reactivities of hydrogens in both the primary and secondary amino groups are equal and independent, the ratio  $k_2/k_1$  is 0.5. Charlesworth<sup>71</sup> found the groups had equal reactivities in the phenyl glycidyl ether/aniline and the N-methyl aniline/DGEBA systems suggesting that substitution effects were insignificant in aromatic amine/epoxy systems. However, more recent studies of epoxy/amine systems by Matejka and Dusek<sup>70</sup> and Matejka<sup>72</sup> found the ratio to be less than 0.5, indicating the reactivities of the amino hydrogens are dependent on the state of substitution.

The overall reaction scheme of an epoxy - amine system is outlined in Equations 2.16 to 2.19<sup>73</sup>:



where E, A<sub>1</sub>, A<sub>2</sub>, and A<sub>3</sub> represent the epoxide, primary amine, secondary amine and tertiary amine molecules respectively. [HX]<sub>0</sub> signifies a hydroxyl catalyst impurity initially present in the system, whilst [HX]<sub>A</sub> is the catalytic hydroxyl group formed during the amine-epoxy reaction. It is assumed in this reaction scheme that the molecules [HX]<sub>0</sub> and [HX]<sub>A</sub> act as true catalysts and are not expended in any side reactions. The rate constants  $k_1$  (Equation 2.16) and  $k_2$  (Equation 2.18) refer to the autocatalyzed reaction of epoxy with primary and secondary amine respectively, whereas the rate constants  $k_{1c}$  (Equation 2.17) and  $k_{2c}$  (Equation 2.19) relate to the

impurity-catalyzed reaction of an epoxy with primary and secondary amines, respectively<sup>16</sup>. If  $e$ ,  $a_1$ ,  $a_2$  and  $x$  are the concentrations of E,  $A_1$ ,  $A_2$  and  $(HX)_A$  at time  $t$ , respectively, and if the concentration  $C_0$  of impurity catalyst  $[HX]_0$ , is assumed to remain constant during the reaction then the rate of reaction of epoxide at time,  $t$  can be given by<sup>16,73</sup>:

$$\frac{d\alpha}{dt} = k_1 e a_1 x + k_2 e a_2 x + k_{1c} e a_1 C_0 + k_{2c} e a_2 C_0 \quad \text{Equation 2.20}$$

### Primary and Secondary Aliphatic Amines

A range of aliphatic amines are used industrially to cure epoxy resins: simple aliphatic amines, linear and branched aliphatic polyamines, alicyclic polyamines and aliphatic amines containing aromatic groups. Common aliphatic amine curing agents include polymethylene diamines (e.g. DAO - see Figure 2.9), diethylenetriamine, triethylenetetramine and tetraethylene pentamine. Aliphatic amines typically have low viscosities and are freely miscible with DGEBA resins. In most commercial systems cured at ambient temperatures, gelation occurs in approximately one hour and the cure is completed after 24 hours<sup>74</sup>.

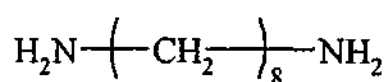


Figure 2.9 The structure of DAO

### Aromatic Amines

A number of aromatic amines are also used as curing agents for epoxy resins. Examples include diaminodiphenyl sulphone, 4,4'-diaminodiphenyl methane (DDM - see Figure 2.10), 1,3-phenylene diamine and dianilinoether.

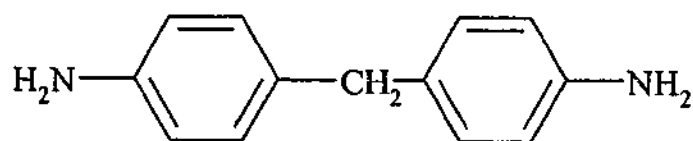


Figure 2.10 The structure of DDM

The incorporation of the rigid benzene ring of the aromatic amine into the epoxy network results in a significantly higher heat distortion temperature than could be obtained using aliphatic amines as the curing agent<sup>75</sup>. Aromatic amines are generally crystalline solids of high melting point and of lower basicity than aliphatic amines. This factor when combined with lower solubility in epoxy resins often means that high cure temperatures are required, frequently followed by a postcure at an elevated temperature<sup>76</sup>.

### 2.2.3 Anhydride cure of Epoxies

The catalyzed reaction of anhydrides with epoxies is another mechanism by which epoxies may be cured. Generally the epoxy/anhydride reaction proceeds quite slowly and a small amount of accelerator, such as a tertiary amine, imidazole, alcohols, acids or onium salt is added to accelerate the reaction<sup>77</sup>. The general anionic curing mechanism is shown in Figure 2.11<sup>25,78-80</sup>.

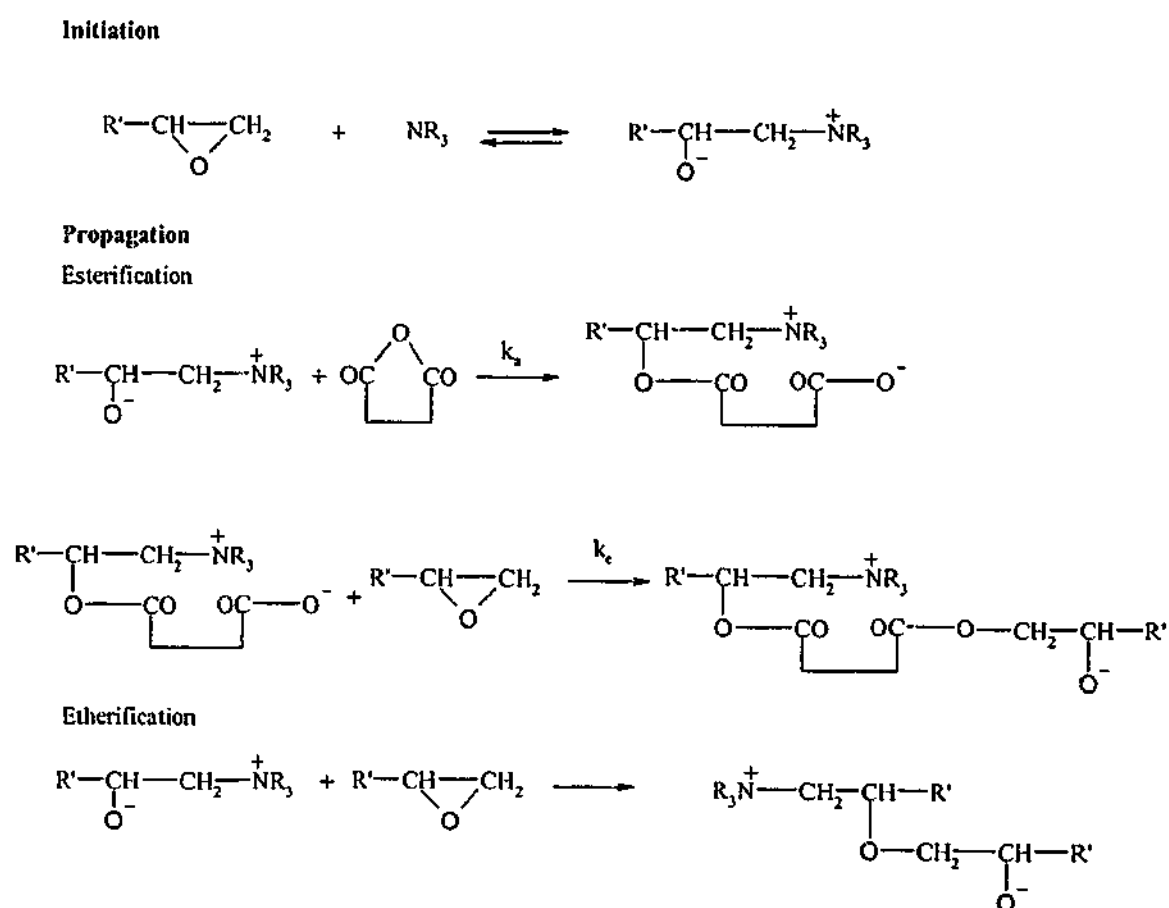


Figure 2.11 Reaction mechanisms for polymerization process of epoxies using anhydrides<sup>25,80</sup>

The kinetics of anhydride cured epoxies are less well understood compared to

amine cured epoxies. The tertiary amine accelerator is reversibly bound to the epoxide and the tertiary nitrogen atom is transformed into a quaternary one. Propagation proceeds predominantly via the alkoxide anion reaction with anhydride and the carboxylate anion with epoxide (where  $k_a > k_e$ , see Figure 2.11)<sup>25</sup>. Etherification between the epoxy and an alkoxide anion can also occur when an excess of epoxy is used<sup>80</sup>. The reaction may be complicated by the possible regeneration of the tertiary amine from the propagating chain and subsequent re-initiation, thus a definitive set of kinetic expressions has not been established<sup>25</sup>.

### 2.2.4 Imidazole cure of Epoxies

A number of imidazoles are very effective curing agents for epoxies. Resins cured with imidazoles exhibit excellent resistance to chemicals and to oxidants, have high thermal resistance, dimensional stability and good dielectric properties<sup>81</sup>. The curing of epoxies by imidazoles is a complex process. Farkas and Strohm<sup>81</sup> postulated that the reaction involved the attack of the terminal carbon of the epoxy functional group by the pyrrole-type nitrogen of the imidazole to produce the 1:1 imidazole:epoxy adduct, and this adduct reacted further with a second epoxy group to form the 1:2 imidazole:epoxy adduct. These adducts were assumed to be the catalysts that initiated the polymerization process and, therefore, the imidazole became permanently incorporated into the epoxy network<sup>81,82</sup>. In other studies Barton and Shepard<sup>83</sup> postulated that the reaction involved the attack of epoxy functional group by the basic pyridine-type nitrogen resulting in the formation of both 1:1 and 2:1 adducts. The mechanism of Barton and Shepard<sup>83</sup> has been generally accepted for 1,3 di-substituted imidazoles, but not for 1-substituted imidazoles (which have substitution on one nitrogen atom). For the anionic polymerization of epoxide groups with 1-substituted imidazoles, such as 1-methylimidazole (1-MeI), Dearlove<sup>84</sup> has proposed a mechanism in which the initiating species was the 1:1 adduct (produced via the attack of the pyridine-type nitrogen) as illustrated in Figure 2.12.

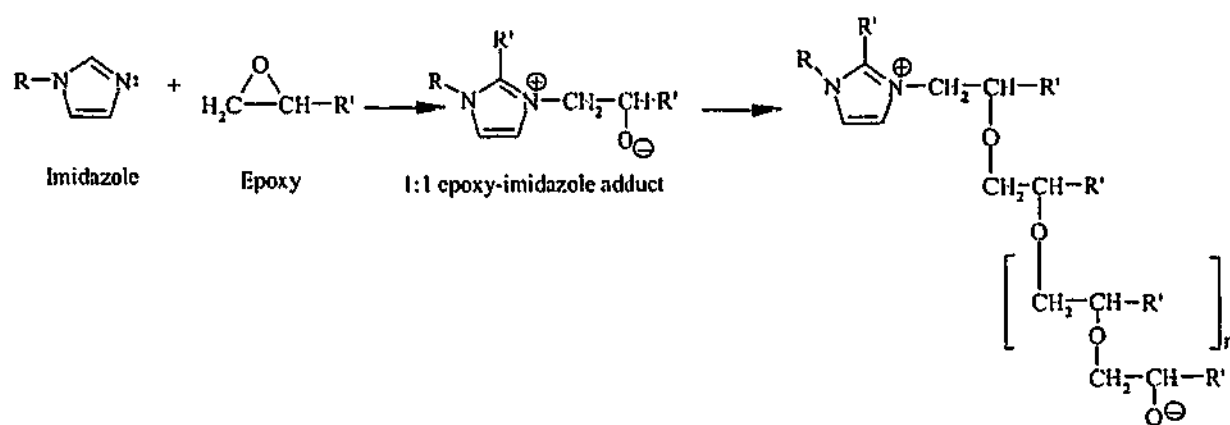


Figure 2.12 Reaction mechanisms for polymerization process of epoxies using imidazoles<sup>84</sup>.

### 2.2.5 Properties and Uses of Epoxy Resins

One of the major uses of epoxy resins is as a surface coating material due to their toughness, flexibility, adhesion and chemical resistance. The excellent chemical resistance of epoxy resins enables them to be used in many corrosive environments such as storage tanks and piping for acids, alkalis, chlorinated brine, salts and oils<sup>85</sup>. Epoxy resins are also used in molding and laminating to make glass fibre-reinforced articles as they offer far superior mechanical strength, chemical resistance and electrical insulation properties compared with unsaturated polyesters. One of the few disadvantages of epoxies is cost and it is for this reason they have not replaced polyester resins in all applications.

## 2.3 Vinyl esters

### 2.3.1 Structure and properties

Vinyl esters are a blend of a vinyl monomer (usually styrene) with unsaturated esters of epoxy resins and they exhibit many of the properties of epoxies but also have the advantage of the processability of polyesters<sup>86</sup>. The most common vinyl ester resins are a reaction product of methacrylic acid and oligomers of the diglycidyl ether of bisphenol-A, which is dissolved in styrene monomer<sup>17,86,87</sup>. The structure of the bisphenol-A epoxy based vinyl ester monomer is illustrated below in Figure 2.13.

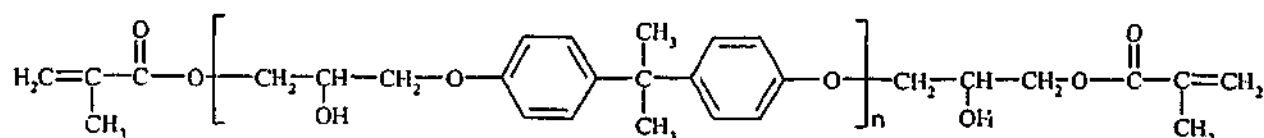


Figure 2.13 The structure of bisphenol-A epoxy methacrylate<sup>17,86,87</sup>

Apart from the bisphenol-A epoxy based vinyl esters, there are a number of others which are commercially available. Novolac epoxyacrylate resins (Figure 2.14) have been utilized for improving the thermal resistance and high temperature corrosion resistance of vinyl ester resins. Inclusion of the novolac structure within the vinyl ester increases the aromatic component and delivers more crosslink sites in pendant positions along the backbone of a molecule.

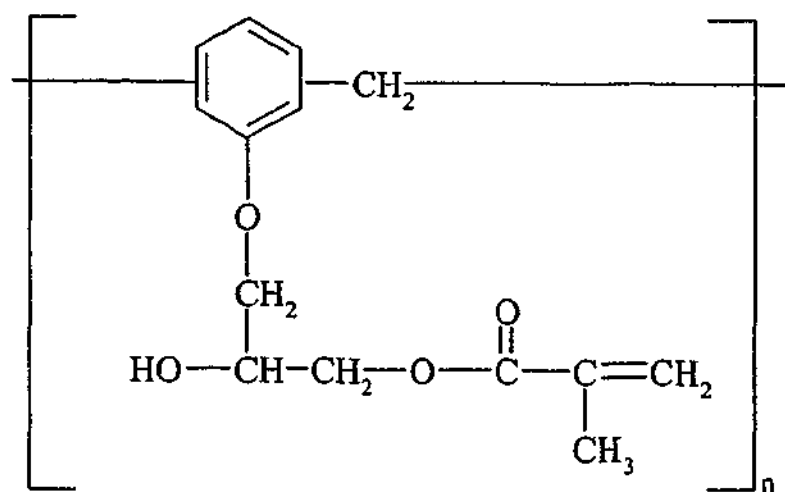
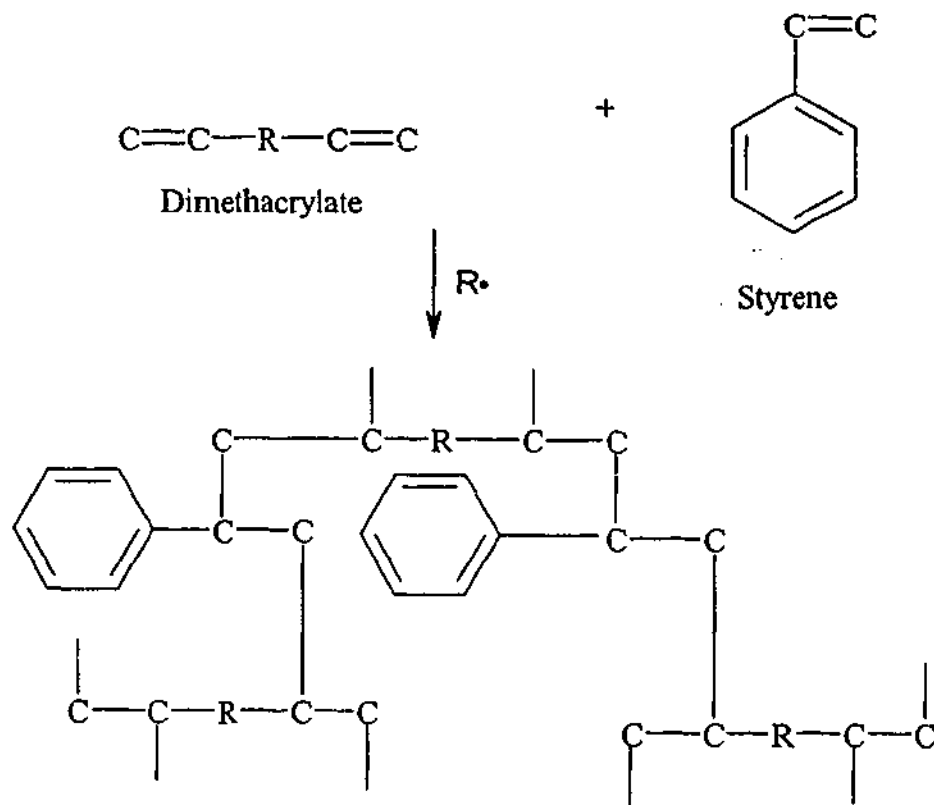


Figure 2.14 The Novolac epoxy acrylate structure<sup>86</sup>

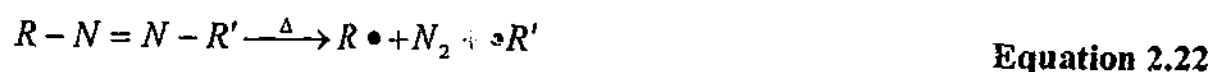
### 2.3.2 Curing mechanisms

Vinyl esters are processed using free radical initiated polymerization<sup>17,41</sup>. A schematic of the general curing reaction of vinyl esters is illustrated in Figure 2.15. Organic



**Figure 2.15 Schematic of the radical initiated polymerization of vinyl ester**

peroxides ( $\text{R}-\text{O}-\text{O}-\text{R}'$ ) and aliphatic azo compounds ( $\text{R}-\text{N}=\text{N}-\text{R}'$ ) are two of the more common families of free radical initiators which decompose thermally to produce free radicals<sup>88,89</sup>. The organic peroxides usually decompose by initial cleavage of the oxygen-oxygen bond to produce two oxygen-centered free radicals (Equation 2.21) and the azo compounds decompose by diazo cleavage to produce nitrogen and two alkyl radicals (Equation 2.22)<sup>88,89</sup>.



A large number of peroxide and azo initiator systems are commercially available. For room temperature cure, redox initiator systems are used such as methyl ethyl ketone peroxide (MEKP) with cobalt naphthenate or alternatively benzoyl peroxide (BPO) and dimethyl aniline<sup>41,86,88-92</sup>. At elevated temperatures t-butyl perbenzoate,

t-butyl peroctoate and peroxy dicarbonate peroxides are often used as initiators for vinyl esters<sup>41,86,88,89</sup>.

Photo-induced polymerization using photoinitiators is another pathway by which thermosets and more specifically vinyl esters and dimethacrylates can be polymerized. The technique of photopolymerization in neat thermosets has been well documented<sup>21,35,93-99</sup> and is a very rapid and precise method for producing crosslinked polymers and has many applications, from dental composite resins<sup>21,97-100</sup> through to microlithography applied to integrated chip design<sup>101</sup>. There are many photo-initiator systems used in curing or crosslinking processes<sup>93,102</sup> and these can be divided into two groups – photo fragmentation (in which the excited initiator decomposes into two radicals) or photo redox (where the excited initiator is reduced by another species to produce two radicals). An example of the latter is the camphorquinone (CQ)-amine pair<sup>97,99</sup>. The photo-redox mechanism of CQ/amine involves the intersystem crossing of the CQ excited singlet state to a triplet followed by the formation of an excited complex (exciplex) by an electron transfer from the tertiary amine to the photo-excited carbonyl compound<sup>97,99</sup>. Ketyl radicals are also formed but are generally slower to initiate polymerization<sup>103</sup>. The mechanism is outlined in Figure 2.16.

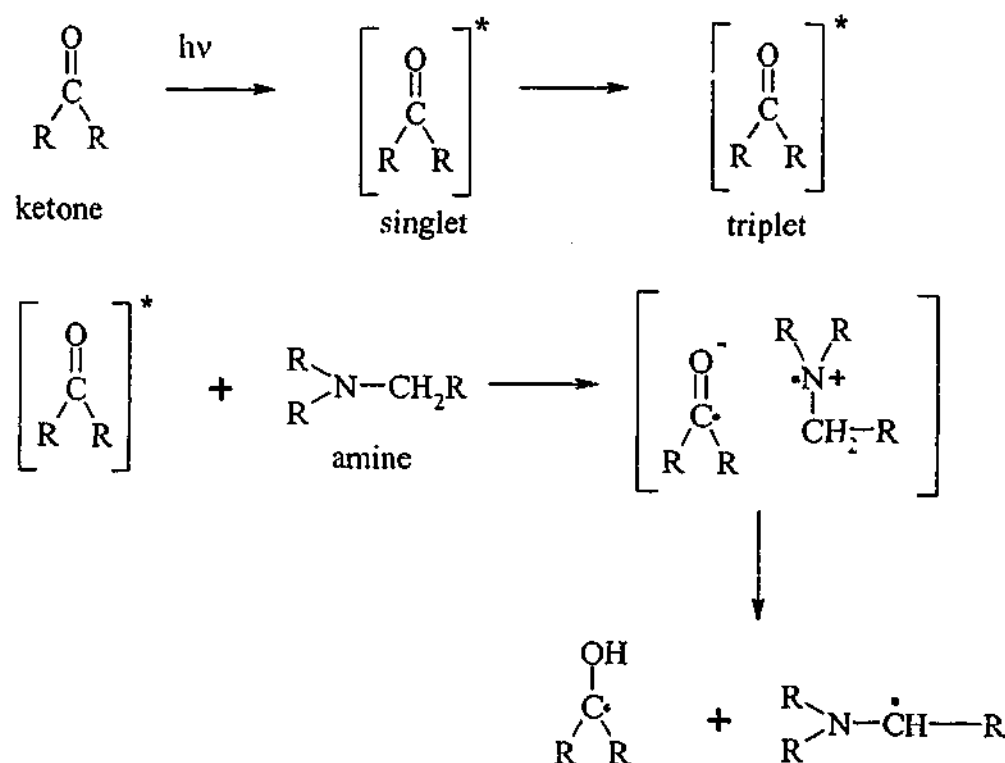


Figure 2.16 The photoinitiation mechanism for the ketone/amine system<sup>97,99</sup>

A special type of this class of photofragmentation initiators is iniferters (*initiator-transfer-terminator*) that form radicals only during irradiation. Due to the

reversible nature of the photofragmentation the concentration of the propagating species is very low, thus reducing the incidence of radical-radical termination and resulting in a living radical polymerization mechanism<sup>104-109</sup>. An example of this is p-xylylene bis(N,N-diethyl dithiocarbamate) (XDT) which on irradiation produces a chain initiating carbon-centered radical and a sulphur-centered dithiocarbamate radical which can reversibly terminate the propagating chains, as shown in Figure 2.17.

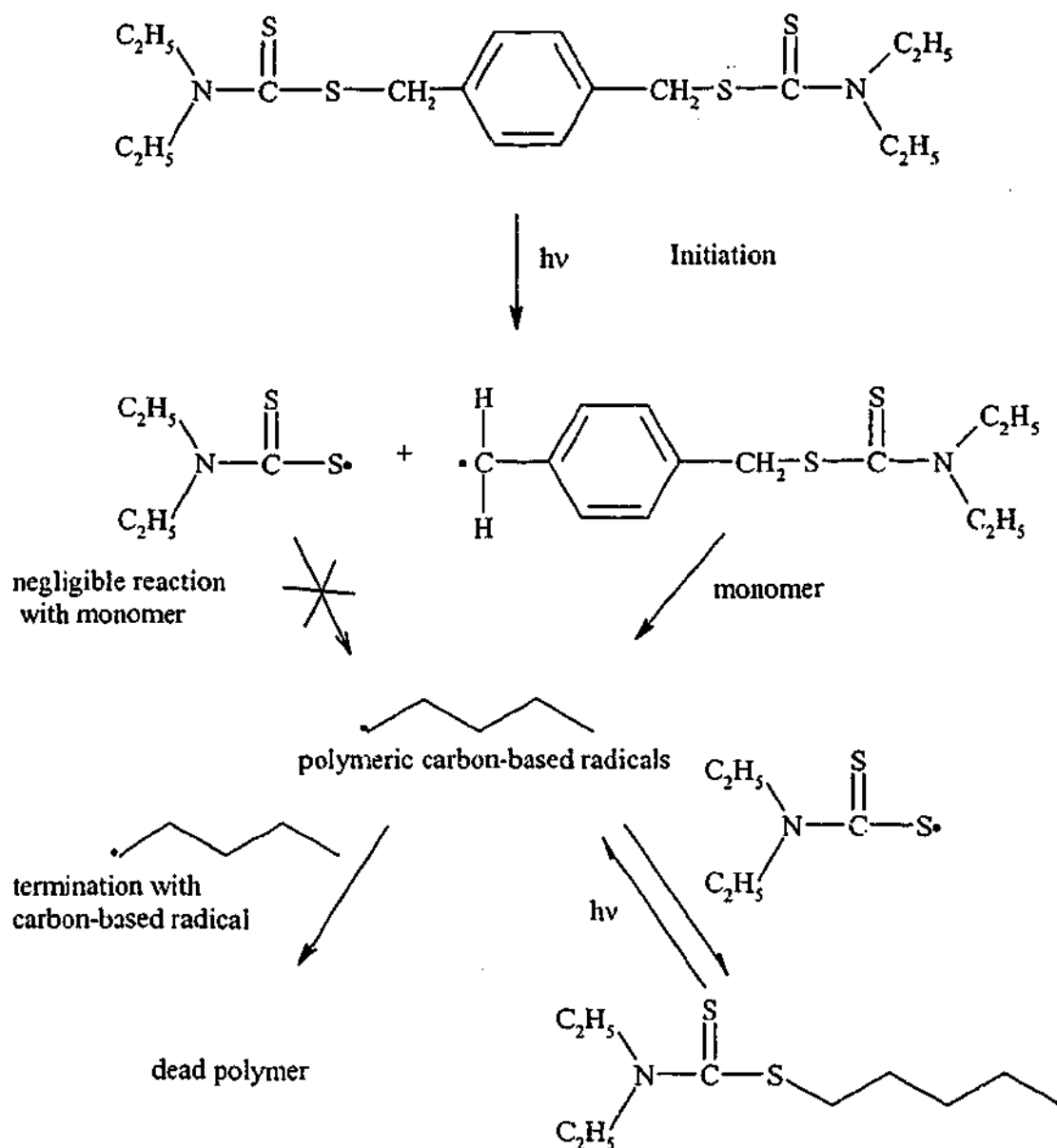


Figure 2.17 The living radical polymerization mechanism for XDT<sup>102</sup>

Extensive research has been undertaken on the curing kinetics of VERs using differential scanning calorimetry (DSC) and Fourier transform infrared spectroscopy (FTIR)<sup>17,110-117</sup>. Cook *et al.*<sup>17</sup> studied the effect of temperature, peroxide initiator and co-catalyst (cobalt octoate) concentration on the DSC cure kinetics of VERs and compared these with gel times. The rate of polymerization of the VER rose with increasing peroxide concentration, but the rate passed through a maximum with cobalt octoate concentration. In contrast, the gel times decreased steadily with increase in peroxide and

cobalt octoate concentration and this behaviour was explained by a kinetic scheme in which the cobalt not only catalyzes the formation of radicals, but also destroys the primary and polymeric radicals<sup>17</sup>. The DSC cure kinetics of vinyl ester resins have been modeled using a modified phenomenological kinetic model for autocatalytic cure<sup>118</sup>:

$$\frac{d\alpha}{dt} = (k_1 + k_2\alpha^m)(\alpha_{\max} - \alpha)^n \quad \text{Equation 2.23}$$

where  $k_1$  and  $k_2$  are the kinetic rate constants,  $\alpha$  is the degree of cure and  $\alpha_{\max}$  is the maximum conversion dependent on the cure temperature. Dua *et al.*<sup>115</sup> successfully modified the autocatalytic kinetic model<sup>118</sup> to fit experimental FTIR data for the cure of a vinyl ester resin. Dua and co-workers<sup>115</sup> studied the effects of styrene concentration, temperature, catalyst and initiator concentration on the cure kinetics. The reactivity ratios of the styrene and methacrylate were calculated to be close to zero suggesting initial copolymerization. Other authors<sup>113</sup> have successfully used other models based on free radical copolymerization theories to fit the curing kinetics in vinyl ester resin systems.

Work by Ganem *et al.*<sup>116</sup> suggested three distinct kinetic stages during the radical initiated copolymerization of DGEBA-based vinyl ester resins and styrene. During the first stage it is presumed that the copolymerization kinetics were dominated by the intrinsic reactivity of styrene and methacrylate double bonds. The noticeable decrease in the reactivity of methacrylate units towards themselves marked the end of stage one and the onset of gelation (observed visually and confirmed by solubility experiments). In the second stage styrene monomer molecules were considered to diffuse relatively unrestricted within the network, whereas the methacrylate units, because of their larger size and network connectivity, were increasingly more immobilized and reacted less with themselves. At the end of the second stage, approximately 45% of the initial methacrylate double bonds remained unreacted, amongst which 20% were estimated to be bonded to the network. In the third stage<sup>116</sup>, the methacrylate copolymerization was considered to have ceased, but the styrene continued to react via homopolymerization until halted by vitrification. Despite these different modes of polymerization, the polymers did not exhibit significant phase separation as dynamical mechanical studies by Varma *et al.*<sup>119</sup> did not show separate glass transition temperatures. Brill and Palmese<sup>117</sup> found similar results - the styrene

conversion was lower than the methacrylate conversion in the initial stages of polymerization in a VEF system, however the styrene continued to homopolymerize after the conversion of methacrylate groups had ceased.

### 2.3.3 Properties and Uses of Vinyl ester Resins

Vinyl esters are easily processable but exhibit resistance to degradation by corrosive and hostile environments, which may be mainly attributed to the crosslinked structure, the sterically hindered ester groups, and the bulky, chemically resistant bisphenol-A group within the structure. This resistance enables their use in many applications, ranging from corrosion barriers in tanks, pipe and ducting and linings in metal tanks to skin coats used in swimming pools, boats, and spas and sandwich composites<sup>41,120</sup>.

Vinyl ester resins can be categorized into two groups depending on which epoxy they are based. Vinyl esters based on bisphenol-A type epoxy (see Figure 2.13) are most commonly used because of their excellent all round properties. They are resistant to a wide range of chemicals across the pH range, have a relatively high level of toughness and can be used at relatively high temperatures for load bearing components<sup>86</sup>. The second group of vinyl esters are those based on the novolac epoxy structure (see Figure 2.14) - these vinyl esters are characterized by a higher crosslink density, which leads to increased stability at higher temperatures as well as better organic solvent resistance<sup>86,121-123</sup>.

## 2.4 Polymer Blends

In the early stages of the polymer industry, property modification was usually achieved through copolymerization. More recently multi-component polymer systems have been used to manufacture products with exceptional chemical and physical properties. Some of the most common are mechanically blended thermoplastic polymers which often exhibit two phase structure due to the lack of enthalpic interaction between the component polymers<sup>124</sup>. Other common multi-component polymers include graft and block copolymers. Conventionally, for crosslinked polymers, properties were optimized by use of appropriate comonomers. An alternative to copolymerization is IPN

formation that represents a mechanism by which different polymers types can be physically combined.

### 2.4.1 Interpenetrating Polymer Networks

As first proposed by Sperling<sup>6,125</sup> IPNs are ideally a composition of two (or more) chemically distinct polymer networks held together exclusively by their permanent mutual entanglements (Figure 2.18a). This definition has been generalized to include semi-IPNs where only one of the components forms a network (Figure 2.18b). IPNs can be formed by one of two methods. A sequential IPN is one where the first network is formed and then swollen with a second crosslinking system that is subsequently polymerized. Such systems have great potential for the development of unusual gradient morphologies. The second type is the simultaneous IPN in which the two network components are polymerized together (see Figure 2.19) and it is this type that is investigated in the present study.

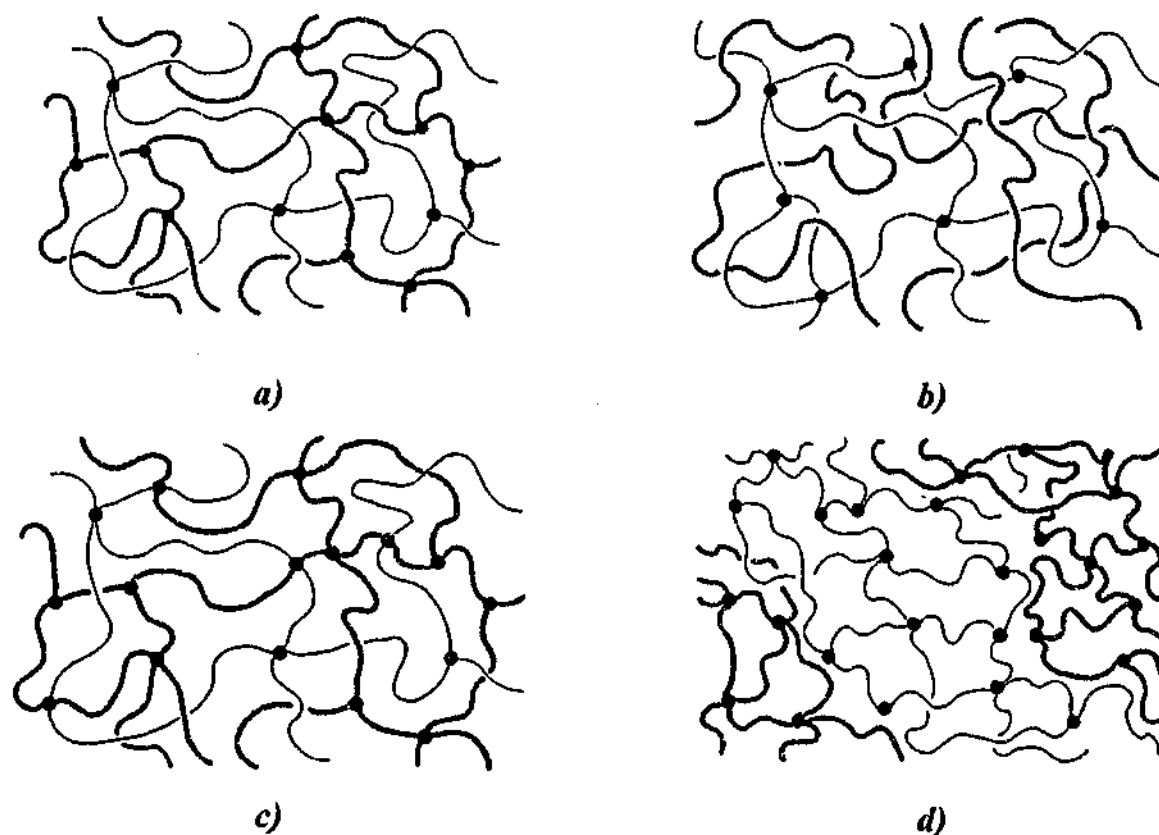


Figure 2.18. a) Idealized structure of an IPN; b) semi-IPN; c) grafted IPN; d) phase separated IPN

In an IPN formed simultaneously, both monomers (or linear prepolymers) A and B with their respective curing agents and initiators are combined together in bulk (melt), solution or dispersion (Figure 2.19)<sup>6</sup>, prior to polymerization.

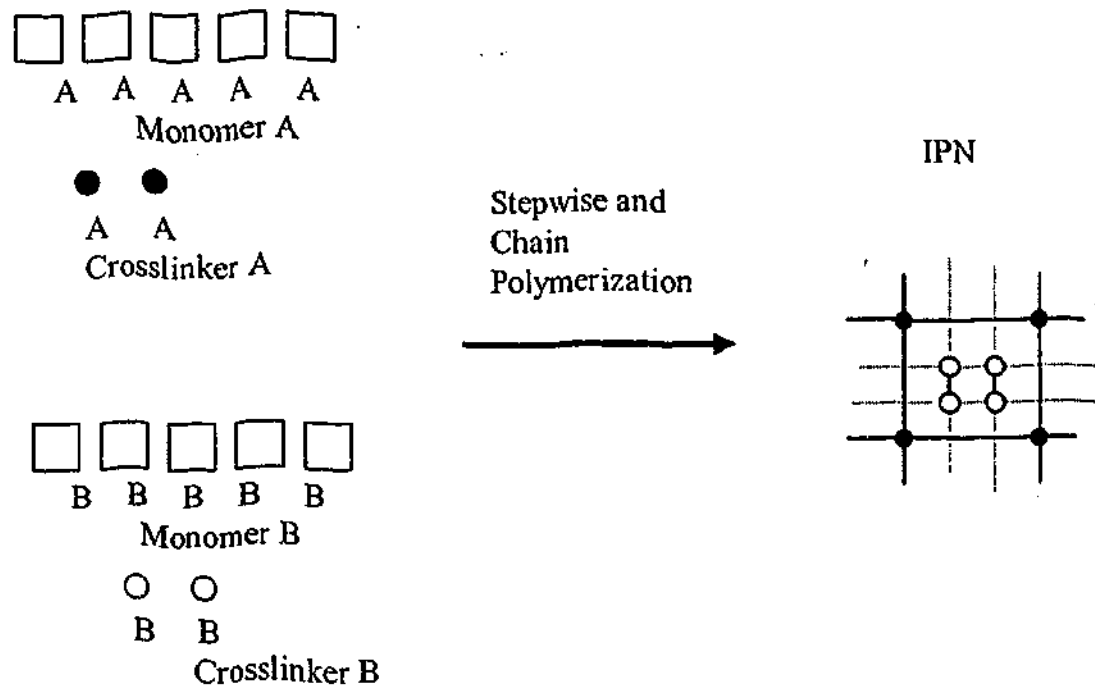


Figure 2.19. Simultaneous IPN formation (adapted from Sperling *et al.*<sup>6</sup>)

## 2.4.2 Kinetics of Formation of IPNs

### *Complications in IPN cure*

The crosslinking components within the IPNs are generally formed by different polymerization modes (such as polymerization by a combination of chain-growth and step-growth mechanisms). However, the cure kinetics of each component can affect each other and consequentially effect the overall cure rate, final cure and hence properties of the resulting IPNs. There are a number of factors that can lead to these complications in the curing of IPNs. First, interactions between the components of one network and the initiators of the other may accelerate or retard reaction. As an example, in a study of the cure of epoxy/polyester resins IPNs, Lin and Chang<sup>5</sup> observed a complexation between the cobalt salt catalyst of the polyester and the diamine curative

for the epoxy. Second, the rate of reaction of one component might be expected to be reduced due to the dilutional effects by the other components<sup>126</sup>. In addition, it is known that during free radical polymerization (see Section 2.3.2), the reaction may become diffusion controlled (such as with the termination process<sup>37-39,127</sup>) and so the change in viscosity of the IPN due to the reaction of one component may also affect the curing behaviour of the second component as suggested by Jin *et al.*<sup>128</sup>. If a thermosetting system is cured at a temperature below its maximally attainable  $T_g$ , vitrification may occur during cure (see Section 2.1.1), thus slowing the final stages of reaction and limiting the final degree of cure. But in an IPN, if the first component reacts more slowly than the second component, the former may act as a plasticizer to the cure of the latter, allowing faster reaction of the second component and full cure without vitrification. Evidence for this has been reported by Lin and Chang<sup>5</sup>. In contrast, a fast polymerization of the second component may retard the reaction of the first component due to the presence of additional crosslinks in the system causing earlier vitrification and preventing further reaction of the first component. Also it is known that in some densely crosslinked polymers, the surrounding network architecture may trap reactive groups<sup>129</sup>. Hence it might be expected that in IPNs, the developing skeletal structure of one network might exert a topological restraint on the development of the other network reducing the rate and final extent of reaction of the other component. In addition, although the selection of different polymerization modes of each of the crosslinking systems such as chain-growth and step growth mechanisms is intended to prevent copolymerization, grafting reactions (depicted in Figure 2.18c), may occur between the two polymer networks<sup>2</sup>. In a study of polyester/amine-cured epoxy IPNs by Subramaniam and McGarry<sup>3</sup> a significant amount of intersystem grafting occurred and FTIR investigations indicated that this was partially due to the Michaels addition reaction<sup>130-132</sup> between the amine curative for the epoxy and the double bonds of the polyester.

Recently, Lin and coworkers<sup>5,133</sup> have suggested an additional complication in which mutual entanglements formed during the polymerization of IPNs led to a process they termed "network interlock" which provided a sterically hindered environment, reducing reactivity of the component systems. This process might be equivalent to topological restraint, however Lin *et al.*<sup>5,133</sup> appear to suggest that the network interlock effect can occur quite early in the cure and is not restricted to the last stages of polymerization as is found with the structurally-determined topological restraint<sup>129</sup>. Lin

and Chang<sup>5</sup> and Lin *et al.*<sup>134,135</sup> studied the kinetics of cure of IPNs of epoxy (DGEBA) and unsaturated polyesters (UPE) using FTIR and DSC. Lin and Chang *et al.*<sup>5</sup> postulated that during the cure, the 'network interlock' increased the activation energy and reduced the cure rates for both DGEBA and UPE. In fact, experimental results showed a lower cure rate for the UPE in the IPN compared with the neat UPE network formation. However the cure rate of the epoxide groups within the IPN was higher than the neat epoxy system. The higher rate constants for the cure of the epoxide within the IPN was explained by the catalytic effect of hydroxy end groups in the UPE on the epoxide group conversion overcoming the network interlock effect on the cure kinetics. Further experimental results by Lin and Jeng *et al.*<sup>133,136</sup> on simultaneous IPNs based on poly(ethylene glycol) diacrylate and DGEBA showed that the rate constants were lower and activation energies higher for the IPN compared with those of the epoxy and diacrylate components. Thus it would appear that their "network interlock effect" has a kinetic and not a thermodynamic basis.

For IPNs formed from amine-cured epoxy and peroxide-initiated unsaturated polyester, Lin *et al.*<sup>135</sup> found that IPNs exhibited lower  $T_g$ s compared with the neat resins, and they inferred that the sterically hindered environment restrained chain mobility in the curing reactions resulting in lower epoxy and unsaturated polyester conversion resulting in lower  $T_g$ s in the IPNs. In another study by Lin and Lee<sup>137</sup>, the cure of epoxy and methacrylate components of an IPN appeared to be affected by this 'network interlock effect' and as a consequence the scanning DSC exotherm was shifted to higher temperatures compared to the parent resins. Another explanation for the higher exotherm temperatures and lower  $T_g$ s for these IPNs could be the redox reaction between the amine curative for the epoxy and the peroxide initiator for the unsaturated polyester which could cause acceleration of the peroxide decomposition and lead to premature depletion of the initiator system and thus undercuring of the acrylate or polyester may result.

Fan *et al.*<sup>138,139</sup> also used the technique of FTIR in their study of the cure kinetics of VER and polyurethane IPNs. The polyurethane and the vinyl ester components were found to affect the cure of each other in the IPN, leading to lower reaction rates. Because the free radical polymerization of the VER exhibited an induction period, the early stage of the PU network formation (which occurred prior to the VER cure) was considered to be polymerization in a polymer solution. Hence Fan *et al.*<sup>138</sup> argued the

main reason for the depressed rate of PU formation was the decrease in the concentrations of hydroxyl and isocyanate groups and the urethane polymerization catalyst by dilution with the VER. The subsequent cure of the VER was believed to be depressed due to the topological restraint imposed on it by the prior formation of the PU network.

### *Effect of Cure Order on IPN polymerization and morphology*

The polymerization rates of the components within an IPN can be modified so that the reactions occur at similar or different rates depending on the selection of different initiators and/or catalysts. However, the curing rate of one component may affect the subsequent curing rate of the other. Thus, changing the sequence of cure of the components in an IPN can have a significant effect on the cure kinetics and may have a large influence on the resulting phase morphology of the IPN<sup>140-144</sup>.

Hsu and Lee<sup>140</sup> investigated the effect of changing the polymerization sequence in a polyurethane/unsaturated polyester IPN by using either a high temperature peroxide or a low temperature peroxide/amine initiating system for the polyester component. When the high temperature initiator was used, the polyurethane cured first and the conversion of polyurethane in the IPN was higher than in the neat polyurethane due to a plasticization effect by the unreacted polyester monomers, but the polyester only reached 70% conversion, which the authors suggest may be due to a topological restraint. When the low temperature peroxide/amine initiator was used, the polyester polymerized much more rapidly, at a rate similar to the polyurethane. Analysis of the effect of curing order on the cure kinetics was complicated in this system as the amine in the peroxide/amine system had a catalytic effect on the polyurethane cure.

Chou and Lee<sup>141</sup> also investigated the effect of changing the polymerization sequence in polyurethane/unsaturated polyester IPNs by using two peroxides of different activities for the initiation of the polyester. Analysis of the curing kinetics were complicated in this system due to the presence of carboxyl end groups in the unsaturated polyester component which accelerated the polyurethane reaction whilst retarding the polyester cure by grafting reactions. Chou and Lee<sup>141</sup> observed different phase separated morphologies in the IPN depending on the cure temperature and initiator used. All IPNs were phase separated to a degree, but changing the sequence of cure of the components

did affect the extent of phase separation that occurred.

Zhou *et al.*<sup>142,143</sup> studied the effect of using peroxide systems of differing activities for the cure of the methacrylate component in a crosslinked urethane/crosslinked methacrylate IPN. When the lower temperature peroxide initiator was used, the cure rates of crosslinking reaction of the two components were very similar and the IPN exhibited a single-phase morphology. However if the higher temperature peroxide initiator was used, the cure rate of the methacrylate was significantly slower than the urethane and two  $T_g$ s were observed due to phase separation.

Widmaier and Drillier<sup>144</sup> studied the effect of changing the cure order in an acrylate/urethane IPN using combinations of three initiating systems of differing activities for the acrylate component and two different catalysts for the urethane component. Three different types of IPNs were formed - one where the urethane cured first, another where both networks formed simultaneously, and one where the urethane cured last. In the IPN where the urethane cured first, two  $T_g$ s were observed between the  $T_g$ s of the neat polymers, representing a urethane rich phase and an acrylate rich phase. On the other extreme where the acrylate cured first, the  $T_g$ s indicated a pure acrylate phase and a phase-mixed urethane phase. In the IPN where both urethane and acrylate cured at similar rates, a single  $T_g$  was observed.

When using thermal initiators in studies of the cure order of IPN components, it may be difficult to ensure that only one component cures without partial cure of the other component in the IPN. Photopolymerization offers a very precise method of curing specific components within an IPN, such that ideally only one component will cure when irradiated and the other will remain unreacted. Frounchi *et al.*<sup>145</sup> formed a full-IPN from a urethane diacrylate and diethyleneglycol bis(allylcarbonate) in which the diacrylate was initially photocured followed by thermal polymerization of the diallyl monomer with benzoyl peroxide. No evidence of phase separation was observed in this IPN and the polymer had a single glass transition temperature midway between the parent resins. In more elegant studies Udagawa *et al.*<sup>146</sup> and Decker *et al.*<sup>147</sup> simultaneously photocured an IPN of epoxy and acrylate by employing an onium salt photoinitiator to cure the epoxy and a radical photoinitiator for the acrylate. In both IPN systems, the acrylate component polymerized faster and to a greater extent than the

epoxy component. Chou and Lee<sup>148</sup> studied the morphology and dynamic mechanical behaviour of IPNs formed from a thermally cured polyurethane and a photocured unsaturated polyester and found that the structure and properties were dependent on the cure order, however no kinetic studies were undertaken. Yang *et al.*<sup>149</sup> studied IPNs formed from photocured diacrylates and thermally cured urethanes and observed that if the acrylate was cured first, extensive phase separation occurred however reversal of the cure sequence gave a more homogeneous structure.

### 2.4.3 Methods for determining phase separation in IPNs

There are numerous methods for determining if phase separation has occurred in cured-IPNs. DMTA and DSC are common and useful techniques to study the glass transition temperatures and thus phase morphology of IPNs<sup>135,150-153</sup>, provided that the individual components of the IPN have clearly defined and well separated  $T_g$ s. Depending on the scale of phase separation and the phase contrast, the techniques of scanning electron microscopy (SEM)<sup>135</sup> and transmission electron microscopy (TEM)<sup>149</sup> can be useful tools to analyze phase morphology in IPNs. Small Angle Light Scattering (SALS) (typical length scale probed 250-25000 nm) and X-ray (SAXS) (typical length scale probed 0.1-2500 nm)<sup>154</sup> have also been used to study the development of the morphology during IPN formation<sup>155-159</sup> (see Section 2.4.4). Both SAXS and SALS are useful techniques provided that the electron density and refractive index of each phase is sufficiently different<sup>154</sup>. Small angle neutron scattering (SANS) has also been used to investigate phase separation in IPNs but often requires deuteration of one of the components to ensure sufficient neutron density differences between phases<sup>160-162</sup>.

#### *Small Angle Neutron Scattering*

For multiphase polymers SANS can give information about heterogeneities down to a few angstroms, give information about the type of interface being formed between the phase separated regions and give total interfacial area<sup>6,163</sup>. Unlike X-rays which are scattered by electrons with the intensity of scattering increasing with atomic number, neutrons are scattered by the nuclei of atoms and the strength of this scattering is related to their scattering length which is not proportional to atomic number<sup>163</sup>. As a consequence lighter atoms like hydrogen have an advantage in neutron scattering

compared to X-ray scattering. Furthermore, the difference in scattering length of hydrogen and deuterium are significantly different and deuterating a particular phase in a multiphase polymer can give excellent phase contrast<sup>163</sup>. When a polymer sample is placed in the path of a neutron beam, the scattering intensity  $I(Q)$  is the coherent elastic scattering measured at the detector and can be defined as the normalized differential scattering cross section per unit volume  $(d\Sigma(Q) / d\Omega)$  where  $d\Sigma$  (neutrons  $s^{-1}$ ) is the number of neutrons scattered per second into a small solid angle  $d\Omega$ . The scattering vector  $Q$  is described by Equation 2.24 in terms of the wavelength ( $\lambda$ ) of the neutron beam and the angle of the scattered beam ( $\theta$ ) from the samples<sup>163,164</sup>.

$$Q = \frac{4\pi}{\lambda} \sin\left(\frac{\theta}{2}\right) \quad \text{Equation 2.24}$$

The difference in scattering length density of each individual component (scattering length,  $b$ , per unit volume,  $v$ ) gives the contrast factor  $b_v$ <sup>163</sup>:

$$b_v = \frac{b_1}{v_1} - \frac{b_2}{v_2} \quad \text{Equation 2.25}$$

The intensity of scattering is proportional to the square of the contrast factor,  $b_v$  between components in a particular system as indicated in Equation 2.26. The general expression for the absolute scattering intensities  $I(Q)$  in terms of a structure factor  $S(Q)$  and form (or shape) factor  $P(Q)$  for small angle neutron scattering is given by<sup>154</sup>:

$$I(Q) = \frac{d\Sigma(Q)}{d\Omega} = N_s V_s (b_v^2) P(Q) S(Q) \quad \text{Equation 2.26}$$

Here  $P(Q)$  is dimensionless and describes how  $(d\Sigma(Q) / d\Omega)$  is modulated by interference effects between neutrons scattered by different parts of the same scattering center.  $S(Q)$  describes the interference effects between neutrons scattered by different scattering centres in the sample and is dependent on the local order in the sample and the interaction potential between scattering components. The term  $N_s$  is the number of scattering centres per unit volume and  $V_s$  is the volume of the sample illuminated by the neutron beam<sup>163,164</sup>.

Several authors have used the Debye-Bueche model<sup>165</sup> to analyze scattering behaviour in immiscible polymer blends<sup>155,161,166</sup> by determining the correlation length and thus give a scale to the phase separation. The Debye-Bueche model assumes a random distribution of phases (of differing densities) throughout a scattering volume ( $V_s$ ) with different sizes and shapes. For such a system, the probability that two points separated by a distance  $r$  are in the same phase<sup>155,165,166</sup> is given by:

$$I(Q) = V_s b_v^2 \phi_1 (1 - \phi_1) 8\pi\xi^3 \left\{ \frac{1}{(1 + \xi^2 Q^2)^2} \right\} + B \quad \text{Equation 2.27}$$

Where  $\phi_1$  is the volume fraction of component 1,  $b_v$  is the contrast factor per unit volume between component 1 and 2,  $V_s$  is the scattering volume  $\xi$  is the correlation length or average density fluctuation length and  $B$  is the background.

#### 2.4.4 Phase Separation and morphology of simultaneous IPNs

The rates of polymerization of components, crosslinking and phase separation all influence the structure and properties of the IPN formed<sup>8</sup>. During the polymerization of simultaneous IPNs, the gelation of either component A or B (see Figure 2.19) or the phase separation of polymer A from B can occur in any order and the morphology and properties of the resulting IPNs are strongly dependent on these events<sup>6,167</sup>. Ideally the polymerization of the individual components and hence interlocking of the two networks within the IPN should prevent phase separation, although it is documented that entropically-driven demixing and phase separation can occur<sup>7,148,153,167</sup> (see Figure 2.18d) and this process may be enhanced in semi-IPNs<sup>7,167</sup> where the absence of an interlocking structure can allow phase separation. However, if sufficient crosslinking of the components in the IPN occurs before diffusion of the components can occur, phase separation may be largely prevented and a high degree of mixing (close to a single phase morphology) would result<sup>168</sup>. Thermodynamic miscibility of the two components within an IPN is governed by the Gibbs free energy of mixing. The free energy of mixing  $\Delta G_M$ , can be expressed as:

$$\Delta G_M = \Delta H_M - T\Delta S_M \quad \text{Equation 2.28}$$

where  $\Delta H_M$  and  $\Delta S_M$  are the enthalpy and entropy of mixing, and  $T$  the absolute

temperature. According to Flory-Huggins solution theory<sup>169,170</sup>, the free energy of mixing is expressed as:

$$\Delta G_M = RT \left( \chi \phi_1 \phi_2 + \left( \frac{\phi_1}{V_1} \right) \ln \phi_1 + \left( \frac{\phi_2}{V_2} \right) \ln \phi_2 \right) \quad \text{Equation 2.29}$$

where  $V_1$  and  $V_2$  are the molar volumes of components 1 and 2,  $\phi_1$  and  $\phi_2$  are the corresponding volume fractions, and  $\chi$  is the thermodynamic binary interaction parameter and  $R$  is the gas constant. A smaller  $\chi$  value will increase the miscibility of the two polymers<sup>6,8</sup>. As the polymerization proceeds the molecular weight (and thus the molar volumes) of the two IPN components increases, which lowers the entropy of mixing and reduces the miscibility<sup>8,171</sup>. Thus, the degree of mixing is controlled by the balance between thermodynamics and kinetics of cure because diffusion and subsequent phase separation can not occur after crosslinking.

With compatible components, phase separation in IPNs may be almost non-existent. However, complete miscibility is not necessary for complete phase mixing (i.e. interpenetration), since permanent entanglements produced by interpenetration can prevent phase separation<sup>172,173</sup>. IPN structures have been reported ranging from dispersed phase domains of a few micrometers to those without a resolvable domain structure<sup>150,167,174-176</sup>. IPNs have been formed which show either two well defined glass transitions<sup>150</sup>, one transition<sup>135,151,152</sup> or an inward shift of the  $T_g$ s from the original  $T_g$ s of the IPN components<sup>153</sup>. Frisch and Klempner<sup>152</sup> studied a number of different IPNs, which all exhibited one sharp glass transition at a slightly lower temperature than the arithmetic mean of the parent  $T_g$ s.

Lin and Chang<sup>5</sup> claimed that hydrogen bonding between DGEBA and unsaturated polyesters resulted in minimal phase separation in epoxy/polyester IPNs. In their study, the viscosity of blends of uncured DGEBA and unsaturated polyester were found to be higher than either resin and this was attributed to intermolecular hydrogen bonding. The cured network was transparent and exhibited a single broad glass transition temperature which the authors suggested was indicative of a single phase system, however the  $T_g$ s of the parent resins were themselves quite broad and not well separated. FTIR spectroscopy studies by Wang *et al.*<sup>177</sup> on IPNs of DGEBA and bisphenol-A vinyl esters also indicated hydrogen bonding between the hydroxy of the

vinyl ester and the epoxy resin as shown by a shift of the carbonyl absorption of the vinyl ester to a lower wavenumber. DSC and DMTA of these vinyl ester/epoxy IPNs showed a single glass transition temperature which the authors suggested indicated miscibility. However, this is not conclusive as the  $T_g$ s of the parent resins were not well separated. IPNs prepared from epoxy/vinyl ester resins by Dubuisson *et al.*<sup>151</sup> were transparent to visible light and also exhibited single glass transition temperatures, suggesting miscibility; although no indication of the breadth of these  $T_g$ s was given.

Tan *et al.*<sup>159</sup> determined the microphase separation characteristics for an acrylate/epoxy IPN by SAXS using the Debye-Bueche and Guinier method to calculate the correlation lengths of the segregated phases in the IPN. The SAXS analysis showed the size of the segregation zones was 50-100Å depending on composition. Junker *et al.*<sup>155</sup> also used SAXS to investigate phase separation in a poly(carbonate-urethane)/dimethacrylate IPN using similar analytical methods and found the size of the segregation zones varied from 20 to 350 Å depending on the IPN composition.

## 2.5 Physical Properties of cured Thermosets

Thermoset polymers exhibit properties such as high rigidity, thermal and dimensional stability, chemical resistance and insolubility due to their covalent network structure. The enhancement of physical properties of network polymers is particularly noticeable above the glass-transition temperature where creep, compression set, and stress relaxation are all improved relative to uncrosslinked polymers.

### 2.5.1 Yielding and Fracture

The ability of a thermosetting polymer to yield is important in determining the extent of toughening which is obtainable. The relationship between tensile stress ( $\sigma$ ) as a function of distance from the crack tip is illustrated in Figure 2.20. If the yield stress is high ( $\sigma_{y1}$ ) then the stress intensification around the crack tip produces only a small plastic zone ( $r_1$ ) around the crack and little plastic energy is dissipated during fracture (Plastic Energy 1). If the yield stress is reduced to  $\sigma_{y2}$ , then the associated energy

(Plastic Energy 2) is significantly higher. The toughness of a polymer and its resistance to crack growth are generally evaluated by two criteria: the critical stress intensity factor (or fracture toughness)  $K_{Ic}$ , whereby fracture proceeds when the stress field experienced around the crack tip reaches a critical level; and the critical strain energy release rate (or fracture energy),  $G_{Ic}$  whereby fracture only occurs when the mechanical strain energy is greater than the surface and plastic deformation energy.

Yielding in thermosetting polymers can be regarded as deformation on a molecular level in which adjacent molecular segments slip over one another when the stress exceeds a critical level. The volume of the molecular segment involved in this process is known as the Eyring 'activation volume'. Eyring theory<sup>178-180</sup> states that the yielding in thermosetting polymers is an Arrhenius-type rate activated process that involves molecular segments 'jumping' over an energy barrier, ( $\Delta H$ ) which separates them from one equilibrium site to another (see Figure 2.21). At a particular strain rate ( $\dot{\epsilon}$ ) and temperature ( $T$ ), an applied shear stress ( $\tau$ ) lowers the energy barrier for this segmental motion by a quantity  $v\tau$ , where  $v$  is the activation volume ( $v_{flow}$ ). The yield stress is described by the Eyring equation<sup>178-180</sup>:

$$\sigma_y = \frac{2\Delta H}{v_{flow}} + \frac{2kT}{v_{flow}} \ln \left( \frac{\dot{\epsilon}}{\dot{\epsilon}_0} \right) \quad \text{Equation 2.30}$$

Thus a linear relationship is expected between tensile yield strength ( $\sigma_y$ ) and logarithm of strain rate at any given temperature (as  $\dot{\epsilon}_0$  is a constant).

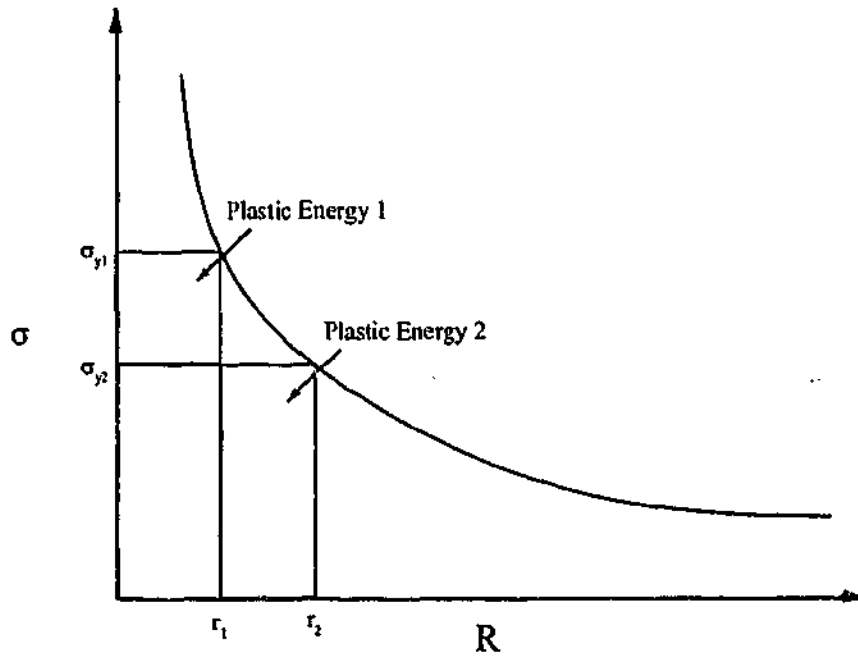


Figure 2.20 Schematic of the theoretical tensile stress as a function of distance from the crack tip for materials with high ( $\sigma_{y1}$ ) and low ( $\sigma_{y2}$ ) yield stress (after Mayr, Cook and Edward)<sup>181</sup>.

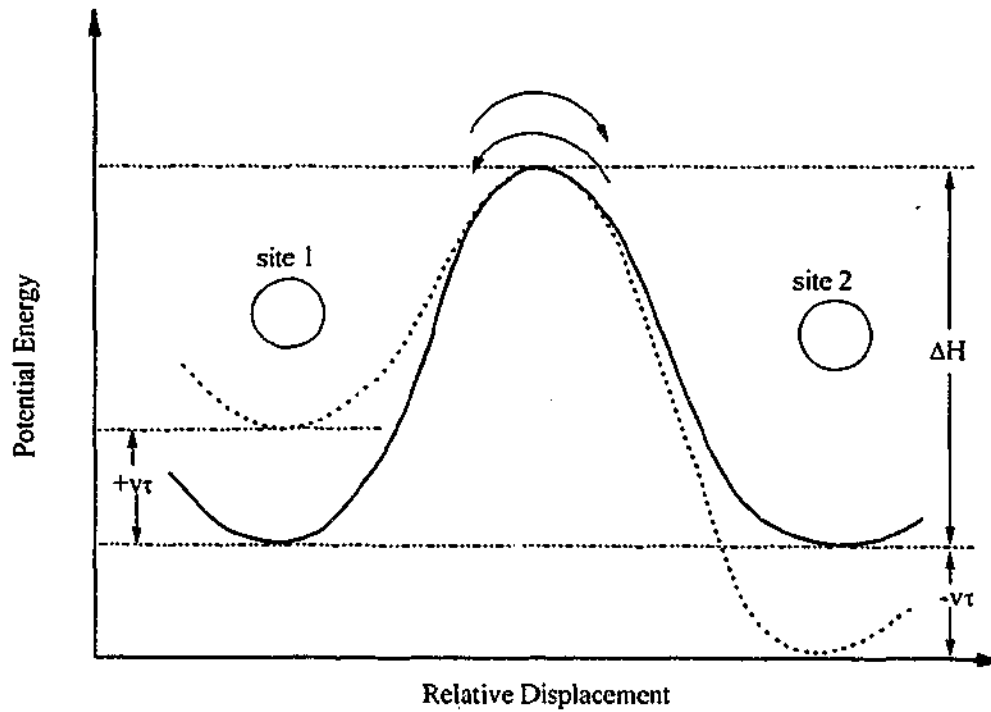
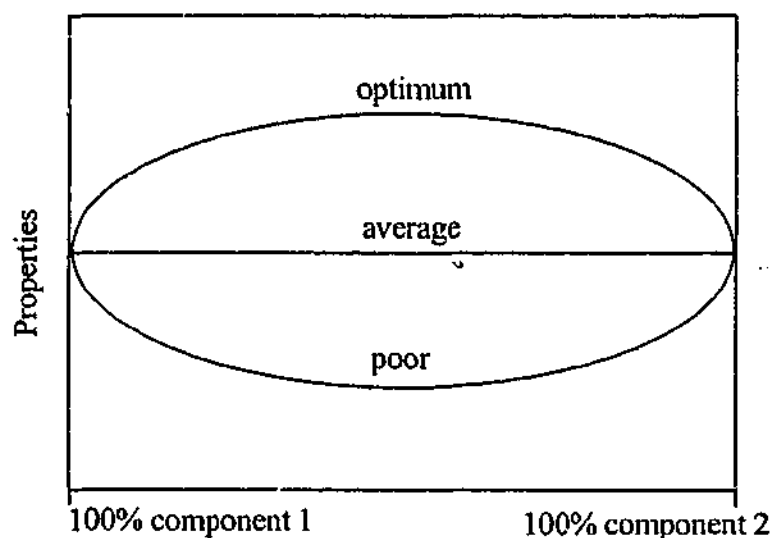


Figure 2.21 The energy barrier between two molecular sites, under an applied shear stress ( $\tau$ )<sup>179,180</sup>

## 2.5.2 Mechanical Properties of IPNs

The formation of IPNs allows unique combinations of polymers and as a consequence have the potential to produce synergistic properties; this is illustrated in

Figure 2.22 where there is a potential for the optimum properties of IPNs to be significantly greater than the average of the two (or more) components of which it is formed.



**Figure 2.22 Schematic of the potential synergistic properties of IPNs**

Lin *et al.*<sup>135</sup> investigated the cure and mechanical behaviour of IPNs formed from amine-cured epoxy and peroxide-initiated unsaturated polyester. They found that IPNs of all compositions exhibited lower  $T_g$ s compared with the neat resins. The 75:25 w/w polyester/epoxy IPN had the lowest  $T_g$ , lowest storage modulus measured by DMTA and highest elongation to break due to its low  $T_g$ , and suggested this was due to entanglements of the two growing networks resulting in uncured components acting as plasticizers within the IPN<sup>5</sup>. The tensile strength at break and fracture energy was also highest in the 75:25 w/w polyester/epoxy IPN, Lin *et al.*<sup>135</sup> attributed this to the greater extent of chain entanglements in the IPN.

Investigations by Rodriguez<sup>182</sup> on epoxy/unsaturated polyester IPNs showed significant increases in tensile strength for the 20/80 and 30/70 blends but the modulus was found to decrease slightly with increasing percentage of the epoxy component. Izod impact data did not indicate any differences between the materials. Subramaniam and M<sup>c</sup>Garry<sup>3</sup> also examined blends of polyesters and epoxies. Mixtures of polyester-styrene and epoxy/amine terminated acrylonitrile butadiene (E/ATBN) yielded a transparent crosslinked material. The inclusion of E/ATBN in the IPN contributed to significant increases in fracture energy and strain to failure, as the rubbery E/ATBN lowered the yield stress and improved the glassy matrix's ability to undergo plastic flow and resulted in an increased blunting of the crack tip.

Park *et al.*<sup>183</sup> studied the mechanical properties of IPNs formed from differing compositions of epoxy and polyester. They observed a higher flexural strength and elastic modulus in the 5:95 w/w blend of unsaturated polyester and epoxy blend than in the neat epoxy/amine or the neat unsaturated polyester. Similar trends were observed in the tensile strength and impact strength data, with the most significant increase in properties being the impact strength. However as the amount of unsaturated polyester added to the blend was increased above 10 wt% the flexural strength, elastic modulus, tensile strength and impact strength decreased to values between those measured for the neat resins. Park *et al.*<sup>183</sup> attributed the enhanced mechanical properties of the IPN to network interlocking between the epoxy and unsaturated polyester causing the matrix to become more rigid due to the restrictions in chain mobility. In this study all samples were cured at room temperature but there was no mention of postcuring and so it may be possible that undercuring occurred which may have affected the validity of the results.

Lin and Lee<sup>184</sup> investigated the dynamic mechanical behavior and impact resistance of a number of fully and semi-interpenetrating polymer networks based on epoxies and acrylics. They found both the full and semi-IPNs exhibited broadened glass transition damping peaks (possibly due to a two-phase structure) which was reflected by an enhancement in impact resistance, Young's moduli and elongation to break.

### 2.5.3 Polymer Degradation

The mechanisms of polymer degradation depend predominantly on the structure of the polymer and exposure conditions. All polymers eventually degrade within the environment to which they are exposed during their life cycle<sup>185</sup>. There are many physical signs of polymer degradation including discolouration, embrittlement, softening, delamination, blistering, cracking, crazing and swelling<sup>186</sup>. Polymer degradation can be broadly classified into a number of mechanisms. Hydrolysis, oxidation, thermal degradation and disintegration or degradation of a physical nature due to absorption, permeation and solvent action are some of the more common mechanisms of polymer degradation<sup>186</sup>.

### Oxidation - thermal

All polymers can be chemically degraded by heat. When heated to the point of bond rupture, polymers can degrade by either random or chain-end scission which produces free radicals<sup>187</sup>. These free radicals can react with oxygen to form smaller oxy and peroxy-radicals and secondary polymer radicals resulting in chain scission. Thermal oxidation is terminated when different free radicals react with each other producing smaller molecules of varying chain length<sup>187</sup>.

### Swelling/solvent uptake

The properties of a polymer (such as  $T_g$ , rigidity and strength) can be impaired by water or solvent uptake<sup>188,189</sup>. In many cases, the uptake kinetics are Fickian, which can be described by Equation 2.31<sup>190</sup> in the initial stages:

$$M_t = M_\infty \left( \frac{4}{\pi} \right) \sqrt{\frac{Dt}{d^2}} \quad \text{Equation 2.31}$$

Here  $D$  is the diffusivity,  $M_\infty$  is the weight gain at saturation,  $M_t$  is the weight at time( $t$ ),  $d$  is the thickness of the material and  $t$  is time. Diffusion can be complicated when the polymer is plasticized by the solvent being absorbed and then the diffusion kinetics are described as non-Fickian.

### Water Sorption

The extent of moisture absorption is mostly determined by the affinity for water molecules of polar groups in cured resins and is known as the hydrophilicity. Hydrophilicity can be quantified by the equilibrium mass fraction of water<sup>188,191,192</sup>:

$$m_\infty = \frac{\text{equilibrium mass} - \text{initial mass}}{\text{initial mass}} \quad \text{Equation 2.32}$$

where  $m_\infty$  depends on the vapour pressure or activity of water and on the temperature<sup>192</sup>. The equilibrium water concentration,  $C_\infty$  (expressed in  $\text{mol.m}^{-3}$ ) can be expressed as:

$$C_{\infty} = \frac{\rho_w}{0.018} m_{\infty} \quad \text{Equation 2.33}$$

where  $\rho_w$  is the density in the wet state.

At low water concentrations Henry's Law relating the water concentration at equilibrium to the water vapor pressure ( $p$ ) can be used to derive the dependency of  $C_{\infty}$  on temperature<sup>191,192</sup>:

$$C_{\infty} = Sp \quad \text{Equation 2.34}$$

where  $S$  is the coefficient of solubility generally expressed in  $\text{mol}\cdot\text{m}^{-3}\cdot\text{Pa}^{-1}$ .

$$C_{\infty} = S_0 p_0 \exp\left(\frac{-H_w - H_s}{RT}\right) \quad \text{Equation 2.35}$$

where  $p_0$  is the water vapour pressure pre-exponential factor,  $H_w$  is the enthalpy of water vapourization (42 kJ/mol)  $H_s$  is the heat of dissolution and  $S_0$  is the water solubility pre-exponential factor.

Experimentally<sup>188,191</sup>,  $C_{\infty}$  can rise or fall with increased temperature. Verdu's group<sup>188,191</sup> has shown this effect of temperature on equilibrium water concentration can be explained by the relationship between  $H_s$  relative to  $H_w$ :  $m_{\infty}$  increases with  $T$  if  $|H_s| < H_w \approx 42 \text{ kJ}\cdot\text{mol}^{-1}$  and decreases with  $T$  if  $|H_s| > H_w \approx 42 \text{ kJ}\cdot\text{mol}^{-1}$ .

The nature of the epoxy resin, polyester or vinyl esters as well as the curing agent can affect the rate of moisture absorption in the polymer networks<sup>193</sup>. A number of studies of water sorption in amine-cured epoxies have been undertaken<sup>188,194,195</sup>. Water uptake was found to be dependent on both the extent of cure and the curing agents used<sup>194</sup>. Amine cured epoxies produce systems with higher hydrophilicity due to the polarity of the amine and can strongly influence water sorption<sup>194</sup>. The effect of moisture absorption is swelling and plasticization of the resins which impairs the mechanical properties.

### Hydrolysis of ester groups (polyesters/vinyl esters)

For significant reaction to occur, water must be absorbed at the surface and then permeate into sub-surface regions. Polyesters and vinyl esters contain terminal ester groups which are subject to hydrolysis<sup>196</sup>. Hydrolysis may be catalyzed by either acids or bases. Compounds may also form within the polymer as a result of accompanying thermal oxidation and these can act as a catalyst for hydrolysis. The rate of hydrolysis is usually limited by the diffusion of the compound into the bulk polymer.

### 2.5.4 Effect of Swelling and Corrosion on Properties

Solvent attack on polymer networks can have a significant effect on strength, modulus, toughness and heat distortion temperature<sup>186</sup> by penetration of solvents into a polymer network causing plasticization<sup>197</sup>. After prolonged exposure to solvents, chemical attack can also occur such as the hydrolysis of ester groups mentioned previously in this Section.

Sonawala and Spontak<sup>198</sup> examined the effects of chemical exposure using a range of solvents, on the mechanical properties of vinyl esters and polyesters. A substantial decrease in flexural and tensile strength was observed for polyesters and to a lesser extent in vinyl ester resins, after prolonged exposure to 1,1,1-trichloroethane. The degradation of both vinyl ester/glass-fibre and polyester/glass-fibre composites was found to be dependent on not only the chemical structure but also the curing processes and the laminates construction. The corrosion resistance of bisphenol-A type vinyl ester resins is obtained predominantly from the phenyl ether linkage in the repeating unit.

Gutierrez et al.<sup>199</sup> investigated the effects of chemical exposure on the mechanical properties of three different epoxy/amine systems. The degradation of the mechanical properties of the epoxy resins were affected by the particular amine curative used and the chemical environment to which they were exposed, however no conclusive structure-property relationships were realized. In studies by Ranney and Parker<sup>200</sup> the chemical resistance of fibreglass-reinforced epoxy resins and fibreglass-reinforced polyester resins were compared, when exposed to a number of different chemically degradative environments. After exposure to a range of hydrocarbons, chlorinated

solvents and oxygen containing compounds for 112 days, the epoxy resin showed minimal weight-gain compared to the polyester resin.

### 2.5.5 Applications of IPNs

There are a number of papers and patents<sup>1,6,201,202</sup> relating to the applications of IPNs and these have been summarized in Table 2.1.

**Table 2.1 Commercial IPN materials (adapted from Cook *et al.*<sup>201</sup>)**

Company/Trade name	Composition/Application
ICI Americas (ITP)	polyurethane/polyester resin IPN for sheet molding compound
Ultracore	Polyester/polyurethane foam IPN reaction spray molding for boats
Amoco Chemical	Polyester/polyurethane IPN for sheet molding and foams
CSI	Polyester/polyurethane IPN for molding of floorboards
DSM	polyester/vinyl ester IPN automotive panels
Dulux	polymethacrylate/melamine latex IPN for paints
Hitachi	vinyl/phenolics IPN for sound dampening
Petrarch (Rimplast)	siloxane/polyurethane IPN for gears
Freeman (Acpol)	acrylic/polyurethane/polystyrene IPN for sheet molding compound

# *Chapter 3*

## *Materials and IPN*

### *preparation*

---

### **3.1 Materials**

The model vinyl ester resin (VER) studied was prepared from a solution of bisphenol-A-diglycidyl-dimethacrylate (bisGMA, see Figure 3.1, supplied by Esschem Co., USA) in 30 wt% styrene monomer (see Figure 3.2, supplied by Huntsman Chemical Company Australia Pty Limited, Australia). Four different types of radical initiators were used to cure this thermosetting component. Methyl ethyl ketone peroxide (MEKP, supplied by Laporte Pty Ltd as a 40 wt% solution in dimethyl phthalate), cumene hydroperoxide (CHP, supplied by Huntsman Chemical Company Australia Pty Limited as a 90 wt% solution in dimethylbenzyl alcohol), benzoyl peroxide (BPO, supplied by Aldrich Chemicals as a 70 wt% suspension in water) and azobisisobutyronitrile (AIBN, supplied by Aldrich Chemicals) were used separately as initiators at a concentration of 1 wt% of the VER component (see Table 3.1 for peroxide initiators). In some studies, cobalt octoate (Co, supplied by Thor Chemicals Australia as a 6 wt% solution in white oil) was used as an accelerator for MEKP at a level of 0.2 w.% based on the VER.

Pure dimethacrylates were also studied – bisphenol-A diglycidyl ether dimethacrylate (bisGMA, supplied by Esschem Co., USA) and diethoxylated bisphenol-A dimethacrylate (DEBPADM, see Figure 3.3, supplied by Sartomer, USA).

A monomeric version of bisGMA, phenyl glycidyl ether methacrylate (PGEMA, see Figure 3.4, synthesised by W.D.Cook<sup>203</sup>) was also studied. Four different types of azo radical initiators were used to cure these dimethacrylates. Azobisisobutyronitrile (denoted AIBN64 supplied by Aldrich Chemicals), 1,1'-azobis(cyclohexanenitrile) (VAZO88, supplied by Dupont), 1,1'-azobis(2,4,4-trimethylpentane) (VR110, supplied by Waco) and 2,2-azobis(2-methylpropane) (AZO168, supplied by Fluka Australia) were used separately as initiators at a concentration of 1 wt% of the VER or methacrylate component (see Table 3.2 for azo initiators).

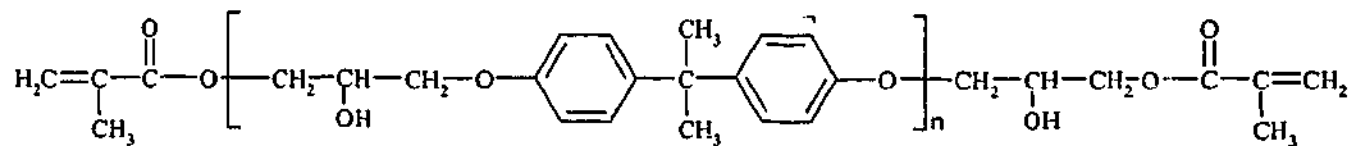


Figure 3.1 Structure of bisGMA ( $n \approx 0.99$  see Section 3.2)

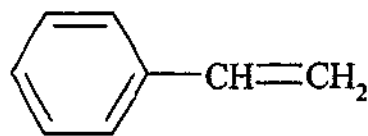


Figure 3.2 Structure of styrene monomer

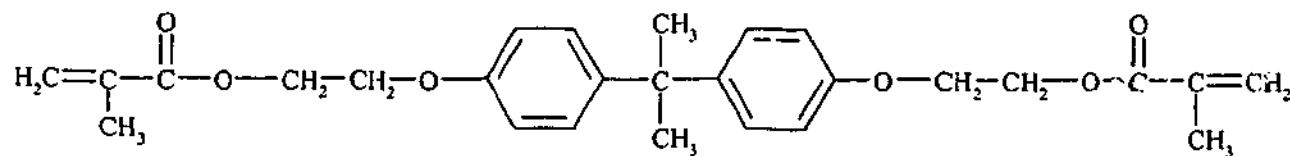


Figure 3.3 Structure of DEBPADM

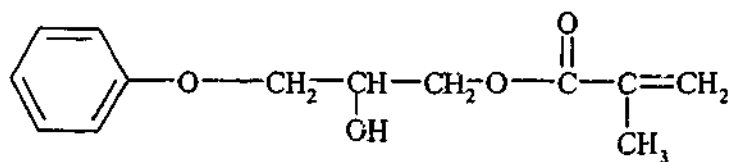
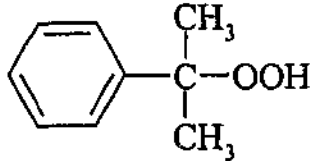
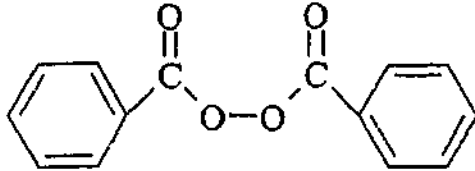


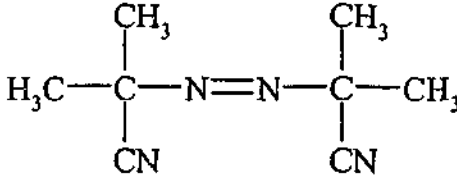
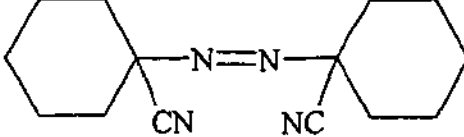
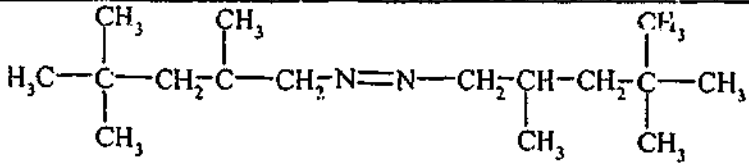
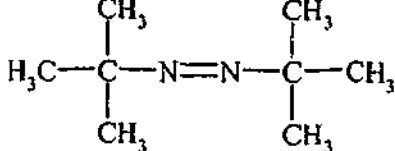
Figure 3.4 Structure of PGEMA

Table 3.1 The structures of the peroxide radical initiators utilized and their 10 hour half life temperatures<sup>204</sup>

Structure	Peroxide Initiator
	Cumene hydroperoxide (CHP) $T_{t \frac{1}{2}=10h} = 140^\circ\text{C}$
$\text{H}_5\text{C}_2-\overset{\text{OOH}}{\underset{\text{OOH}}{\text{C}}}-\text{CH}_3 + \text{H}_3\text{C}-\overset{\text{C}_2\text{H}_5}{\underset{\text{OOH}}{\text{C}}}-\text{OO}-\overset{\text{C}_2\text{H}_5}{\underset{\text{OOH}}{\text{C}}}-\text{CH}_3 + \text{Other structures}$	Methyl ethyl ketone peroxide (MEKP) $T_{t \frac{1}{2}=10h}$ not specified
	Benzoyl Peroxide (BPO) $T_{t \frac{1}{2}=10h} = 71^\circ\text{C}$

\*The 10-hour half life temperatures were obtained from the Polymer Handbook<sup>204</sup>.

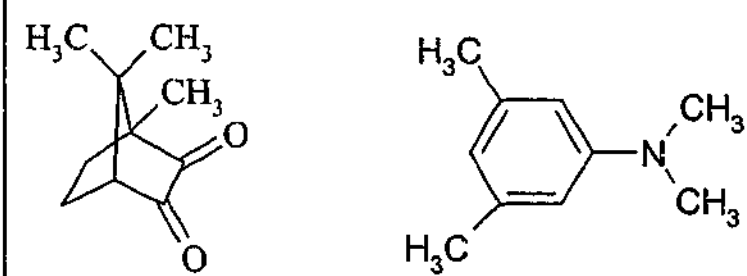
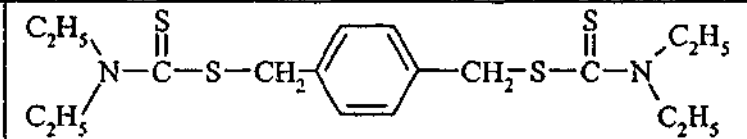
Table 3.2 Structures of the azo initiators used and their 10 hour half life temperatures.

Structure	Azo Initiators and their 10 hour half life temperature
	Azobisisobutyronitrile (AIBN64) $T_{t \frac{1}{2}=10h} = 64^\circ\text{C}$
	1,1'-azobis(cyclohexanenitrile) (VAZO88) $T_{t \frac{1}{2}=10h} = 88^\circ\text{C}$
	1,1'-azobis(2,4,4-trimethylpentane) (VR110) $T_{t \frac{1}{2}=10h} = 110^\circ\text{C}$
	2,2-azobis(2-methylpropane) (AZO168) $T_{t \frac{1}{2}=10h} = 168^\circ\text{C}$

\* The 10-hour half life temperatures were obtained from the azo suppliers<sup>205-207</sup>. Note the number in the code for the initiator gives the 10-hour half-life temperature.

For photocure using visible radiation (ca. 470 nm), 0.25 wt% camphorquinone (CQ, supplied by Aldrich Chemicals) and 0.3 wt% N,N,-3,5-tetramethyl aniline (TMA, supplied by Aldrich Chemicals) was used as a photo-redox initiator, while for the UV-initiated cure, 1 wt% of p-xylylene bis (N,N-diethyl dithiocarbamate) (XDT, synthesised by Mr T.F. Scott using the method given by Otsu and Kuriyama<sup>208</sup>) was used as the photo-initiator. The structures of these photoinitiating systems are illustrated in Table 3.3

Table 3.3 Structures of visible light (470nm) and UV light photoinitiating systems

Initiator system	Structure
CQ/TMA	 <div style="display: flex; justify-content: space-around; margin-top: 10px;"> <div style="text-align: center;"> <chem>C[C@H]1[C@@H]2[C@H](C(=O)O1)C(=O)C2(C)C</chem> CQ         </div> <div style="text-align: center;"> <chem>Cc1cc(C)c(N(C)C)cc1</chem> TMA         </div> </div>
XDT	 <chem>CCN(CC)C(=S)SCH2c1ccc(cc1)CSC(=S)N(CC)CC</chem>

The epoxy oligomer was diglycidyl ether of bisphenol-A (DGEBA, see Figure 3.5, Araldite GY-9708-1 supplied by Ciba Geigy) with  $n = 0.15$  (see Section 3.2). A monomeric form of DGEBA, 1,2 epoxy-3-phenoxy propane (PGE, see Figure 3.6, supplied by Aldrich) was also investigated. The amine curing agents used in stoichiometric amounts (equimolar NH and epoxy groups) for the cure of DGEBA were: butylamine (BA, supplied by Ajax Chemicals), 1,8-diamino-octane (DAO, supplied by Aldrich), aniline (An, supplied by Unilab) and 4,4'-diamino-diphenyl methane (DDM, supplied by Aldrich). Butylamine and aniline are monomeric forms of the crosslinking DAO and DDM, respectively (see Figure 3.7). An anionic initiator was also used to cure the epoxy system and was 1-methyl imidazole (1-MeI, see Figure 3.8, supplied by Ciba Geigy), used at a level of 2 or 5 wt% (as specified). Stoichiometric amounts (1:1 anhydride to epoxy group) of the anhydrides cis-1,2 cyclohexanedicarboxylic anhydride (CHDCA, see Figure 3.9, supplied by Aldrich

Chemicals) and/or n-dodecylsuccinic anhydride (DDSA, see Figure 3.9, supplied by TCI chemicals Tokyo) were used for the cure of the epoxy resin. The epoxy/anhydride cure was accelerated with N,N-dimethylbenzylamine (DMBA, see Figure 3.9, supplied by Aldrich Chemicals) which was used at a level of 2 wt% of the total anhydride in the system.

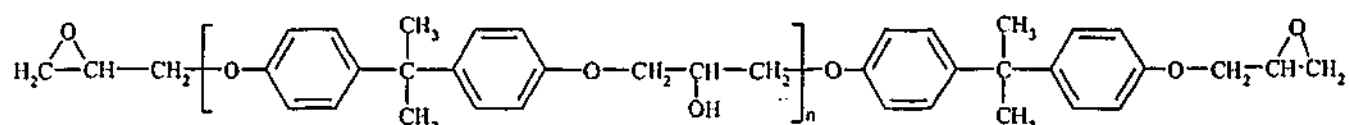


Figure 3.5 Structure of DGEBA ( $n=0.15$ -see Section 3.2)

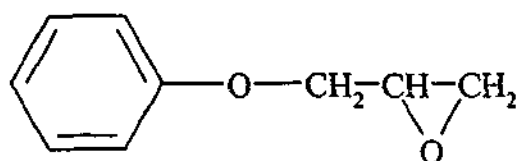
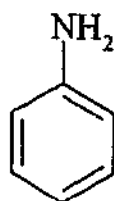
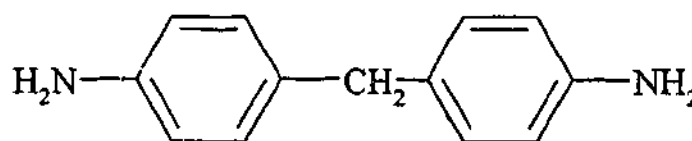


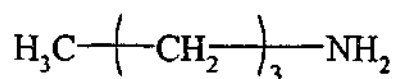
Figure 3.6 Structure of PGE



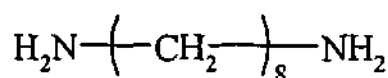
aniline



DDM



butylamine



DAO

Figure 3.7 Structures of monofunctional amines and corresponding diamines

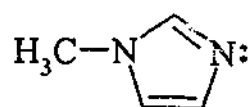


Figure 3.8 Structure of 1-Mel

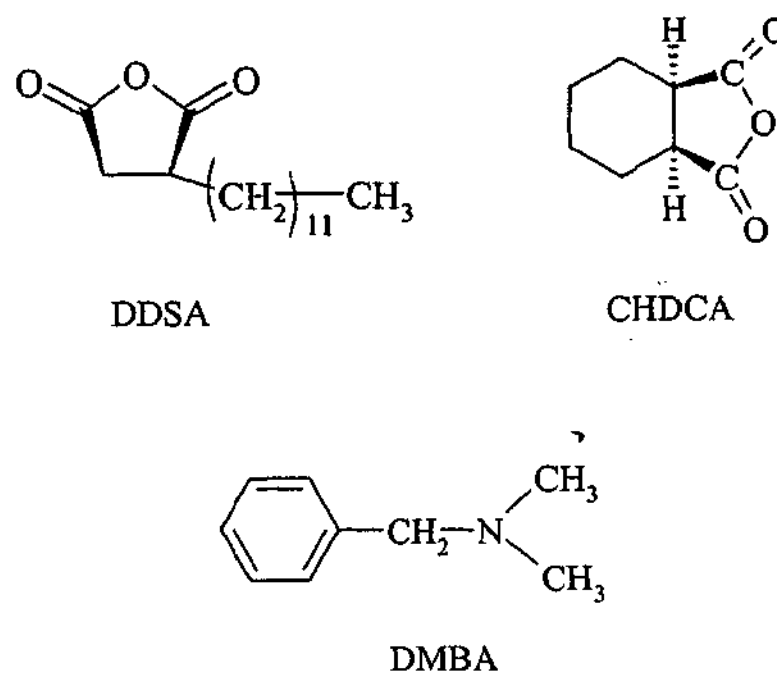


Figure 3.9 Structures of DDSA, CHDCA and DMBA.

### 3.2 Resin characterization

The molecular weights of the bisGMA and DEBADM were determined by the titration of the  $\alpha,\beta$ -unsaturation with morpholine<sup>209</sup>. The unsaturation was reacted quantitatively with morpholine in the presence of acetic acid catalyst to form tertiary amines. The excess morpholine was back titrated with acetic anhydride to form the amide, which was neutral in the reaction medium. The tertiary amine was then titrated with methanolic hydrochloric acid, in the presence of an indicator. The amount of tertiary amine formed is a direct measure of the  $\alpha,\beta$ -unsaturation compound originally present. From this technique the molecular weight of bisGMA was found to be 490 g/mol (compared with the theoretical value of 514 g/mol;  $n=1$ ) and the molecular weight of DEBADM was found to be 470 g/mol (compared with the theoretical value of 452 g/mol) assuming that both monomers were bifunctional.

The molecular weight of DGEBA (Araldite GY-9708-1) reported by Ciba Geigy was 372 g/mol. The styrene equivalent molecular weight of the DGEBA (Araldite GY-9708-1) was estimated to be 368 g/mol by gel permeation chromatography (GPC) using a 2 column Machery-Nagel (KF801 and KF803) instrument. For the GPC experiments,

tetrahydrofuran was used as the solvent at a flow rate of 1mm/min. The GPC was calibrated with polystyrene standards using a Waters Refractometer R410 detector and a Waters 484 UV Spectrometer (wavelength 254nm) detector\*. For all stoichiometric calculations the molecular weight of DGEBA was taken as the average of these values (i.e. 370 g/mol).

### 3.3 IPN preparation and cure

#### 3.3.1 Model VER, neat dimethacrylate and neat epoxy systems

The model VER was prepared from 70wt% bisGMA mixed with 30wt% styrene monomer. The styrene was added in stages to the bisGMA resin and was blended with a large glass stirring rod until the required wt% was reached and the resin was homogeneous. The AIBN was finely ground with a mortar and pestle prior to its addition to the resins and mixed for 2 minutes with the model VER, neat DEBPADM and neat bisGMA, but then allowed to sit for 30 minutes until the AIBN dissolved completely. The other liquid and solid initiators were added separately at 1wt% to the resins and were mixed for 2 minutes at ambient temperature before being tested.

2 or 5 wt % (as specified) of 1-MeI was added to the epoxy resin and mixed for 2 minutes before being tested. The liquid aliphatic and aromatic amines BA and An were blended in stoichiometric quantities (equimolar amino hydrogens and epoxy groups) to the epoxy resin at room temperature. Since DDM and DAO are crystalline solids, a stoichiometric amount of the diamine and DGEBA were heated separately to the melting point of the diamine (see Table 3.4) prior to being mixed for 2 minutes and rapidly cooled to ambient temperature. The crystalline CHDCA and DDSA anhydrides and a stoichiometric quantity of DGEBA were also separately heated to the melting points of the anhydride (see Table 3.4) prior to their mixing and then rapid cooling to ambient temperatures. For mixtures of anhydrides, a 50:50 wt% ratio of CHDCA and

---

\* Thanks to Dr. J. Galy for performing gel permeation chromatography experiments at LMM, INSA Lyon.

DDSA was heated to 50°C before mixing with DGEBA heated to the same temperature. The epoxy/anhydride mixes were cooled to ambient temperatures before the addition of DMBA (as 2wt% of the anhydride) as an accelerator. After mixing the blends were kept at ambient temperature for a very short period before being tested.

**Table 3.4 Melting points of epoxy curatives as measured by scanning DSC at 5°C/min**

<b>Amine curative</b>	<b>Melting point</b>
DAO	40°C
DDM	90°C
CHDCA	32°C
DDSA	74°C

### **3.3.2 IPNs and partial IPN systems**

The IPNs were blended at room temperature with ratios of 25:75, 50:50 or 75:25 by weight of methacrylate component to epoxy component. Each component was mixed (as outlined in Section 3.3.1.) with initiator/catalyst separately before being combined to form the IPN mixture.

In some cases, studies were performed to investigate the effect of the presence or omission of one of the reactive components (such as the epoxy curative or the radical initiator) on the cure of the IPN - in these studies the ratio of the remaining individual components were maintained at the normal level as in the IPN. These systems were prepared by the combination of all of the components of one system prior to the addition of the components of the second system, e.g. for the VER/AIBN:DGEBA combination, the AIBN was added to the VER and mixed for 2 minutes and allowed to stand for a further 30 minutes prior to the addition of the DGEBA.

# *Chapter 4*

## *Experimental Techniques*

---

### **4.1 Fourier Transform Infrared Spectroscopy (FTIR)**

#### **4.1.1 Mid-FTIR**

Studies of the cure were followed using Fourier transform mid-infrared spectroscopy using a Perkin-Elmer FT1600. Potassium bromide (KBr) powder was pressed into 6mm radius and ca 0.5mm thick discs at 10 tonnes of pressure under vacuum for 3 minutes. All samples were mixed at room temperature and sandwiched between two KBr discs before being placed in the spectrometer and scanned over the range 4000-400 $\text{cm}^{-1}$  with a resolution of 4 $\text{cm}^{-1}$ . Samples were cured in an oven at 70°C or 110°C over a number of hours (depending on the rate of cure of each specimen) during which they were periodically removed and scanned in the FTIR. After 24 hours of cure, the specimens were postcured at temperatures between 150 and 200°C depending on the specific system under investigation. The epoxy absorption<sup>77</sup> at 915 $\text{cm}^{-1}$ , the unreacted vinyl double bonds of styrene<sup>116,210</sup> at 778 $\text{cm}^{-1}$  and 1630 $\text{cm}^{-1}$  and the methacrylate stretch<sup>210</sup> at 1645 $\text{cm}^{-1}$  (see Table 4.1)<sup>77,116,210</sup> were used to calculate the conversion after allowance for overlapping peaks. All spectra were internally standardized using the phenyl peak of styrene<sup>116</sup> at 700  $\text{cm}^{-1}$  and/or DGEBA<sup>77</sup> peak at 1508  $\text{cm}^{-1}$  (see Table 4.1)<sup>77,116,210</sup>. Generally the variations in intensity of the internal standard peak were only observed for the initial spectrum taken at room temperature (zero time) and the spectrum of the postcured sample. Due to the overlap of the epoxy and styrene peaks in the region

910-915  $\text{cm}^{-1}$ , and the overlap of the styrene and methacrylate peaks in the region 1630-1645  $\text{cm}^{-1}$ , separation was achieved as outlined below.

*In pure styrene monomer:*

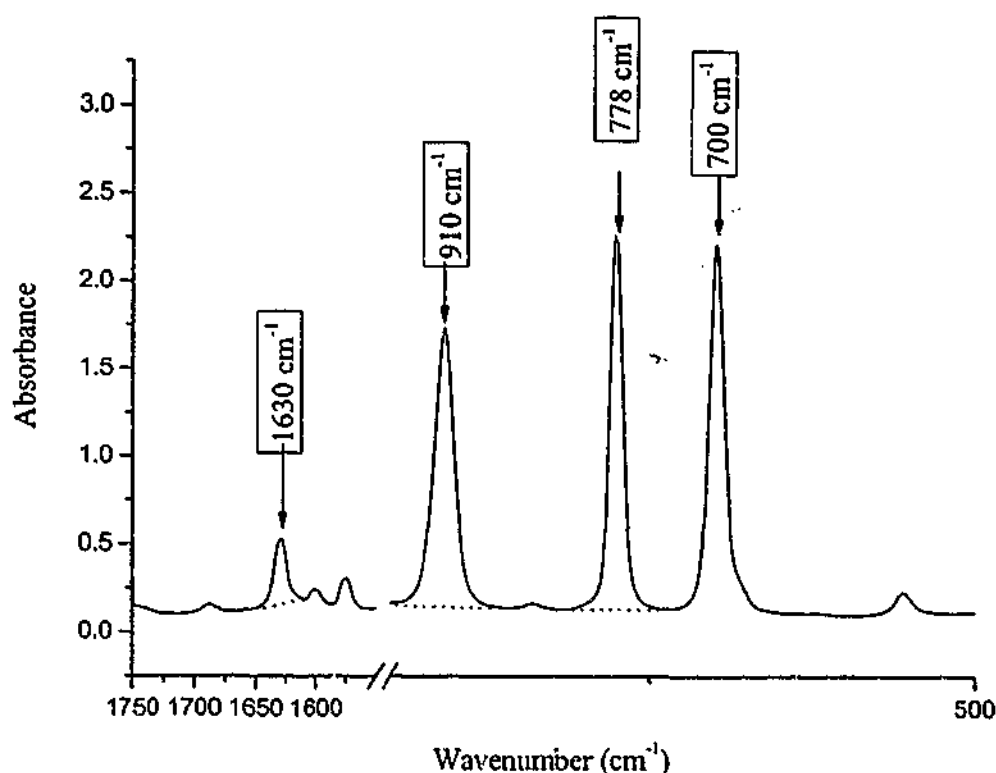


**Figure 4.1** mid-FTIR spectra of the pure styrene monomer

The mid-FTIR spectra of the pure styrene monomer is illustrated in Figure 4.1. The peaks at 1630, 910 and 778  $\text{cm}^{-1}$  are due to unreacted vinyl double bonds<sup>116,210</sup> and as mentioned previously the peak at 700 $\text{cm}^{-1}$  is due to the phenyl peak of styrene<sup>116,210</sup> (see also Table 4.1). Two conversion factors ( $C_{st778/910}$  and  $C_{st778/1630}$ ) were obtained from the ratio of the area of the styrene monomer peak ( $A_{stm}$ ) at 778  $\text{cm}^{-1}$  to the styrene peaks ( $A_{stm}$ ) at 910  $\text{cm}^{-1}$  and 1630  $\text{cm}^{-1}$  respectively – see Equations 4.1 and 4.2.

$$C_{st778/910} = \frac{A_{stm(778\text{cm}^{-1})}}{A_{stm(910\text{cm}^{-1})}} \quad \text{Equation 4.1}$$

$$C_{st778/1630} = \frac{A_{stm(778\text{cm}^{-1})}}{A_{stm(1630\text{cm}^{-1})}} \quad \text{Equation 4.2}$$

*In a binary system of epoxy and model vinyl ester resin:*

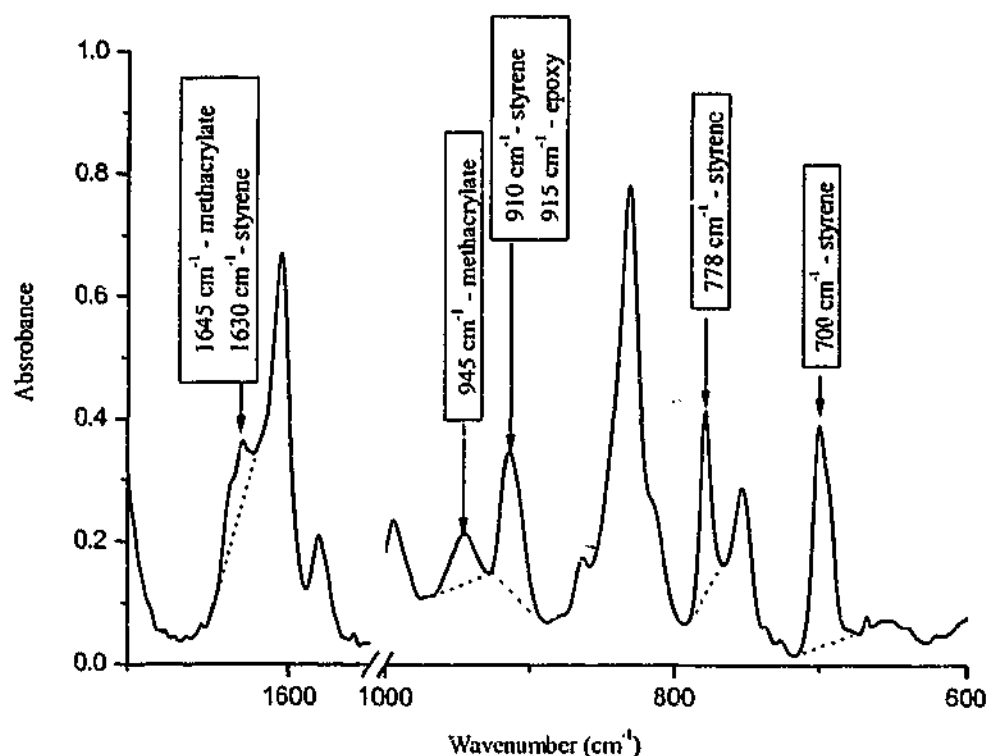


Figure 4.2 mid FTIR spectra of DGEBA/BA:VER/AIBN unreacted system as an example of all the peaks on interest used in this work.

The mid-FTIR spectra of an IPN example (in this case DGEBA/BA:VER/AIBN IPN) is illustrated in Figure 4.2 with the position and identification of the main peaks of interest clearly noted (see also Table 4.1). The conversion factors that were developed from the spectra of pure styrene monomer were then used in the binary systems of epoxy and model vinyl ester (for example the DGEBA/BA:VER/AIBN IPN as illustrated in Figure 4.2) to extract the styrene component from the regions at 910-915  $\text{cm}^{-1}$  (overlapping of styrene and epoxy peaks) and 1630-1645  $\text{cm}^{-1}$  (overlapping of styrene and methacrylate peaks) – see Equations 4.3 to 4.5.

$$A_{\text{stb}(910\text{cm}^{-1})} = \frac{A_{\text{stb}(778\text{cm}^{-1})}}{C_{\text{st}778/910}} \quad \text{Equation 4.3}$$

$$A_{\text{epb}(915\text{cm}^{-1})} = A_{\text{epb/stb}(910\text{cm}^{-1}+915\text{cm}^{-1})} - A_{\text{stb}(910\text{cm}^{-1})} \quad \text{Equation 4.4}$$

$A_{\text{stb}}$  is the proportion of the peak area due to the styrene absorption in the binary systems. As the styrene peak at 778  $\text{cm}^{-1}$  is not significantly disrupted by other peaks (see Figures 4.1 and 4.2), the reaction of styrene can be monitored by the decrease in this peak. Dividing the styrene peak at 778  $\text{cm}^{-1}$  in the binary system by the conversion

factor ( $C_{st778/910}$ ) obtained from the spectra of pure styrene monomer gives the proportion of the overlapped peaks of styrene and epoxy at  $910-915\text{cm}^{-1}$  due to styrene (see Equation 4.3). Thus the proportion of the peak area at  $910-915\text{cm}^{-1}$  due to the epoxy absorption in the binary systems ( $A_{epb}$ ) can be determined (see Equation 4.4). The other separation of styrene and methacrylate at  $1630$  and  $1645\text{cm}^{-1}$  was based on a similar analysis using Equation 4.2 and Equation 4.5 giving the proportion of the peak at  $1630-1645\text{cm}^{-1}$  which is the contribution of the methacrylate absorbance.

$$A_{\text{methb}(1645\text{cm}^{-1})} = A_{\text{methb/stb}(1645\text{cm}^{-1}+1630\text{cm}^{-1})} - \frac{A_{\text{stb}(778\text{cm}^{-1})}}{C_{\text{st778/1630}}} \quad \text{Equation 4.5}$$

The relative conversions of the various reactive species within the monomer blend were then evaluated from the Beer-Lambert Law<sup>211</sup>:

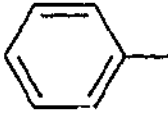
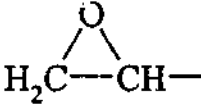
$$A = \epsilon cd \quad \text{Equation 4.6}$$

where  $\epsilon$  is an integrated molar absorptivity,  $c$  is the molar separation and  $d$  is the path length. Thus assuming that Beers law is obeyed, the conversion is given by:

$$\alpha = 1 - \frac{A_t}{A_0} \quad \text{Equation 4.7}$$

where  $\alpha$  is the conversion,  $A_t$  is the integrated absorbance of the characteristic peak at time  $t$  and  $A_0$  is the integrated absorbance of the characteristic peak at time zero. The conversion of the reactive groups were determined from the decrease in area of the characteristic peaks (see Figures 4.1 and 4.2 and Table 4.1) using the Grams Analyst software version 3.1B. This program used the tangent baseline method to calculate the area of the methacrylate peak between  $1655-1615\text{cm}^{-1}$  and the epoxy peak between  $930-900\text{cm}^{-1}$ . Due to the presence of overlapping peaks in the region between  $900-1000\text{cm}^{-1}$  this tangent baseline technique introduces approximately  $\pm 2\%$  uncertainty in the calculation of the conversion.

Table 4.1 Band assignment for chemical groups from mid-FTIR absorption spectra<sup>77,116,210</sup>

Chemical Name	Wavenumber (cm <sup>-1</sup> )	Band assignment of reactant or product
styrene	778, 910 and 1630	$\text{—CH=CH}_2$ unreacted vinyl double bonds
	700	 benzene ring (Internal standard)
bisGMA	945* and 1645	$\begin{array}{c} \text{—C=CH}_2 \\   \\ \text{CH}_3 \end{array}$ unreacted methacrylate double bonds
DGEBA	915	 epoxy group
	830 and 1508	 benzene ring (Internal standard)

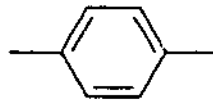
#### 4.1.2 near FTIR band

Fourier transform near infra-red spectroscopy was also utilized to measure the cure kinetics with a Nicolet 550 FTIR at a resolution of 4 cm<sup>-1</sup>. The liquid sample was contained by a silicone gasket, which was sandwiched between two glass plates coated with conductive indium-tin oxide and having a path length of 1 mm. A voltage was applied across the glass plates which heated the sample in the assembly as described by

\* The absorption at 945 cm<sup>-1</sup> was not used as a measure of methacrylate conversion in the mid FTIR studies as it was superimposed with a broad peak which disturbed the area/height calculations.

Rey *et al.*<sup>212</sup>. The reaction temperature was maintained at 70°C as measured with a thermocouple, which was inserted into the liquid. The characteristic peaks in the near infrared region for the epoxy group, styrene unsaturation and methacrylate unsaturation are 6070, 6135 and 6166 cm<sup>-1</sup> respectively<sup>212,213</sup>. The area under the epoxy absorption peak at 6070 cm<sup>-1</sup> was used directly to calculate the conversion of the epoxy groups. Unfortunately, the vinyl resonances of the styrene (6135cm<sup>-1</sup>) and methacrylate (6166cm<sup>-1</sup>) groups overlap. Since previous mid-FTIR<sup>214,215</sup> (see also Section 5) had indicated that the rate of cure of styrene and methacrylate vinyl groups were very similar, the NIR vinyl resonances were not separated, but their total area was measured to give an average vinyl group conversion. After isothermal cure at 70°C for 450 minutes the samples were postcured at 160°C for 2 hours (unless stated otherwise). Since the peaks lie on a curved spectrum, a 4<sup>th</sup> order polynomial was fitted to the spectrum of the “fully cured” sample and this approximation of the underlying spectral baseline was subtracted from the NIR spectra. The area under these peaks was used to calculate the conversion of the epoxy and methacrylate groups in the uncured, partially cured and “fully cured” systems.

**Table 4.2 Band assignments for chemical groups from near-FTIR absorption spectra<sup>212,213</sup>.**

Chemical Name	Wavenumber (cm <sup>-1</sup> )	Band Assignment
styrene	6135	$-CH=CH_2$ unreacted vinyl double bonds
bisGMA	6166	$\begin{array}{c} -C=CH_2 \\   \\ CH_3 \end{array}$ unreacted methacrylate double bonds
DGEBA	6070	$\begin{array}{c} O \\ \diagup \quad \diagdown \\ H_2C-CH- \end{array}$ epoxy group
	4065	 benzene ring (Internal standard)

## 4.2 Differential Scanning Calorimetry (DSC)

### Scanning DSC

The kinetics of the cure were measured with a Perkin-Elmer DSC-7, operated in scanning mode (5°C/min) under a N<sub>2</sub> atmosphere. The N<sub>2</sub> gas flow rate was maintained at ca. 20 cc/min. The temperature and enthalpy were calibrated using high purity indium (transition point = 156.61°C, transition energy = 28.45 J/g) and purity zinc (transition point = 419.47°C) standards. A baseline was recorded using two empty aluminium pans that were scanned over the same temperature range of the experiment then subsequently subtracted from the scan of the sample by the Perkin Elmer PC Series Software (Version 3.1). Approximately 8-15 mg of the IPN resins were sealed in aluminium pans and scanned from 40 to 300°C. In a number of cases the Perkin-Elmer Intracooler was also used for subambient runs from -10 to 300°C. The specimens were subsequently re-run from 40 to 300°C to determine the T<sub>g</sub>s of the polymers using the mid-point method. In most cases a minimum of 2 samples were measured for any one experiment to ensure reproducibility. All exotherm energies are reported as Joules per gram of total resin (pure resin or IPN resin). A typical exotherm obtained from a temperature scan from 50-250°C of the neat DGEBA/1-MeI resin system is shown in Figure 4.3. In some cases, and particularly in IPN systems, multiple peaks were recorded in the DSC scans and, where possible, the overlapping peaks were approximately resolved by dropping a vertical line from the heat flux curve to the baseline at the temperature corresponding to the lowest heat flux and integrating the underlying curve to obtain the individual heats of polymerization.

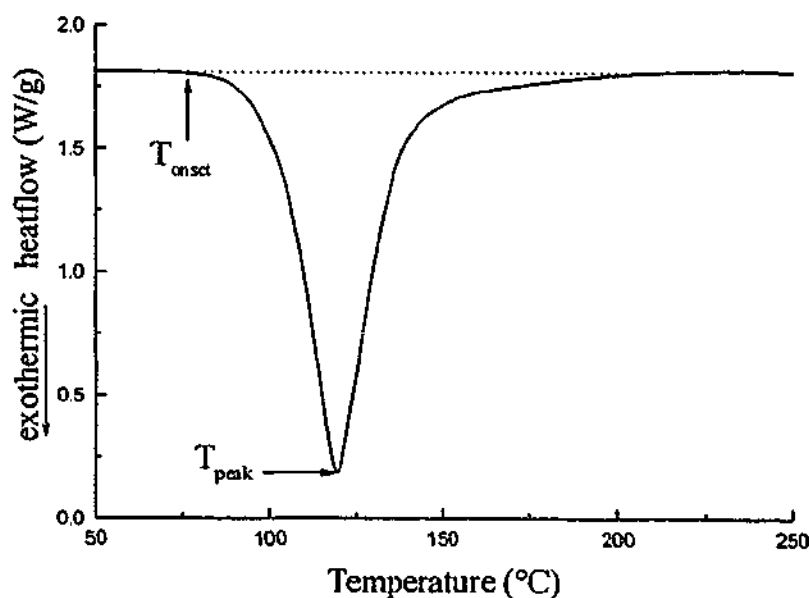


Figure 4.3 A representative exotherm produced from scanning DSC

### Isothermal photopolymerization mode

The photopolymerization kinetics were measured with a Perkin-Elmer DSC-7, operated in isothermal mode under a N<sub>2</sub> atmosphere. The instrument was modified to allow the irradiation of the sample as discussed by Cook<sup>216</sup>. This modification involved the use of a bifurcated fibre optic lead (glass for visible light and quartz for UV), which approximately balanced the thermal heating effect of the source. The standard DSC pan lids were removed and replaced with transparent PET covers to allow irradiation of the resin. Fine aluminium rings were placed in each sample pan holder and PET covers (cut to size with two small holes punched near the outside edge to allow for circulation of N<sub>2</sub>) were placed above the rings to minimize thermal noise in the system. The sample (5-8 mg) was spread as a thin layer (ca 0.5mm) over the base of the aluminium sample pan and the pan was left un-sealed to allow photocuring. The sample pan was placed in the DSC sample pan holder and covered with the PET cover before being left for 20 minutes at either 50°C or 100°C under a N<sub>2</sub> atmosphere to minimize the effect of dissolved oxygen and to equilibrate the sample temperature. No induction was observed in the photocuring of the dimethacrylate and no thermal cure of the epoxy was observed at 50°C, however at 100°C approximately 10% cure occurred in the epoxy component of the IPN during the 20 minute equilibration. Isothermal scans were repeated on the fully cured samples and the data was subtracted from all curing scans to eliminate thermal effects from the light sources.

For visible light photopolymerization, the sample was initiated with a Visilux-2 dental photocuring source (3M, USA) which emits radiation predominantly in the 450-500nm range but had a maximum emittance near 470nm<sup>97</sup> which is the wavelength of maximum absorbance for CQ. The unattenuated radiation intensity at the base of the DSC sample pan was 2 mW cm<sup>-2</sup> nm<sup>-1</sup> at 470nm<sup>97</sup>, but for most studies the radiation intensity was reduced by placing neutral density filters between the source and the fibre optic bundle. For ultraviolet light photopolymerization, the sample was initiated with a Spectroline SB-100PC/FA ultraviolet lamp (Spectronics). A glass bi-convex lens (Oriel, USA) was used to further focus the UV radiation (predominantly 365 nm) on to the fibre optic entrance. The unattenuated radiation intensity at the sample pans, measured using an International Light IL1700 radiometer fitted with a SED033/UVA/W detector was 0.50 mW cm<sup>-2</sup> at 365nm. In both cases, a shutter was used to allow an accurate

control of the exposure time of the sample by the light source. A standard exotherm produced from photopolymerization of DEBPADM/CQ/TMA with visible light is shown in Figure 4.4. For consequent scanning DSC of these samples the sample pans were removed and the lid clamped immediately before the sample was scanned as specified previously in this work.

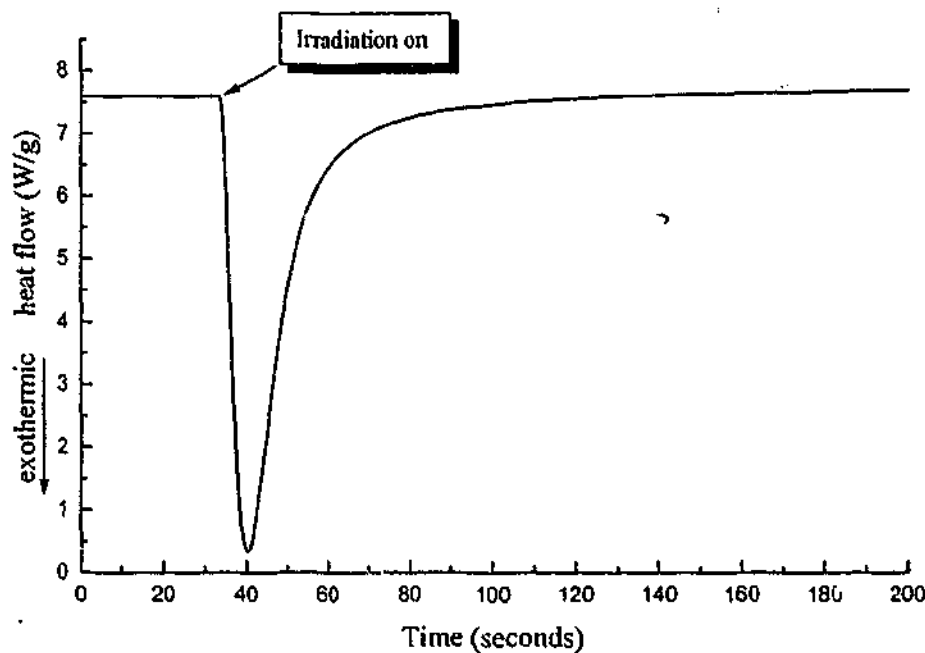


Figure 4.4 A representative exotherm produced by photopolymerization of DEBPADMA/CQ/TMA with visible light.

### 4.3 Soxhlet Extractions

The un-grafted linear epoxy was extracted from the network forming VER in semi-IPNs of VER/AIBN:DGEBA/BA and VER/AIBN:DGEBA/An with chloroform as a solvent using a soxhlet apparatus as illustrated in Figure 4.5. The sample was placed in a pre-dried paper soxhlet (dried under vacuum at 50°C for 24 hours) tube before further drying at 50°C under vacuum for a further 24 hours prior to extraction. The un-grafted linear epoxy was extracted with chloroform under reflux for 24 hours. After extraction the specimen was dried at 50°C for a further 24 hours prior to being weighed to an accuracy of 0.01mg.

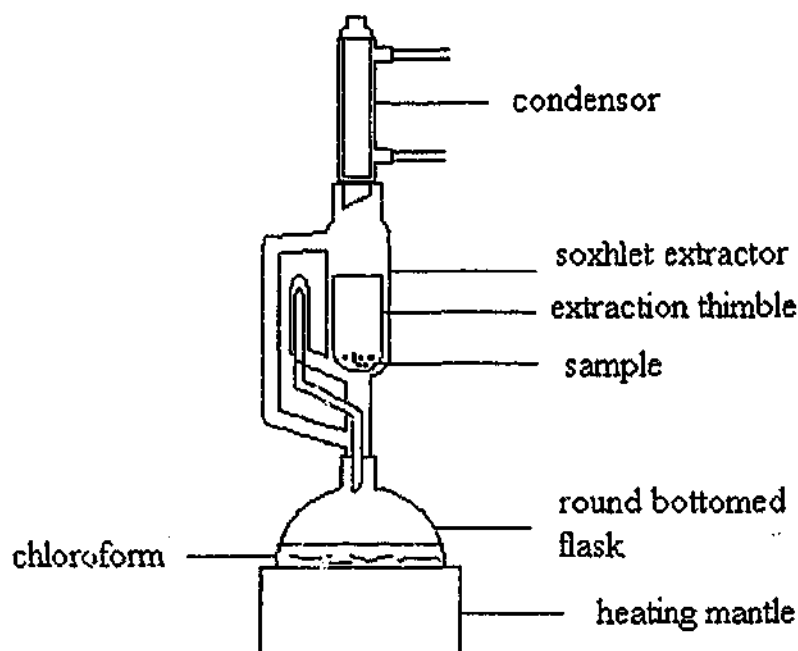


Figure 4.5 Schematic of the Soxhlet extraction

## 4.4 Rheology

The changes in the steady shear viscosity during cure of the neat resins and their IPNs were followed via a Contraves Rheomat 115 type viscometer at 70°C using a cup and bob arrangement (1mm gap) at a shear rate of 10 s<sup>-1</sup>. Gelation is commonly determined as the stage when the steady shear viscosity diverges to infinity<sup>23,44</sup> and so the gel times were obtained by extrapolating the reciprocal of the viscosity to zero. All steady shear experiments were repeated to ensure reproducibility.

Dynamic rheology of the systems were obtained at 70°C with angular frequencies varying from 1 rad/s to 100 rad/s via a Rheometrics Dynamic Analyzer (RDAII) using 40 mm diameter parallel plates, ca 0.5 mm gap and an average shear strain of 40% which enhanced the sensitivity of the instrument to the gelation phenomena. Gelation was determined by two criteria from this dynamic rheology data. The time at which the real ( $G'$ ) and the loss ( $G''$ ) shear moduli showed power law behaviour and so  $\tan\delta$  became frequency independent was one definition<sup>50</sup>. In addition, since gelation is accompanied by the formation of an elastic network, the time at which  $G'$  attained a value of 1 Pa, was also used as an operational definition which corresponds to the detection limit of the experimental set-up.

Dynamic rheology which accentuated the vitrification phenomena of the systems

was also performed at 70°C as above but using the Rheometrics RDAII and the Bohlin CS-50 with ca 10 mm diameter parallel plates, and average shear strains varying from 40% (when liquid) to 0.016 % (when solid). The onset of the glass transition temperature is often defined<sup>217</sup> as occurring where the real shear modulus attains a value in the region of  $10^7$ - $10^8$  Pa. Since the rheometers become insensitive for stiff materials, the vitrification time was operationally defined when  $G' = 10^7$  Pa. All dynamical experiments were repeated to ensure reproducibility, however the values of shear modulus obtained during the measurement of the gelation and vitrification properties may not have been strictly comparable due to the different instrumentation and experimental set-up used to accentuate the respective behaviors.

The dynamic mechanical behaviour of the fully cured resins and IPNs were measured with a Rheometrics RDAII (rectangular specimens in torsion) or a Rheometrics Mark IV DMTA (rectangular samples in dual cantilever flexure). In the dual cantilever bending test, both ends of the sample are clamped to a rigid frame and the drive shaft was clamped to the center of the sample (see Figure 4.6). The glass transition temperature was determined by the maximum in  $\tan\delta$  at 1 Hz in the dynamic mechanical thermal analysis spectrum. The modulus of the rubbery region was measured at 50°C above the glass transition temperature of the sample. Bar samples of thickness ca 1mm and width ca 6mm were tested in both Rheometrics torsion and flexure setups. The bar samples were cured for 24 hours at 70°C and then postcured at 180°C for 2 hours (except where otherwise stated). All DMTA experiments of the fully cured materials were repeated to ensure reproducibility. The error of the modulus was estimated to be ca.  $\pm 5$ -10 %.

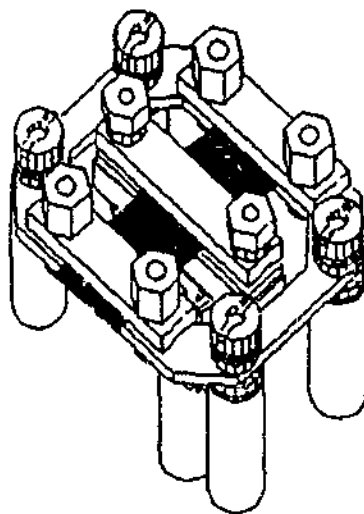


**Figure 4.6 Dual Cantilever Bending test frame with sample.**

## 4.5 Density Measurements

The densities of a selection of fully cured resin systems (to be used in the SANS study) were measured using a Micrometrics pycnometer. The pressure attained by the fill and purge cycle was 17.5 psi. Approximately 2g of cured resin (dried at 50°C under vacuum for 12h) weighed to an accuracy of  $\pm 0.01$ mg was sealed in the pressure chamber prior to measurement. An average of 10 measurements of the density were taken of each sample.

## 4.6 Small Angle Neutron Scattering (SANS)

SANS experiments were performed at NIST\*. The 8m SANS spectrometer was configured to a sample-detector distance of 3.6m, off centre angle of 3.5°, with a central incident neutron wavelength of 12 Å (25% spread). The momentum transfer range probed was  $0.0006 \text{ \AA}^{-1} < Q < 0.09 \text{ \AA}^{-1}$ . The data was reduced to absolute differential cross section per unit volume (in  $\text{cm}^{-1}$ ) by calibration using a porous silicon standard of known differential cross-section. The background scattering (without a sample in the beam line), scattering due to stray neutrons and cosmic radiation (beamline blocked with cadmium-strong neutron absorber) and incoherent scattering (predominantly due to the hydrogen nuclei in the sample) were removed from the scattering data using the IgorPro software attached to the SANS spectrometer. SANS was performed on plate samples of the resins (thickness of 0.2mm to 0.3mm) which were machined from samples (thickness 2mm) which had been cured for 24 hours at 70°C and then postcured at 170°C for 2 hours (with exception to the VER/AIBN system which was only postcured to 150°C for 2 hours).

## 4.7 Water Uptake of Cured Resins

Samples for water uptake were prepared from plate samples of ca 1mm thickness were cured for 24 hours at 70°C and then postcured at 170°C for 2 hours, with

---

\* The SANS experiments and data reduction was kindly performed at NIST, Gaithersburg by Dr Min Lin on samples formulated and prepared by the author.

the exception of the VER/AIBN system, which was only postcured to 150°C for 2 hours. After complete curing (confirmed by repeating DSC scans for the  $T_g$ ) the samples were machined into rectangular samples of dimension 1cm×2cm. Prior to water sorption testing the samples were dried in a vacuum oven at 50°C.

The water sorption tests were carried out at ENSAM, Paris by Dr Ilhame Merdas on the samples at 75% relative humidity at three temperatures 50, 70 and 90°C. Each test was duplicated to check for reproducibility. Throughout the duration of exposure, the samples were periodically weighed using a laboratory balance with a relative precision of 0.01mg.

## 4.8 Mechanical Properties of Cured Resins

### 4.8.1 Compression Testing

IPN and neat resin samples were cured in 10mm diameter cylindrical Teflon™ molds of length 16mm<sup>218</sup> for 24 hours at 70°C, then postcured at 170°C for 2 hours. The samples were then cooled slowly over a period of 4 hours before being de-molded.

The uniaxial compression yield experiments were performed at 22±2°C using a Instron 4504 mechanical testing instrument with a 1 kN load cell with strain rates of 0.588, 0.0588 and 5.88×10<sup>-3</sup> min<sup>-1</sup> (corresponding to crosshead speeds from 10 to 0.1mm/min). The Instron 4504 was calibrated and balanced using the Instron Merlin software internal balance and calibration program. The Young's modulus was determined from the initial linear region of the stress-strain curve – a minimum of 4 repeat samples were tested. The modulus results were corrected for internal compliance of the rig using a method described by Cook *et al.*<sup>219</sup>. The true sample stiffness  $K_S$  was related to the apparent stiffness of the sample  $K_A$  by the equation:

$$\frac{1}{K_S} = \frac{1}{K_A} + \frac{1}{K_R} \quad \text{Equation 4.8}$$

Here  $K_R$  is the stiffness of the rig in compression (using a parallel sided steel specimen having high stiffness) and was measured to be 4.1×10<sup>4</sup> Nmm<sup>-1</sup>. However, since the stiffness of the polymer sample was significantly lower than the stiffness of the steel

specimen used to obtain  $K_R$ , the correction factor was small. The average yield stress (determined from a minimum of 4 samples tested) for samples at each different strain rate was defined as the point where the stress passed through a maximum or otherwise as the obvious knee in the stress-strain plot.

### 4.8.2 Flexural Testing

Flexural testing was completed on specimens of dimensions 2mm×10mm×25mm using the same curing procedure as the DMTA samples. Testing was performed using a small, steel, three point bend setup as illustrated in Figure 4.7 in accordance with the ASTM standard<sup>220</sup>. The flexural strength was calculated using Equation 4.9:

$$\sigma = \frac{3Fl}{2bd^2} \quad \text{Equation 4.9}$$

where  $F$  is the force at break,  $l$  is the span length,  $b$  is the width of the sample and  $d$  is the thickness of the sample.

The flexural modulus was calculated from the force-displacement curve using Equation 4.10:

$$E = \frac{Fl^3}{4bd^3x} \quad \text{Equation 4.10}$$

Where  $F$  is the load measured in the linear region of the curve at displacement  $x$ . Testing was performed at  $22\pm 2^\circ\text{C}$  on an Instron 4504 mechanical testing instrument at a crosshead speed of 0.2mm/min, with a minimum of 3 samples used for each material.

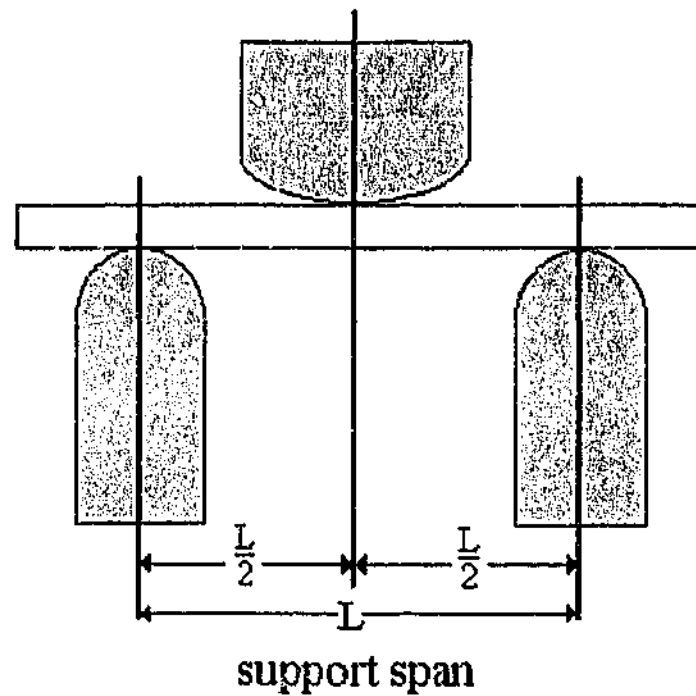


Figure 4.7 Loading nose and support diagram for 3 point bending test setup

### 4.8.3 Error Analysis

A minimum of four specimens per sample, were used in the compression and flexural tests. The average and the standard deviation (Std. Dev.) were calculated for  $n$  samples and are represented in Tables 10.3 and 10.4.

$$\text{Std. Dev.} = \sqrt{\frac{n \sum x^2 - (\sum x)^2}{n(n-1)}}$$

Equation 4.11

# *Chapter 5*

## *Kinetics of Formation of networks*

---

### **5.1 Aliphatic and Aromatic Amines based IPNs**

#### **5.1.1 Introduction**

The cure behaviour of a series of IPNs formed from a model VER and an amine cured epoxy resin has been studied by scanning DSC and isothermal mid-FTIR. This study of semi- and full-IPNs and numerous combinations of the components within them, gives an important understanding of the possible interactions between the VER and the epoxy, potential grafting reactions, effects of dilution, plasticization and vitrification, all of which are essential in building a solid base of knowledge of IPNs and understanding their structure-property relationships.

#### **5.1.2 Differential scanning calorimetry of IPN cure and extraction studies**

##### **(a) AIBN initiated systems**

The scanning DSC of the An- and DDM-cured DGEBA and the AIBN-initiated VER are shown in Figure 5.1 The two epoxy systems show single broad exotherms at

159 and 138°C respectively— the reason for this difference in cure temperatures is due to an induction effect, attributable to *para*-substitution of alkyl groups on aniline as discussed by Wise *et al.*<sup>16</sup>. The heats of polymerization for the neat DGEBA/An and DGEBA/DDM were 421 J/g and 373 J/g corresponding to 97.4 kJ/mol and 87.5 kJ/mol, which were similar to the energy involved in opening the epoxy ring during cure reported by Barton<sup>221</sup> for the DGEBA/DDM system (91.4 kJ/mol) and close to that found by Wise *et al.*<sup>16</sup> during the cure of epoxy/diamine systems (98-99 kJ/mol). The VER exhibits a sharp peak at 92°C with a small shoulder near 110°C - the cause for the shoulder is unclear but similar DSC traces have been observed previously for VER resins<sup>17</sup>. Based on the heat of polymerization for methyl methacrylate of 56.2 kJ/mol<sup>17,222</sup> and styrene 67.4 kJ/mol<sup>17,223</sup>, the theoretical heat of copolymerization of the VER was calculated as 340.7 J/g (based on a bisGMA molecular weight of 490 g/mol obtained by titration – see Section 3.2). The observed heat of polymerization of VER/AIBN was 327 J/g, suggesting 96% cure. The scanning DSC curing traces of the semi-IPN of AIBN/VER:DGEBA:An and the full-IPN of AIBN/VER:DGEBA/DDM are also shown in Figure 5.1. The DSC traces of the IPN systems appear to show two exothermic peaks: one narrow peak superimposed over a much broader peak, corresponding in part to the cure of the VER and of the epoxy-amine network, respectively. The VER/AIBN peak at 97 and 102°C in the IPNs is shifted to higher temperatures than in the parent VER/AIBN (92°C) as a result of reduced reaction rates. In a similar study of the cure of an IPN formed from diamine-cured DGEBA and a radically cured diacrylate resin, Lin and Chang<sup>5</sup> proposed a “network interlock effect” in which mutual entanglements between the two polymer networks produced a sterically hindered environment resulting in the reduction in the rate constant of the diacrylate resin. However, it is more likely that this rate reduction is due to dilution of the reactants by the other components as suggested by Yang and Lee<sup>126</sup> (see Section 2.4.2). In contrast, the epoxy peak occurs at similar temperatures in the parent resin and the IPN. This may be due to phase separation of the epoxy component, so that the concentration of reactants in this phase are undiluted. Alternatively, this may be due to a combination of opposing factors - the effect of dilution would be to decrease the reaction rate however the preference of H-bonding OH groups on the bisGMA molecule could counter this effect as it is known that the epoxy-amine reaction is catalyzed by H-bonding groups<sup>66,73</sup> (see Section 2.2.2). The overall heat of polymerization associated with the peaks in the semi-IPN of VER/AIBN:DGEBA:An (373 J/g) and the full-IPN of VER/AIBN:DGEBA/DDM (400 J/g) corresponds closely to that expected from the

average of their constituent parent resins (see Table 5.1). In addition, the similarity of cure behaviour of the VER and epoxy components in the IPNs and in the neat resins suggests that the curing mechanism of each component is not greatly affected by the presence of the other, probably due to the lack of chemical interaction between the components of the parent systems and in particular between AIBN and the amines. This is in accord with research showing that azo compounds are generally not susceptible to chemically induced decomposition<sup>90</sup>, unlike that observed for peroxides<sup>41,86,88,90-92,224</sup>. Since the curing behaviour of the IPN is not affected by the extent of network formation *per se*, the subsequent studies of IPNs containing aromatic amine curatives were restricted to the monomeric amine species, aniline, because its liquid nature simplified the preparation of the IPN mixture.

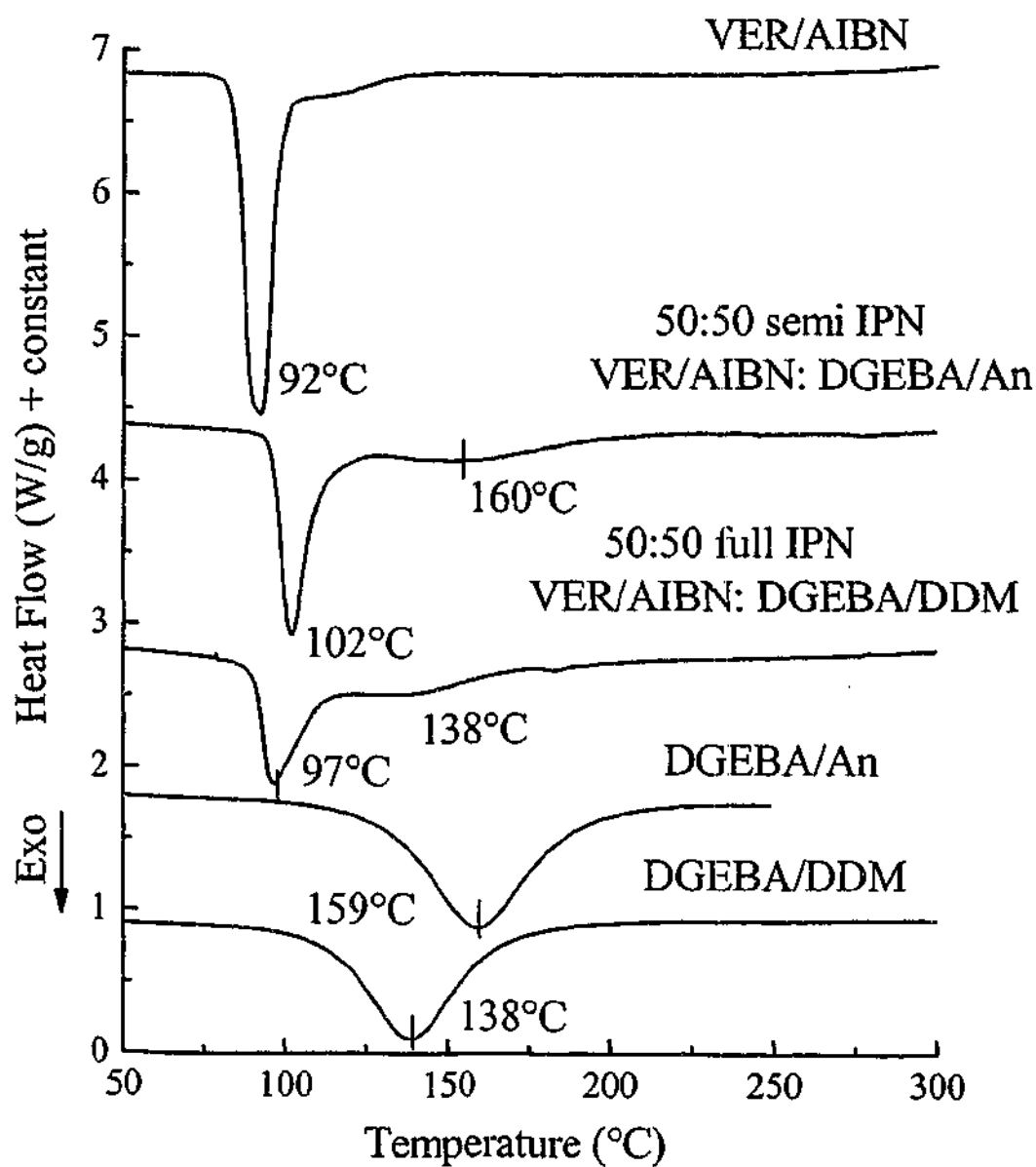


Figure 5.1 DSC scans of the 50:50 VER/AIBN:DGEBA/An semi-IPN, the 50:50 VER/AIBN:DGEBA/DDM full-IPN and the parent resin systems

Analogous to the investigations of the IPNs involving aromatic amine-cured DGEBA systems, the IPNs involving aliphatic amines of butylamine and crosslinking diamino-octane were also studied. Due to their chemical similarity, the curing behaviour of DGEBA/BA and DGEBA/DAO were almost identical as noted by Mayr *et al.*<sup>181</sup>, both exhibited broad exotherms at 90°C (Figure 5.2). The heats of polymerization for the neat DGEBA/BA and DGEBA/DAO were 398 J/g and 424 J/g corresponding to 88.1 kJ/mol and 93.7 kJ/mol, which is close to that reported in the literature on similar systems<sup>16,225</sup>. The neat VER/AIBN resins exhibited a narrow exotherm at 92°C with a corresponding exotherm of 327 J/g. Due to the proximity of the exotherm curves for the parent resins, it was not possible to comment on dilutional or catalytic effects of each component on the other. The DSC traces of the 50:50 semi-IPN and 50:50 full-IPN are similar to those obtained from the sum of the neat resin components, with the total heat of polymerization for the semi- and full-IPNs being close to that predicted from the average of the cure of the component resin systems (see Table 5.2). As a result of the similarity between the curing behaviour of the semi-IPN and full-IPN, further studies of IPNs containing aliphatic amine curatives were restricted to the monomeric amine species, butylamine, because its liquid nature simplified the preparation of the IPN mixture.

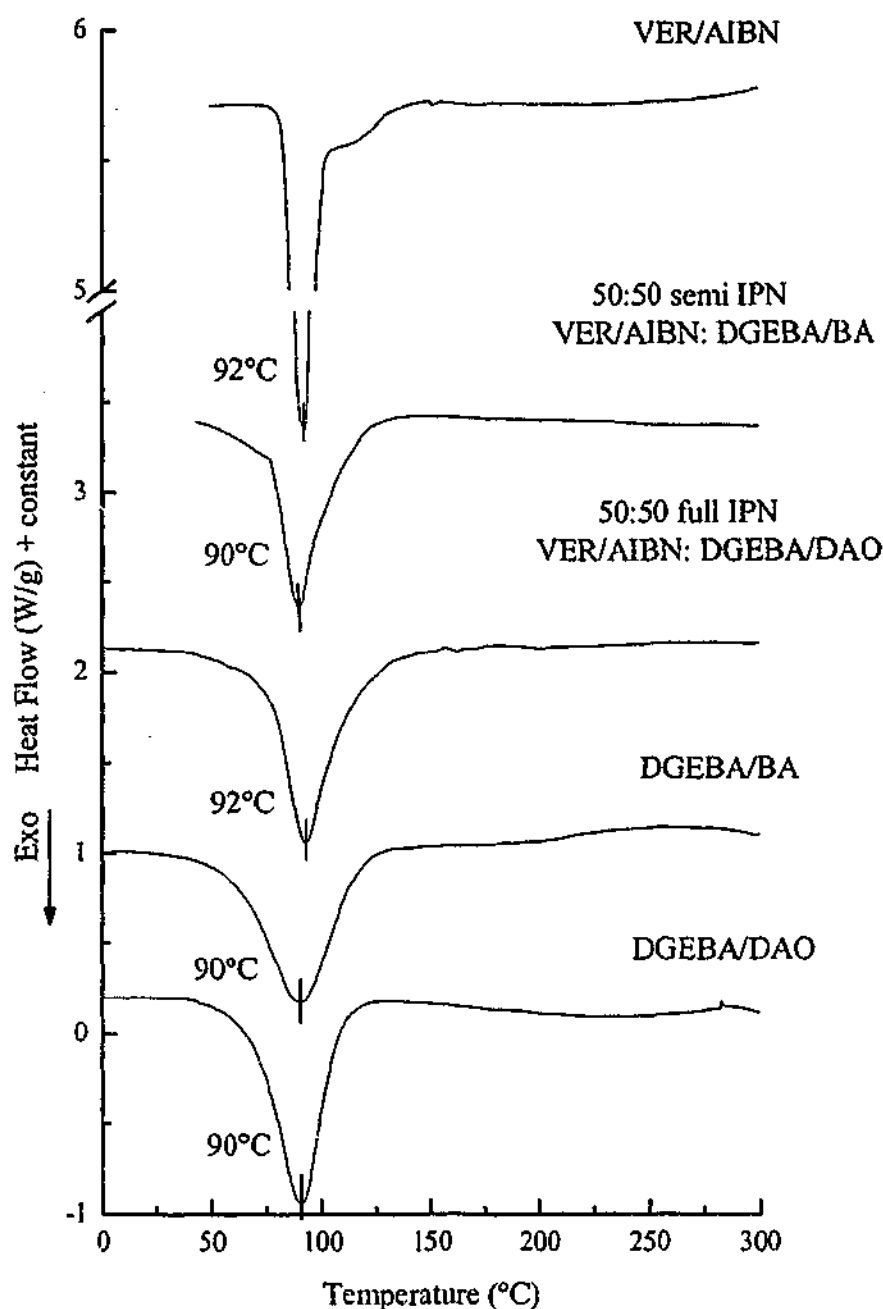


Figure 5.2 DSC scans of 50:50 VER/AIBN:DGEBA/BA, semi-IPN, 50:50 VER/AIBN

To provide further information of the curing behaviour in the IPNs, studies were made of IPN systems containing only some of the components. For example, a DSC scan of the VER/AIBN:BA combination (see Table 5.2) - where the weight fractions of components is as in the IPN except that it contains no DGEBA, indicated a quite complete exotherm attributable to the VER exhibiting a total heat of polymerization (309 J/g for the VER/AIBN component, allowing for the dilution of the resin by BA) which is close to that expected for full polymerization of the neat VER/AIBN system (327 J/g). However some evidence of potential grafting reactions between the IPN components can be observed. For example, the initiator-free systems bisGMA:An and

bisGMA:BA (which are analogs to VER/AIBN:DGEBA/An and VER/AIBN:DGEBA/BA) should not show significant reaction of the methacrylate groups since thermal cure of VER in the absence of radical initiator was found to require temperatures above 200°C. However mid-FTIR spectroscopy indicated that a reaction occurred at 70°C, leading to a consumption of methacrylate groups, as shown in Figure 5.3. This reaction is presumably the Michael addition<sup>130</sup>, in which a nucleophile (the amine) attacks the electron deficient double bond (the methacrylate group) followed by the transfer of a proton. The Michael reaction between secondary amino hydrogen and the fumarate double bond in unsaturated polyester resins is well documented<sup>130-132</sup> - see Section 2.4.2. Investigations of epoxy/polyester IPNs by Subramaniam and McGarry<sup>3</sup> indicated a significant amount of intersystem grafting occurred partially due to the Michael's addition reaction between the amine curative for the epoxy and the double bonds of the polyester. A schematic of grafting of the epoxy and dimethacrylate due to the Michael's addition is outlined in Figure 5.4. The extent of methacrylate reaction in the bisGMA:BA system is higher than for bisGMA:An - this is what would be expected for Michael addition because the aliphatic amine is a stronger base<sup>226</sup>. A comparison of the curing kinetics of the VER component in the IPN with the bisGMA/amine reaction suggest that although the consumption of methacrylate double bond due to the Michael reaction is less than that due to free radical polymerization by AIBN, it is still significant. It is interesting to note that despite the approximately equimolar ratio of NH and methacrylate groups present in these systems, cure at 70°C for 24 h did not produce complete reaction of the methacrylate groups in the bisGMA/amine systems and that postcure at 150°C for 3h only resulted in approximately 20% conversion.

The un-grafted epoxy component in the postcured 50:50 semi-IPNs of VER/AIBN:DGEBA/BA and VER/AIBN:DGEBA/An was extracted with chloroform (as described in Section 4.3) and it was found that, after 24 hrs of extraction, 22.2 wt% of the epoxy component was grafted to the VER network in the VER/AIBN:DGEBA/BA semi-IPN and 5.3 wt% of the epoxy component was grafted to the VER network in the VER/AIBN:DGEBA/An semi-IPN. The higher grafting in the VER/AIBN:DGEBA/BA IPN than in the VER/AIBN:DGEBA/An IPN is qualitatively consistent with the higher infra-red conversions of vinyl groups for the bisGMA/BA system than the bisGMA/An system as shown in Figure 5.3.

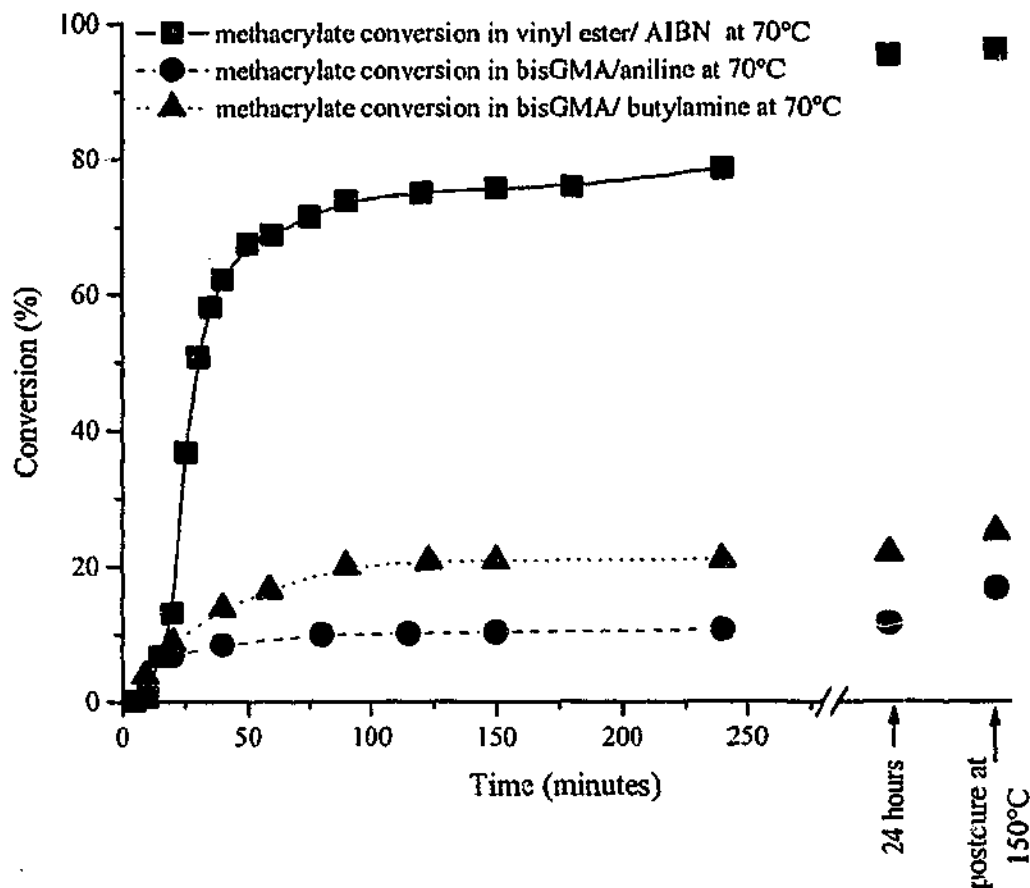


Figure 5.3 Mid-FTIR methacrylate conversion (measured from the decrease in methacrylate absorption at  $1645\text{cm}^{-1}$ )<sup>\*</sup> versus time for the VER/AIBN, bisGMA/BA and bisGMA/An at  $70^\circ\text{C}$ .

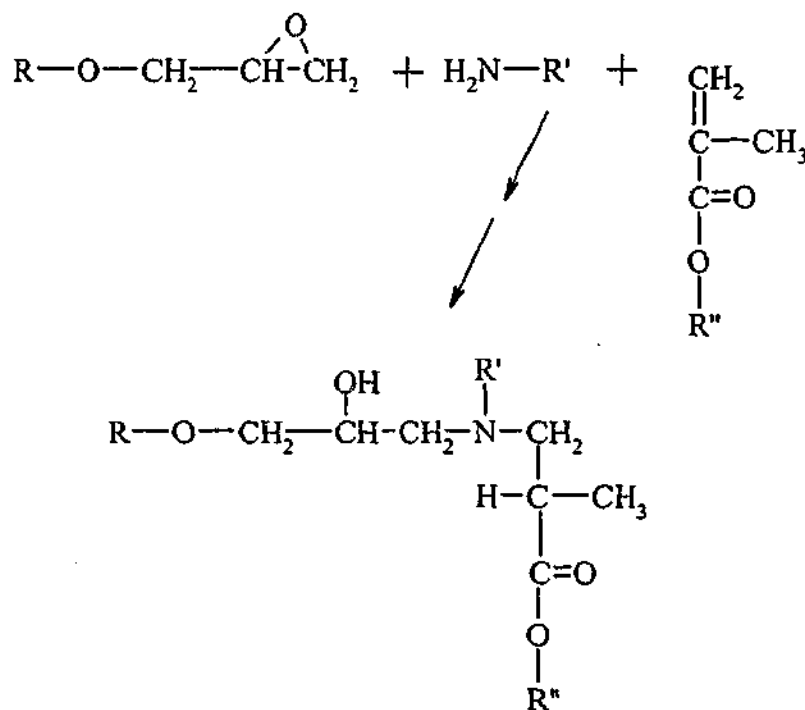
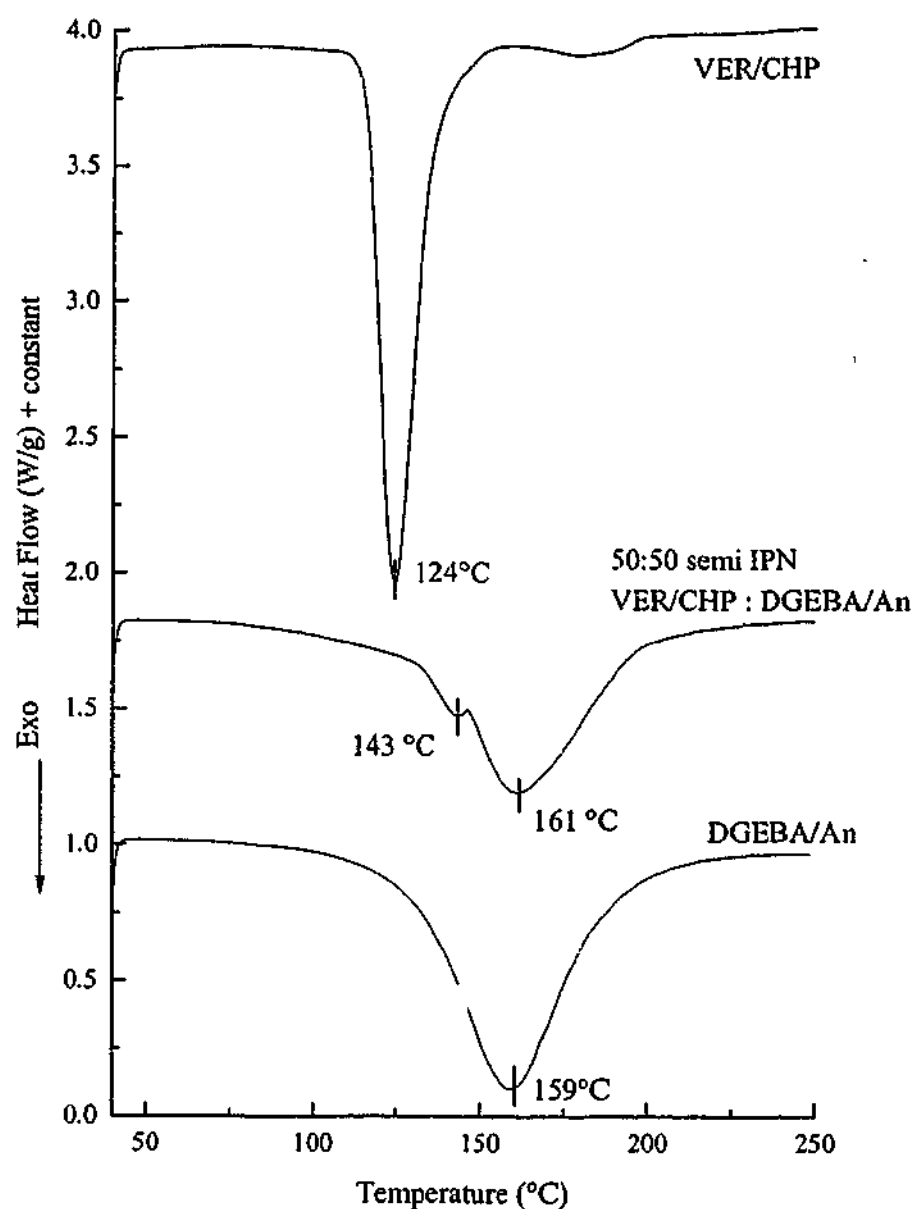


Figure 5.4 Schematic of the Michael's addition of an amine across the methacrylate unsaturation leading to grafting of the epoxy and dimethacrylate networks.

<sup>\*</sup> Please note that the Michael addition reaction was not quantitatively followed by the consumption of amine groups at  $3500\text{cm}^{-1}$  as indicated previously<sup>3,4</sup> due to the overlapping absorptions of the hydroxy groups of the bisGMA which were also present in this region.

**(b) CHP initiated systems**

The VER/CHP:DGEBA/An system shows two DSC exothermic curing peaks (Figure 5.5) which are similar to the DSC peaks found for the VER/AIBN:DGEBA/An system (Figure 5.1), except that the first peak in the VER/CHP:DGEBA/An semi-IPN is much smaller. The dominant curing exotherm at 161°C in the IPN corresponds to that of the DGEBA/An component, which exhibits a peak at 159°C in the parent resin. The invariance of the epoxy peak temperature in the IPN and the neat resin, indicates a constant epoxy cure rate, and as discussed above may be due to the combination of a rate reduction due to dilution in the IPN and the rate acceleration due to the catalytic effect of H-bonding of the epoxy-amine transition state<sup>66,73,224</sup> with the bisGMA hydroxy groups (see Equations 2.16-2.20) or due to the similar effect of the dimethyl benzyl alcohol in the CHP solution or phase separation. The smaller peak observed at 143°C attributed to vinyl polymerization in the IPN DSC trace occurs at a significantly higher temperature than that in the neat VER/CHP resin (125°C), indicating a reduction in the VER cure rate. This may be due to a dilutional effect from the DGEBA and/or due to a reduction of the activity of the CHP. The latter may be caused by redox interactions between the peroxide and the amine - it is known that in some cases amines can catalyze the decomposition of peroxides<sup>41,86,88,90-92,224</sup> to radicals but perhaps in the present case, the redox reaction may result in non-radical products which causes a reduction in radical formation. The total heat of polymerization for the IPN (378 J/g) is very close to the average of the individual components (370 J/g), suggesting that full cure can be obtained for this system under reasonable curing conditions.



**Figure 5.5 DSC scans of the CHP-initiated VER, the An-cured DGEBA and the 50:50 VER/CHP:DGEBA/An semi-IPN**

Figure 5.6 shows the DSC curing exotherms for the 50:50 VER/CHP:DGEBA/BA system. In this particular semi-IPN, the DGEBA/BA cures faster than the VER/CHP and so the first exotherm peak of the 50:50 IPN represents the partial cure of the epoxy component. The second DSC peak at 136°C presumably represents the partial cure of the VER network by CHP-derived radicals. However, this system appears to have significant inter-component interaction. A broad exothermic peak is observed in the IPN at 220°C, which may be attributed to thermal cure of the VER resin. This assignment is confirmed by the DSC scan of VER:DGEBA/BA (omitting the peroxide) which shows the peak cure of the epoxy at 89°C (with an exotherm of 202 J/g corresponding to complete cure of DGEBA/BA) and a broad exotherm at 220°C which is close to the exotherm found during non-catalyzed thermal

cure of VER (see Figure 5.6 and Table 5.2). This thermal cure of residual vinyl groups in the complete IPN system indicates that the CHP has been unable to fully cure the VER component, perhaps due to catalytic decomposition of CHP by butylamine, causing a significant loss of radicals. It is interesting to note that even after scanning up to 300°C, the IPN is not fully cured as shown by the small heat of polymerization (259 J/g, Table 5.2) compared with the expected average value of the parent resins (358 J/g). One possible explanation for the reduction in heat of polymerization is that the CHP concentration is rapidly consumed by redox reactions with the butylamine, causing premature peroxide decomposition and subsequent depletion of radicals similar to the effect of dead-end radical polymerization<sup>227-229</sup>. This is in contrast to the VER/AIBN:DGEBA/BA system which showed virtually full cure (Figure 5.2 and Table.1).

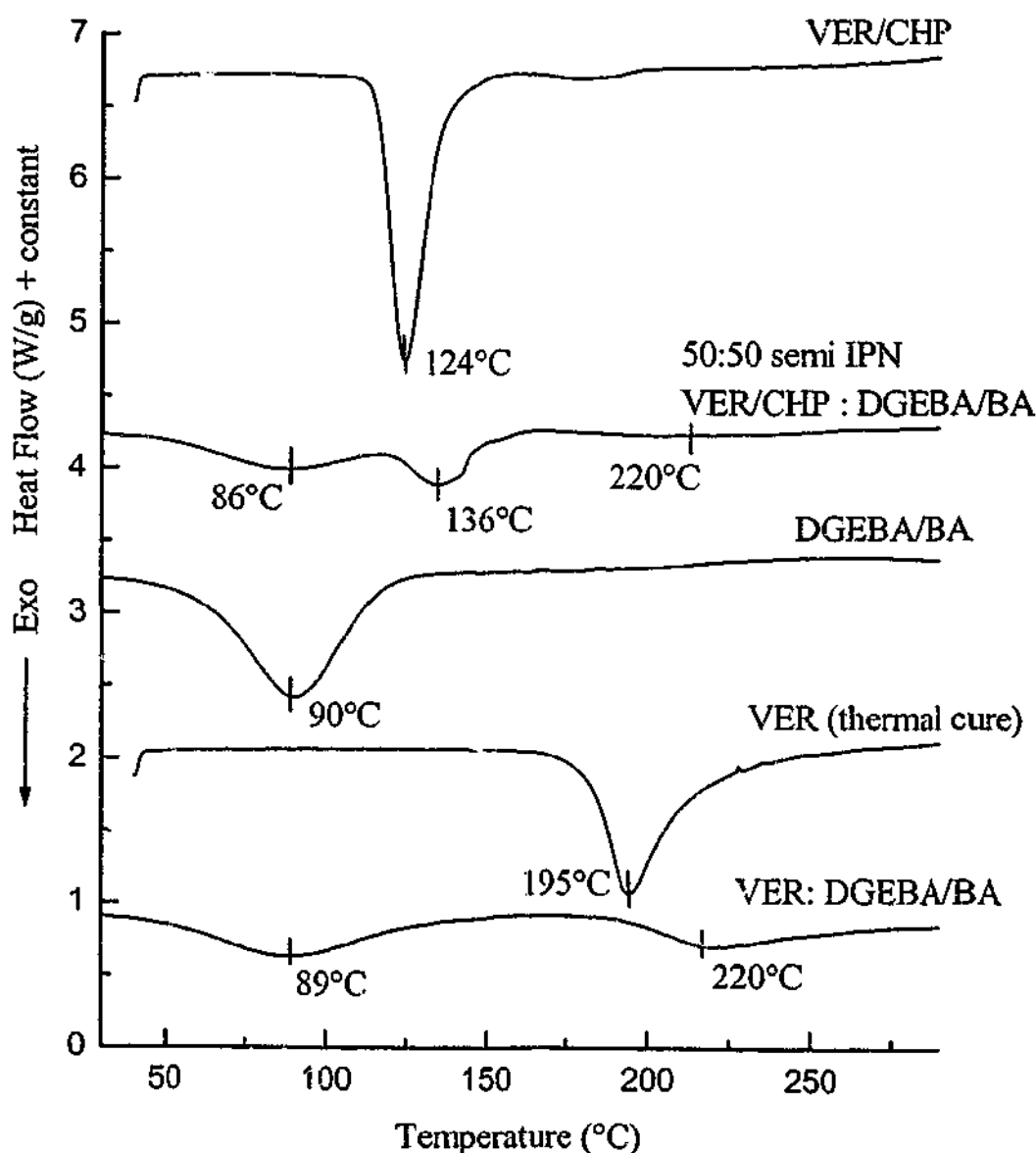


Figure 5.6 DSC scans of the VER/CHP:DGEBA/BA semi-IPN, the parent resins, the thermal cure of VER and the system VER:DGEBA/BA (without radical initiator).

**(c) BPO initiated systems**

The IPN systems containing the BPO initiated VER resin showed interesting behaviour. The 50:50 VER/BPO:DGEBA/BA semi-IPN exhibited two DSC peaks (see Figure 5.7). The lower temperature exotherm at 86°C corresponds very closely to the curing exotherm in the neat DGEBA/BA system (90°C). The shift of this peak to lower temperatures is opposite to that expected from dilution and may be due to the accelerating effect of the OH groups from the bisGMA or the water in the BPO paste. The second peak at approximately 229°C corresponds closely to that of the VER thermal curing temperature (195°C). The total heat of polymerization was measured to be approximately 249 J/g (integration range 0-275°C), which is lower than that expected from an average of the parent resins (340 J/g). As observed in the VER/CHP:DGEBA/BA system, the reduction in heat of polymerization may be due to the consumption of BPO by redox reactions with the butylamine, causing premature peroxide decomposition and subsequent depletion of radicals similar to the effect of dead-end radical polymerization<sup>227-229</sup>. The DSC traces in the semi-IPN also exhibited considerable noise above 250°C, possibly due to volatilization of unreacted species within the system and this may have effected the measurement of the heat of polymerization.

The 50:50 VER/BPO:DGEBA/An system (Figure 5.7) also exhibits two exothermic peaks, at approximately 138°C and at 213°C. The peak at 138°C (which would be expected to be due to epoxy cure) occurs at a lower temperature than the epoxy cure peak in the neat DGEBA/An (150°C), possibly due to acceleration of the DGEBA/An reaction by the bisGMA hydroxyl groups or the water stabilizer in the BPO paste. Alternatively it may be an artificial result caused by an overlap of the epoxy peak with a lower temperature peak due to partial cure of the VER. The higher temperature curing exotherm in the IPN corresponds closely to the thermal VER cure (195°C - see Table 5.2). The total heat of polymerization was measured to be 260 J/g (integration range 25-275°C), which is lower than that expected from an average of the parent resins (352 J/g). Similar to the VER/BPO:DGEBA/BA system, the reduction in heat of polymerization may be due to the consumption of BPO by redox reactions with the amine (in this case aniline), causing premature peroxide decomposition and subsequent depletion of radicals similar to the effect of dead-end radical polymerization<sup>227-229</sup>.

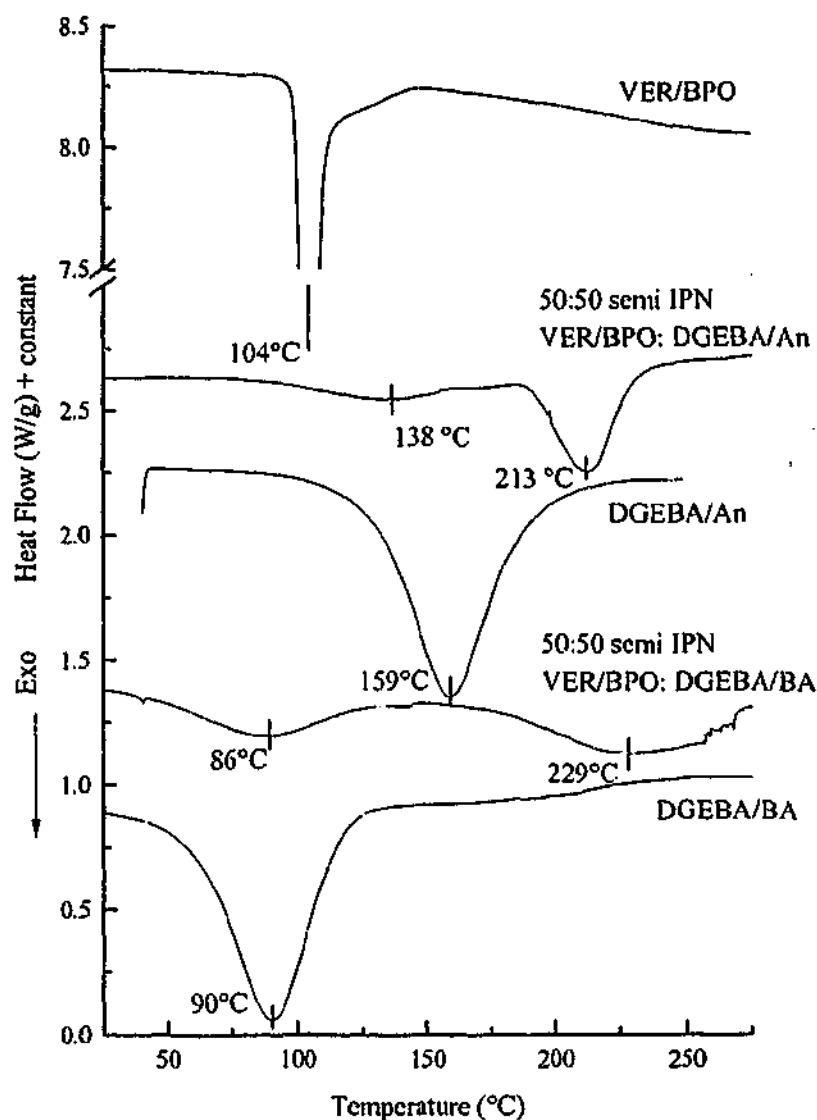
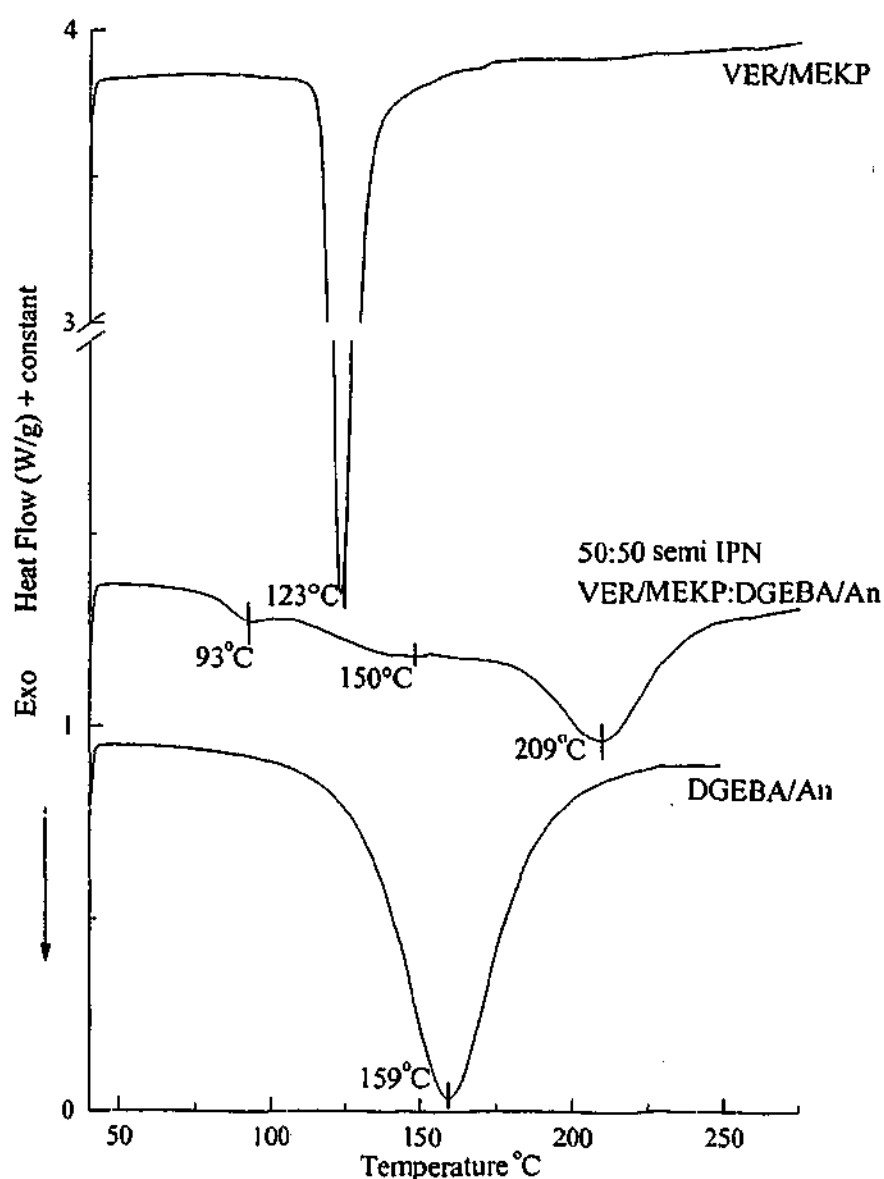


Figure 5.7 DSC scans of the 50:50 VER/BPO:DGEBA/An and VER/BPO:DGEBA/BA semi-IPNs and the parent resins.

#### (d) MEKP initiated systems

The DSC scan of the VER/MEKP system (Figure 5.8) shows a sharp exotherm at 123°C while DGEBA cured with aniline exhibits a broad exotherm at 159°C. The 50:50 blend of the two systems has a very broad exotherm region with overlapping peaks at 93°, 150° and 209°C, suggesting that complex interactions have occurred between the components. The first peak may be due to the cure of VER by the accelerated decomposition of MEKP by aniline – Many workers<sup>41,86,88,90-92,224</sup> have reported that aromatic amines can undergo a redox reaction with peroxides, resulting in enhanced radical production. The second peak at 150°C may be associated with the DGEBA/An cure, perhaps accelerated by the bisGMA hydroxyl groups, as discussed above. The final peak at 209°C may be due to thermal cure of the VER components due

to premature loss of radical initiator in the early stages of the VER cure. The total heat of polymerization of the IPN is 380 J/g, which is similar to the average of the enthalpies of the pure systems (370 J/g), suggesting that full cure has been attained, but only after high temperature cure (up to 275°C), with a significant contribution to this exotherm pertaining to the high temperature thermal curing of VER.



**Figure 5.8** DSC scans of the 50:50 VER/MEKP:DGEBA/An semi-IPN and the parent resins.

The scanning DSC of DGEBA cured with butylamine (Figure 5.9) exhibits a broad low temperature DSC peak (89°C) compared with the higher temperature and narrower peak at 124°C, due to VER/MEKP cure. However the blend of the two systems produces two quite broad peaks at 89°C and 218°C. The heat of polymerization for the lower

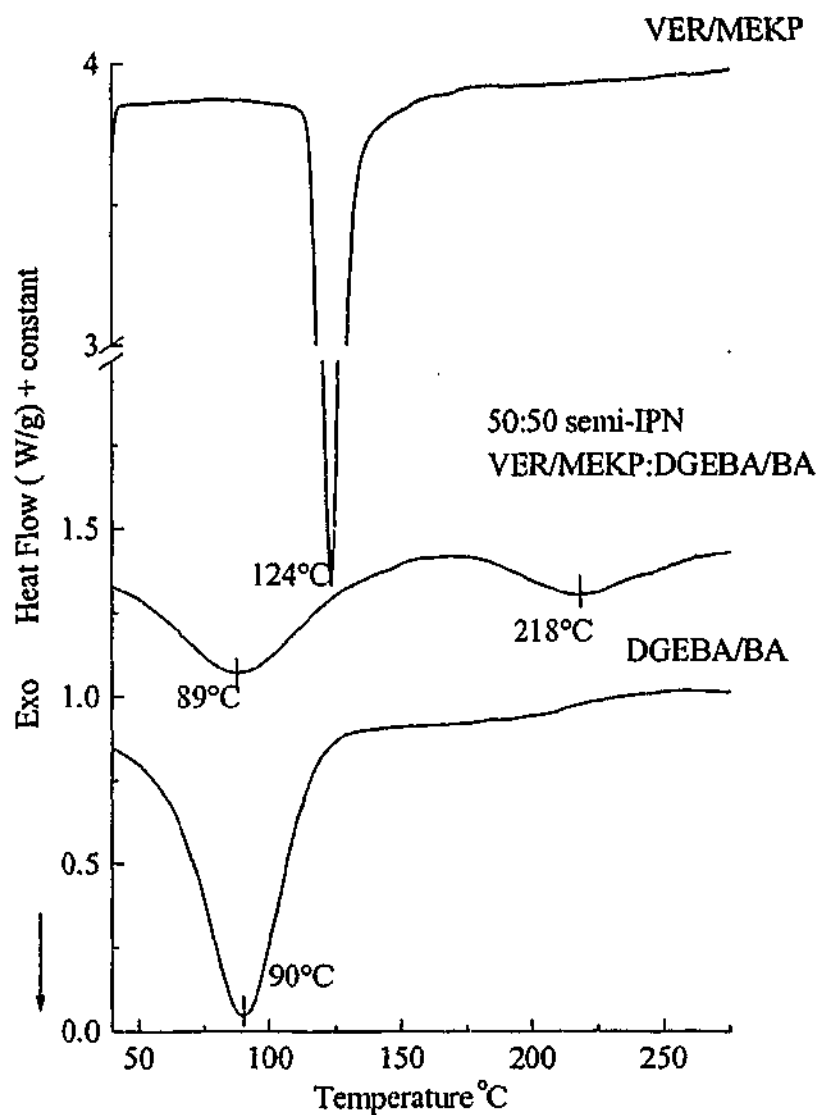


**Figure 5.9 DSC scans of VER/MEKP:DGEBA/BA and the parent resins**

temperature peak of the IPN (approximately 245 J/g) is greater than 50% (199 J/g) of the heat of polymerization of the DGEBA/BA system, suggesting that partial cure of the VER component is also occurring within this lower temperature peak at temperatures much less than for neat resin. Such behaviour has been suggested above for the VER/MEKP:DGEBA/An and possibly the VER/BPO:DGEBA/BA system. One possible explanation of the apparent absence of a separate peak due to MEKP cure of the VER may be the amine-accelerated peroxide decomposition<sup>41,86,88,90-92,224</sup> as discussed previously. The presence of a residual exotherm peak at 218°C, which is close to the peak at 195°C found in the thermal cure of VER without initiator (Table 5.2), suggests that the redox reaction between the MEKP and BA causes premature depletion of the peroxide (occurring at ca 90°C) before full VER cure is attained and that further thermal cure of the VER component occurs at 218°C. The total heat of polymerization for the two exothermic peaks of the 50:50 semi IPN of VER/MEKP:DGEBA/BA is 317 J/g (integrated from 50-275 °C) which is less than the weighted average of the

VER/MEKP cure and the DGEBA/BA (359 J/g), suggesting a significant degree of under-curing for this particular system.

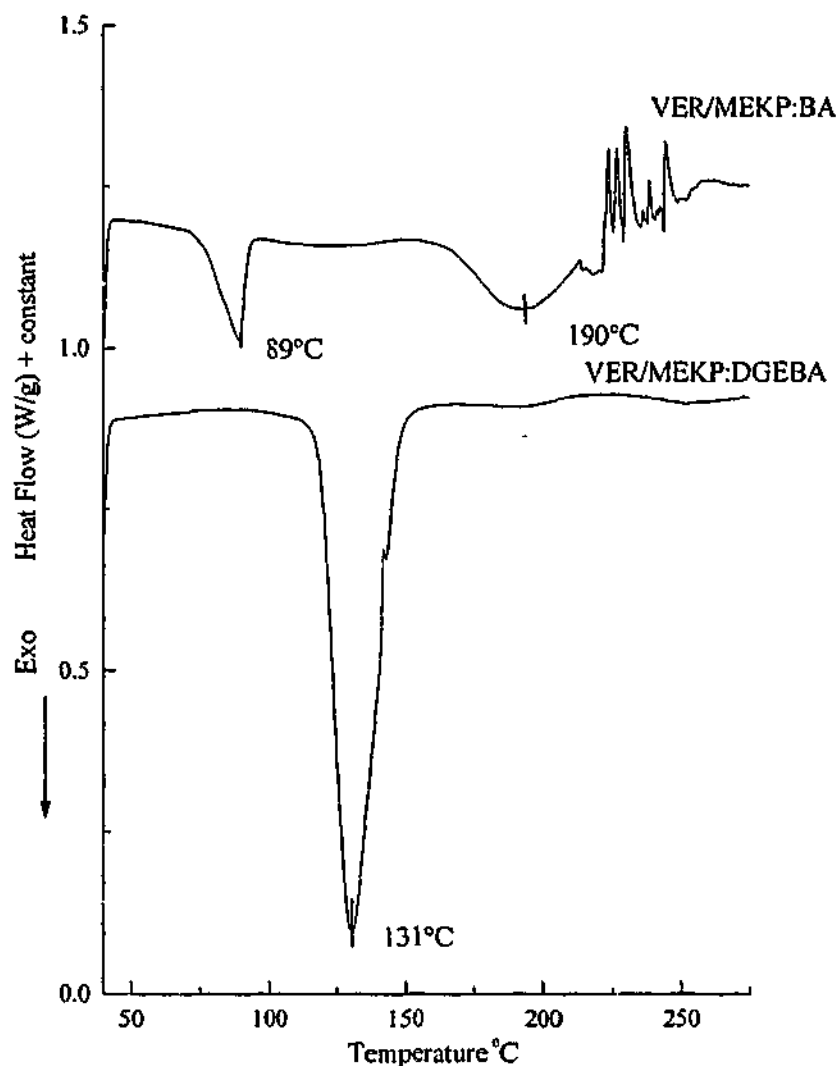


**Figure 5.10 Variations of the VER/MEKP:DGEBA/BA semi-IPN system - DSC thermograms of VER/MEKP:BA and VER/MEKP:DGEBA.**

Variations of the VER/MEKP:DGEBA/BA system were studied to provide more complete explanations for the unusual cure behaviour in this series of IPNs. The top DSC curve in Figure 5.10 shows the interfering effects of BA on the VER/MEKP cure - the first curing exotherm peak at 89°C has a heat of polymerization of only 19 J/g in comparison with the parent resin of VER/MEKP which exhibits an exotherm peak at 123°C and a heat of polymerization of 320 J/g (see Table 5.2). The second peak near 190°C in the VER/MEKP:BA system is consistent with thermal cure of the VER (c/f Figure 5.6). The DSC trace shows considerable noise above 210°C and this may be due to loss of the volatile amine by evaporation. A comparison of the VER/MEKP scan in Figure 5.9 and the VER/MEKP:DGEBA scan in Figure 5.10 also reveals the dilutional effect of uncured DGEBA resin on the cure of the VER/MEKP resin - the VER curing

peak is shifted from 124°C in the neat resin to 131°C in the DGEBA-diluted resin.

Figure 5.11 illustrates the differences between two semi-IPNs cured with and without the presence of the accelerator cobalt octoate. As discussed previously and shown in Figure 5.8, the VER/MEKP:DGEBA/An semi-IPN exhibits a complicated DSC curve with peaks at 93°, 150° and 209°C. When cobalt octoate is included in the system, the small peak at 93°C is magnified and shifted to a lower temperature (75°C) confirming that the production of radicals from MEKP has been enhanced by the redox reaction of cobalt and MEKP. However this peak at 75°C in the VER/MEKP/Co:DGEBA/An system is much smaller (approximately 21 J/g) than is observed for VER/MEKP/Co cure (321 J/g with a peak at 80°C - see Table 5.2) so that some of the activity of the MEKP must have been lost by interactions with aniline. In contrast, the VER/MEKP:DGEBA/BA system showed similar DSC curves with and without Co indicating that much of the MEKP activity was destroyed by side reactions with the amine with the result that the thermal cure of the dimethacrylate was the main cure mechanism.

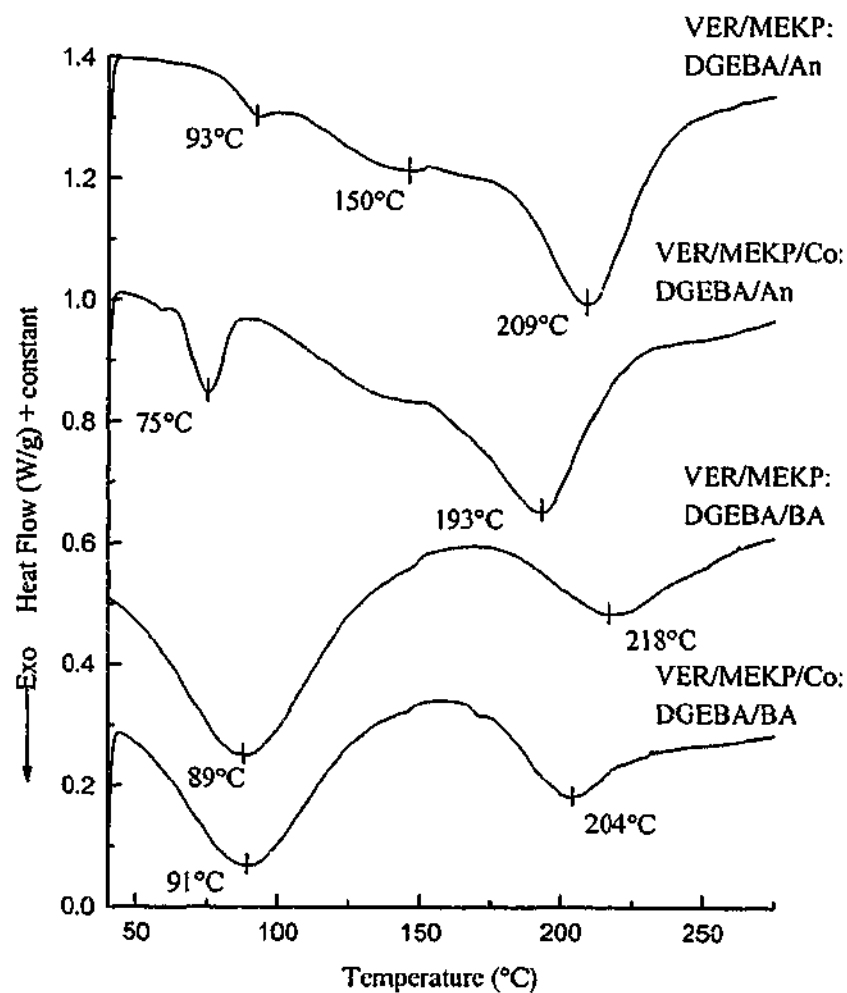


Figure 5.11 The effects of cobalt octoate accelerator on the scanning DSC cure of VER/MEKP/Co:DGEBA/An and VER/MEKP/Co:DGEBA/BA

**Table 5.1 Heat of polymerization and peak temperatures for individual peaks for IPNs involving aromatic amine-cured epoxies**

System	Curing Peak (°C)	$\Delta H$ (J/g)	Integration range (°C)
<i>AIBN initiated systems</i>			
VER/AIBN	Peak 1: 92°C	327	50-275
50:50 VER/AIBN:DGEBA/An	Peak 1: 102°C Peak 2: 159°C	375	50-275
50:50 VER/AIBN:DGEBA/DDM	Peak 1: 97°C Peak 2: 133°C	400	50-275
DGEBA/An	Peak 1: 159°C	421	50-250
DGEBA/DDM	Peak 1: 138°C	373	50-250
<i>CHP initiated systems</i>			
VER/CHP	Peak 1: 125°C	318	50-250
50:50 VER/CHP:DGEBA/An	Peak 1: 143°C Peak 2: 161°C	378	
DGEBA/An	Peak 1: 159°C	421	50-250
<i>BPO initiated systems</i>			
VER/BPO	104°C	283	50-200
50:50 VER/BPO:DGEBA/An	Peak 1: 138°C Peak 2: 213°C	260	25-275
DGEBA/An	Peak 1: 159°C	421	50-250
<i>MEKP initiated systems</i>			
VER/MEKP	123°C	320	45-275
VER/MEKP/Co	80°C	321	45-275
50:50 VER/MEKP:DGEBA/An	Peaks at: 93°C, 50°C, 209°C	380	
50:50 VER/Co/MEKP:DGEBA/An	Peak 1: 75°C Peak 2: 193°C	Peak 1: 21 Peak 2: 280	45-275
DGEBA/An	Peak 1: 159°C	421	50-250
<i>Other mixed systems</i>			
VER/MEKP:An	Peak 1: 90°C Peak 2: 220°C	Peak 1: 12 Peak 2: 94	45-275
VER/MEKP/Co:An	Peak 1: 84°C Peak 2: 181°C	Peak 1: 84 Peak 2: 36	45-275
VER/Co:An	Peak 1: 190°C Decomposition of volatiles at 250-260°C	218	50-275
MEKP/Co:DGEBA/An	151°C	444	45-275
MEKP:DGEBA/An	149°C	449	45-275
VER:An	190°C	195	45-275

**Table 5.2 Heat of polymerization and peak temperatures for individual peaks for IPNs involving aliphatic amine-cured epoxies**

System	Curing Peak (°C)	$\Delta H$ (J/g)	Integration range (°C)
<i>AIBN initiated systems</i>			
VER/AIBN	Peak 1: 92°C	327	50-275
50:50 VER/AIBN:DGEBA/BA	90°C	379	45-275
50:50 VER/AIBN:DGEBA/DAO	92°C	395	0-275
DGEBA/BA	90°C	398	0-275
DGEBA/DAO	90°C	424	0-275
<i>CHP initiated systems</i>			
VER/CHP	Peak 1: 125°C	318	50-250
50:50 VER/CHP:DGEBA/BA	Peak 1: 86°C Peak 2: 136°C Peak 3: 205°C	259	45-275
DGEBA/BA	90°C	398	0-275
<i>BPO initiated systems</i>			
VER/BPO	105°C	283	50-200
50:50 VER/BPO:DGEBA/BA	Peak 1: 86°C Peak 2: 229°C	Peak 1: 101 Peak 2: 148	0-275
DGEBA/BA	90°C	398	0-275
<i>MEKP initiated systems</i>			
VER/MEKP	123°C	320	45-275
VER/MEKP/Co	80°C	321	45-275
50:50 VER/MEKP:DGEBA/BA	Peak 1: 89°C Peak 2: 218°C	Peak 1: 245 Peak 2: 72	50-275
50:50 VER/MEKP/Co:DGEBA/BA	Peak 1: 91°C Peak 2: 204°C	Peak 1: 162 Peak 2: 78	50-275
DGEBA/BA	90°C	398	0-275
<i>Other mixed systems</i>			
VER/AIBN:BA	96°C	324	45-275
MEKP:DGEBA/BA	89°C	390	45-275
Co/MEKP:DGEBA/BA	89°C	341	45-275
VER/MEKP/Co:DGEBA	Peak 1: 85°C Peak 2: 193°C	Peak 1: 134 Peak 2: 19	45-275
VER/MEKP/Co:BA	Peak 1: 118°C Peak 2: 197°C	Peak 1: 16 Peak 2: 42	45-275
VER/Co:DGEBA/BA	Peak 1: 91°C Peak 2: 203°C	Peak 1: 142 Peak 2: 82	45-275
VER/MEKP:BA	Peak 1: 89°C Peak 2: 190°C	Peak 1: 19 Peak 2: 40	45-275
VER/BA	Peak 1: 125°C Peak 2: 195°C	Peak 1: 20 Peak 2: 40	25-275
VER (thermal cure)	195°C	320	100-275
VER/MEKP:DGEBA	131°C	161	25-275
VER:DGEBA/BA	Peak 1: 89°C Peak 2: 220°C	Peak 1: 202 Peak 2: 108	25-275

### 5.1.3 Fourier transform infra-red spectroscopy of IPN cure

#### (a) AIBN initiated systems

Figure 5.12 shows the variation in the mid-FTIR spectrum during the cure of the VER/AIBN:DGEBA/An semi-IPN. The main change appears to be the reduction in magnitude of the methacrylate ( $1645\text{cm}^{-1}$ ), styrene ( $778$ ,  $910$  and  $1650\text{cm}^{-1}$ ) and epoxy ( $915\text{cm}^{-1}$ ) peaks as cure proceeds.

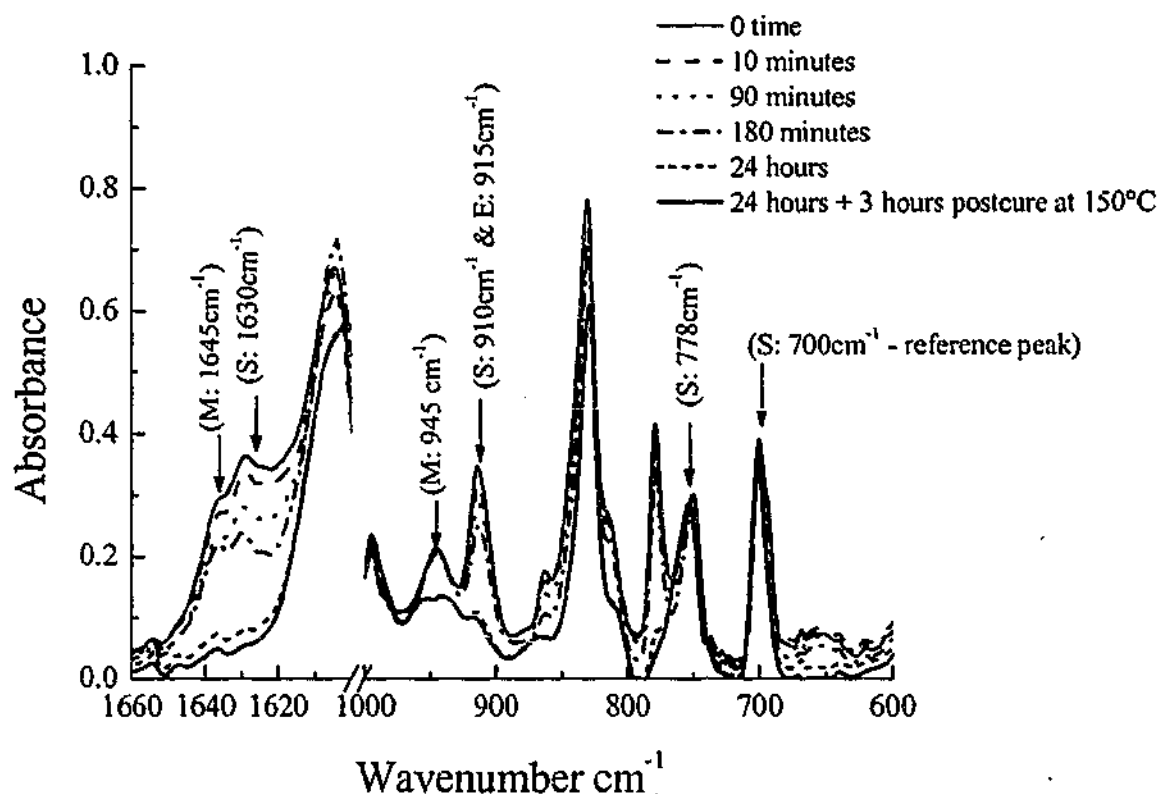
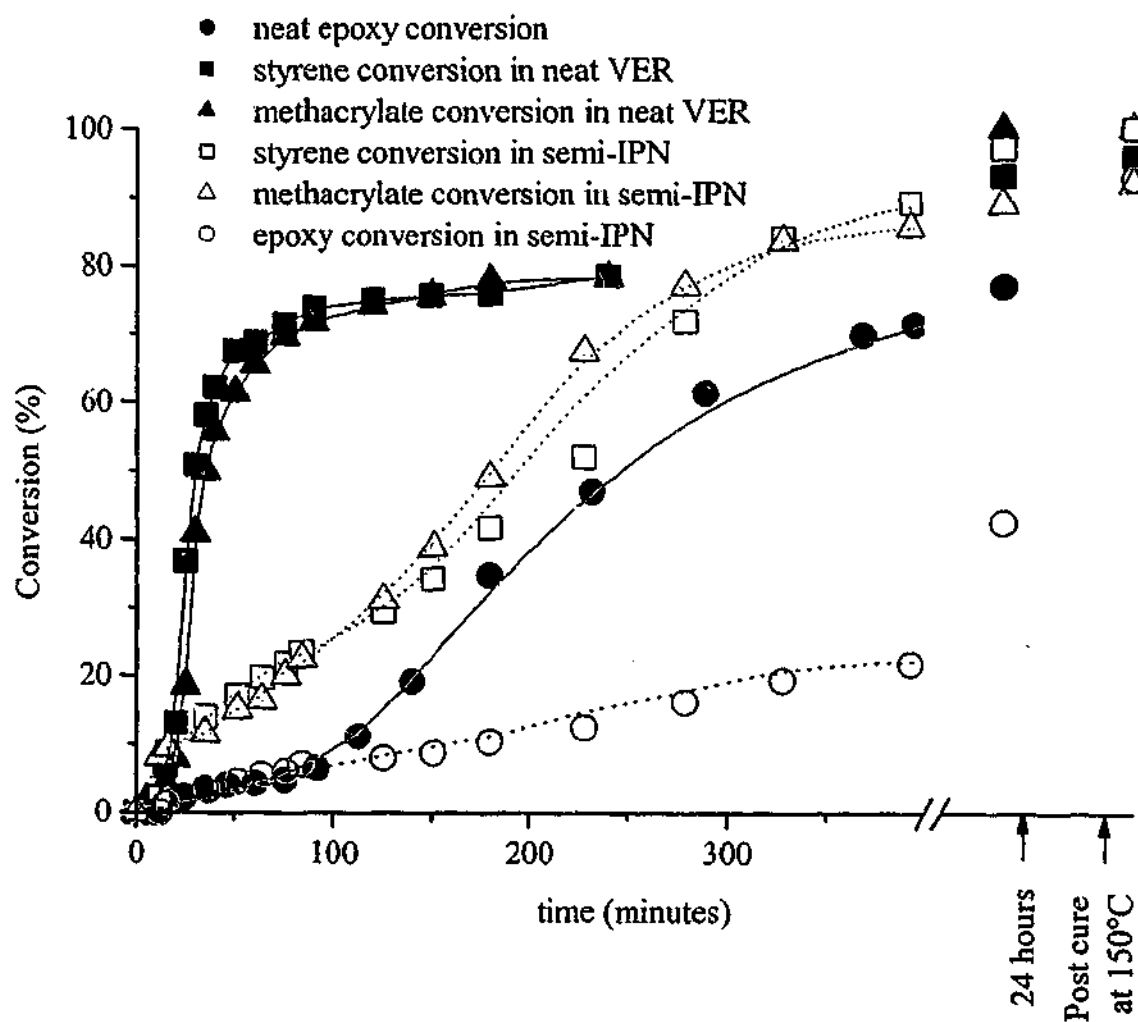


Figure 5.12. FTIR spectra for the cure of 50:50 VER/AIBN:DGEBA/An at  $70^{\circ}\text{C}$  illustrating the epoxy (E), methacrylate (M) and styrene (S) characteristic peaks.

The conversion with time of styrene, methacrylate and epoxy groups during cure of the IPN at  $70^{\circ}\text{C}$  are shown in Figure 5.13. During the isothermal cure of both the vinyl ester system and the 50:50 IPN, the styrene and methacrylate conversion data exhibit brief induction periods, presumably due to the presence of free radical inhibitors in the resins. The conversions of styrene and methacrylate groups are significantly delayed in the VER/AIBN:DGEBA/An system compared with the neat VER/AIBN system, as suggested by the DSC studies (see Section 5.2.1). The decrease in the rate of C=C conversion in the semi-IPN may be partly attributable to the dilution of the reactants by the DGEBA resin as discussed above. However after 300 minutes cure at

70°C, the IPN system exhibits a higher level of conversion of both styrene and methacrylate groups, compared with the neat VER. Since the reaction of DGEBA is very slow in the IPN, the increased conversion of vinyl groups in the IPN may be due to the presence of unreacted DGEBA in the IPN that acts as a plasticizer by enhancing mobility within the system and hence enabling a higher degree of reaction before vitrification occurs (see Section 2.1.1). This behaviour is similar to that observed by Jin *et al.*<sup>128</sup> for polyurethane-monomethacrylate/trimethacrylate IPNs. However, postcuring of the VER and of the IPN at 150°C caused almost complete vinyl conversion in both networks, confirming that the undercure of the epoxy was due to vitrification of the IPN.



**Figure 5.13** Conversion versus time for the epoxy, methacrylate and styrene in the 50:50 VER/AIBN:DGEBA/An and the parent resins at a cure temperature of 70°C

As shown in Figure 5.13, the rate of epoxy conversion in the VER/AIBN:DGEBA/An semi-IPN is very similar to that in the neat DGEBA/An system up to 100 min. The apparent similarity of epoxy cure rate up to 100 min may be the combined result of a dilutional effect and a rate accelerating effect in the IPN, discussed

above. However after 100 min, the epoxy conversion in the IPN is retarded in comparison with the neat resin, which may be due to the dominance of the dilutional effect. Close to full conversion of the epoxy was observed after postcure at 150°C which is close to the  $T_g$ s of the two components, indicating that the presence of the VER network does not produce a significant topological restraint on the cure of the epoxy.

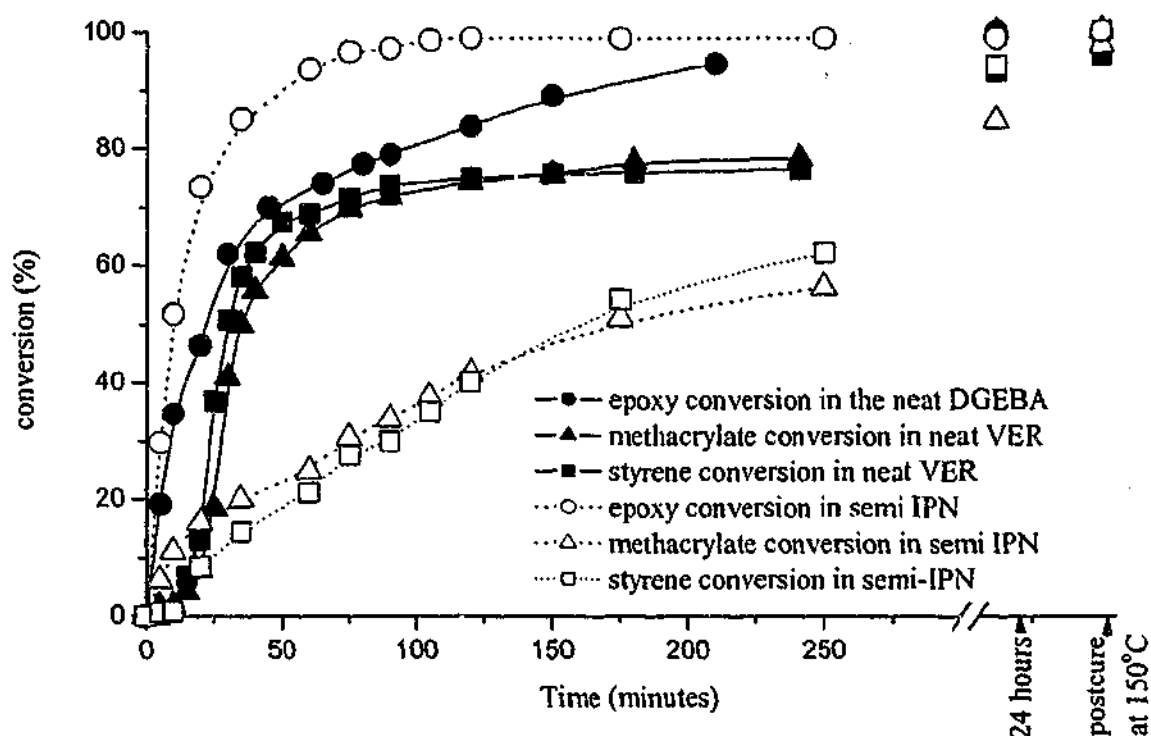


**Figure 5.14** Conversion versus time for the epoxy, methacrylate and styrene in the 50:50 VER/AIBN:DGEBA/BA semi-IPN and the parent resins at a cure temperature of 70°C

The conversion with time of styrene, methacrylate and epoxy groups for the VER/AIBN:DGEBA/BA semi-IPN is shown in Figure 5.14. The conversions of styrene and methacrylate groups are significantly delayed in the VER/AIBN:DGEBA/BA system possibly due to dead-end polymerization<sup>227-229</sup> resulting from a depletion of active radicals by their reaction with amine to form a less active species. However, this does not explain why full cure was not attained on postcure or why full cure was observed by DSC (Figure 5.2). An alternative explanation, supported by other data (see Chapter 8) is that phase separation occurs during cure, resulting in a low  $T_g$  (epoxy rich) phase and a VER rich phase. For the epoxy component, the final conversion at 70°C in the IPN and the neat resin is close to 100% because the low  $T_g$  of DGEBA/BA (67°C by DMTA) prevents vitrification in the epoxy phases (see 2.4.1 and 2.4.2). However, at 70°C the VER rich phase would vitrify prior to complete conversion (see Figure 5.14)

because its  $T_g$  is greater than the curing temperature. In confirmation of this postcuring of the VER and of the IPN at 150°C caused almost complete conversion of styrene and methacrylate groups.

### (b) CHP initiated systems

The conversion of the reactive groups at 70°C in the neat resins and the 50:50 VER/CHP:DGEBA/An semi-IPN is shown in Figure 5.15. The cure of styrene and the methacrylate groups is significantly slower in the IPN than in the VER resin, in agreement with the DSC results. The IPN and the neat VER both show full conversion of the styrene and methacrylate groups when postcured at 150°C (above the maximum  $T_g$  of the parent resins). While it was found in the VER/AIBN:DGEBA/An system that

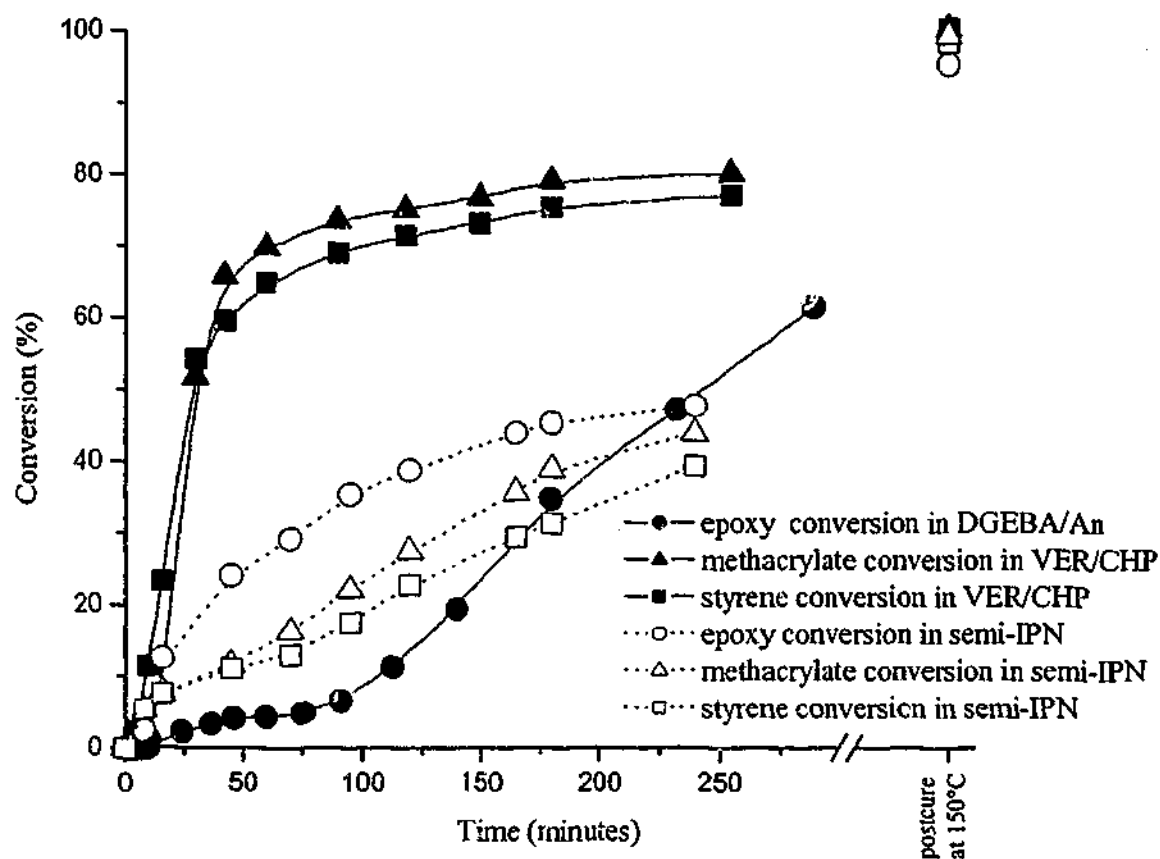


Figure 5.15 FTIR conversion versus time for the 50:50 VER/CHP:DGEBA/An and the parent resins at 70°C.

the epoxy component enhanced the VER cure through a plasticizing mechanism, in the VER/CHP:DGEBA/An system, the epoxy reacts at a similar rate to the VER components and so there are fewer small molecules able to act as plasticizers of the VER component. This may account for the lower level of cure of the VER components (c/f the VER/AIBN:DGEBA/An IPN) when cured at 70°C due to vitrification of the

## VER/CHP:DGEBA/An IPN.

The epoxy conversion is initially faster in the VER/CHP:DGEBA/An semi-IPN (Figure 5.15), than in the neat resin. As mentioned earlier, this may be a catalytic effect of the hydroxy groups in the bisGMA molecule on the diamine/epoxy reaction<sup>73</sup>, however the initial epoxy cure rate is also faster in the CHP-initiated IPN (Figure 5.15) than in the AIBN-initiated IPN (Figure 5.13) and this may be due to the additional accelerating effect of the hydroperoxy groups. After approximately 250 minutes, the cure rate of the epoxy in the IPN becomes less than the neat epoxy and this may be partly due to a dilution effect in the IPN.

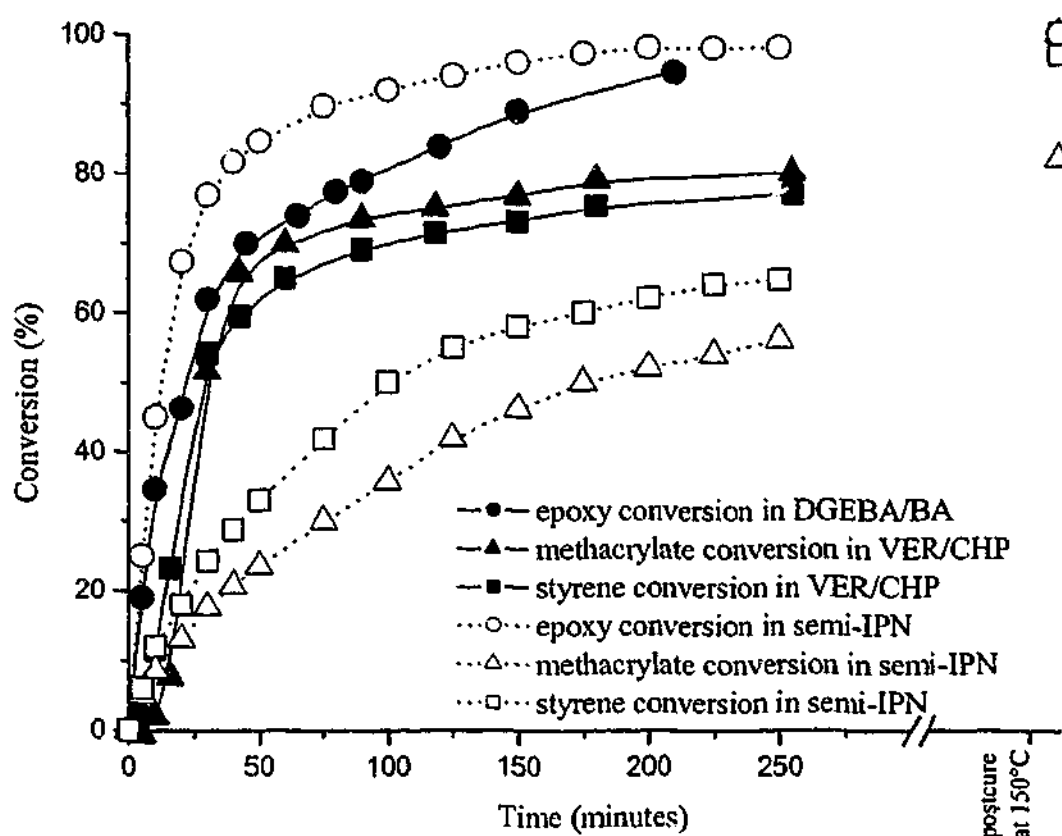


Figure 5.16 FTIR conversion versus time for 50:50 VER/CHP:DGEBA/BA and the parent resins at 70°C.

The conversion of the reactive groups at 70°C in the neat resins and the 50:50 VER/CHP:DGEBA/BA semi-IPN is shown Figure 5.16. The conversions of styrene and methacrylate groups are significantly delayed in the VER/CHP:DGEBA/BA system possibly due to the vitrification of the epoxy network at the curing temperature of 70°C – as suggested for the VER/AIBN:DGEBA/BA semi-IPN (see Figure 5.14). In this system it is the DGEBA that cures more rapidly than the model VER. Since the reaction of the VER is slower in the IPN, the increased conversion of epoxy groups in the IPN may be due to the presence of unreacted VER in the IPN, which acts as a plasticizer by enhancing mobility within the system and hence enabling a higher degree of reaction

before vitrification occurs. There appears to be a premature loss of peroxide initiator due to interactions between the amine and the peroxide because even after postcuring at 150°C the methacrylate component in the IPN could not reach full conversion.

### 5.1.4 Conclusions

The polymerization behaviour of IPNs formed from radically-initiated VER and amine-cured epoxy has been investigated by temperature-ramping DSC from 0°C to 300°C and by isothermal mid-FTIR at a curing temperature of 70°C. Apart from a dilutional (solvent) effect by the other components on the VER cure, the DSC studies showed that IPNs formed with AIBN-initiated VER exhibited the most independent cure behaviour. In contrast, initiation of the VER component by BPO, CHP and MEKP all showed strong interactions between the peroxide and the amine, particularly for aliphatic amines. The cure of the DGEBA resin was less affected by the radical initiator, however there is evidence that the hydroxy groups of bisGMA (or in the diluent of the peroxide) caused acceleration of the epoxy cure by H-bonding catalysis<sup>66,73</sup>. Evidence for grafting reactions (presumably by Michael addition) between the amine groups of the epoxy-amine system and the methacrylate groups of the VER were demonstrated by FTIR and extraction studies.

More detailed studies of the IPN cure by isothermal FTIR showed that the cure rate of one of the components affected the level of cure of the second component. Thus the presence of unreacted components (such as DGEBA or amines) of the epoxy system could plasticize the IPN and enable a higher level of reaction in the VER before vitrification occurred. In addition, if one of the components (such as the VER component) attained a high level of cure early in the formation of the IPN, the high level of crosslinking contributed to premature vitrification, which limited the extent of cure of the other component. Due to these complications in the cure of IPNs, the kinetic expressions discussed in Section 2.2 and 2.3 could not be applied. None of the curing behaviour could be attributed to the "network interlock" process suggested by Lin and co-workers<sup>133,137,230</sup>. In most cases, near-complete cure of the IPN components could be attained by postcuring above the  $T_g$  of the component networks. Topological constraint by one network on the full cure of the other component was relatively limited for the systems showed.

## 5.2 Imidazole based IPNs

### 5.2.1 Introduction

In this section the polymerization kinetics for full and semi IPNs based on a model VER and an imidazole-cured epoxy resin have been studied by scanning DSC and isothermal FTIR. The chemical interactions between the VER initiating system and the imidazole curative, effects of plasticization by one component of the cure of the other and effects of vitrification have been examined.

### 5.2.2 Differential scanning calorimetry of IPN cure

#### (a) AIBN initiated systems

The temperature ramping DSC cure behaviours of the AIBN-initiated VER, the 1-MeI initiated DGEBA and their IPNs are shown in Figure 5.17. The DSC thermograms of the neat VER/AIBN and the DGEBA/1-MeI (5 wt%) exhibit single peaks with slight shoulders at the higher temperature side of the exotherms whereas the IPNs of the vinyl ester resin and DGEBA epoxy (Figure 5.17) show two distinct exotherms. The observed heat of polymerization of VER/AIBN was 327 J/g, suggesting 96% cure (c/f theoretical – see Section 5.1.2). The heat of polymerization for the neat DGEBA/1-MeI was 471 J/g corresponding to 92 kJ/mol, which was similar to the energy involved in opening the epoxy ring during epoxy cure, as reported in the literature for epoxy/imidazole systems (97-103 kJ/mol)<sup>231,232</sup> and within the range reported for DGEBA/amine systems<sup>16,221,225</sup>. Based on the close correspondence of peak temperatures in the neat and blended systems, the lower and upper exotherms in the DSC traces of the IPNs can be attributed to the vinyl ester and DGEBA cure, respectively. The designation of the lower and upper exotherms to the cure of vinyl ester and epoxy respectively is confirmed by variations in the composition of this system. The resolved contributions to the DSC exotherm show that the areas of the lower and upper peaks are approximately proportional to the weight fractions of VER and epoxy components in the IPN respectively as shown in Table 5.3. In addition, the total polymerization enthalpies for the 75:25, 50:50 and 25:75 blends of

VER/AIBN:DGEBA/1-MeI are 364, 415 and 444 J/g, which are comparable with the weighted averages of the enthalpies for the individual components of 362, 399 and 435 J/g, respectively, suggesting that 'full' cure was achieved at moderate temperatures and that blending had not impaired the curing ability of each resin.

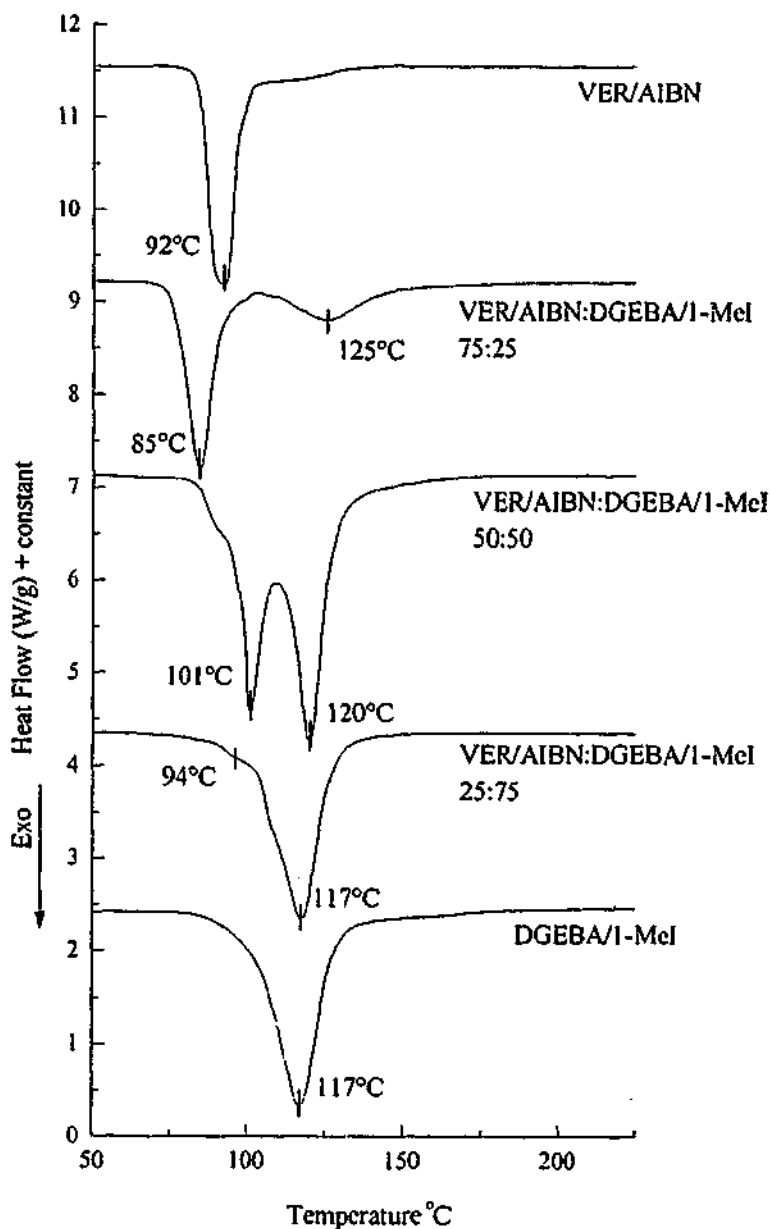


Figure 5.17 DSC scans of VER/AIBN, DGEBA/1-MeI (5 wt%) and their IPNs.

The curing exotherm peak of the vinyl ester component shifted from 92°C to 101°C in the 50:50 VER/AIBN:DGEBA/1-MeI IPN and the epoxy exotherm shifted from 117°C to 120°C in the 50:50 IPN (Figure 5.17). Similar behaviour was also observed for IPNs prepared from diamine-cured DGEBA and VER (see Section 5.1) and may be due to dilution of the reactants, which reduces the rate of cure and therefore raises the peak temperature. However the 75:25 VER/AIBN:DGEBA/1-MeI IPN exhibits an acceleration of the cure of the VER - the reason for this observation is

unclear because catalytic decomposition of AIBN is not expected. In a similar study of the cure of an IPN formed from diamine-cured DGEBA and a radically cured diacrylate resin, Lin and Chang<sup>5</sup> proposed a "network interlock effect" in which mutual entanglements between the two polymer networks produced a sterically hindered environment resulting in the reduction in the rate constant of the diacrylate resin. However this argument does not seem to be applicable to the data shown in Figure 5.17 because the epoxy network does not start to develop until the cure of the VER is nearly complete.

**Table 5.3 Summary of the DSC analysis of the VER cured with various radical initiators, DGEBA cured with 1-MeI and the IPNs formed from these resins.**

System	Curing Peak (°C)	$\Delta H$ (J/g)	Integration range (°C)
<b>AIBN and 1-MeI initiators</b>			
VER/1%AIBN	92°C	327	50-275
75:25 VER/1 wt% AIBN: DGEBA/5 wt% 1-MeI	Peak 1: 85°C Peak 2: 125°C	Peak 1: 250 Peak 2: 114	50-275
50:50 VER/1 wt% AIBN: DGEBA/5 wt% 1-MeI	Peak 1: 101°C Peak 2: 120°C	Peak 1: 176 Peak 2: 239	50-275
25:75 VER/1 wt% AIBN: DGEBA/5 wt% 1-MeI	Shoulder: 94°C Peak: 118°C	444	50-275
DGEBA/5 wt% 1-MeI	117°C	471	50-275
<b>CHP and 1-MeI initiators</b>			
VER/1 wt% CHP	125°C	318	50-250
75:25 VER/1 wt% CHP: DGEBA/5 wt% 1-MeI	Peak 1: 104°C Peak 2: 124°C Peak 3: 242°C	Peak 1: 343 Peak 2: 102 Peak 3: 12	50-250
50:50 VER/1 wt% CHP: DGEBA/5 wt% 1-MeI	Peak 1: 95°C Peak 2: 122°C Peak 3: 244°C	Peak 1: 133 Peak 2: 254 Peak 3: 8	50-250
25:75 VER/1 wt% CHP: DGEBA/5 wt% 1-MeI	Peak 1: 83°C Peak 2: 115°C Peak 3: 245°C	Peak 1: 56 Peak 2: 375 Peak 3: 4	50-250
DGEBA/5 wt% 1-MeI	117°C	471	50-275
1wt%CHP:DGEBA/5 wt% 1-MeI	114°C	468	50-275
VER/1wt% CHP: 5 wt% 1-MeI	Peak 1: 107°C Peak 2: 191°C	Peak 1: 308 Peak 2: 22	50-275
<b>MEKP and 1-MeI initiators</b>			
VER/ 1 wt% MEKP	123°C	320	45-275
50:50 VER/1 wt% MEKP: DGEBA/5 wt% 1-MeI	Peak 1: 87 °C Peak 2: 120 °C Peak 3: 225 °C	Peak 1: 8 Peak 2: 232 Peak 3: 64	45-275
DGEBA/5 wt% 1-MeI	117°C	471	50-275
MEKP:DGEBA/5 wt% 1-MeI	114°C	470	50-275
VER/1wt% MEKP:5 wt% 1-MeI	Peak 1: 106°C Peak 2: 233°C	Peak 1: 302 Peak 2: 23	50-275
<b>BPO and 1-MeI initiators</b>			
VER/1 wt% BPO	105°C	323	50-200
50:50 VER/1 wt% BPO: DGEBA/5 wt% 1-MeI	Peak 1: 91°C Peak 2: 121°C Peak 3: 235°C	Peak 1: 34 Peak 2: 203 Peak 3: 34	45-275
DGEBA/ 5 wt% 1-MeI	117°C	471	50-275
VER/1wt% BPO:5 wt% 1-MeI	Peak 1: 93°C Peak 2: 204°C	Peak 1: 302 Peak 2: 19	50-275
1wt% BPO:DGEBA/5 wt% 1-MeI	116°C	Peak 1: 472	50-275
<b>Thermal Cure</b>			
VER	195°C	320	100-275

The curing behaviour of the systems discussed above are complicated by the presence of three curing components – styrene, methacrylate and epoxy. To try to simplify these IPNs and to investigate the effect of network formation in one component on the cure of the other, a series DSC scans of semi- and full-IPNs based on the linear PGEMA and its crosslinking counterpart bisGMA and PGE and its crosslinking

counterpart DGEBA were studied and are shown in Figure 5.18. The neat bisGMA/AIBN and neat PGEMA/AIBN systems both exhibit single exotherm peaks at 99 and 84°C respectively. The reason for the different peak temperatures is unknown but may be associated with different levels of inhibitors in the resins (see section 2.1.3). Based on the heat of polymerization for methyl methacrylate of 56.2 kJ/mol<sup>17,222</sup>, the theoretical heat of polymerization of the bisGMA was calculated as 229.4 J/g (based on a bisGMA molecular weight of 490 g/mol obtained by titration – see Section 3.2). The observed heat of polymerization of bisGMA/AIBN was 175 J/g, suggesting 76% cure. Based on the same heat of polymerization for methyl methacrylate of 56.2 kJ/mol<sup>17,222</sup>, the theoretical heat of polymerization of the PGEMA was calculated as 238.1 J/g. The observed heat of polymerization of PGEMA/AIBN was 240 J/g, suggesting 100% cure (within error). The neat DGEBA/1-MeI and neat PGE/1-MeI system also produced single exotherms at 117°C and 124°C respectively. As mentioned previously, the heat of polymerization for the neat DGEBA/1-MeI was 471 J/g corresponding to 92 kJ/mol and similar to that reported in the literature<sup>16,225</sup>. The heat of polymerization for the neat PGE/1-MeI was 515 J/g corresponding to 81.3 kJ/mol, which is a little lower than reported in the literature for the epoxy ring opening<sup>16,225</sup>. The resulting 50:50 IPNs of bisGMA/AIBN:PGE/1-MeI and PGEMA/AIBN:DGEBA/1-MeI both show two distinct exotherms. Based on the close correspondence of peak temperatures in the neat and blended systems, the lower and upper exotherms in the DSC trace can be attributed to the methacrylate and epoxy cure respectively. In the 50:50 bisGMA/AIBN:PGE/1-MeI IPN the bisGMA curing exotherm shifted from 99 to 102°C and the PGE exotherm shifted from 124 to 130°C, as expected from dilution effects. Similar shifts in exotherm were observed in the 50:50 PGEMA/AIBN:DGEBA/1-MeI IPN where the exotherm due to the PGEMA shifted to 89°C (c/f 84°C for the neat PGEMA/AIBN) and the exotherm due to the DGEBA shifted to 129°C (c/f 117°C for the neat DGEBA/1-MeI).

The resolved contributions to the DSC exotherm show that the areas of the lower and upper peaks are approximately proportional to the weight fractions of dimethacrylate and epoxy components in the IPN (see Table 5.4), indicating that the cure of individual components in the IPNs were relatively independent. This study agrees with the results in Section 5.12 indicating that network formation in the IPN does not significantly affect the cure.

As will be shown in Section 8.2 the 50:50 bisGMA/AIBN:PGE/1-MeI IPN is

phase separated whereas the 50:50 PGEMA/AIBN:DGEBA/1-MeI IPN is miscible. The fact that similar dilutional effects are observed in both systems may result from a high level of phase mixing and the absence specific partitioning of the reacting components between the phases.

**Table 5.4 Summary of the DSC analysis of the bisGMA/AIBN, PGEMA/AIBN, DGEBA/1-MeI, PGE/1-MeI and the IPNs formed from these resins.**

System	Curing Peak (°C)	$\Delta H$ (J/g)	Integration range (°C)
bisGMA/1%AIBN	99°C	175	50-200
PGEMA/1 wt%AIBN	84°C	240	50-200
50:50 bisGMA/1 wt% AIBN: PGE/5 wt% 1-MeI	Peak 1: 102°C Peak 2: 130°C	Peak 1: 101 Peak 2: 295	50-250
50:50 PGEMA/1 wt% AIBN: DGEBA/5 wt% 1-MeI	Peak 1: 89°C Peak 2: 129°C	Peak 1: 123 Peak 2: 245	50-250
PGE/5 wt% 1-MeI	124°C	515	50-275
DGEBA/5 wt%1-MeI	117°C	471	50-275

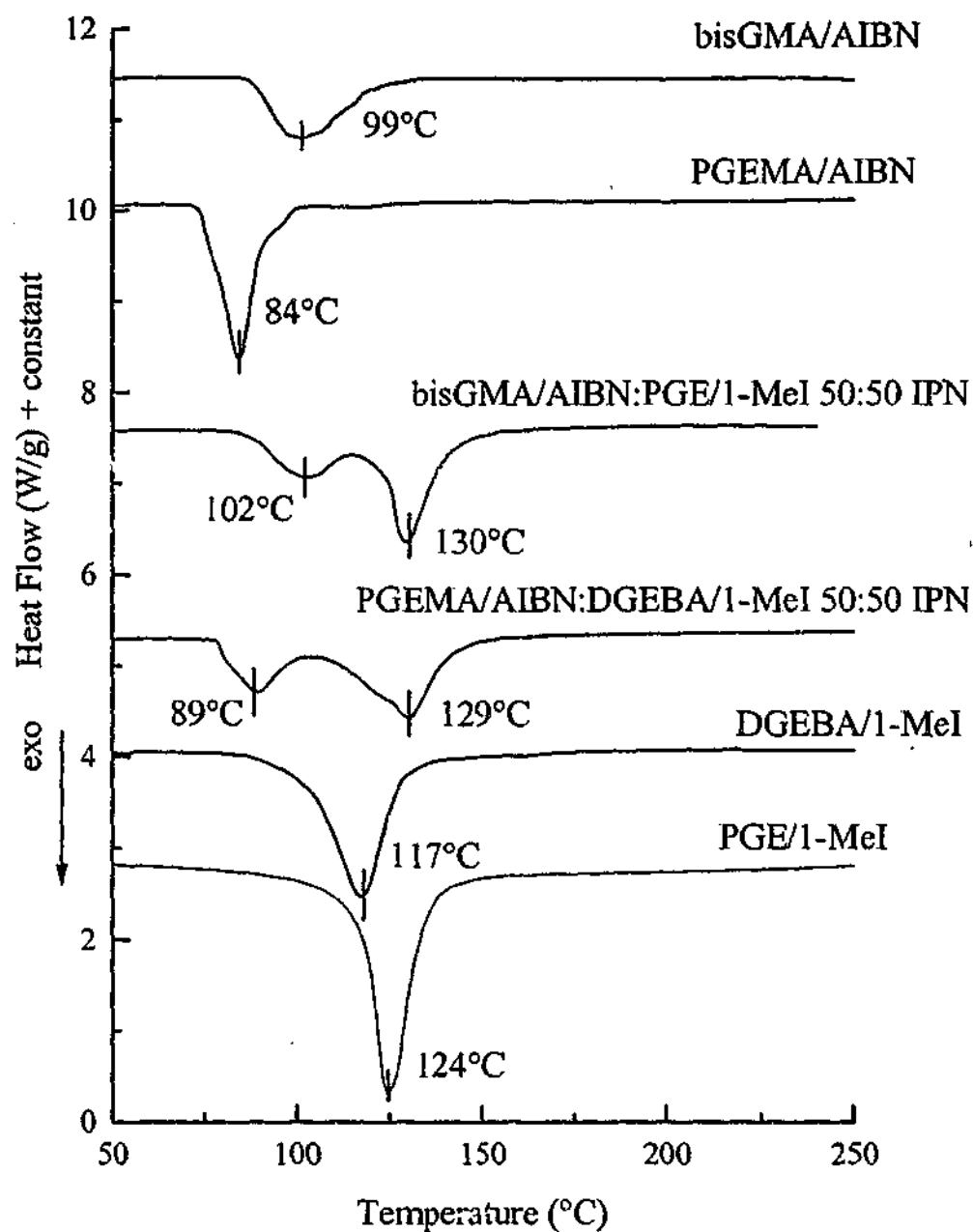


Figure 5.18 DSC scans of bisGMA/AIBN, PGEMA/AIBN, DGEBA/1-MeI (5 wt%), PGE/1-MeI (5 wt%) and their IPNs.

#### (b) CHP initiated systems

The DSC thermograms of the VER/CHP resin and the DGEBA/1-MeI resins exhibit single major peaks while each of the 50:50 IPNs exhibit two well resolved exotherms (Figure 5.19). Based on the size of the peaks in the IPNs for the three compositions (75:25, 50:50 and 25:75), the lower and higher temperature exotherms observed may be attributed to the cure of vinyl ester and epoxy components respectively. The polymerization enthalpy and temperature at the peak for each system are listed in Table 5.3. The total heat of polymerization (measured from 50°C to 250°C) for the 50:50 blend is 387 J/g which is only slightly less than the average of the

enthalpies for the individual exotherms (395 J/g), suggesting that nearly full cure can be obtained with these IPNs at moderate temperatures. However, the enthalpy associated with the first peak (133 J/g; estimated by the peak resolution method discussed in Section 4.2) is less than that expected for complete polymerization of the VER (159 J/g) - the remainder of this enthalpy may be included in the epoxy cure exotherm at 122°C and in the broad exotherm (8 J/g) at temperatures around 200°C, which has previously been attributed to thermal cure for the VER component (see Section 5.1).

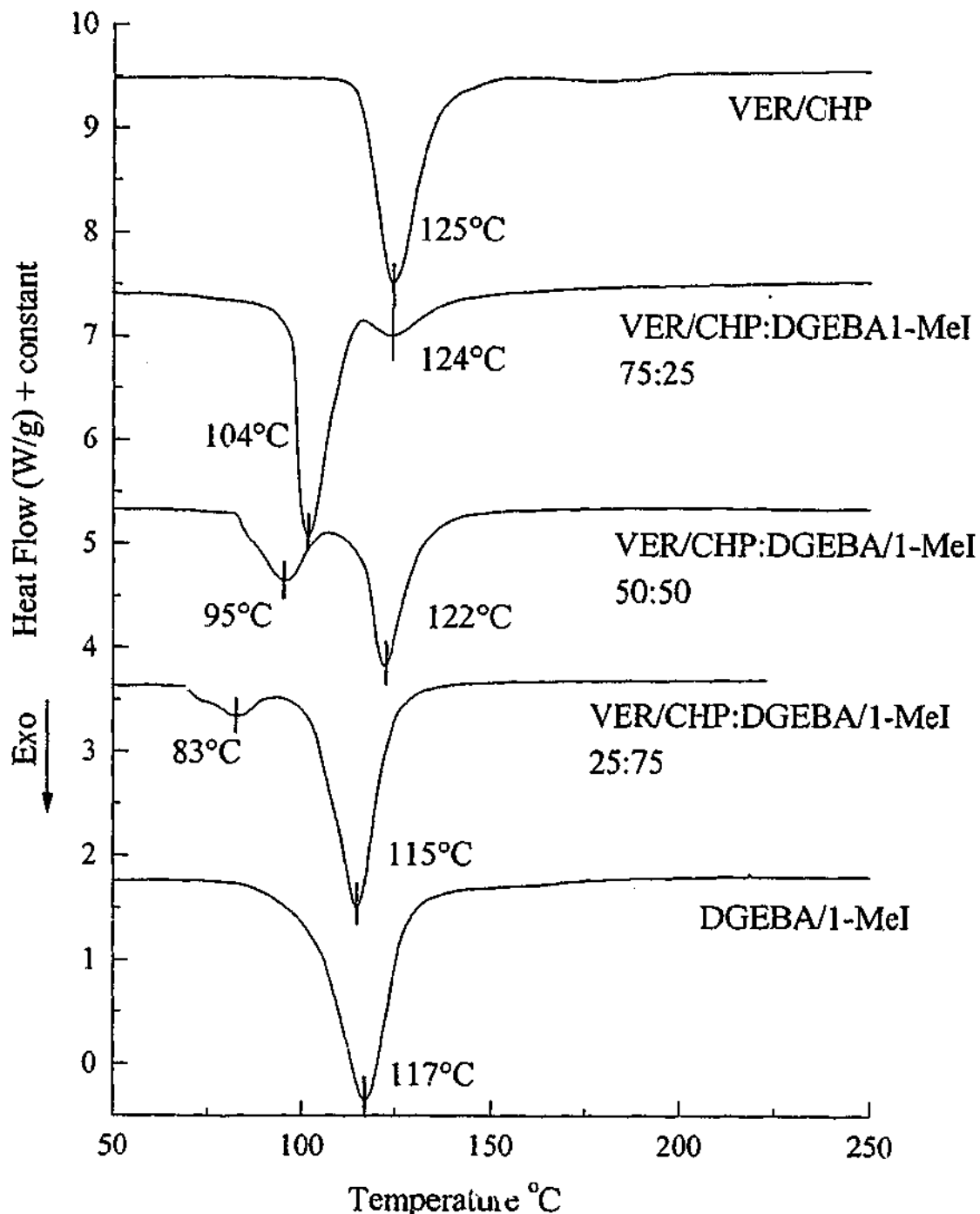


Figure 5.19 DSC scans of VER/CHP, DGEBA/1-MeI (5 wt%) and their IPNs

The small shift of the temperature of the epoxy exotherm peak from 117°C to 122°C in Figure 5.19 can be attributed to dilution effects within the 50:50 blend as

found above with the AIBN-cured IPN. In contrast, dilution effects cannot account for the downward shift of the VER exotherm peak from 125°C to 95°C (in the 50:50 blend) for the vinyl ester cured with CHP. This unusual behaviour may be attributed to a redox reaction between the CHP and 1-MeI - similar redox reactions between aromatic amines and peroxides have been observed by a number of workers<sup>41,86,88,90-92,224</sup> (see Section 2.3.2). These redox reactions may cause premature decomposition of the peroxide and enhance radical production, resulting in the observed acceleration of the cure of the vinyl ester component. To confirm the acceleration of the cure of the vinyl ester resin by the imidazole in the 50:50 blend, a separate sample of the VER/CHP systems was blended with 5% 1-MeI and studied by scanning DSC (see Table 5.3). Close to full cure of the VER was observed, with a small amount of thermal cure (20 J/g) at 191°C. The temperature of the main exotherm peak for the VER/CHP:1-MeI has shifted to 107°C, compared with 125°C for the vinyl ester resin initiated with CHP alone, confirming that the imidazole accelerates the rate of radical production and hence the rate of cure. Surprisingly this peak occurs at a lower temperature (95°C) in the IPN than in the VER/CHP:1-MeI system - the reason for this is unclear.

### (c) MEKP initiated systems

The DSC thermograms of the VER/MEKP and the DGEBA/1-MeI resins exhibit single exothermic peaks respectively, however the DSC thermogram of the 50:50 IPN of epoxy and vinyl ester exhibits three significant exothermic peaks (Figure 5.20), indicating that much more complex interactions are occurring between the components in the IPNs. The total polymerization enthalpy and the temperature at each exotherm peak are listed in Table 5.3 for each system. The total heat of polymerization for the 50:50 blend (304 J/g, integrated from 45°C to 275°C) is substantially less than that predicted from the average of the enthalpy for the individual component exotherms (average of the VER/MEKP and DGEBA/1-MeI, i.e. 396 J/g). One possible explanation for the reduction in heat of polymerization is that the MEKP concentration is rapidly consumed by redox reactions with the imidazole, causing premature peroxide decomposition and subsequent depletion of radicals similar to the effect of dead-end radical polymerization<sup>227-229</sup>. Alternatively, the 1-MeI may also reduce the MEKP by a side reaction, which does not produce radical species, thus also causing premature depletion of the peroxide. These processes would be observed as a decrease in the heat of polymerization and a lower peak exotherm temperature for the vinyl ester resin

component. On this basis, the small peak at 87°C could be due to the accelerated but incomplete polymerization of the vinyl ester resin. This assignment is consistent with the accelerated VER cure when 5 wt% 1-MeI was added to the VER/MEKP system (see Table 5.3) resulting in a large peak at 106°C due to accelerated VER cure. Surprisingly, this peak occurs at a higher temperature and develops a greater exotherm than in the IPN - the reason for this is unclear. The VER/MEKP:1-MeI system also shows a small, broad peak at 233°C. This peak occurs close to the peak around 225°C in the IPN and is similar to the broad exotherm at 195°C observed for the vinyl ester resin when thermally cured without added initiator. In contrast, the DSC cure of the MEKP:DGEBA/1-MeI blend (containing no VER) shows no significant decrease in polymerization enthalpy of the epoxy groups compared with the pure system (see Table 5.3). On this basis, the middle peak at 120°C in the IPN may be identified with cure of the epoxy component - the enthalpy of this peak (232 J/g) is similar to the contribution expected from the pure epoxy system (236 J/g) suggesting that the epoxy achieves close to full cure. The shift of the peak exotherm of the epoxy from 117°C in the neat resin to 120°C in the IPN may be attributed to dilution effects within the blend as found with the AIBN- and CHP-containing IPN systems.

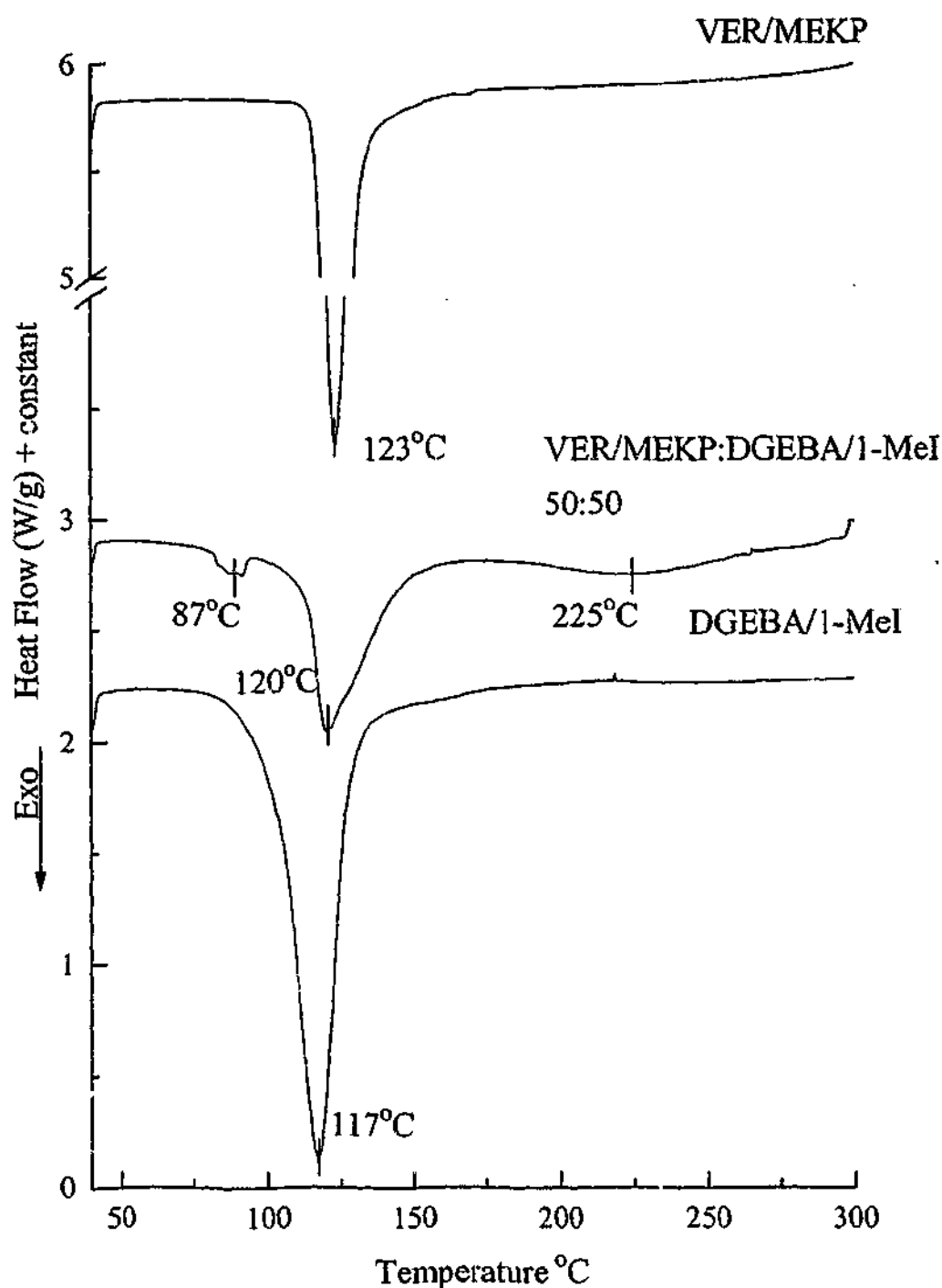


Figure 5.20 DSC scans of VER/ MEKP, DGEBA/ 1-MeI (5 wt%) and their 50:50 IPN.

(d) BPO initiated systems

The DSC thermograms (see Figure 5.21) of the BPO-initiated vinyl ester resin and the 1-MeI initiated epoxy resin both exhibit single primary peaks whereas the 50:50 IPN of the epoxy and vinyl ester resins exhibits three exotherms – a small exotherm at 91°C, a larger peak at 121°C and a broad exotherm around 235°C. On the basis of their

proximity to the parent resins, the lower and intermediate temperature exotherms observed in the 50:50 blend may represent the partial cure of vinyl ester and epoxy respectively, whereas the broad peak at high temperatures can be assigned to thermal cure of the remaining VER components, as discussed earlier. The exothermic VER curing peak at 91°C is significantly lower than in the neat VER system (104°C) and can be attributed to the reduction of the BPO by the 1-MeI causing accelerated radical production similar to that observed in both the CHP and MEKP cured IPNs. This is confirmed by the shift of the curing peak of VER/BPO from 104° to 93°C when 5 wt% of 1-MeI is added (see Table 5.3) and is similar to the behaviour found for MEKP-cured systems. The broad peak around 235°C in the IPN is close to the broad high temperature exotherm at 203°C in the VER/MEKP:1-MeI system and corresponds with the exotherm at 195°C observed for the vinyl ester resin when thermally cured without added initiator. The upwards shift of the peak temperature of the epoxy component exotherm in the VER/BPO:DGEBA/1-MeI IPN, from 117°C to 121°C, can be attributed to dilution effects within the 50:50 blend as found in the AIBN, CHP and MEKP cured IPNs. The exotherm enthalpy of the epoxy peak in the IPN (203 J/g) is less than that expected for full cure (236 J/g); however, this may be within the experimental error associated with the separation of overlapping peaks.

The total heat of polymerization for the 50:50 blend (237 J/g not including the thermal component of the VER cure of 34 J/g at 235°C) is substantially reduced from the average of the enthalpies for the individual exotherms of VER/BPO and DGEBA/1-MeI (i.e. 397 J/g) suggesting that the VER component does not fully cure at normal curing temperatures. This decrease in size of the VER component exotherm in the IPN can be explained by the premature decomposition of the BPO by the 1-MeI, as discussed above, which causes dead-end radical polymerization<sup>227-229</sup>. Alternatively BPO may be depleted by a side reaction that does not produce radical species, thus decreasing the heat of polymerization. The lower total heat of polymerization for the 50:50 blend may have also been due to the undercure of the epoxy component if sufficient 1-MeI had been consumed in the redox reaction with the BPO.

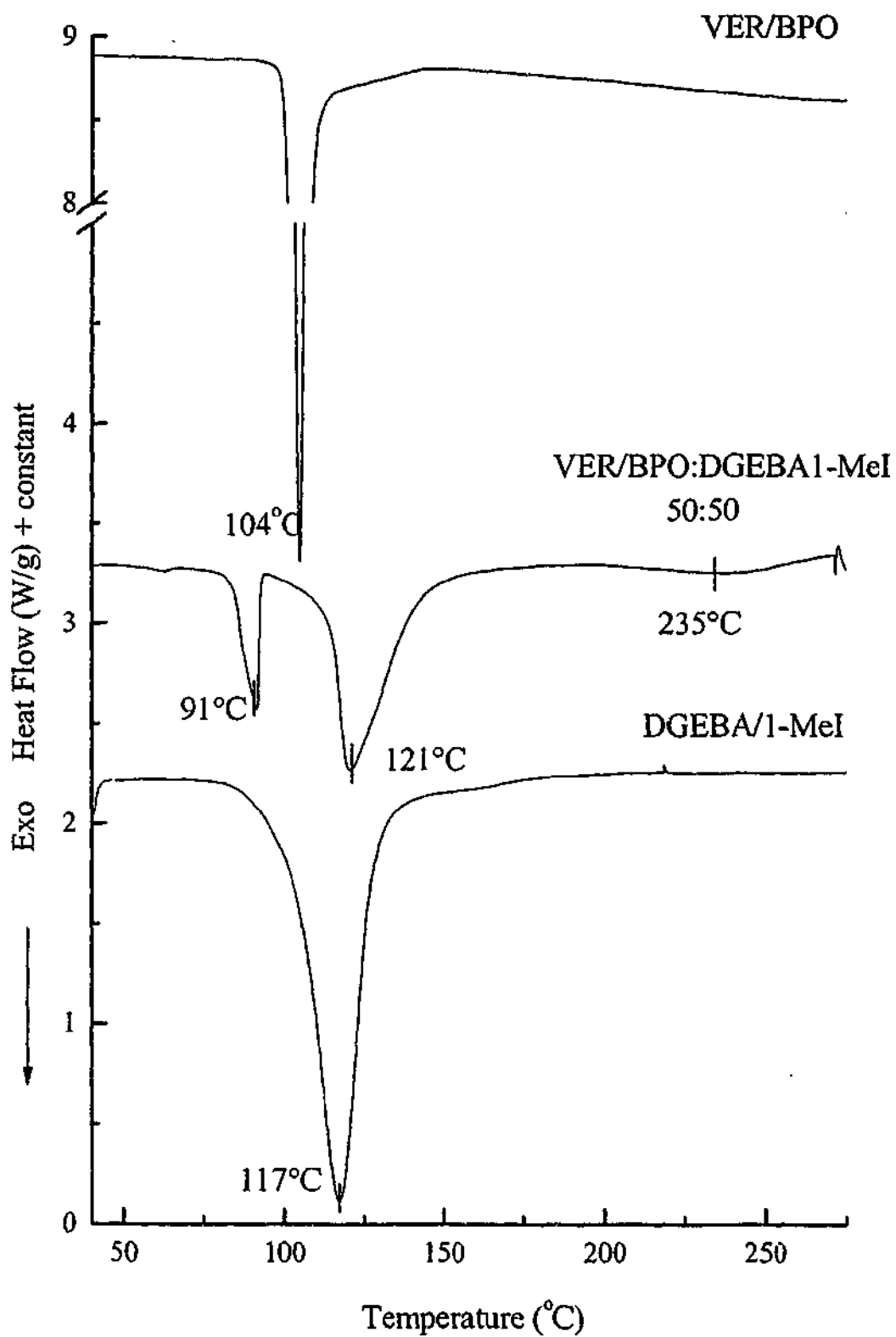


Figure 5.21 DSC scans of the VER/BPO and DGEBA/1-MeI (5 wt%) resins and their 50:50 IPN

### 5.2.3 Fourier transform infra-red spectroscopy of IPN cure

#### (a) AIBN initiated systems

Figure 5.22 illustrates the variation in the FTIR spectrum during the cure of the VER/AIBN:DGEBA/1-MeI IPN - the main changes appear to be the reduction of the magnitude of the absorption peaks associated with the methacrylate ( $1645\text{ cm}^{-1}$ ), styrene ( $778, 910$  and  $1630\text{ cm}^{-1}$ ) and epoxy ( $915\text{ cm}^{-1}$ ) groups.

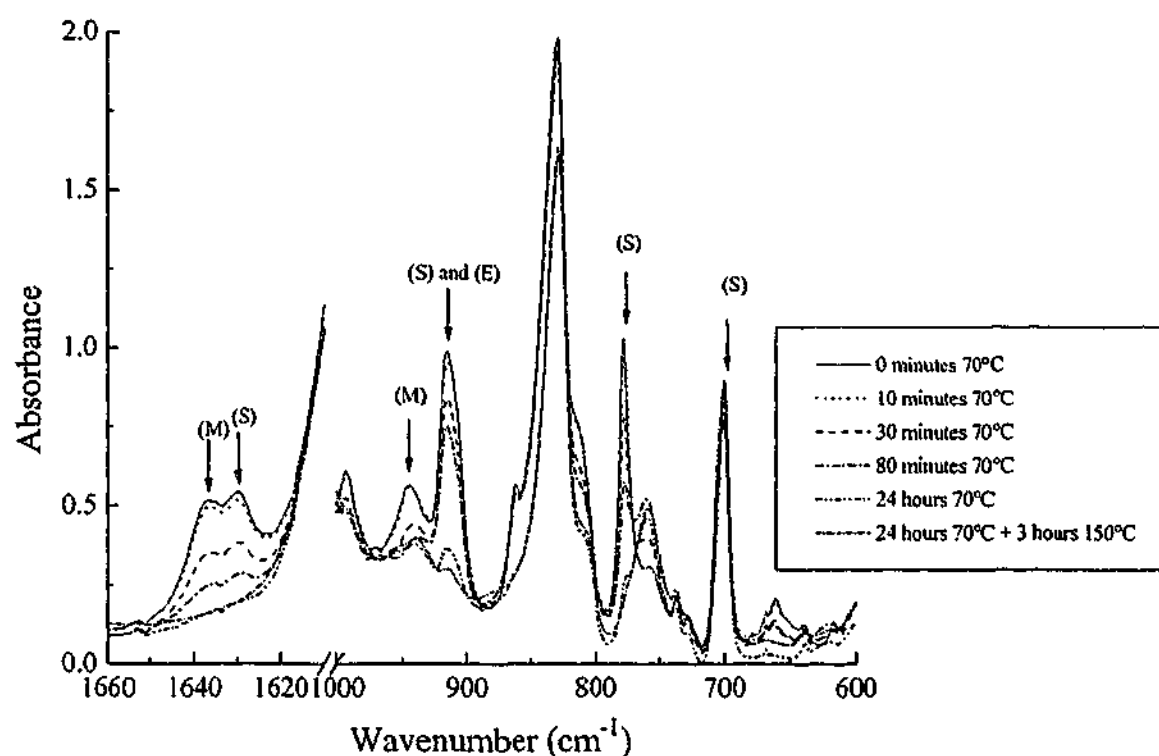
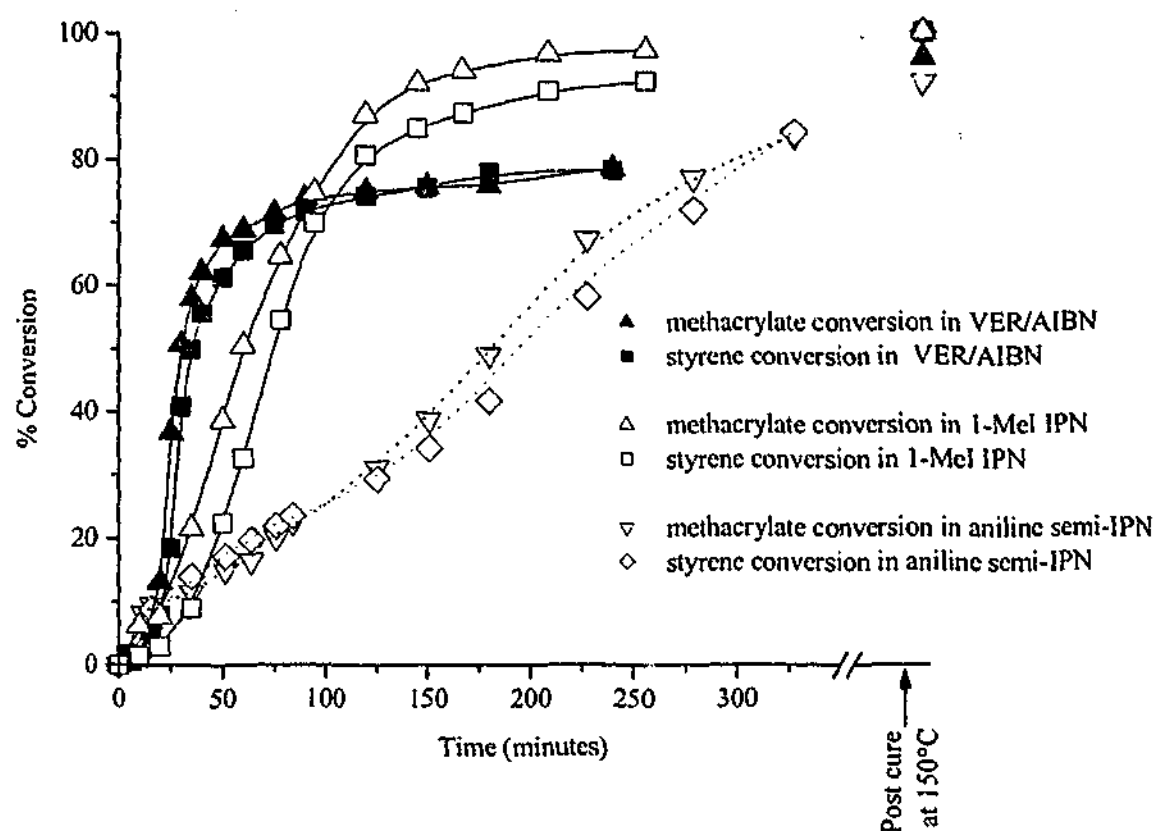


Figure 5.22 FTIR spectra in the region from  $1660\text{ cm}^{-1}$  to  $1600\text{ cm}^{-1}$  and from  $1000\text{ cm}^{-1}$  to  $600\text{ cm}^{-1}$  of the 50:50 VER/AIBN:DGEBA/1-MeI (5 wt%) IPN cured at  $70^\circ\text{C}$  for varying times and after post-cure at  $150^\circ\text{C}$  for 3 hours.

Typical conversion-time data for the reaction of the vinyl groups in the neat VER at  $70^\circ\text{C}$  are shown in Figure 5.23. As predicted from the similar reactivity ratios of the methacrylate groups of dimethacrylate, and styrene<sup>116</sup>, both groups copolymerize at similar rates. The VER shows incomplete cure at  $70^\circ\text{C}$  (see Figure 5.23) but close to full cure was observed during isothermal cure at  $110^\circ\text{C}$  (see Figure 5.24). This difference can be attributed to the effect of vitrification during cure which occurs when crosslinking raises the glass transition temperature to the curing temperature<sup>233</sup> (see

Section 2.1.1). Thus, when the polymerization was conducted at an isothermal cure temperature that was significantly below the  $T_g$  of the fully cured VER (169°C), incomplete cure resulted. However, regardless of the initial isothermal cure temperature, nearly complete cure occurred upon postcure of the resin at 150°C.



**Figure 5.23** Dimethacrylate and styrene conversion versus time in the pure VER/AIBN system and in the 50:50 blend of VER/AIBN:DGEBA/1-MeI at 70°C. The dashed lines show the cure behaviour of the IPN formed with VER/AIBN:DGEBA/aniline (see also Figure 5.13)

As observed in the isothermal curing study of aniline or butylamine based IPNs (see Section 5.1.3), the styrene and methacrylate conversion in both the vinyl ester system and the 1-MeI based IPN exhibit brief induction periods (see Figure 5.23), presumably due to the presence of free radical inhibitors in the resins. Isothermal infrared spectroscopy undertaken at 110°C showed negligible induction periods (see Figure 5.24) as would be expected for a rate acceleration. At each given temperature, the methacrylate groups within the IPN initially polymerize more slowly compared with the pure resin. This decrease in reaction rate can be attributed to the dilution of the reactants by the DGEBA resin; in agreement with the DSC results for this IPN (see

Section 5.2.2(a)). In Section 5.1, FTIR studies of semi-IPNs formed from a vinyl ester resin with DGEBA cured by a stoichiometric amount of primary amine (either aniline or butylamine) also showed a similar reduced polymerization rate for styrene and methacrylate, suggesting that a dilution effect was operative. However, when this data and in particular the data for the aniline-containing IPN data is compared (see Figure 5.23) with that for the IPNs containing imidazole, it is apparent that the IPN containing a primary amine reacts more slowly. This difference in cure rates may be attributed to the retardation of the vinyl ester polymerization by the large quantities of aniline or butylamine that are present in a much higher concentration than the imidazole curing agents. This hypothesis is supported by the work of Imoto *et al.*<sup>90</sup> who showed that dimethyl aniline reduced the polymerization rate in the AIBN-initiated methyl methacrylate and suggested that this effect was due to radical transfer to the amine, which was incapable of re-initiating the polymerization.

Similar to that found previously for the VER/AIBN:DGEBA/An IPN (see Section 5.1.2), the VER/AIBN:DGEBA/1-MeI IPN exhibits a higher level of conversion of both styrene and methacrylate units compared with the neat resins (see Figure 5.23). This increase in final conversion of styrene and methacrylate groups may be attributed to the presence of the unreacted DGEBA in the system since the cure of the epoxy resin is much slower than that of the VER (compare Figure 5.23 and Figure 5.25). Thus, if the IPN is considered to be miscible (or partly miscible), the unreacted DGEBA can act as a plasticizer during the cure of the VER components, enabling greater mobility within the system and hence a greater degree of conversion for the styrene and methacrylate units prior to vitrification of the resin – see Section 2.1.1 and 2.4.2.

Typical conversion-time data for the reaction of the vinyl groups in the neat VER/AIBN and the 50:50 VER/AIBN:DGEBA/1-MeI at 110°C are shown in Figure 5.24. The induction period which was clearly visible at 70°C has virtually disappeared and the methacrylate and styrene groups in the neat VER/AIBN and the 50:50 VER/AIBN:DGEBA/1-MeI IPN reach close to 100 % conversion in less than 10 minutes. Due to this rapid cure, all conversions are within error of each other and no valid comparisons were made between the neat and IPN systems at 110°C.

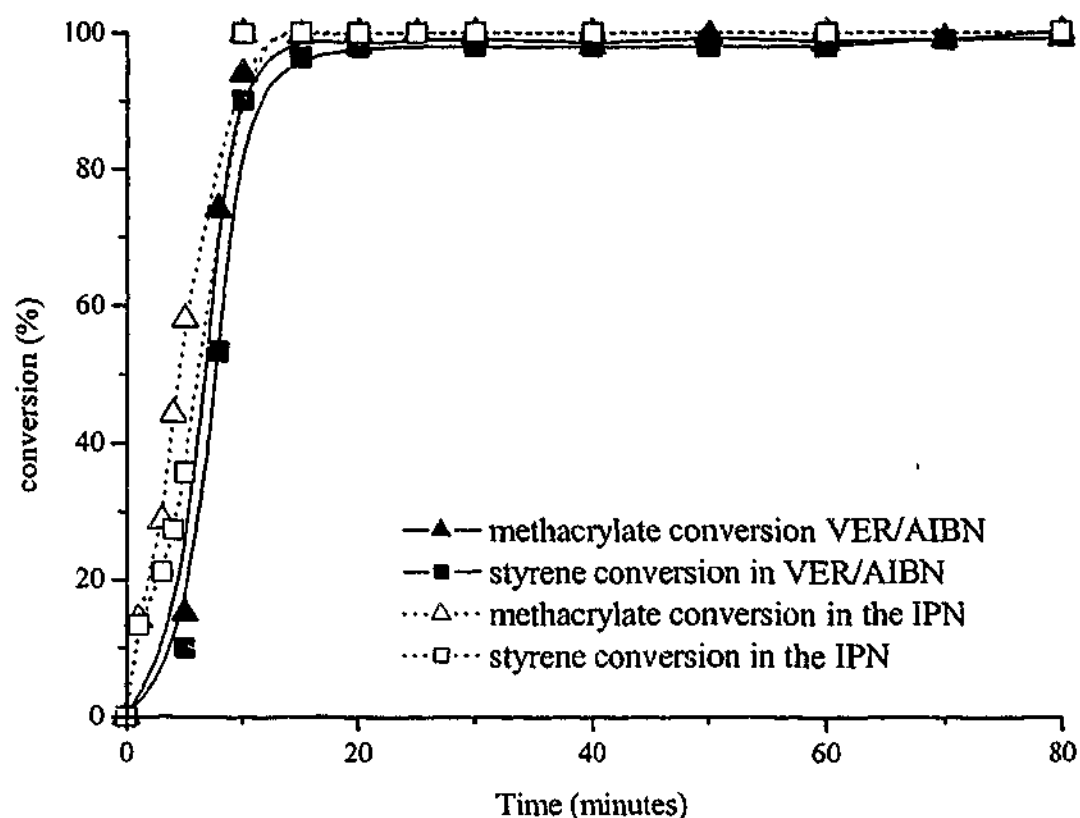


**Figure 5.24** Dimethacrylate and styrene conversion versus time in the pure VER/AIBN system and in the 50:50 blend of VER/AIBN:DGEBA/1-MeI at 110°C.

The isothermal conversion-time plots for the epoxy groups in neat DGEBA as measured by FTIR at 70°C and 110°C are illustrated in Figure 5.25. Although the FTIR conversion-time data was only semi-quantitative (see Chapter 4), the epoxy conversion curve at 70°C suggests a two-stage cure process. This process has been previously observed<sup>231</sup> during isothermal (but not scanning) DSC cure studies and is believed to be associated with the distinct stages of formation of the 1:1 adduct and of polymerization (see Section 2.2.4). As discussed above for the VER system, the epoxy groups are not fully reacted (80% conversion) after 24 hours at 70°C because this is well below the  $T_g$  of the fully cured epoxy resin (the  $T_g$  of DGEBA/1-MeI (2 wt%) was 185°C by DMTA) and so vitrification occurs during cure<sup>233</sup>.

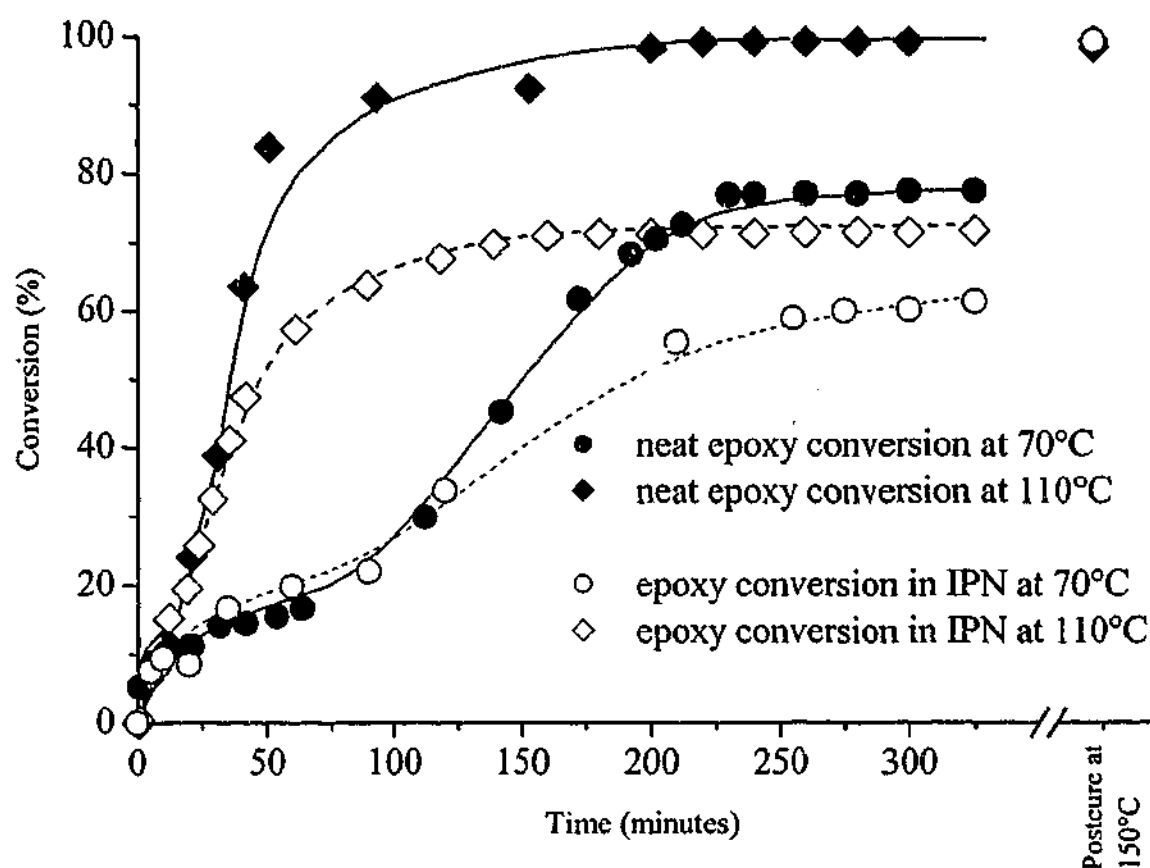


**Figure 5.25** Epoxy conversion versus time for the neat DGEBA/1-MeI (5 wt%) resin and in the 50:50 blend of the model VER/AIBN:DGEBA/1-MeI (5 wt%).

In the early stages of cure of the epoxy groups, the neat epoxy system and the IPN appear similar (see Figure 5.25) - the data is not sufficiently accurate to distinguish between them. However, as the reaction proceeds, the cure rate in the IPN is slower than in the neat system, as observed by DSC (see Figure 5.17), possibly due to a dilutional effect. It is interesting to note that the plateau conversions of the epoxy groups in the IPN cured at 70°C was significantly lower than in the neat resin at these temperatures. This may be explained in terms of the vitrification of the IPN during cure<sup>233</sup>, as suggested in Section 5.1.2 for the VER/AIBN:DGEBA/An IPN. A comparison of Figure 5.23 with Figure 5.25 indicates that the VER components polymerize at a much faster rate than does the epoxy component. Thus if the IPN is considered as a single phase material, an increase in its crosslink density by the curing of the VER component may raise the  $T_g$  of the IPN so much that the material vitrifies before complete reaction of the DGEBA. When the systems were cured at 110°C, the epoxy conversion in the neat resin was almost 100%, but less than full cure was attained in the IPN perhaps due

to premature vitrification of the IPN as a result of the high level of crosslinking provided by the VER component as suggested in Section 5.1.3(a). In partial support of the vitrification explanation, Figure 5.25 shows that nearly full conversion of the epoxy groups can be attained when the IPN is postcured at 150°C. Alternatively, the "network interlock effect"<sup>5,133</sup> (see Section 2.4.2) may retard the cure of the epoxy in the presence of the already formed VER network, due to steric hindrance and restricted chain mobility. However, the network interlock mechanism does not explain why postcuring at 150°C produces near complete epoxy cure in the IPN.

#### (b) CHP initiated systems

Figure 5.26 illustrates the conversion of styrene and methacrylate species obtained by FTIR at 70°C in the neat and IPN systems. The reaction of the methacrylate and styrene groups in the neat VER exhibited a short induction period, probably due to radical inhibition, however this induction period is significantly reduced for the IPN systems. In contrast to the AIBN initiated VER systems, the conversion of both styrene and methacrylate is faster in the CHP-containing IPN which agrees with the DSC data (see Table 5.3) and confirms that the imidazole does act as a promoter causing enhanced radical production from the CHP. Similar to that observed in the IPN systems initiated with AIBN (see Figure 5.25), the cure rates of the VER components are faster than the epoxy (compare Figures 5.26 and 5.27) and as a result the final isothermal conversion of both styrene and methacrylate groups is higher for the IPN than for the neat system due to the plasticization of the developing VER network by the unreacted DGEBA, thus delaying vitrification in this time regime. Accelerated cure behaviour was observed in FTIR studies at 110°C but here full cure was observed during the isothermal phase.

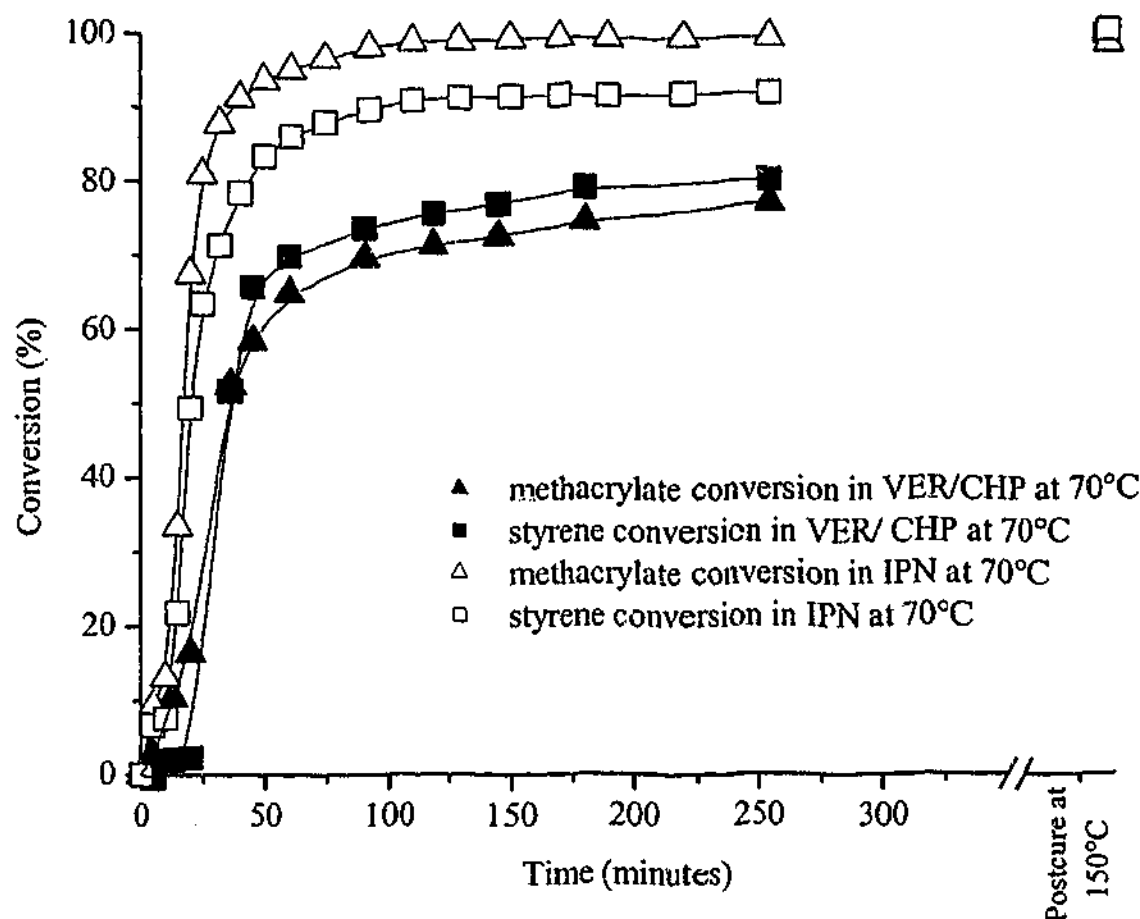


**Figure 5.26** Dimethacrylate and styrene conversion versus time in the pure VER/CHP system and in the 50:50 blend of VER/CHP:DGEBA/1-MeI at 70°C.

The conversion of the epoxy groups in the neat DGEBA/1-MeI resin and the VER/CHP:DGEBA/1-MeI IPN, obtained from isothermal FTIR at both 70°C and 110°C, is illustrated in Figure 5.27. As expected, the rate of polymerization is faster at the elevated isothermal temperature of 110°C compared with 70°C. In agreement with the DSC data (see Figure 5.19); the initial rate of conversion of epoxy groups in the IPN is slower than in the neat epoxy system, perhaps due to dilution by the surrounding VER, as suggested for the VER/AIBN:DGEBA/1-MeI IPNs. Also in agreement with the previously presented data, the final epoxy conversion at 70°C is higher for the neat DGEBA resin than for the IPN, possibly due to vitrification caused by the high level of crosslinking of the VER component in the IPN. This is confirmed by the observation that, postcuring at 150°C (which is close to the  $T_g$ s of the individual components) leads to an epoxy conversion of greater than 95% in the IPN. When the resins were cured at an isothermal temperature of 110°C, the final conversion of the epoxy component was still incomplete and this may result from the vitrification effect caused by the high level

of crosslinking of the VER component as discussed above (see Sections 5.1.3(a) and 5.2.3(a))

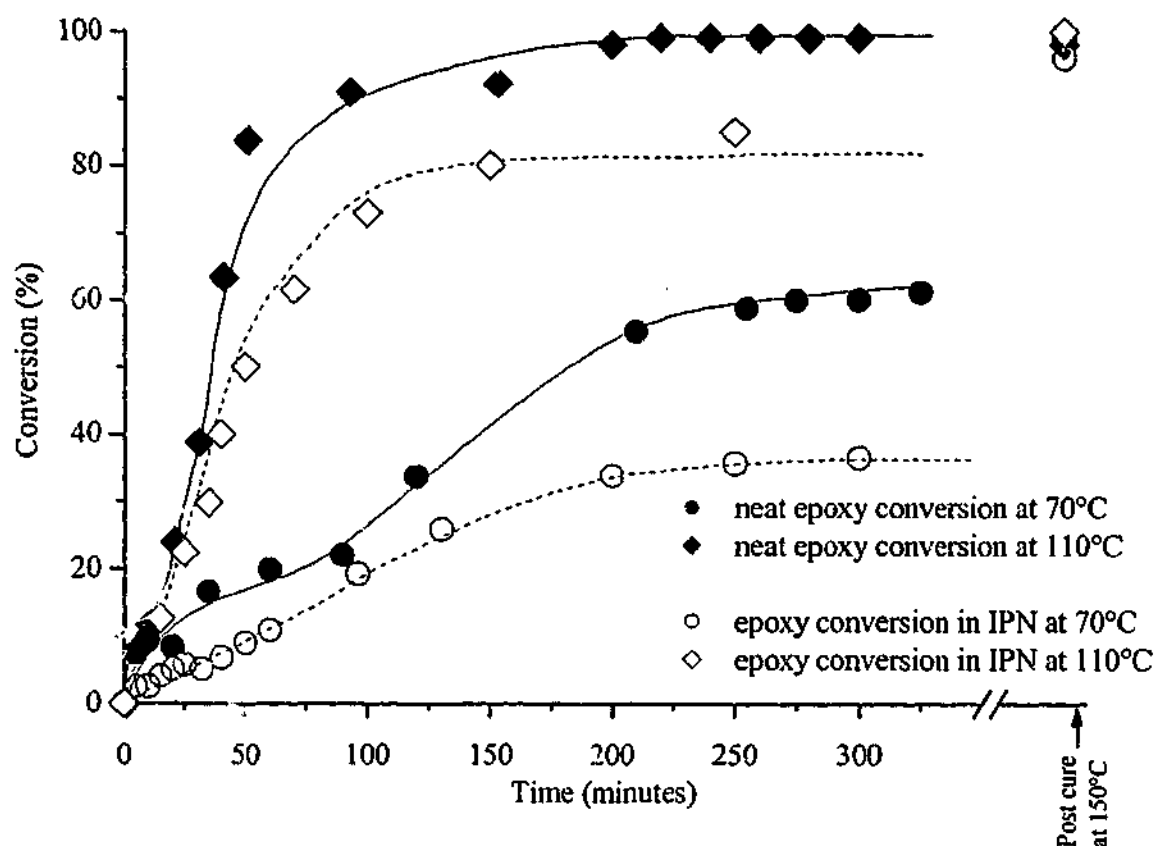
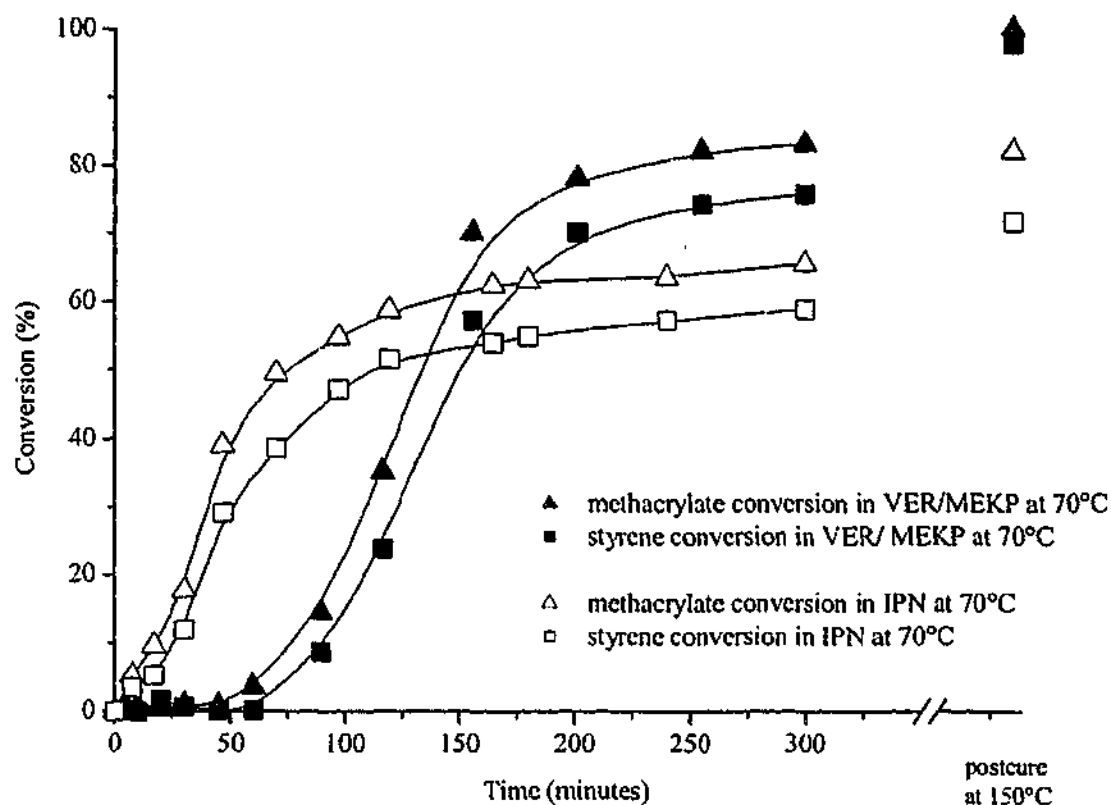


Figure 5.27 Epoxy conversion versus time for both the neat DGEBA/1-MeI resin and in the 50:50 blend of VER/CHP:DGEBA/1-MeI

### (c) MEKP initiated systems

The FTIR conversions of styrene and methacrylate units in both the pure VER/MEKP resin and the IPN at 70°C are shown in Figure 5.28. In contrast to the extensive induction period found for the conversion of vinyl ester components in the neat resin, a minimal induction period is observed for both the styrene and methacrylate groups within the IPN at 70°C (Figure 5.28) and the initial polymerization rate is higher in the IPN as was observed with the CHP-containing IPNs. These results support the DSC data (Figure 5.20) suggesting accelerated decomposition of the MEKP initiator by the 1-MeI tertiary amine. For the neat resin, the conversion of styrene and methacrylate groups at 70°C attains a plateau conversion of approximately 70% and 80% respectively due to vitrification (see Section 2.1.1), and both groups reach close to full cure after postcuring at 150°C. In contrast, the IPN conversion of the styrene and methacrylate groups level out at approximately 50% and 60% respectively and even after the postcure

at 150°C, the styrene and methacrylate units within the IPN only reach 70% and 80% conversion, respectively. This is consistent with the DSC studies of this system (Table 5.3) and further confirms the degradation of the MEKP by the imidazole causing either a dead-end effect<sup>227-229</sup> or depletion of radicals by a non-radical-producing side reaction.



**Figure 5.28** Dimethacrylate and styrene conversion versus time in the VER/MEKP system and in the 50:50 blend of VER/MEKP:DGEBA/1-MeI (5 wt%) at 70°C.

Figure 5.29 compares the epoxy conversion in the neat DGEBA/1-MeI and the MEKP-initiated IPN. As found for the IPN systems radically initiated by CHP (see Section 5.2.3(b)) and AIBN (see Section 5.2.3(a)), the epoxy conversion within the IPN is significantly retarded in comparison with the neat system, due to a dilution effect and perhaps due to the crosslinking of the VER component prior to significant epoxy cure, as discussed earlier. Full cure of the epoxy groups in the IPN was attained on postcure at 150°C.

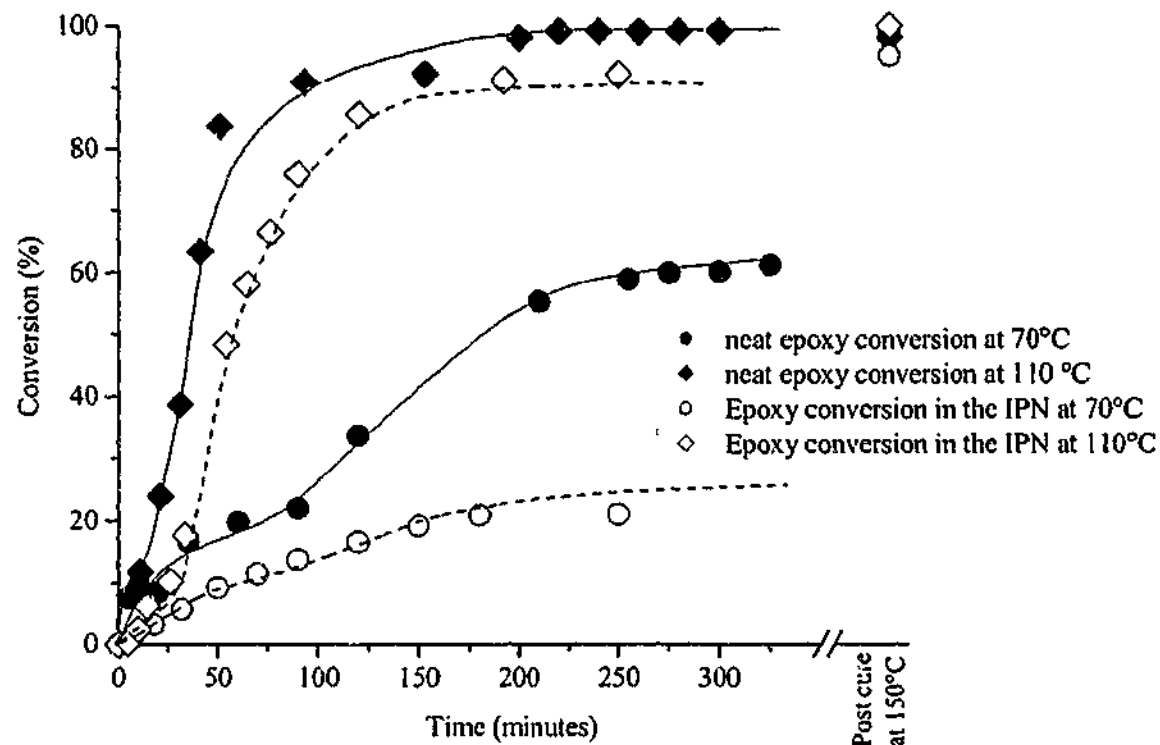


Figure 5.29 Epoxy conversion versus time for both the neat system of DGEBA/1-MeI and in the 50:50 blend of VER/MEKP:DGEBA/1-MeI at 70 and 110°C.

### 5.2.4 Conclusions

IPNs were prepared from imidazole-cured DGEBA and radical-cured VER. The AIBN-containing IPNs did not show significant interaction effects between the VER and epoxy components, and for the AIBN- or CHP- initiated systems, full cure of the VER was achieved at moderate temperatures as indicated by the scanning DSC heat of polymerization and from the isothermal FTIR conversion-time data. However, all of the peroxide-initiated IPN systems exhibited an apparent redox reaction between the 1-MeI amine and the peroxide, causing accelerated decomposition of the peroxides to radicals, and hence this accelerated the rate of cure of the vinyl ester component. In the case of MEKP and BPO, the cure of the vinyl species was incomplete due to loss of initiator activity, perhaps by non-radical redox reactions - full cure was not achieved even at high temperatures for these two IPNs.

The extent of epoxy cure was nearly complete at moderate temperatures for all IPN systems. This suggests that even if interactions occurred between the initiator systems, there was sufficient residual imidazole to allow full cure.

In general, dilution effects of the reacting DGEBA system by the VER components were observed for the IPNs in the early stages of the cure. In addition, during isothermal cure at 70°C, unreacted DGEBA monomer plasticized the IPN allowing a higher plateau conversion of the vinyl groups in the IPN, provided there were no strong interactions between the 1-MeI and the radical initiators. In contrast, when the conversion of the VER component was near complete, the subsequent reaction of the epoxy was limited by vitrification of the IPN associated with the high level of crosslinking in the VER component.

## 5.3 Anhydride based IPNs

### 5.3.1 Introduction

In this section the polymerization kinetics for IPNs formed from a model VER and an anhydride-cured epoxy resin have been studied by scanning DSC. This system was chosen as an alternative to the amine-cured epoxy based IPNs, as it was observed in Sections 5.1 and 5.2 that a number of interactions occurred between amines and other components within these IPNs.

### 5.3.2 Differential scanning calorimetry of IPN cure

The cure behaviours of the AIBN-initiated VER, the CHDCA/DMBA cured DGEBA and the resulting 50:50 IPN is shown in Figure 5.30. The DSC thermograms of the neat VER/AIBN and the DGEBA/CHDCA/DMBA exhibit single peaks at 92°C and 144, whereas the 50:50 VER/AIBN:DGEBA/CHDCA/DMBA shows two distinct exotherms. The observed heat of polymerization of VER/AIBN was 327 J/g, suggesting 96% cure (c/f theoretical – see Section 5.1.2). The heat of polymerization of the epoxy system was 330 J/g corresponding to 122 kJ/mol, which was a little higher than the energy involved

in opening the epoxy ring during cure of the uncatalyzed tetraepoxy/anhydride systems (105-106 kJ/mol) reported by Corcuerra *et al.*<sup>234</sup>. Based on the close correspondence of peak temperatures in the neat and blended systems, the lower and upper exotherms in the DSC trace of the 50:50 IPN can be attributed to the VER and DGEBA cure, respectively. The exotherm due to the VER/AIBN cure is shifted from 92 to 95°C, perhaps due to a dilution effect by the epoxy component and the exotherm due to the DGEBA/CHDCA/DMBA has shifted from 144 to 150°C due to the corresponding dilution effect by the VER. The total heat of polymerization (332 J/g) is very close to the mean of the parent resins (329 J/g) and the resolved contributions to the DSC exotherm show that the areas of the lower and upper peaks are approximately proportional to the weight fractions of VER and epoxy components in the IPN respectively - the discrepancy in these values may be due to the method by which the exotherm contribution from each component is measured (see Section 4.2).

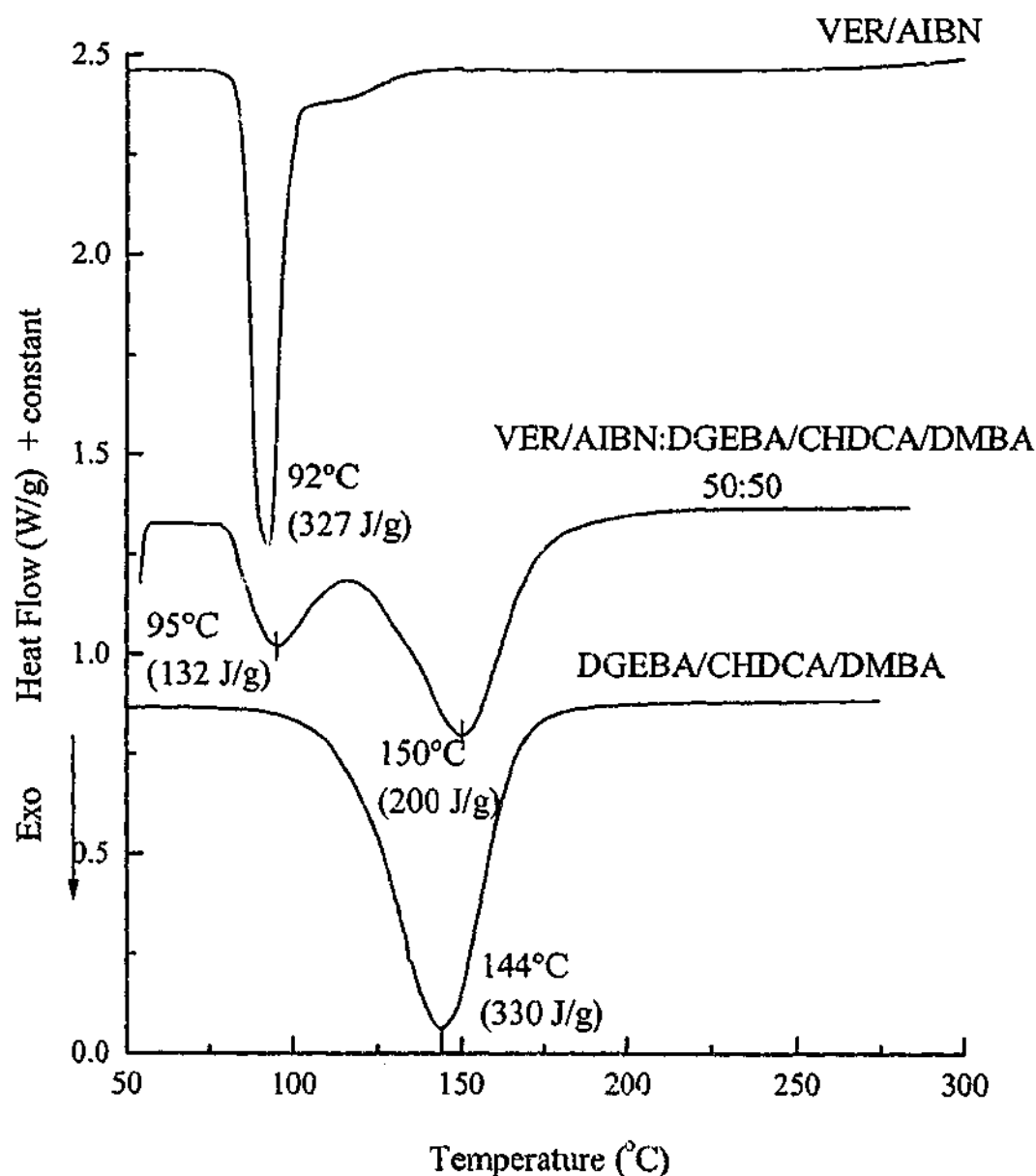


Figure 5.30 DSC scans of VER/AIBN, DGEBA/CHDCA/DMBA and the 50:50 IPN

### **5.3.3 Conclusions**

Both the VER/AIBN and DGEBA/CHDCA/DMBA components within the IPN produced exotherms at slightly higher temperatures compared to their parent resins due to dilution effects. The 50:50 VER/AIBN:DGEBA/CHDCA/DMBA IPN did not show any significant interactions between the VER and the epoxy components (as seen in some of the previously discussed systems). The heats of polymerization measured for the IPN indicated that close to full cure was achieved.

# *Chapter 6*

## *Chemorheology of IPNs and correlation with near FTIR*

---

### **6.1 Introduction**

The changes in rheology of a thermoset as it cures are very important to its application but evolution of the rheology can also provide vital information on the cure kinetics, phase separation, gelation and vitrification. Rheological and NIR spectroscopic investigations have been undertaken for two different IPNs based on a model VER cured with AIBN and an epoxy monomer cured either with 1-MeI, or with a stoichiometric quantity of DDM. The VER/AIBN:DGEBA/1-MeI IPN was selected as it exhibited minimal interactions between components (see Section 5.2) and close to full cure could be achieved while the VER/AIBN:DGEBA/DDM IPN was chosen as a more complicated system in which a number of interactions occurred (identified in Section 5.1).

### **6.2 Curing Kinetics**

Typical NIR spectra of VER/AIBN:DGEBA/1-MeI (using 2 wt% 1-MeI rather than the standard level of 5 wt%) are shown in Figure 6.1 obtained during isothermal cure at 70°C. The level of imidazole was reduced in an attempt to reduce the discoloration of the cured DGEBA/1-MeI resin caused by the 1-MeI, and curing studies (see Chapter 7) indicated the level of cure of the DGEBA was not lowered by this reduction. The absorptions due to the styrene ( $6135\text{cm}^{-1}$ )<sup>212</sup> and methacrylate

$(6166\text{cm}^{-1})^{212}$  species rapidly decrease in the initial 25 minutes of isothermal cure at  $70^\circ\text{C}$  while the epoxy group absorption  $(6073\text{cm}^{-1})^{213}$  decreases less rapidly due to its lower polymerization rate. After postcure at  $160^\circ\text{C}$ , however, the epoxy reaction appeared to be essentially complete. Unfortunately, the vinyl resonances of the styrene ( $6135\text{cm}^{-1}$ ) and methacrylate ( $6166\text{cm}^{-1}$ ) groups overlap. Since previous mid-FTIR investigations (see Sections 5.1.3 and 5.2.3) indicated that the rate of cure of styrene and methacrylate vinyl groups are very similar, the NIR vinyl resonances were not separated

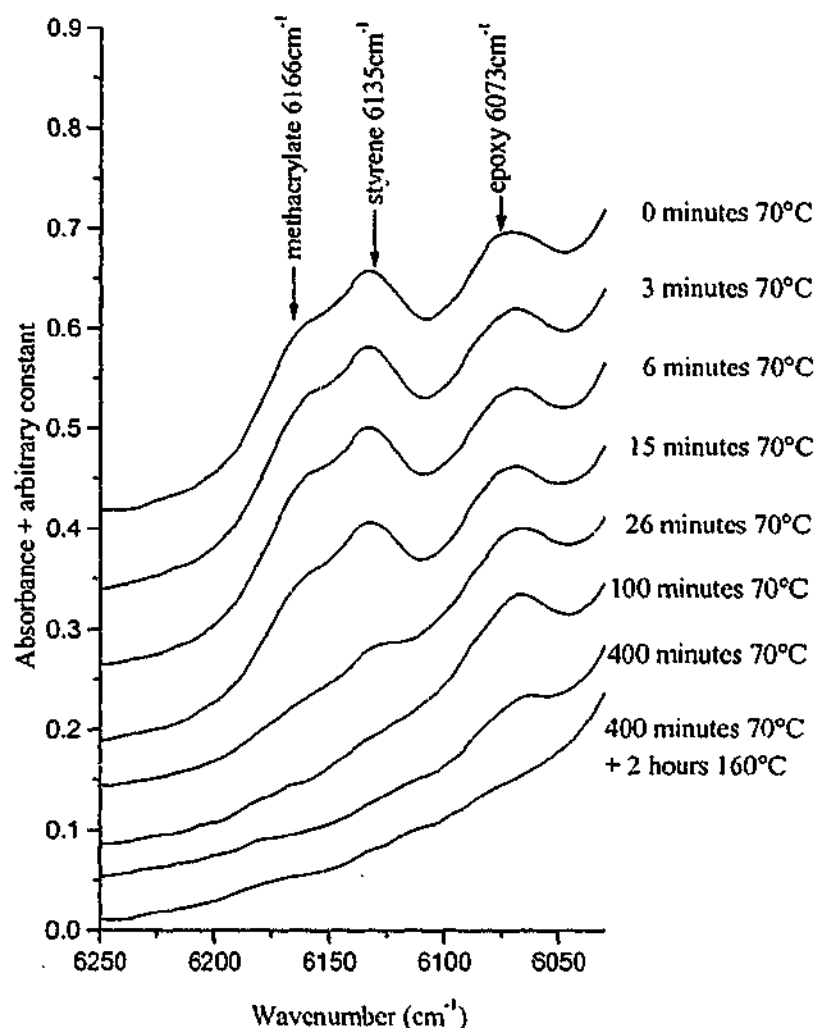


**Figure 6.1** Near infra-red spectra during cure of the 50:50 VER/AIBN:DGEBA/1-MeI IPN at  $70^\circ\text{C}$ .

in the present study, but their total area was measured to give the total vinyl group conversion. As observed in the isothermal curing study of aniline, butylamine and imidazole based IPNs (see Sections 5.1.3 and 5.2.3), the vinyl conversion in the neat VER/AIBN, 1-MeI- and DDM-based IPNs exhibit brief induction periods (see Figure 6.2), presumably due to the presence of free radical inhibitors in the resins. Figure 6.2 shows that the rate of conversion of styrene and methacrylate species in the neat VER/AIBN is faster than in the 50:50 IPN of DGEBA/1-MeI:VER/AIBN and, more

significantly faster than in the 50:50 IPN of DGEBA/DDM:VER/AIBN. If the effect of dilution of the VER component by the epoxy component on the rate constant is ignored, then one would expect the VER to polymerize more slowly in the IPN than in the neat resin system due to the reduction in concentration of the reactant components. Thus the lower rate of vinyl group conversion in the IPNs may be due (in part) to the dilution of the VER reactants, as we have observed elsewhere (see Chapter 5 and Section 2.4). Figure 6.2 also shows that the vinyl groups in the VER/AIBN:DGEBA/DDM IPN cure more slowly than in the VER/AIBN:DGEBA/1-MeI IPN. This may result from the reaction of the isobutyl radicals or the polymer chain radicals with the DDM amino groups forming less reactive amine radicals. This explanation is consistent with similar observations that the polymerization of methyl methacrylate can be either retarded or inhibited by aromatic primary amines<sup>235</sup>, as discussed in Section 5.2.3. In the VER/AIBN:DGEBA/DDM system, the DDM concentration is much higher than the 1-MeI concentration in the VER/AIBN:DGEBA/1-MeI system and so the DDM radical reaction would be more likely and may explain its slower cure.

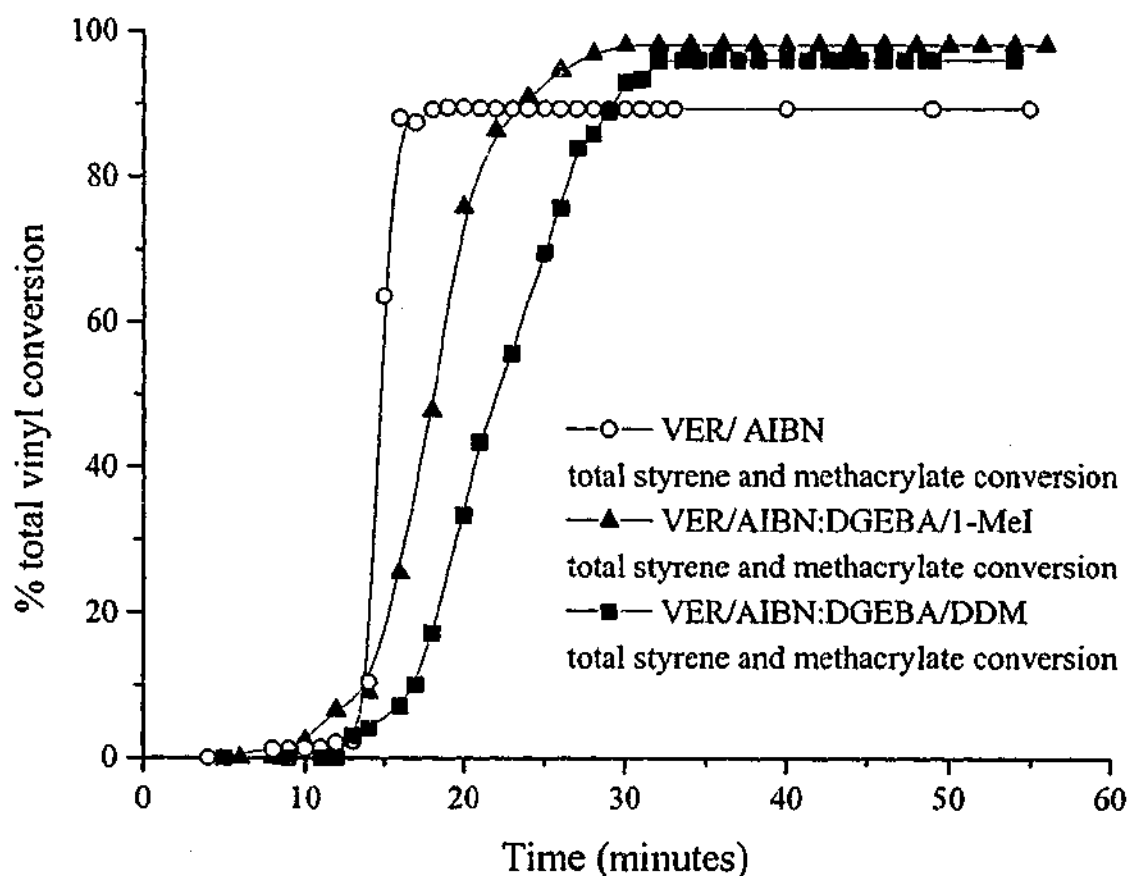


Figure 6.2 Comparison of the total vinyl conversion in the neat VER/AIBN system, the 50:50 VER/AIBN:DGEBA/1-MeI and VER/AIBN:DGEBA/DDM IPNs at 70°C.

The conversion of the vinyl groups in the neat VER reaches a plateau value of ca. 90% at 70°C (see Figure 6.2). This premature cessation of the reaction is presumably due to vitrification of the matrix<sup>14,56</sup> which reduces the molecular mobility and hence reactivity, because the  $T_g$  of the post-cured VER (169°C)\* is much greater than the isothermal cure temperature employed (70°C). Both IPN systems exhibit a higher final conversion of styrene and methacrylate groups compared with the neat VER/AIBN system. As suggested earlier (see Figure 5.13 and Figure 5.23), this increase in conversion may be due to the presence of the unreacted DGEBA from the more slowly reacting epoxy component of the IPN that acts as a plasticizer providing greater mobility within the system and hence allowing a higher degree of vinyl conversion before vitrification occurs.

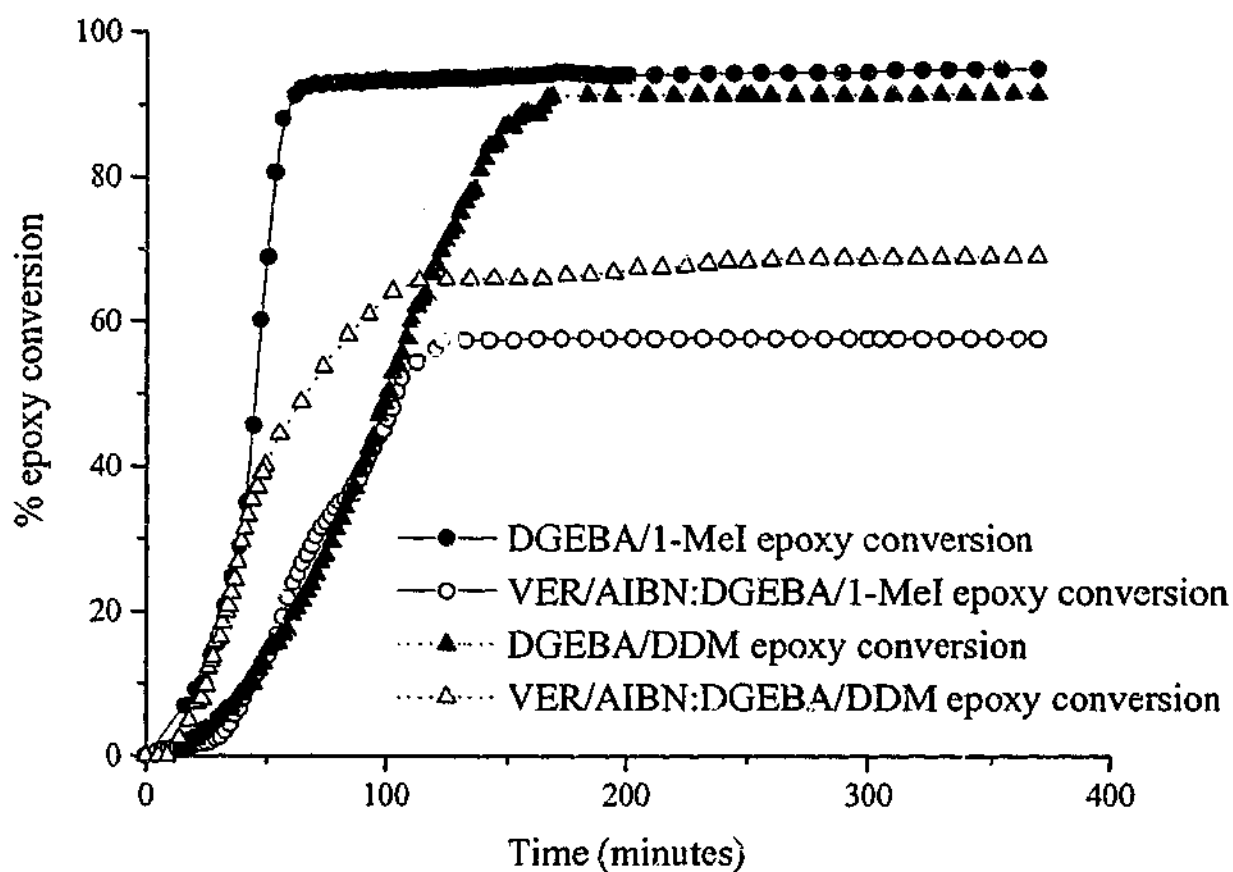


Figure 6.3 Comparison of epoxy conversion in the neat DGEBA systems, the 50:50 wt% VER/AIBN:DGEBA/1-MeI and VER/AIBN:DGEBA/DDM IPNs at 70°C.

The dependence of epoxy group conversion on cure time is illustrated in Figure 6.3. For both IPNs and their parent resins, the rate of consumption of epoxy groups is not as rapid as observed for the styrene and methacrylate groups as noted above. For the imidazole-cured system, the rate of epoxy conversion in the IPN is lower than in the

\* Early DMTA studies<sup>236</sup> suggested that the  $T_g$ s for the VER and epoxy were lower than reported here. This has since been proved incorrect and may have been due to incorrect temperature calibration of the instrument.

neat resin. This observation is consistent with results presented in Chapter 5 and can be explained in terms of a dilution effect such that the presence of the vinyl ester component within the IPN reduces the concentration of 1-MeI and epoxy species and thus slows the rate of the polymerization reaction. In contrast, Figure 6.3 shows an enhanced rate of epoxy conversion in the VER/AIBN:DGEBA/DDM IPN system compared with the epoxy conversion in the neat system. As discussed in Section 2.1.2 and Section 5.1.2, it is well known that the amine/epoxy reaction is catalyzed by H-donors<sup>66,73</sup> and it is possible that the presence of the hydroxy groups in the bisGMA molecule act as a catalyst of the epoxy-amine reaction which offsets any dilutional effect, with the result that the rate of epoxy conversion within the VER/AIBN:DGEBA/DDM IPN is actually enhanced. Alternatively, the IPN may be phase separated when the epoxy component cures so that its components are not diluted by the VER. The epoxy conversion approaches a plateau of approximately 90-95% (after 450 minutes at 70°C) in the neat DGEBA/1-MeI and DGEBA/DDM systems (see Figure 6.3). This conversion limit may be caused by vitrification of the network during cure at 70°C because the fully cured resins have  $T_g$ s of 185°C (DGEBA/1-MeI with 2 wt% 1-MeI) and 189°C (DGEBA/DDM), which are greater than the curing temperature. More significantly, the conversion of the epoxy group approaches a plateau of approximately 60% and 70% (after 450 minutes at 70°C) in the VER/AIBN:DGEBA/1-MeI and VER/AIBN:DGEBA/DDM IPNs respectively which is significantly lower than in the neat systems. If it is assumed that the IPN is one phase (or if a certain level of miscibility exists) then the difference between the plateau conversions of the neat epoxy resin and in the IPN can be interpreted in terms of the degree of cross-linking in the VER component as suggested previously (see Section 5.2.3). After curing at 70°C for only 30 minutes, the VER component in the IPN is nearly fully cured (see Figure 6.2) and so its contribution to the crosslink density of the IPN would be high. Therefore the  $T_g$  of the IPN (or the epoxy-rich phase if partially phase separated) would have been raised by the prior cross-linking of the VER component so that during cure at 70°C, the epoxy component may only polymerize partially before the IPN vitrifies. In fact, full conversion of the epoxy component in the IPNs is not observed until after postcuring above the  $T_g$  of both pure components, indicating that vitrification was responsible for incomplete epoxy cure. The observation that the epoxy component in the IPN can be fully cured shows that the presence of the VER network does not exert a significant topological restraint on the capability of the epoxy to cure.

### 6.3 Gelation

The changes in the steady shear viscosity during cure of the thermoset blends and their respective pure components at 70°C are shown in Figure 6.4. Using the gel point criteria of viscosity divergence (see Section 2.1.4), the neat VER/AIBN system gelled at 8 minutes. The two neat epoxy systems, DGEBA/1-MeI and DGEBA/DDM, gelled at 57 minutes and 115 minutes, respectively. It would appear that the neat VER/AIBN system gels earlier than the epoxy resin because the VER/AIBN system polymerizes faster and because gelation of divinyl systems occurs at low conversions<sup>33</sup> (see 2.1.3) - in fact a comparison of the NIR and rheology data for the VER/AIBN system suggests the conversion of vinyl groups at gel point is less than 2% (Table 6.1).

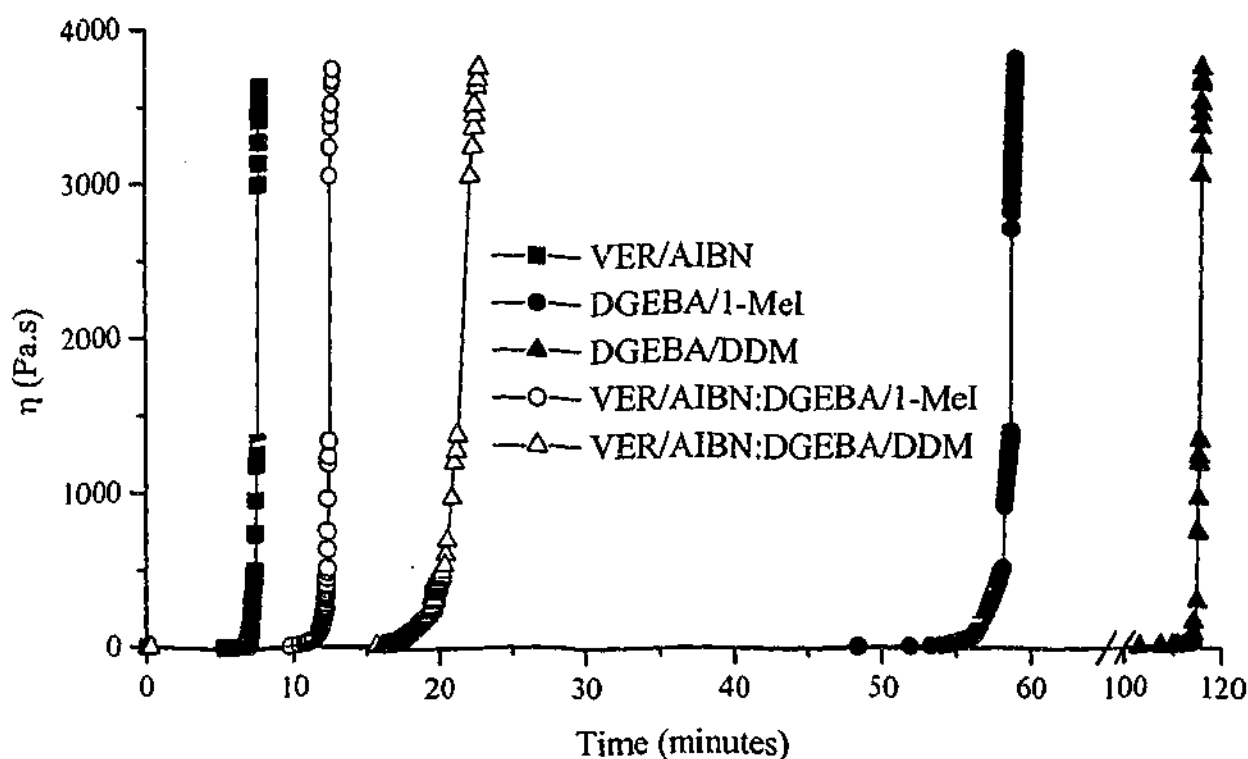


Figure 6.4 Steady shear viscosity versus time for the pure components and respective blends at 70°C

In contrast, the epoxy systems polymerize more slowly and the conversions at the gel points are expected to be higher. For DGEBA/DDM, the high conversion at the gel point (measured to be 60%- compared to the theoretical value<sup>23,31</sup> of 57%- see Section 2.1.2) is a result of the step growth nature of the reaction. The DGEBA/1-MeI system should gel at a relatively high conversion for a chain growth polymerization because the kinetic chain length of the anionic chain growth polymerization of epoxy groups is relatively low<sup>237</sup> however the measured value (70% - see Table 6.1) is higher than expected. The VER/AIBN:DGEBA/1-MeI IPN and the VER/AIBN:DGEBA/DDM IPN

gelled (as determined by steady shear rheometry) at 12 minutes and 21 minutes respectively. The proximity of the gel times for the VER/AIBN:DGEBA/1-MeI and VER/AIBN:DGEBA/DDM IPNs to that of the neat VER system is close and the resemblance of their viscosity indicates that gelation in the IPNs is determined by gelation of the VER component. The gelation times of VER/AIBN, VER/AIBN:DGEBA/1-MeI and VER/AIBN:DGEBA/DDM also correlates well with the near-FTIR data, which shows that the rate of vinyl conversion in the VER/AIBN resin is fastest, the rate in the VER/AIBN:DGEBA/1-MeI IPN is intermediate and that for the VER/AIBN:DGEBA/DDM IPN the vinyl cure is slowest.

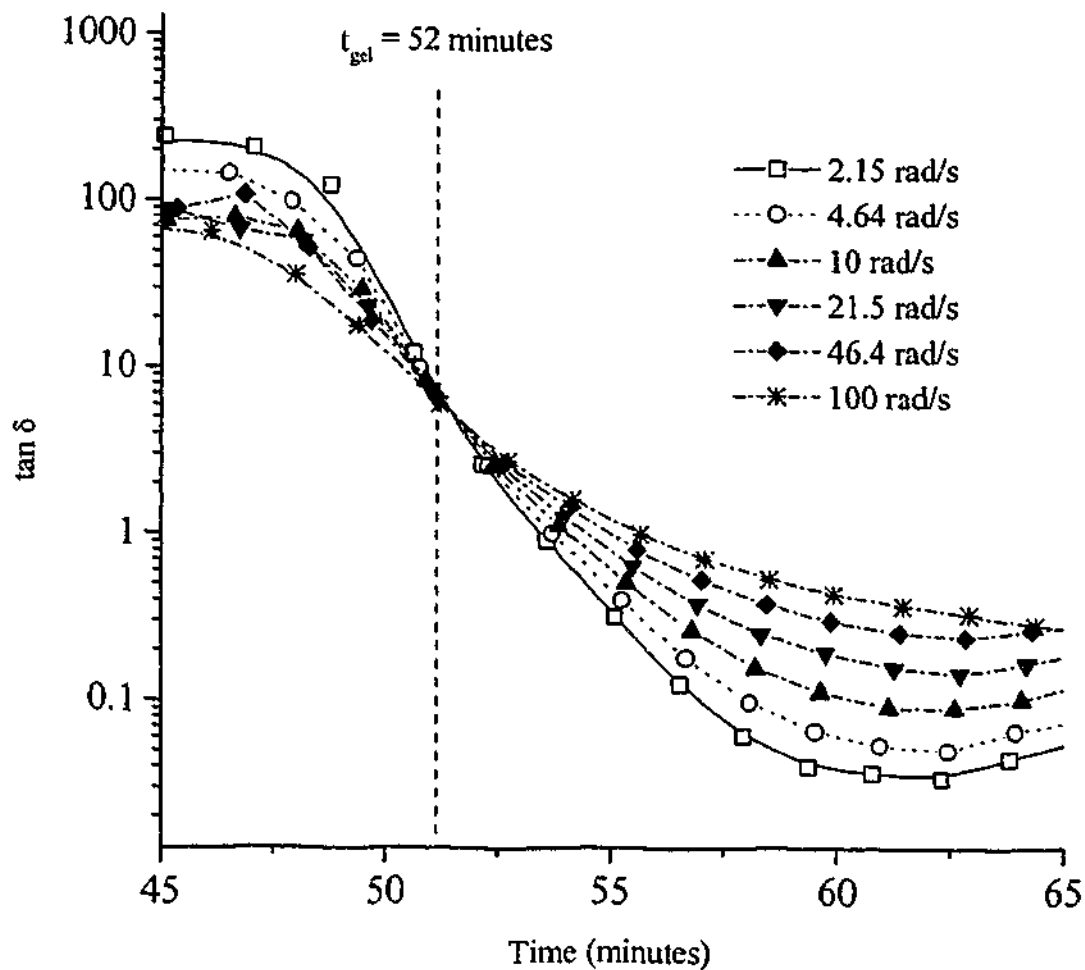
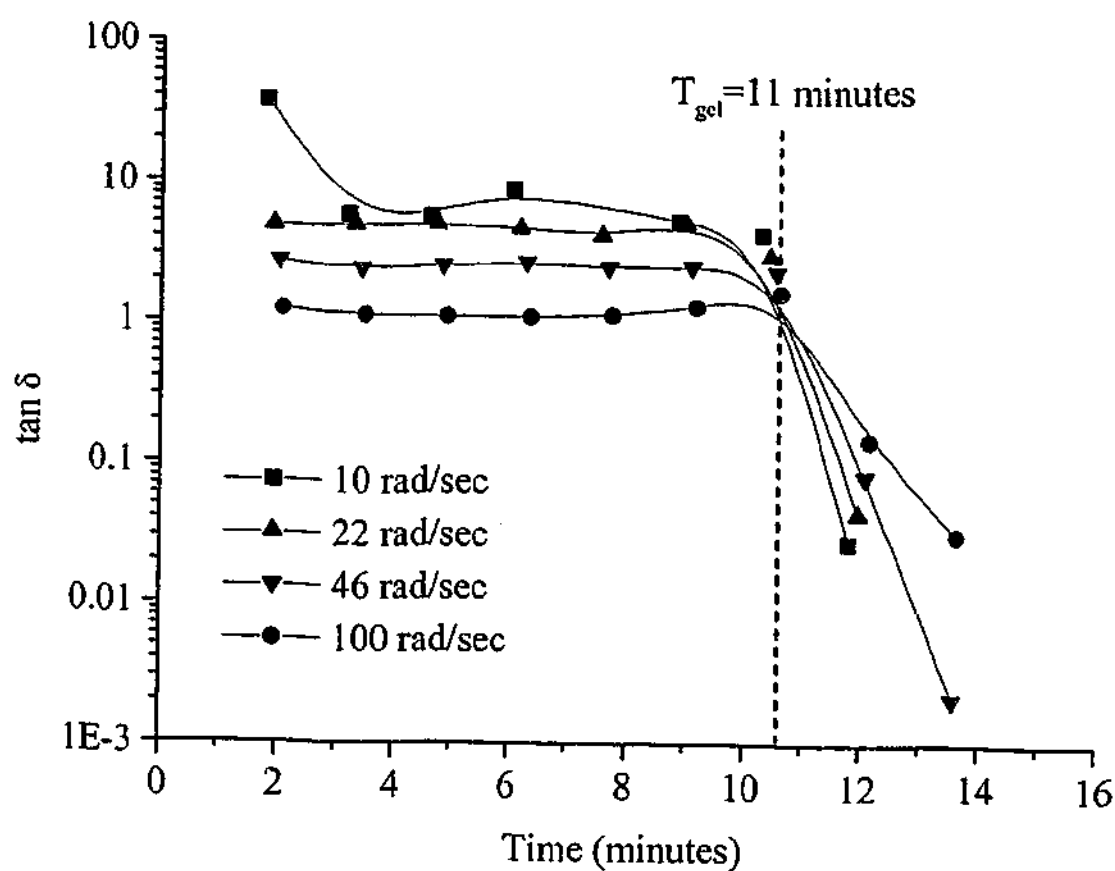


Figure 6.5 Frequency dependence of  $\tan \delta$  as a function of reaction time for neat DGEBA/1-MeI at 70°C

The frequency independence of  $\tan \delta$  at the gel point is commonly observed as a 'frequency crossover point' (see Section 2.1.4) - below the gel point, the  $\tan \delta$  decreases

with increasing frequency whereas the reverse is observed above the gel point. A frequency crossover in  $\tan\delta$  for the pure DGEBA/1-MeI system is illustrated in Figure 6.5 indicating the gel point at 52 minutes. This value agrees quite well with the steady shear viscosity experiments, which indicated a gel point at 57 minutes (Table 6.1). The corresponding dynamic rheometry behaviour for the VER/AIBN:DGEBA/1-MeI IPN is illustrated in Figure 6.6 and shows a frequency crossover for the IPN at 11 minutes, in good agreement with the 12 minute gel time determined by steady shear rheometry (see Table 6.1). A frequency crossover in  $\tan\delta$  for the pure DGEBA/DDM system was observed at 112 minutes. This value also agrees quite well with the steady shear viscosity experiments, which indicated a gel point at 115 minutes (Table 6.1). The corresponding dynamic rheometry behaviour for the VER/AIBN:DGEBA/DDM IPN is illustrated in Figure 6.7 and shows a frequency crossover for the IPN at 13 minutes,



**Figure 6.6** Frequency dependence of  $\tan\delta$  as a function of reaction time for VER/AIBN:DGEBA/1-MeI at 70°C

slightly shorter than the 21 minute gel time determined by steady shear rheometry Table 6.1 shows that the value of the power-law exponent  $n$  (see Chapter 2), calculated from  $\tan\delta$  via Equation 2.13, varies from 0.48 to 0.98 which lies within the range 0.33-1.0 (see Section 2.1.4) predicted from various gelation theories<sup>54</sup>.

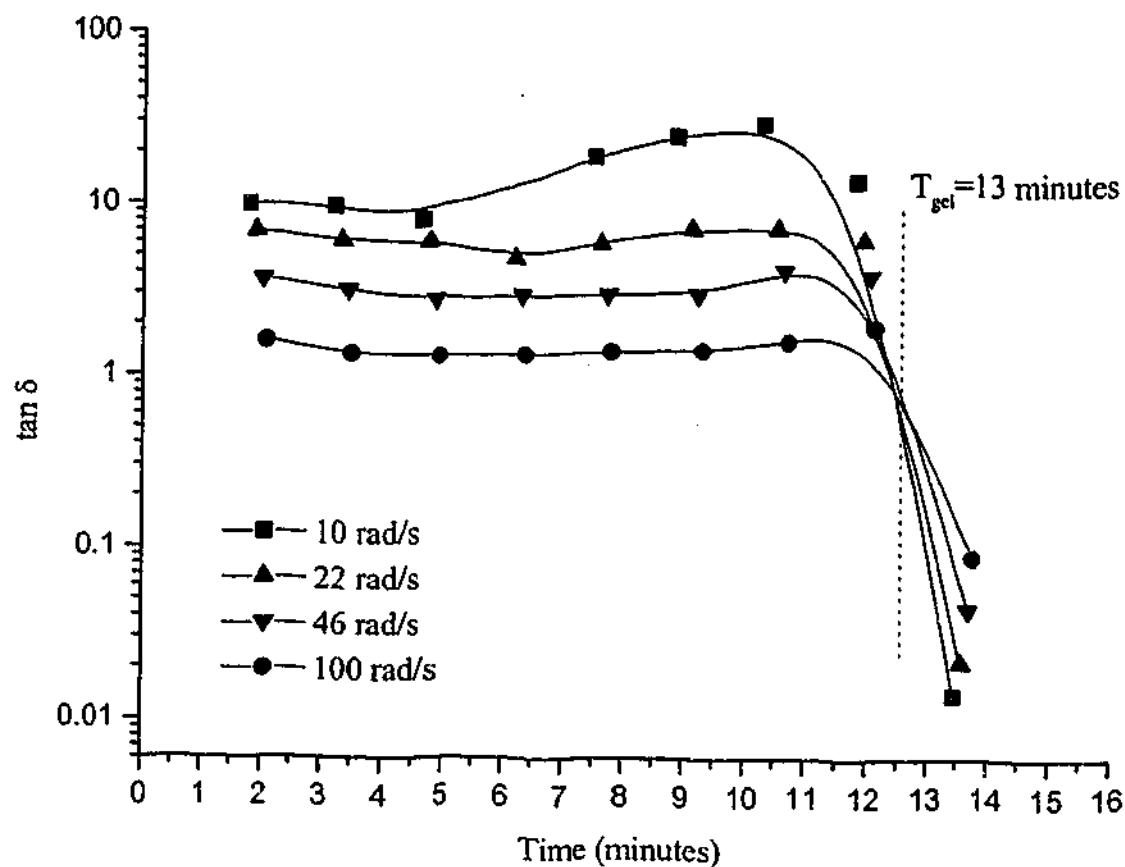


Figure 6.7 Frequency dependence of  $\tan \delta$  as a function of reaction time for VER/AIBN:DGEBA/DDM at 70°C

Figure 6.8 illustrates the dependence of real modulus ( $G'$ ) on cure time for the pure components and their respective blends. In each system, there is a time regime in which the modulus starts rapidly rising because of the increasing number of crosslinks being added to the hyper-branching structure as it develops into a three dimensional gel. As revealed in Table 6.1, the operational definition of gelation as the stage where  $G'$  equals 1 Pa (see Section 4.4), gives an approximation to the gel time which agrees reasonably well with the more rigorous methods.

The gel times of the network-forming systems and the corresponding conversions of the reactive functional groups (obtained by NIR- see Section 6.2) are listed in Table 6.1. For the free radical polymerized VER/AIBN system, gelation occurs at such low conversions that the crossover of  $\tan \delta$  could not be observed, hence the times at which  $G'$  equaled 1 Pa and when the steady shear viscosity diverged to infinity were used to determine the gel point. The gel points of the IPNs are close to that of the VER/AIBN system and occur at low conversions of the vinyl groups, showing that the gelation of the IPN is very much dependent on the gelation of the VER/AIBN component of the IPN. Table 6.1 reveals that the gel times of the IPNs are longer than

for the neat VER and this is consistent with the effect of dilution on the reaction rate (for VER/AIBN:DGEBA/DDM and VER/AIBN:DGEBA/1-MeI) and cure retardation by amine-radical interactions (for VER/AIBN:DGEBA/DDM) as suggested earlier (see Section 5.1.3). The effect of dilution on the gelation time of the IPN components is further supported by dilution studies of the VER with xylene - Figure 6.8 shows that the gelation of the resin was delayed when it was diluted by 50 wt% xylene.

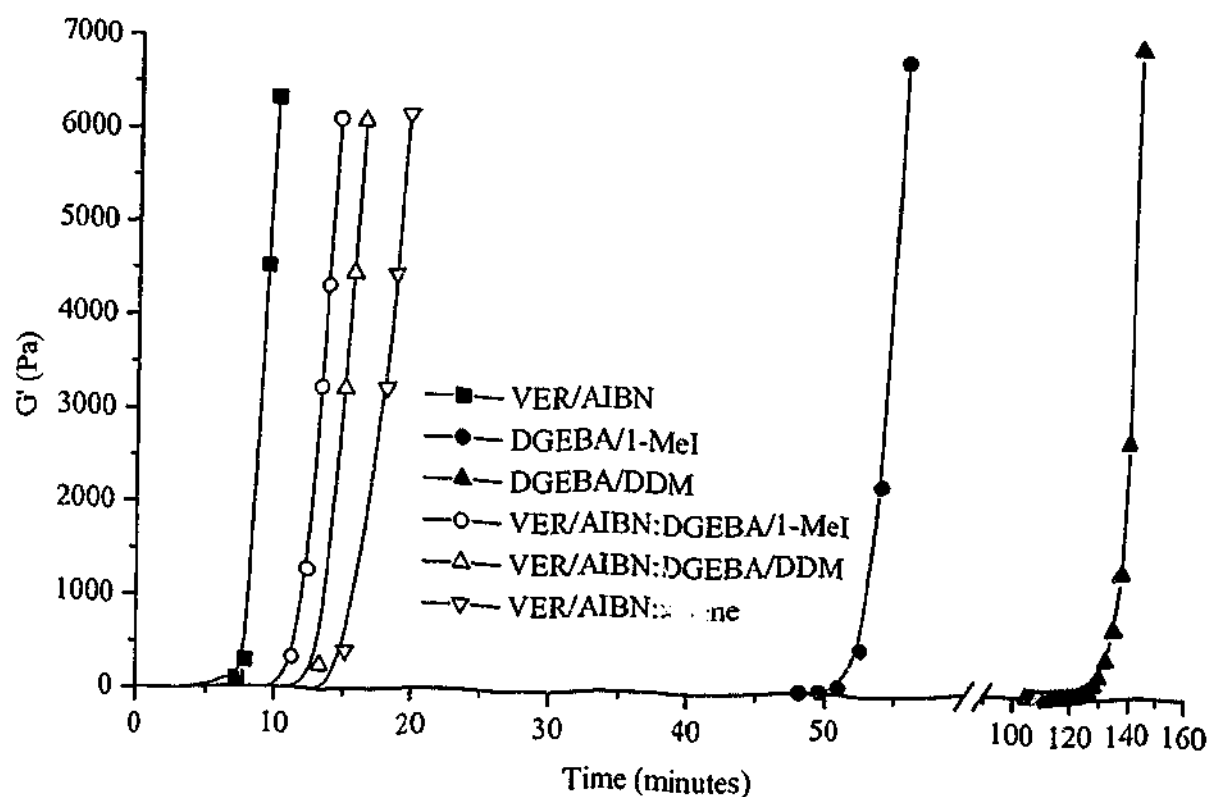


Figure 6.8 Real modulus ( $G'$ ) at 22 rad/s as a function of reaction time for the neat resins and the 50:50 IPNs and for a 50:50 mixture of VER and xylene at 70°C, near the gelation point.

## 6.4 Vitrification

Figure 6.9 and Figure 6.10 show the development of the real modulus with time, highlighting the rheological changes occurring in the final stages of cure. The vitrification times (taken to be the time when  $G'$  equals  $10^7$  Pa) and the corresponding vinyl and epoxy conversions at the onset of vitrification for the neat resins and IPNs are listed in Table 6.2. All neat resin systems vitrified at high conversions when cured at 70°C. The VER/AIBN system was the first to approach the vitrification region, with the real modulus attaining a value of  $10^7$  Pa after curing at 70°C for approximately 30 minutes. The neat epoxy resins reached the vitrification region well after this time - vitrification occurs at 145 minutes for DGEBA/1-MeI and at 180 minutes for the

DGEBA/DDM system. In contrast, the IPNs vitrify at much later times of 260 minutes for the VER/AIBN:DGEBA/1-MeI IPN and 435 minutes for the VER/AIBN:DGEBA/DDM IPN.

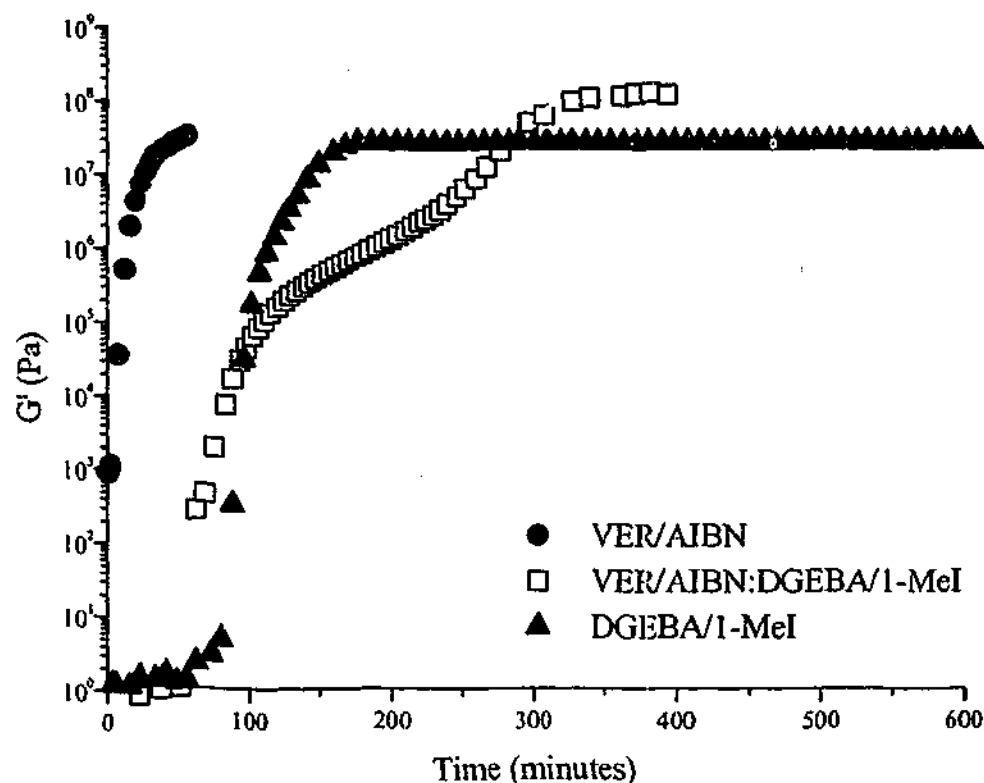


Figure 6.9 Real modulus ( $G'$ ) at 22 rad/s as a function of time for the 50:50 VER/AIBN:DGEBA/1-MeI IPN and the parent resins in the vitrification region at 70°C.

For the parent resins, there is a correlation between the rheological vitrification time and that measured from the NIR conversion data (see Table 6.2), although the latter values are generally significantly smaller than the former. This difference is explained by the different sensitivity of vitrification on cure as measured by the two methods. Similarly, for the IPNs, the vitrification times determined by NIR are smaller than the rheological values, however there is no correlation between the two. This lack of agreement may be a reflection of the fact that small changes in reaction can have dramatic effects on the modulus in the transition region and that this is further complicated in an IPN because there are two reaction processes building up the structure.

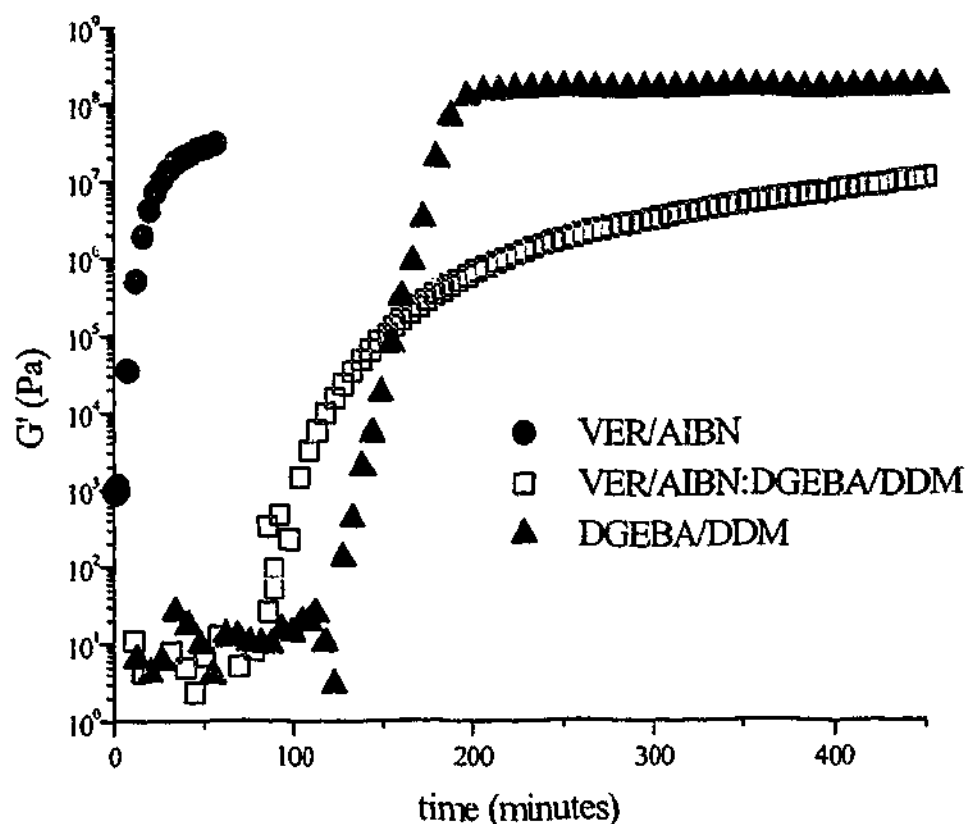


Figure 6.10 Real modulus ( $G'$ ) at 22 rad/s as a function of time for the 50:50 wt% VER/AIBN:DGEBA/DDM IPN and the parent resins in the vitrification region at 70°C.

It is interesting to note that for the IPNs, the modulus slowly rises to the glass-like plateau over a long period of time compared with the parent resins. For VER/AIBN:DGEBA/1-MeI, there appears to be two steps in the development of the modulus. These observations are qualitatively consistent with the conversion data (Figure 6.3) because the modulus of the VER/AIBN:DGEBA/1-MeI IPN develops from the point where the first component (the VER) gels through to the stage where the more slowly reacting component (the epoxy resin) finally vitrifies. In contrast, a two stage development of the real shear modulus is not evident for the VER/AIBN:DGEBA/DDM IPN, possibly due to the greater overlap of the time regimes where the VER and the DGEBA/DDM components are curing.

Table 6.2 shows that the coconversion of vinyl and epoxy groups at the vitrification point was incomplete in the neat parent resins because the curing temperature (70°C) was less than the maximally attainable  $T_g$ . However, the vinyl group conversion was marginally higher in the IPNs than in the neat resin system while the epoxy conversions in the IPNs were significantly lower at vitrification. This is

consistent with the observations that the VER is the faster polymerizing component and its reaction is aided by the plasticizing effect of the more slowly reacting DGEBA component - in contrast the cure of the DGEBA is prematurely interrupted by vitrification as a result of the high level of crosslinking in the VER component, as discussed in Section 5.1.3 and 5.2.3.

**Table 6.1 Summary of rheology and kinetics at the gel point at 70°C.**

System	VER/ AIBN	DGEBA/ 1-MeI	DGEBA/ DDM	VER/AIBN: DGEBA/ 1-MeI	VER/AIBN: DGEBA/DDM
Gel time from steady shear viscosity	8 minutes	57 minutes	115 minutes	12 minutes	21 minutes
Gel time determined from the time when $G' = 1$ Pa	5 minutes	46 minutes	98 minutes	9 minutes	11 minutes
Gel time from $\tan\delta$ crossover	Not clearly observed	52 minutes	112 minutes	11 minutes	13 minutes
$\tan\delta$ at gelation and power-law exponent (in brackets)	Not clearly observed	5.5 (0.88)	43.2 (0.98)	1.25 (0.57)	0.94 (0.48)
NIR conversion of total C=C groups at gelation ( $\tan\delta$ crossover)	<ca 2%*	-	-	<ca 2%	<ca 2%
NIR conversion of epoxy groups at gelation ( $\tan\delta$ crossover)	-	70 %	60 %	<ca 1%	<ca 1%

\* determined at  $G' = 1$  Pa

**Table 6.2 Summary of rheology and kinetics at the onset of vitrification (at  $G' = 10^7$  Pa) at 70°C**

System	VER/AIBN	DGEBA/ 1-MeI	DGEBA/ DDM	VER/AIBN: DGEBA/1-MeI	VER/AIBN: DGEBA/DDM
Vitrification time at $G' = 10^7$ Pa	30 minutes	145 minutes	180 minutes	260 minutes	435 minutes
Vitrification time (plateau in conversion)	15 minutes	60 minutes	170 minutes	140 minutes	90 minutes
NIR conversion of total C=C groups at vitrification	90%	-	-	98%	96%
NIR conversion of epoxy groups at vitrification	-	93%	90%	57%	68%

## 6.5 Conclusion

IPNs were prepared from a model VER and two epoxy resin systems and the rheometry was compared with NIR conversions at 70°C. For all systems, the rate of consumption of epoxy groups was slower than that found for the vinyl groups. The rate of vinyl (styrene and methacrylate) conversion in the 50:50 VER/AIBN:DGEBA/DDM was found to be slower than in the 50:50 VER/AIBN:DGEBA/1-MeI, and the rates of vinyl conversion in both IPNs were slower than in the neat VER/AIBN resin. This decrease in rate in the IPNs is partly due to the dilution of the VER reactants by the other components as previously observed by DSC and mid-FTIR studies of similar systems (see Chapter 5). In addition, a more dilute system may also promote cyclization, resulting in an increase in the critical conversion and thus delay gelation. In addition, for the VER/AIBN:DGEBA/DDM IPN, the DDM amino groups interacted with the radicals and retarded the cure rate of the vinyl groups. The rate of epoxy conversion in VER/AIBN:DGEBA/1-MeI was slower than in the neat DGEBA/1-MeI, which is also consistent with dilutional effects. In contrast, for the 50:50 VER/AIBN:DGEBA/DDM IPN, the epoxy group reaction was faster compared with the epoxy conversion in the neat system, due to the presence of the hydroxy groups in the bisGMA molecule acting as a catalyst of the epoxy-amine reaction, which offset any dilutional effect by the VER components.

The similarity between the gel points for the VER/AIBN system and the IPNs indicated it was the gelation of the VER component rather than the gelation of the epoxy component that had the dominant effect on the overall gel point of the IPN. The gelation was fastest in the neat VER/AIBN system and was slowest in the VER/AIBN:DGEBA/DDM IPN which correlated well with the NIR vinyl conversion data for VER/AIBN, VER/AIBN:DGEBA/1-MeI and VER/AIBN:DGEBA/DDM systems. The delayed gelation of the IPNs was due, in part, to a dilutional effect (confirmed by the study of a xylene diluted VER/AIBN resin) and in part due to amine-radical interactions.

All systems vitrified in the latter stages of the reaction because the isothermal cure temperature was well below the glass transition temperature of the resin

components. Compared with the parent resins, the real modulus for both IPNs rose more slowly to the glassy region and was consistent with the NIR results. The degree of conversion of the vinyl and epoxy groups when the parent resins and their IPNs vitrified was interpreted in terms of the plasticization of the VER component by DGEBA and the vitrification of the IPN prior to full cure of the epoxy component caused by the high level of crosslinking contributed by the VER component.

# *Chapter 7*

## *Azo initiator selection to control the curing order in epoxy/dimethacrylate IPNs*

---

### **7.1 Introduction**

In Chapters 5 and 6 the cure kinetics and rheology of IPNs formulated from DGEBA cured with a range of amines and a model VER mixture initiated by various radical sources were investigated. Two classes of effects were observed. The dilution effect and the influence of vitrification on the kinetics are innate to the cure of IPNs. In addition, chemical interactions between components which are specific only to the particular system investigated were observed. A number of effects were identified and are discussed in the conclusions of these chapters. In this chapter DSC and FTIR studies were undertaken on the cure of IPNs formed with imidazole-cured DGEBA and with either DEBPADM or bisGMA polymerized by a range of azo initiators (AIBN64, VAZ088, VR110 and AZO168) with differing decomposition rates. These systems avoid the Michael addition and minimized interactions between the radical initiator and the epoxy curative, and the range of azo initiators used enable the effect of curing order on the cure kinetics and final conversion to be investigated.

## 7.2 Curing Kinetics

### *bisGMA-based IPNs*

The temperature-ramping DSC scans for bisGMA/AIBN64, DGEBA/1-MeI and the 50:50 IPN are shown in Figure 7.1. Based on the heat of polymerization for methyl methacrylate of 56.2 kJ/mol<sup>17,222</sup>, the theoretical heat of polymerization of the bisGMA was calculated as 229.4 J/g (based on a bisGMA molecular weight of 490 g/mol obtained by titration – see Section 3.2). The observed heat of polymerization of bisGMA/AIBN was 175 J/g, suggesting 76% cure. The exotherm of DGEBA/2 wt% 1-MeI is located at a similar temperature and has a similar energy as that found for the resin cured with 5 wt% of 1-MeI. The heat of polymerization of DGEBA/2wt% 1-MeI was 475 J/g, corresponding to 92.5 kJ/mol, which was similar to that found in the literature for epoxy/imidazole systems (97-103 kJ/mol)<sup>231,232</sup> and similar to that reported in the literature for the cure of epoxy/diamine<sup>16,221,225</sup>. The DSC thermograms of the neat bisGMA/AIBN64 and the neat DGEBA/1-MeI exhibit single peaks whereas the corresponding 50:50 bisGMA/AIBN64:DGEBA/1-MeI IPN shows two distinct exotherms. The lower and upper exotherms in the DSC trace of the 50:50 IPN can be attributed to the bisGMA and DGEBA cure, respectively, because the resolved contributions to the DSC exotherm of the IPN show that the heats associated with the lower and upper peaks are approximately proportional to the weight fractions of bisGMA and epoxy components in the IPN respectively (see Figure 7.1). The bisGMA and DGEBA curing exotherms are shifted to higher temperatures in the IPN, as was found in the VER/AIBN:DGEBA/5wt% 1-MeI IPN (see Section 5.2.2), which is consistent with the effects of dilution, as discussed in Chapters 5 and 6. The shape of the exotherm due to the dimethacrylate cure is sharper in the IPN than in the parent resin which also suggests that the free radical polymerization kinetics are influenced by the presence of the epoxy components. The total heat of cure of the 50:50 IPN (326 J/g) is close to the weighted average of the parent resins (325 J/g - see Table 7.1) and is 92% of the average theoretical heat of polymerization for the 50:50 IPN (352 J/g) calculated from bisGMA (229 J/g) and the epoxy (from the epoxy ring opening value of 92 kJ/mol).

**Table 7.1 Summary of the DSC analysis of the bisGMA/AIBN64, DEBPADM/AIBN64, DEBPADM/VAZO88, DEBPADM/VR110, DEBPADM/AZO168, DGEBA/1-MeI and the IPNs formed from these resins**

System	Curing Peak (°C)	$\Delta H$ (J/g)	Integration range (°C)
bisGMA/AIBN64	99 °C	175 J/g	50-200
bisGMA/AIBN64:DGEBA/1-MeI 50:50 wt %	Peak 1. 104°C Peak 2. 127°C	Peak 1. 104 J/g Peak 2. 222 J/g	50-250
DGEBA/2wt % 1-MeI	118 °C	475 J/g	50-250
DEBPADM/AIBN64	78°C	220 J/g	50-200
DEBPADM/AIBN64:DGEBA/1-MeI 75:25	Peak 1. 86°C Peak 2. 127°C	Peak 1. 191 J/g Peak 2. 103 J/g	50-250
DEBPADM/AIBN64:DGEBA/1-MeI 50:50	Peak 1. 95°C Peak 2. 126°C	Peak 1. 138 J/g Peak 2. 226 J/g	50-250
DEBPADM/AIBN64:DGEBA/1-MeI 25:75	Peak 1. 90°C Peak 2. 123°C	Peak 1. 58 J/g Peak 2. 386 J/g	50-250
DGEBA/2 wt% 1-MeI	118°C	475 J/g	50-250
DEBADM/VAZO88	93°C	225 J/g	50-200
DEBADM/VAZO88:DGEBA/1-MeI 50:50 IPN	Peak 1. 115°C Peak 2. 127°C	301 J/g	50-250
DGEBA/2 wt% 1-MeI	118°C	475 J/g	50-250
DEBADM/VR110	129°C	220 J/g	50-275
DEBADM/VR110:DGEBA/1-MeI 50:50 IPN	Peak 1. 131°C Peak 2. 155°C	285 J/g	50-275
DGEBA/2 wt% 1-MeI	118°C	475 J/g	50-250
DEBPADM/2wt%AZO168	184°C	177 J/g	100-275
DEBPADM/2wt%AZO168: DGEBA/1-MeI 50:50 IPN	Peak 1. 134°C Peak 2. 153°C Peak 3. 217°C	305 J/g	50-275
DGEBA/2 wt% 1-MeI	118°C	475 J/g	50-250

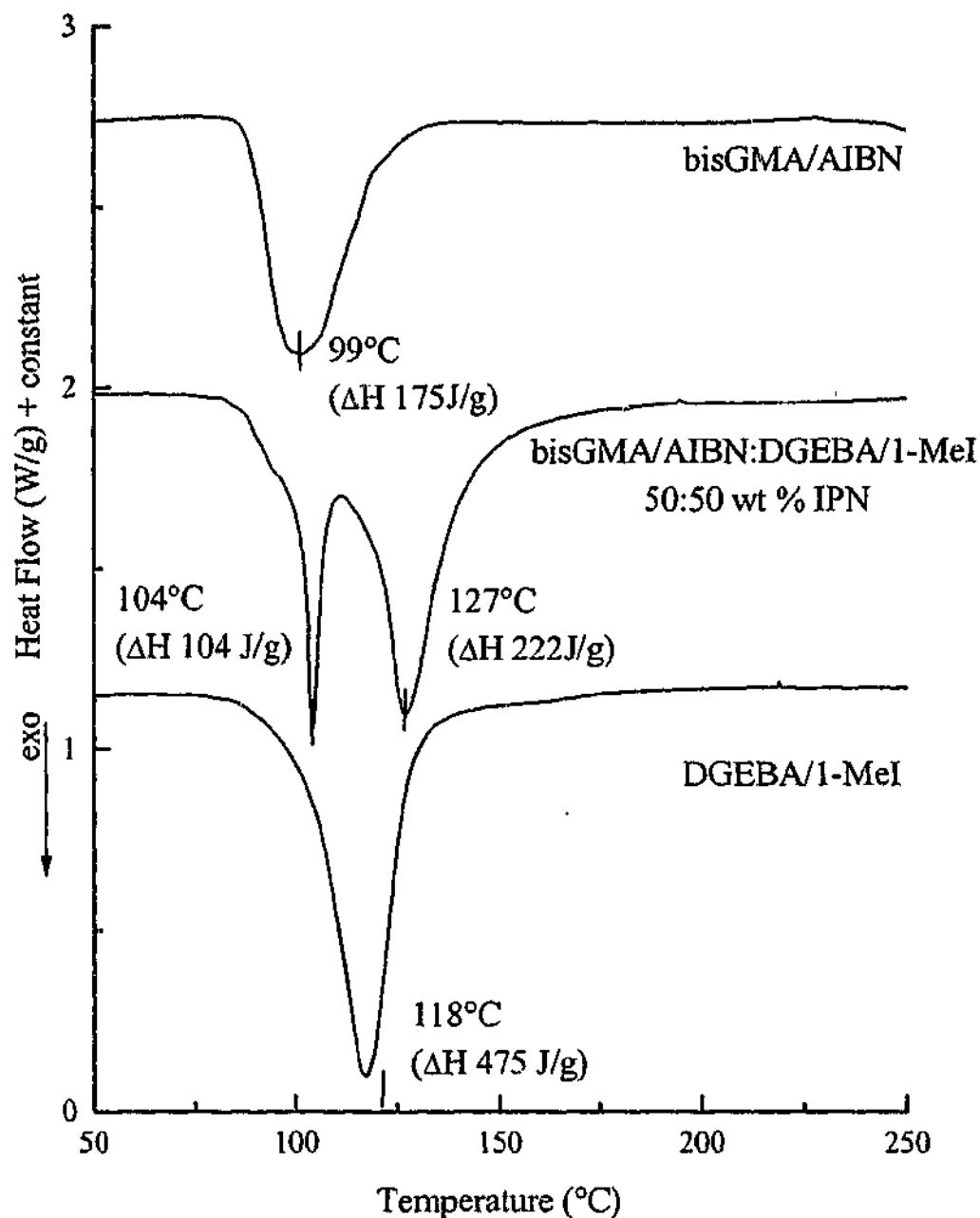


Figure 7.1 DSC scans of bisGMA/AIBN64, DGEBA/I-MeI and their IPNs

#### *DEBPADM-based IPNs*

Figure 7.2 shows the DSC thermograms for the neat DEBPADM/AIBN64 and DGEBA/I-MeI systems and their IPNs. As found for the bisGMA based IPNs, the DEBPADM-based IPNs (Figure 7.2) show two distinct exotherms in contrast to the neat resins. The lower and upper exotherms in the DSC trace of the IPNs can be attributed to the polymerization of the DEBPADM and DGEBA components, respectively and this is confirmed by the analysis of the 75:25 and 25:75 blends of this system - the resolved contributions to the DSC exotherm of the lower and upper peaks are approximately proportional to the weight fractions of DEBPADM and epoxy components in the IPN respectively (see Table 7.1). The peak exotherm temperature for each component in the

IPN appears to be shifted to higher temperatures than in the parent resins, due to dilution effects, as observed for the 50:50 bisGMA/AIBN64:DGEBA/1-MeI IPN.

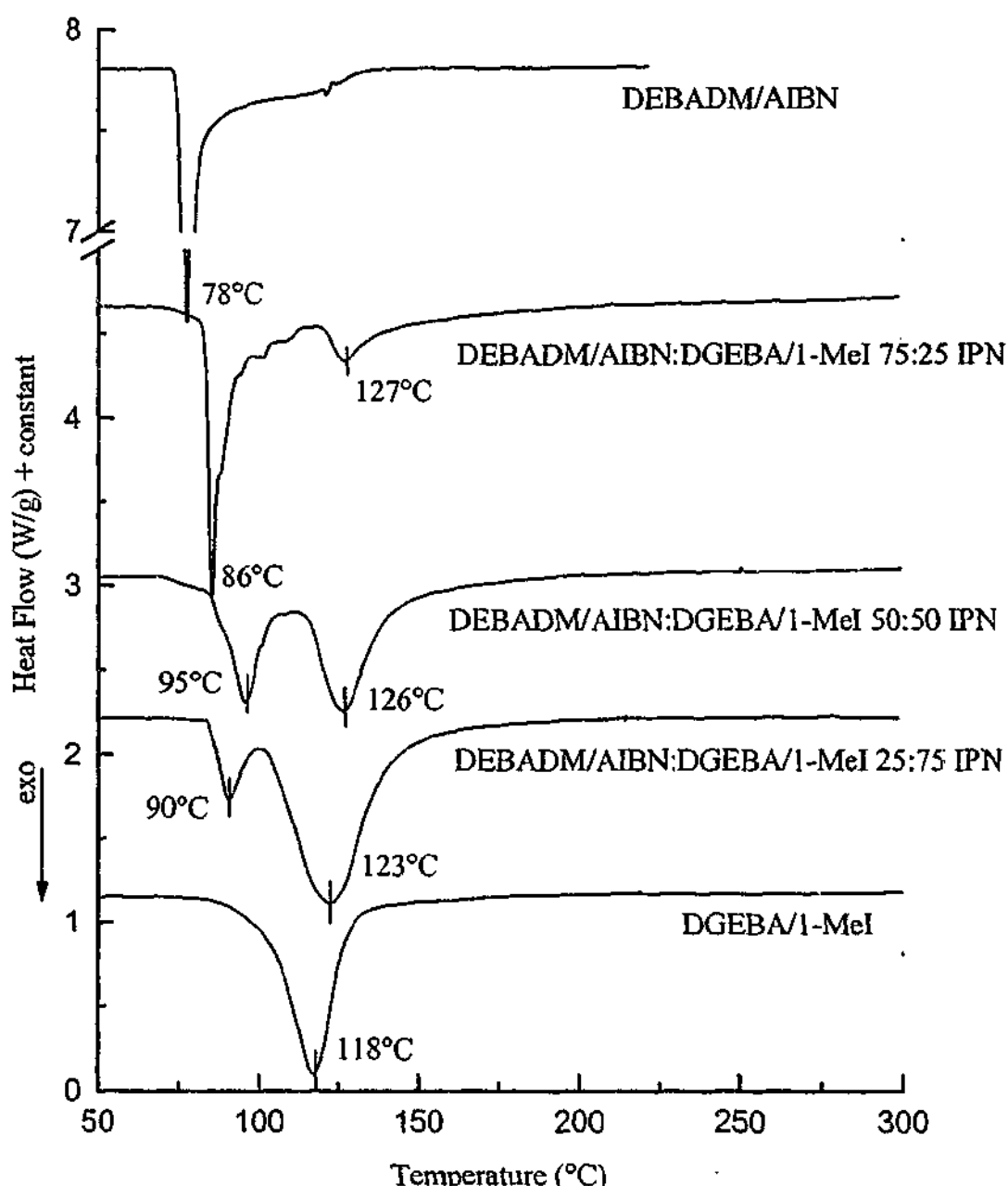


Figure 7.2 DSC scans of DEBADM/AIBN64, DGEBA/1-MeI and their IPNs

The effect of the chemical nature of the azo initiator on the cure of DEBPADM is shown in Figure 7.3 and 7.4 and Table 7.1. The neat resin initiated by either AIBN64 (10 hr half-life temperature 64°C), VAZO88 (10 hr half-life temperature 88°C) or AZO168 (10 hr half-life temperature 168°C) showed one major peak but the DEBPADM/VR110 (10 hr half-life temperature 110°C) system exhibits several peaks, perhaps due to the presence of isomers or impurities in the initiator. Based on the heat of polymerization for methyl methacrylate of 56.2 kJ/mol<sup>17,222</sup>, the theoretical heat of polymerization of the DEBPADM was calculated as 239.2 J/g (based on a DEBPADM molecular weight of 470 g/mol obtained by titration – see Section 3.2). The observed

heat of polymerization of the neat DEBPADM/AIBN64 was 220 J/g suggesting 92% conversion. The heats of methacrylate polymerization using VAZO88 (225 J/g, 94% conversion) and VR110 (220 J/g, 92% conversion) were similar but much lower conversion was obtained with 1wt% AZO168 (134 J/g, 56 % conversion) or even with 2wt% AZO168 (177 J/g, 74% conversion). This suggests that there exists a balance between having a cure temperature which is adequate for dissociation of the azo-initiator to radicals and one which causes depolymerization or degradation of the dimethacrylate, as suggested elsewhere<sup>21</sup>.

The AIBN64 and VAZO88 initiators (see Figure 7.3) cause exotherms of the neat dimethacrylate at 86°C and 93°C, respectively, which occur at lower temperatures than the peak exotherm for the neat epoxy system (118°C), while VR110 and AZO168 produce exotherms (see Figure 7.4) at 129°C and 184°C respectively, which is higher than produced by the epoxy system. As a result, the order of the curing peaks in the IPNs is reversed for the latter two initiators - in the AIBN64 and VAZO88 initiated IPNs, the dimethacrylate cures before the DGEBA/1-MeI component, however for the VR110 and AZO168-initiated IPNs, the dimethacrylate curing exotherm occurs after the epoxy component. The peak exotherm temperature of the epoxy component of the IPN is shifted to higher temperatures (between 126°C and 134°C, depending on the azo initiator) than the neat resin (118°C), as expected of a dilution effect. For the IPNs containing the AIBN64, VAZO88 and VR110, the dimethacrylate peak is also shifted due to dilution. However the DSC cure behaviour in the 50:50 DEBPADM:AZO168:DGEBA:1-MeI IPN (with 2 wt% of AZO168 initiator) does not follow these trends but exhibits an epoxy peak at 134°C, another peak at 154°C and a shoulder at 217°C, indicating more complex interaction between the components<sup>+</sup>. The peak at 154°C may involve partial cure of the dimethacrylate but it is unclear why it occurs so much lower than the parent resin (184°C). The broad shoulder at 217°C in the AZO168-based IPN may be due to the thermal cure of the DEBPADM resin or degradation, because the DSC of uninitiated DEBPADM (not shown) has a small exotherm peak at 178°C (with 42 J/g and corresponding to 17% conversion), followed by an even higher temperature exotherm with a peak temperature of approximately 290°C.

---

<sup>+</sup> DSC peaks were observed at 146°C and 221°C in the DEBPADM/AZO168:DGEBA/1-MeI system using only 1wt% of AZO168, but this system shows substantial undercure (164 J/g) due to incomplete methacrylate polymerization. Similarly in the neat DEBPADM/AZO168 using only 1wt % AZO168 undercure (134 J/g or 56% conversion) was also observed.

Table 7.1 lists the experimental heats of polymerization for the IPNs. Comparison of the total heat of polymerization for the 50:50 DEBPADM/AIBN64:DGEBA/1-MeI IPN (364 J/g) with the weighted average (357 J/g) of the theoretical heats of polymerization for the DEBPADM (239 J/g) and the epoxy (475 J/g), shows that full cure is achieved. The 50:50 IPN of DEBPADM/VAZO88:DGEBA/1-MeI gives a heat of polymerization of 301 J/g which is 86% of what would be expected from the weighted mean (350 J/g) of DEBPADM/VAZO88 and DGEBA/1-MeI and is 84% of that expected value from the

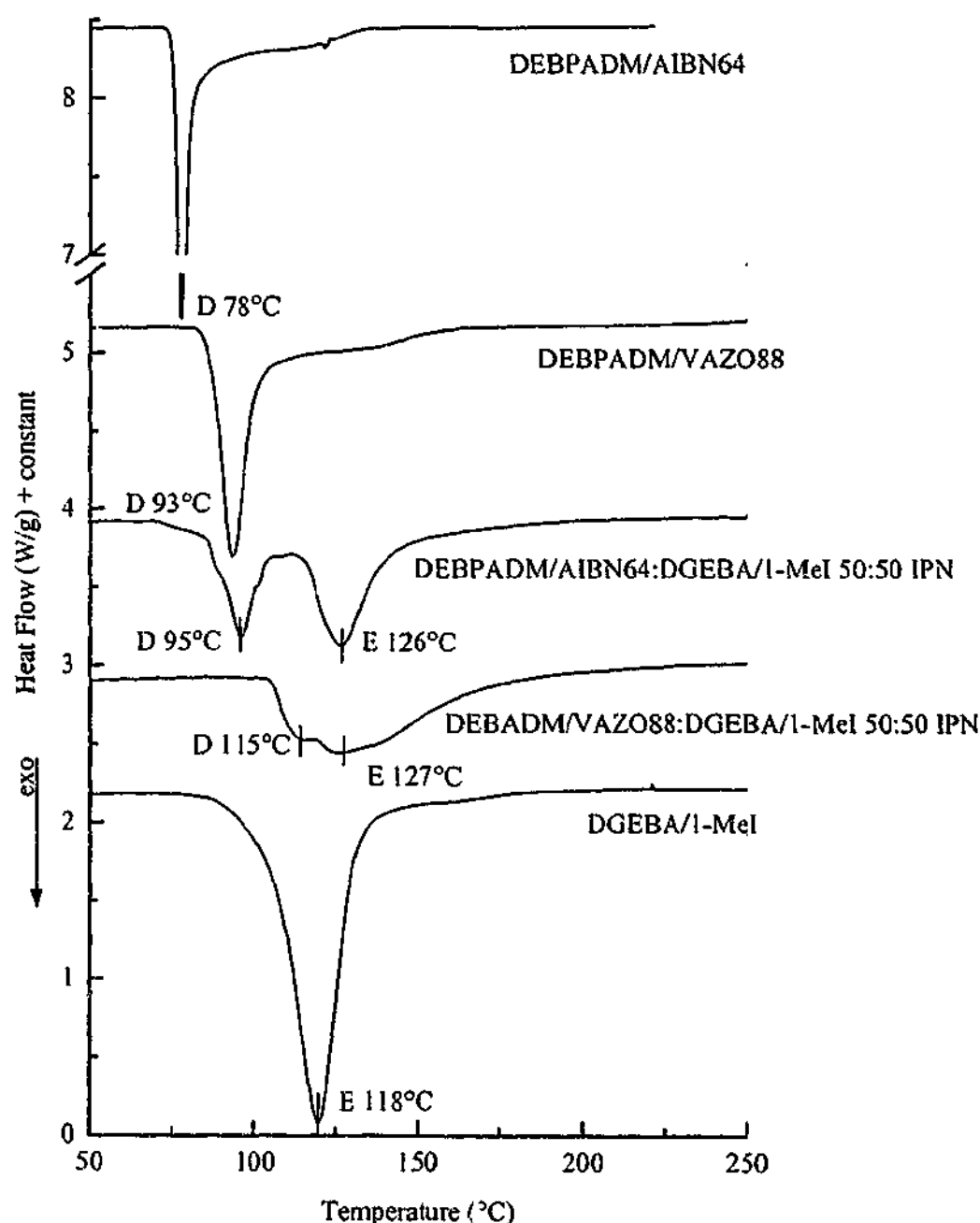


Figure 7.3 DSC scans of DEBPADM/AIBN64, DEBPADM/VAZO88, DGEBA/1-MeI and their IPNs. (D= dimethacrylate peak; E = epoxy peak)

weighted mean of the theoretical heats of polymerization (357 J/g), suggesting that the cure of the components affects one another. Similarly, the 50:50 IPN of DEBPADM/VR110:DGEBA/1-MeI gives a heat of polymerization of 285 J/g which is

82 % of that expected from the weighted mean for DEBPADM/VR110 and DGEBA/1-MeI (347 J/g) or 80% of expected value from weighted mean of the theoretical heats of polymerization (357 J/g). Interestingly, despite the more complicated DSC profile of the DEBPADM/AZO168:DGEBA/1-MeI IPN (using 2wt% AZO168) the measured heats of polymerization for this IPN is 85% of the expected cure, although this includes the high temperature exotherm at 217°C (and uses a wider integration range of 50 to 275°C).

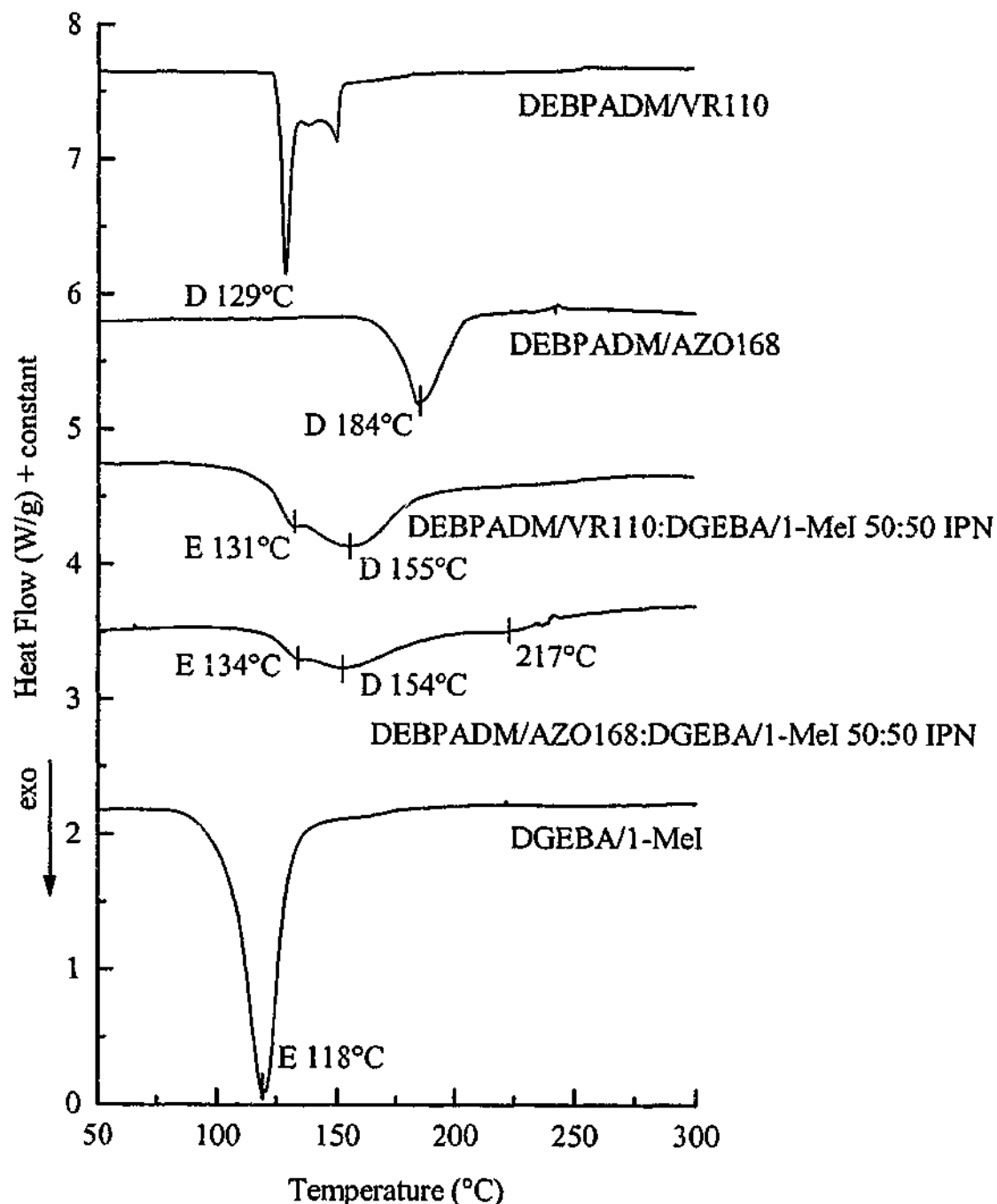


Figure 7.4 DSC scans of DEBPADM/VR110, DEBADM/AZO168 and DGEBA/1-MeI and the 50:50 IPN. (D= dimethacrylate peak; E = epoxy peak)

Mid-FTIR spectra (Figure 7.5) of the 50:50 DEBPADM/AIBN64:DGEBA/1-MeI IPN illustrates the consumption of epoxy and methacrylate groups during cure. The corresponding conversion data are shown in

Figure 7.6 for the 50:50 DEBPADM/AIBN64:DGEBA/1-MeI IPN and its parent resins at 70°C. Figure 7.6 shows that the cure of methacrylate in the 50:50 DEBPADM/AIBN64:DGEBA/1-MeI IPN is almost complete prior to any polymerization of the epoxy because AIBN64 is a low temperature initiator. Thus the

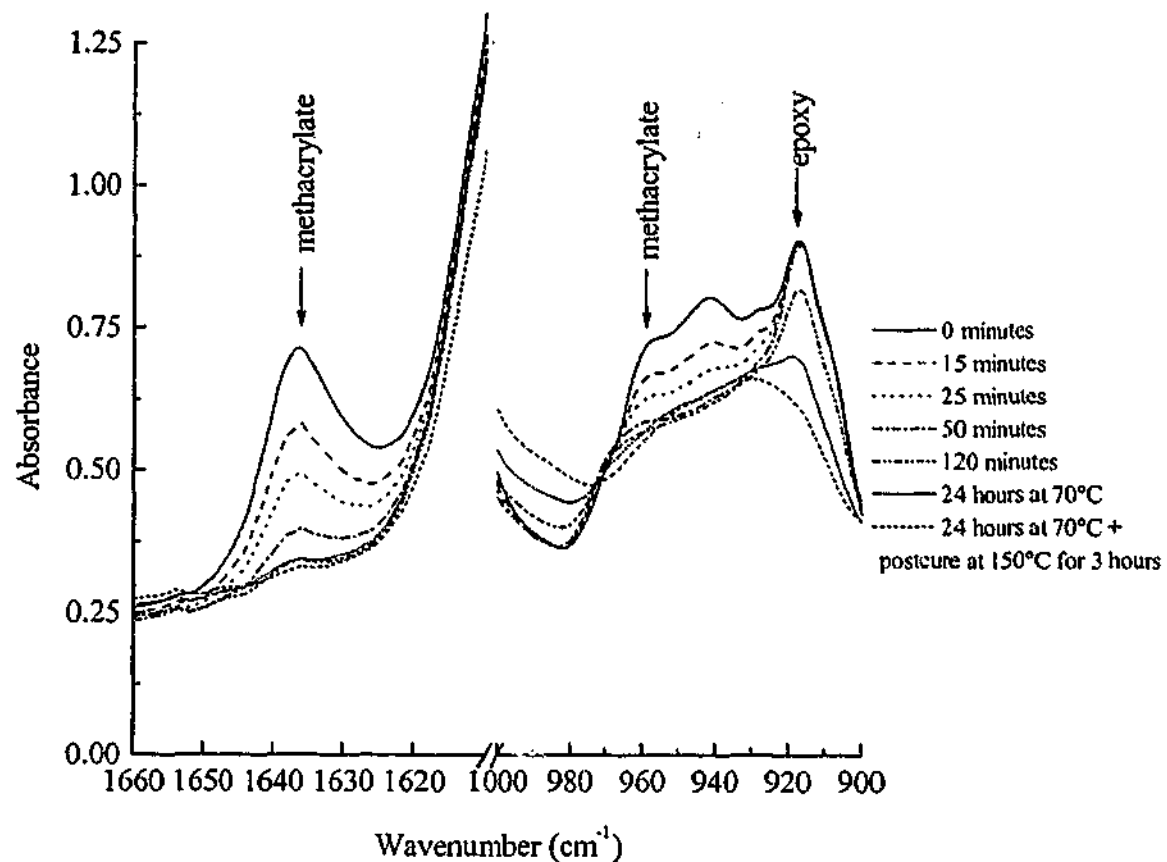


Figure 7.5 FTIR spectra in the region from 1660  $\text{cm}^{-1}$  to 1600  $\text{cm}^{-1}$  and from 1000 $\text{cm}^{-1}$  to 900 $\text{cm}^{-1}$  for the 50:50 DEBPADM/AIBN64:DGEBA/1-MeI IPN cured at 70°C for varying times and after post-cure at 160°C for 3 hours.

cure of the methacrylate and the epoxy are well separated, which agrees with the DSC data for this system (see Figure 7.3). For the 50:50 DEBPADM/VR110:DGEBA/1-MeI IPN containing a higher temperature initiator, the polymerization rate of methacrylate and epoxy groups is initially quite similar, in agreement with the DSC data for this system (see Figure 7.4). As shown in Chapters 5 and 6, if the curing temperature is low enough so that the IPN can vitrify, a difference in curing rates of the two IPN components will have an effect on the final isothermal conversions of the two species because they react in environments of differing mobility. Assuming that the IPNs are miscible, the more slowly polymerizing component can act as a plasticizer for the more rapidly reacting component so that a higher conversion can be obtained prior to vitrification (see for example, Section 5.2.3(a)). On the other hand, the extent of cure of the more slowly reacting component is limited by the presence of the already formed

network and thus vitrification of the IPN will prevent full cure (see for example Section 5.2.3(a)). Both of these behaviours are clearly evidenced in the DEBPADM/AIBN64:DGEBA/1-MeI IPN (see Figure 7.6). When cured at 70°C, the neat dimethacrylate resin does not cure to its topological limit because the  $T_g$  of the fully cured resin (189°C-see Section 8.2) is well above the curing temperature and so vitrification prevents full cure. However, in the IPN, the more slowly reacting epoxy resin acts as a plasticizer and so the final methacrylate conversion is higher than in the neat DEBPADM/AIBN64 system. Contrasting with this observation, the extent of cure of the more slowly reacting component (the epoxy) in the 50:50 DEBPADM/AIBN64:DGEBA/1-MeI IPN is less than in the neat DGEBA/1-MeI resin due to vitrification of the IPN by the highly crosslinked dimethacrylate component. In confirmation that this behaviour is due to vitrification and is not a topological effect, postcuring of the IPN at 160°C led to almost complete cure of reactive groups.

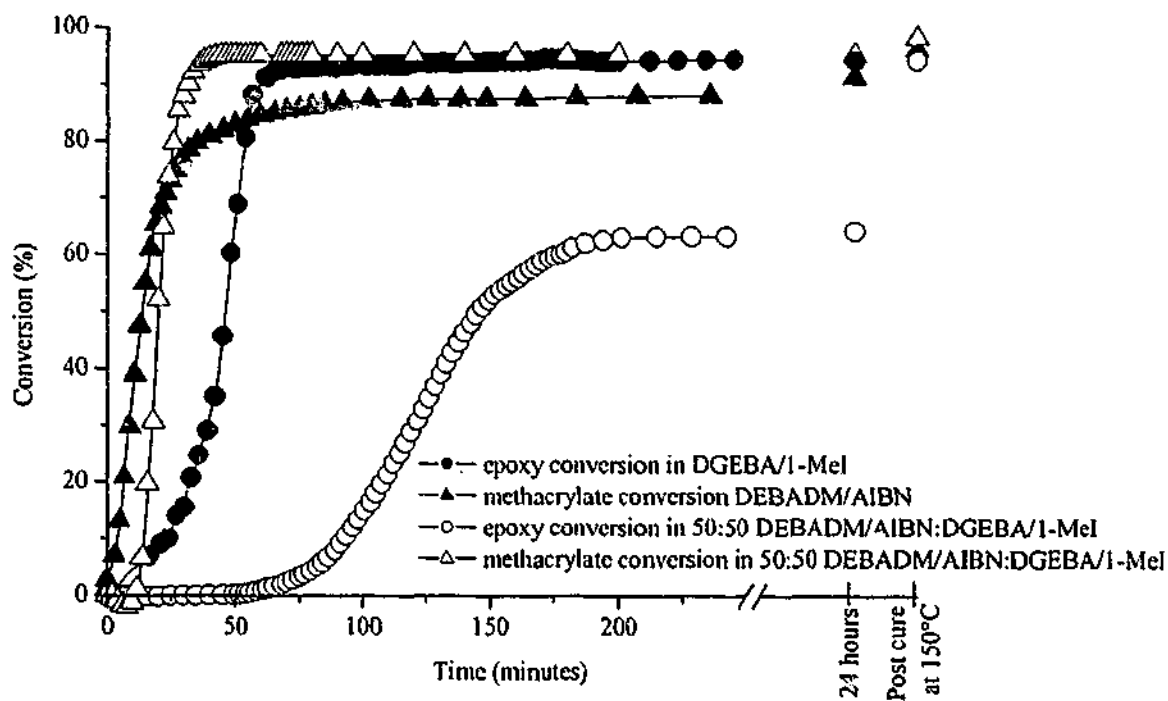
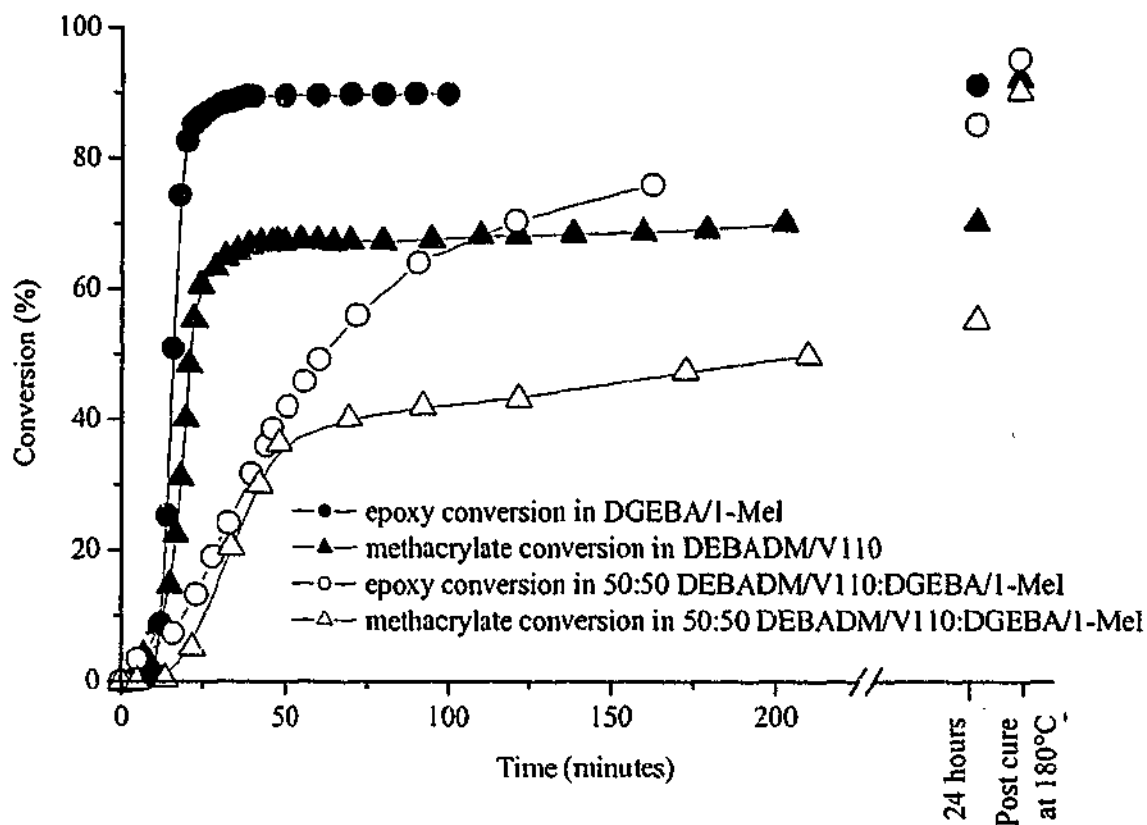
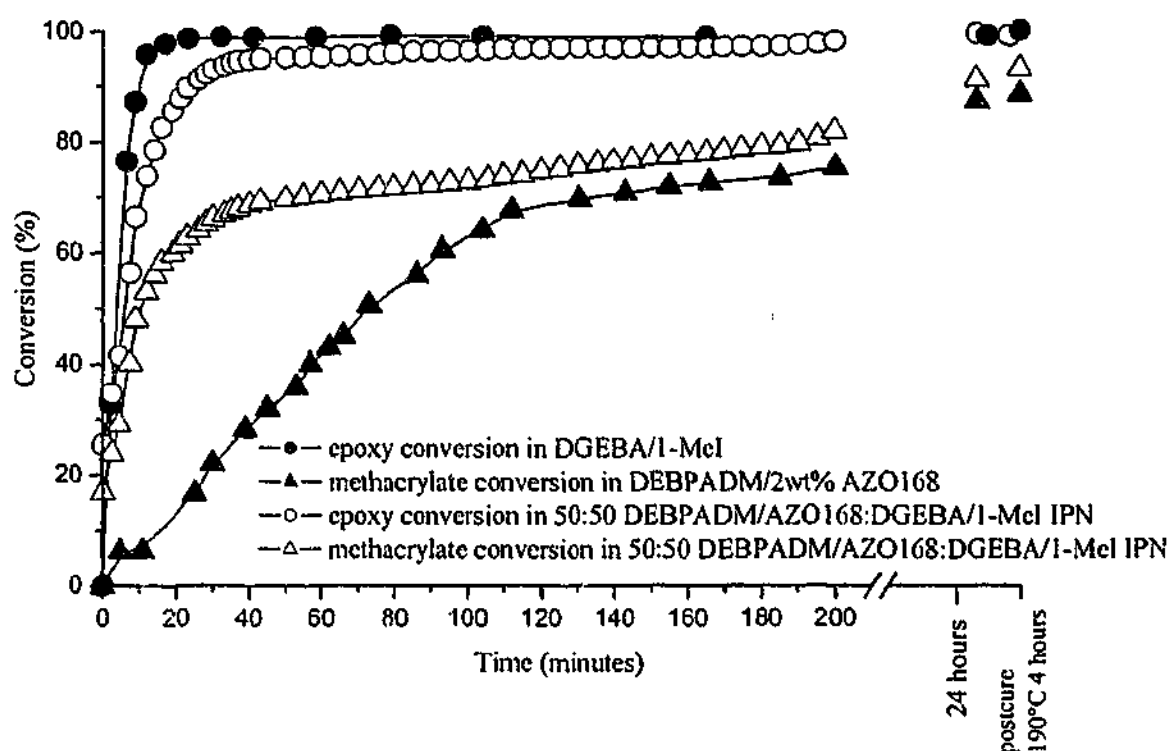


Figure 7.6 Epoxy and methacrylate conversion versus time for the neat resins and in the 50:50 blend of DEBPADM/AIBN64:DGEBA/1-MeI at 70 °C.



**Figure 7.7** Epoxy and methacrylate conversion versus time for the neat resins and in the 50:50 blend of DEBADM/VR110:DGEBA/1-MeI at 110°C.

In the 50:50 DEBADM/VR110:DGEBA/1-MeI IPN (Figure 7.7), the isothermal conversions of methacrylate and epoxy groups are less than for the parent resins because the development of the two network components in the IPN occur at similar rates and so vitrification of the IPN limits full cure of both species. Postcuring at 180°C led to almost complete cure of the epoxy groups and lower but similar extents of cure of the methacrylate groups in the IPN and the neat dimethacrylate. Showing that vitrification of the IPN was the cause of the incomplete polymerization at 70°C.



**Figure 7.8** Epoxy and methacrylate conversion versus time for the neat resins and in the 50:50 blend of DEBPADM/AZO168 (2 wt%):DGEBA/1-MeI at 160°C.

FTIR studies (Figure 7.8) show that the neat DGEBA/1-MeI system polymerized faster than the DEBPADM/AZO168 resin at 160°C, which is consistent with the DSC results (Figure 7.4). In the 50:50 IPN of these resins, the epoxy groups reacted more slowly than in the neat DGEBA/1-MeI resins due to a dilution effect and this is consistent with the scanning DSC results (Figure 7.4). The faster isothermal cure of the methacrylate groups in the IPN is also consistent with the DSC data (Figure 7.4) but the reason for this acceleration is unclear. The final isothermal conversions of the epoxy in the IPN are similar to that in the parent resin because the cure temperature (160°C) is close enough to the maximally attainable  $T_g$ s (see Table 8.2) to allow full cure without vitrification. The final cure of the methacrylate groups in the IPN and neat resin is less than 100% perhaps due to degradation or depolymerization of the polymer at the high isothermal cure and postcure temperatures

### 7.3 Conclusions

DSC and FTIR studies of a range of IPNs prepared from an epoxy resin and

several different azo-initiated dimethacrylates have been undertaken. In the neat DGEBA/1-MeI, DEBPADM/AIBN64, DEBPADM/VAZO88 and DEBPADM/VR110 resins, close to full cure was achieved. For the neat, high temperature DEBPADM/AZO168 resin, full cure was not attained, possibly due to the compromise between using a high enough temperature for azo decomposition while avoiding depolymerization or decomposition of the methacrylate polymer. The IPN cure studies showed that, by appropriate initiator selection, it was possible to interchange the order of cure of the components within the IPN so that either the dimethacrylate or epoxy cured first, without the complications due to interactions between components as observed in Chapter 5. In the isothermal cure of 50:50 DEBPADM/AIBN64:DGEBA/1-MeI, it is the dimethacrylate which polymerizes first because the 10 hr half-life of AIBN is low. As a result, the final conversion of the dimethacrylate in the IPN is enhanced and the epoxy conversion is reduced. However after postcure both groups react nearly completely. For the 50:50 IPN of DEBPADM/VR110:DGEBA/1-MeI the methacrylate and epoxy groups cure at a similar rate and the final isothermal conversions are less than 100%. Postcuring causes almost 100% reaction of the epoxy but the methacrylate groups are not fully cured due to the competition between polymerization and degradation. In the 50:50 IPN of DEBPADM/AZO168:DGEBA/1-MeI, it is the epoxy which cures first, but the high isothermal temperature required to initiate the polymerization of the methacrylate causing further degradation of the methacrylate component producing an incompletely cured system.

# *Chapter 8*

## *DMTA and SANS of cured systems*

---

### **8.1 Introduction**

Dynamical mechanical studies (DMTA) and small angle neutron scattering (SANS) have been performed on a number of the IPN systems in order to probe their phase structure. These IPN systems display a number of different results, from IPNs that produce one  $\tan\delta$  peak (indicative of a single phase system) to systems that are clearly phase separated (showing two  $\tan\delta$  peaks). These DMTA results were correlated with the SANS studies - samples that showed two  $\tan\delta$  peaks also showed scattering in the SANS spectrum. Fitting of the SANS data to various theories gave a scale to this phase separation.

### **8.2 Dynamical Mechanical Thermal Analysis (DMTA)**

#### **VER based IPNs**

##### *The Glass Transition*

The DMTA results for a range of 50:50 IPNs based on VER/AIBN and DGEBA cured with a range of amines and anhydride are listed in Table 8.1. Figure 8.1 shows the real modulus and  $\tan\delta$  versus temperature for the VER/AIBN, DGEBA/1-MeI and the

corresponding 50:50 IPN. The  $T_g$  (taken as a maximum in  $\tan\delta$ ) for the neat VER/AIBN is 169°C and the  $T_g$  for the neat DGEBA/1-MeI is 185°C. The resulting 50:50 VER/AIBN:DGEBA/1-MeI IPN exhibits a single  $\tan\delta$  peak with a maximum corresponding to a  $T_g$  of 189°C which is close to the  $T_g$  of the neat DGEBA/1-MeI, and would occur if the conversion of epoxy, methacrylate and styrene was higher in the IPN. This cannot be confirmed because the conversion in the parent resins and the IPN are all close to 100%.

**Table 8.1. DMTA results for parent resins and their IPNs**

System	$\beta$ relaxation (°C)	$\alpha$ relaxation ( $\tan\delta$ maximum) (°C)	E' of rubbery plateau ( $10^7$ Pa)
VER/AIBN	-80	169	3.0
VER/AIBN: DGEBA/1-MeI	-70	189	4.5
DGEBA/1-MeI	-60	185	4.7
VER/AIBN	-80	169	3.0
VER/AIBN: DGEBA/BA	-69	Peak 1. 71 Peak 2. 141	1.6
VER/AIBN: DGEBA/DAO	-57	Peak 1. 120 Peak 2. 146	2.4
DGEBA/BA	-66	67	-
DGEBA/DAO	-47	119	2.0
VER/AIBN	-80	169	3.0
VER/AIBN: DGEBA/An	-65	Peak 1. 111 Peak 2. 161	0.8
VER/AIBN: DGEBA/DDM	-63	171	2.3
DGEBA/An	-64	109	-
DGEBA/DDM	-50	189	2.0
VER/AIBN	-80	169	3.0
VER/AIBN: DGEBA/CHDCA/ DMBA	-54	157 with a large shoulder	2.1
DGEBA/CHDCA/ DMBA	-41	159	2.0

The DMTA spectra for VER/AIBN, DGEBA/BA, DGEBA/DAO and the resulting semi-IPN and full IPN are illustrated in Figure 8.2. The neat VER/AIBN shows a single  $T_g$  at 169°C, the neat linear DGEBA/BA shows a single  $T_g$  at 67°C and the neat crosslinking DGEBA/DAO shows a single  $T_g$  at 119°C (which is higher than the DGEBA/BA due to the presence of crosslinks). The 50:50 VER/AIBN:DGEBA/BA semi-IPN produces two  $T_g$ s at 71°C and 141°C, the lower  $T_g$  at 71°C due to the epoxy

(neat DGEBA/BA has  $T_g$  of  $67^\circ\text{C}$ ) and the higher  $T_g$  due to the VER (neat VER/AIBN  $T_g$  is  $169^\circ\text{C}$ ). There does not appear to be much difference in the  $T_g$  of the epoxy whether in the neat or IPN system, however the VER  $T_g$  is  $28^\circ\text{C}$  lower in the IPN compared with the neat resin, this may be due to phase mixing of DGEBA/BA with VER or some undercuring of this component. Previous investigations of the cure kinetics of this system (see Section 5.1.2) indicated a Michael addition<sup>130-132</sup> (see Section 2.4.2), between the amine (a nucleophile) and the electron deficient carbon in the methacrylate groups (see Figure 5.4 and Section 5.1.2) in both the VER/AIBN:BA and the VER/AIBN:An systems. Therefore, it may be concluded that although the dimethacrylate conversion in the IPN (97% - see Chapter 5) is similar to that of the neat VER (98%), this is not a direct measure of the level of VER network formation, since it also contains the grafted VER-amine polymer - thus the  $T_g$  of the VER component in this IPN system may be reduced as a result of grafting which may contribute to the compatibility of the two networks noted by a shift of the VER  $T_g$  toward the  $T_g$  of the epoxy. The 50:50 VER/AIBN:DGEBA/DAO full-IPN also exhibits two  $T_g$ s of  $120^\circ\text{C}$  and  $146^\circ\text{C}$ , the lower glass transition at  $120^\circ\text{C}$  can be assigned to the epoxy (neat DGEBA/DAO has  $T_g$  of  $119^\circ\text{C}$ ) while the higher transition is due to the VER (neat VER/AIBN  $T_g$  is  $169^\circ\text{C}$ ). Similarly to that found for the BA based IPN, there does not appear to be much difference in the  $T_g$  of the epoxy whether neat or in the IPN system, however the VER  $T_g$  is  $23^\circ\text{C}$  lower in the IPN compared with the neat resin and this may also be due to the phase mixing or Michael addition reaction causing undercuring of the VER network, as discussed above.

The DMTA spectra for VER/AIBN, DGEBA/An, DGEBA/DDM and the resulting semi-IPN and full IPN are illustrated in Figure 8.3. The neat VER/AIBN shows a single  $T_g$  at  $169^\circ\text{C}$ , the neat linear DGEBA/An shows a single  $T_g$  at  $109^\circ\text{C}$  and the neat crosslinking DGEBA/DDM shows a single  $T_g$  at  $189^\circ\text{C}$  (which is higher than that of DGEBA/An due to the presence of crosslinks). The resulting 50:50 VER/AIBN:DGEBA/An semi-IPN produces two  $T_g$ s at  $111^\circ\text{C}$  and  $161^\circ\text{C}$ , the lower corresponding to the  $T_g$  of the DGEBA/An and the higher corresponding to the VER/AIBN. Similar to the effects of the Michael addition between the BA and the dimethacrylate (see Section 5.1.2) the  $T_g$  of the VER/AIBN component in the phase-separated 50:50 VER/AIBN:DGEBA/BA IPN, Michael addition between the An and the dimethacrylate also occurs, but to a lesser extent (see Section 5.1.2) because the aliphatic amine is a stronger base<sup>226</sup>, so that the downward shift of the  $T_g$  (from  $169^\circ\text{C}$

in the neat VER/AIBN to 161°C in the 50:50 VER/AIBN:DGEBA/An) is not as significant as the 28°C shift observed in the 50:50 VER/AIBN:DGEBA/BA IPN. A larger contribution of the measured dimethacrylate conversion in the BA-based IPN is may also be due to the Michael addition, therefore it is possible that the level of VER network formation was reduced. In contrast, the 50:50 VER/AIBN:DGEBA/DDM IPN produces a single  $T_g$  at 171°C, however, the small difference in  $T_g$  of the parent resins in the DDM base IPN (VER/AIBN - 169°C and DGEBA/DDM - 189°C) makes it difficult to determine whether a two-phase system exists. Thus, based solely on the DMTA data, the 50:50 VER/AIBN:DGEBA/DDM IPN may have complete phase separation, or partial separation with small epoxy-rich or dimethacrylate-rich phases, or complete miscibility.

The DMTA spectra for VER/AIBN, DGEBA/CHDCA and the corresponding IPN is shown in Figure 8.4. The neat VER/AIBN shows a single  $T_g$  at 169°C, the neat DGEBA/CHDCA shows a single  $T_g$  at 157°C and the resulting 50:50 VER/AIBN:DGEBA/CHDCA IPN produces a single  $T_g$  at 159°C with a shoulder on the higher temperature side of the peak suggesting some degree of phase separation in this IPN. Further evidence for this is provided by DMTA studies on mixed anhydride systems in Chapter 9.

### *Rubbery Modulus*

The modulus in the rubbery region is related to the crosslink density (see Equation 2.15); however for materials with a high rubbery modulus, deviations from this relationship have been observed<sup>238</sup>. The rubbery moduli values reported here give a qualitative indication of the crosslink density. The rubbery modulus of the 50:50 VER/AIBN:DGEBA/1-MeI IPN is  $4.5 \times 10^7$  Pa which is between the rubbery modulus of the DGEBA/1-MeI ( $4.7 \times 10^7$  Pa) and the VER/AIBN ( $3.0 \times 10^7$  Pa). The VER/AIBN:DGEBA/DAO ( $2.4 \times 10^7$  Pa), VER/AIBN:DGEBA/DDM ( $2.3 \times 10^7$  Pa) and VER/AIBN:DGEBA/CHDCA ( $2.1 \times 10^7$  Pa) IPNs also all exhibited rubbery modulus values between those recorded for the parent resins. The values of rubbery modulus for the 50:50 VER/AIBN:DGEBA/BA ( $1.6 \times 10^7$  Pa) and VER/AIBN:DGEBA/An ( $0.8 \times 10^7$  Pa) IPNs are low (as expected) due to the uncrosslinked nature of the DGEBA/BA and DGEBA/An of which they consist.

### Relaxational Behaviour

The secondary (or  $\beta$ ) relaxation in the neat VER ( $-80^\circ\text{C}$ ) is generally associated with localized molecular motion of the methacrylate group<sup>239</sup>, as the secondary relaxation of styrene occurs between  $-100^\circ\text{C}$  and  $-140^\circ\text{C}$ <sup>239</sup>. The  $\beta$  relaxation in the neat DGEBA/1-MeI ( $-60^\circ\text{C}$ ) may be due to the localized motion of the bisphenol-A group<sup>240</sup>. The  $\beta$  relaxation of the 50:50 VER/AIBN:DGEBA/1-MeI IPN ( $-70^\circ\text{C}$ ) is a combination of the  $\beta$  relaxation for the two parent resins. The  $\beta$  relaxation for the DGEBA/BA ( $-66^\circ\text{C}$ ) and DGEBA/DAO ( $-47^\circ\text{C}$ ) may be partly due to motion of the bisphenol-A group, but has also been connected with the motion of the hydroxyether groups<sup>240</sup>. Similar to the 1-MeI based IPNs, the aliphatic-amine based IPNs exhibit  $\beta$  relaxation close to an average of the two parent resins. The  $\beta$  relaxation for the DGEBA/An ( $-64^\circ\text{C}$ ) and DGEBA/DDM ( $-50^\circ\text{C}$ ) may be due to similar motions of the bisphenol-A group or hydroxyether groups<sup>241</sup> as observed in the aliphatic-amine based systems<sup>240</sup>. As observed for the aliphatic amine-based IPNs, the aromatic-amine based IPNs exhibit  $\beta$  relaxations close to the average of the two parent resins. The  $\beta$  relaxation for the DGEBA/CHDCA ( $-41^\circ\text{C}$ ) may be due to a combination of the motion of the bisphenol-A group<sup>240,241</sup> and the diester segment from the anhydride<sup>79,242</sup>. The 50:50 VER/AIBN:DGEBA/CHDCA IPN exhibited a  $\beta$  relaxation ( $-54^\circ\text{C}$ ) which occur between the values measured for the parent resins.

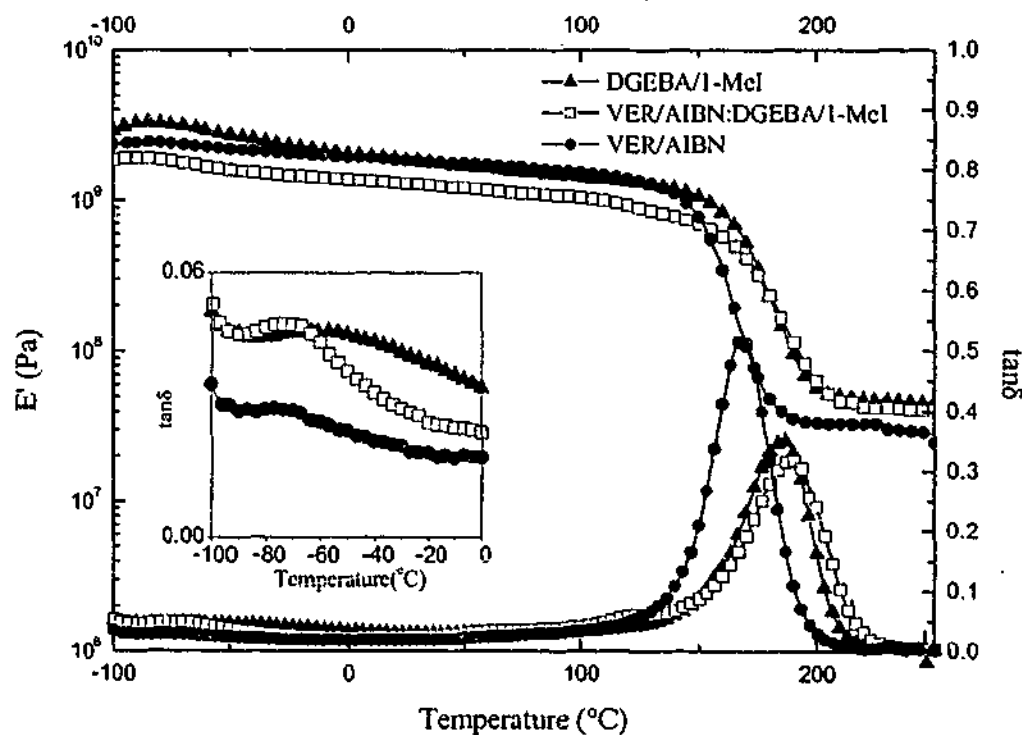


Figure 8.1 DMTA scans of DGEBA/2wt% 1-MeI, VER/AIBN and the corresponding 50:50 IPN.

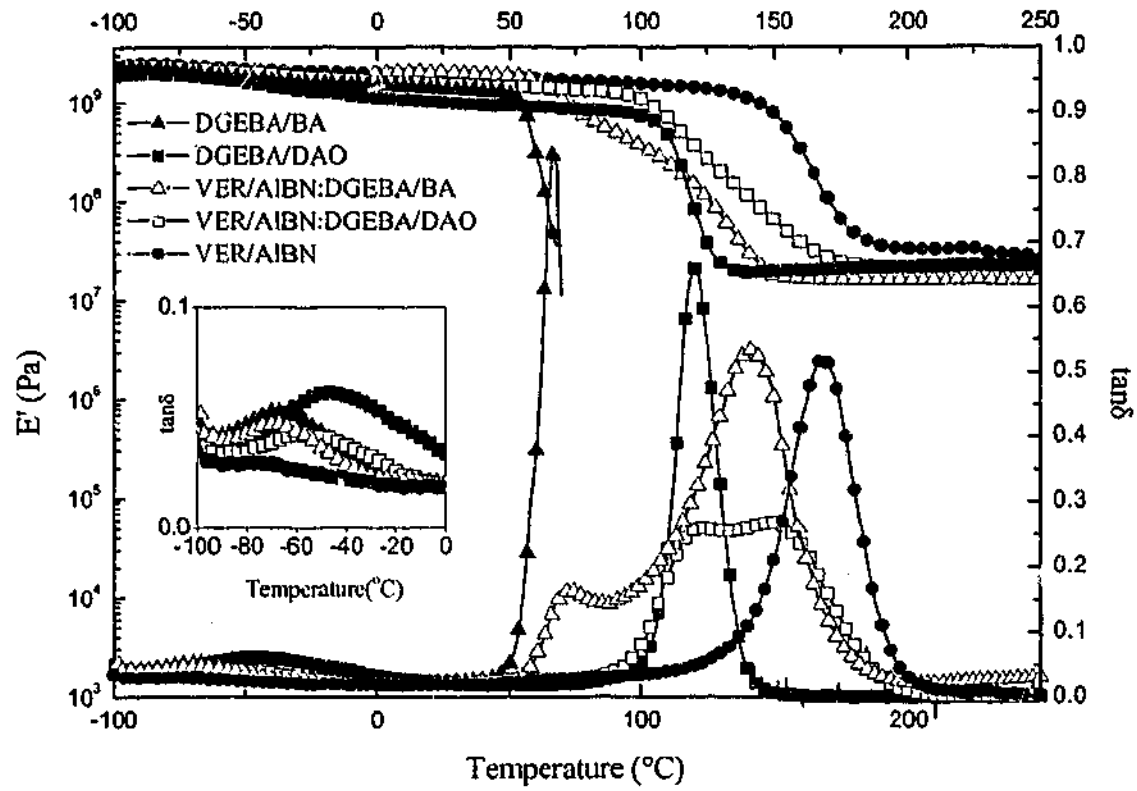


Figure 8.2 DMTA scans of DGEBA/BA, DGEBA/DAO, VER/AIBN and corresponding 50:50 IPNs.

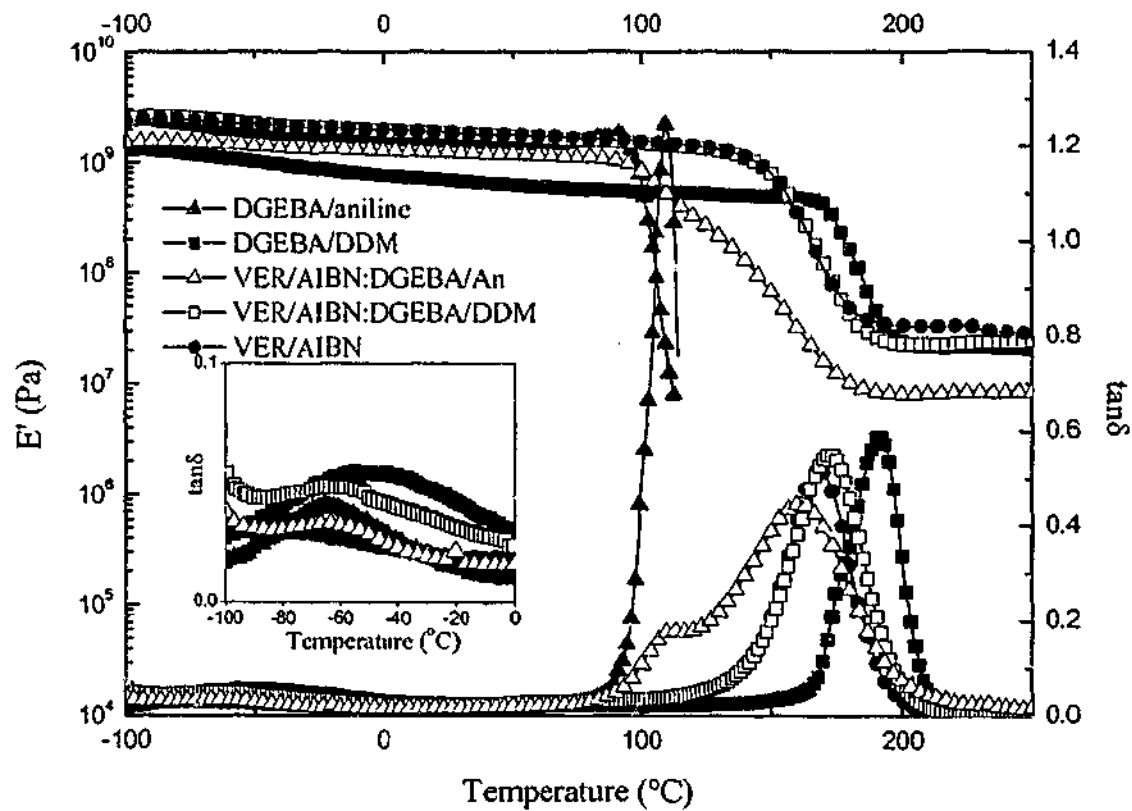


Figure 8.3 DMTA scans of DGEBA/An, DGEBA/DDM, VER/AIBN and corresponding 50:50 IPNs.

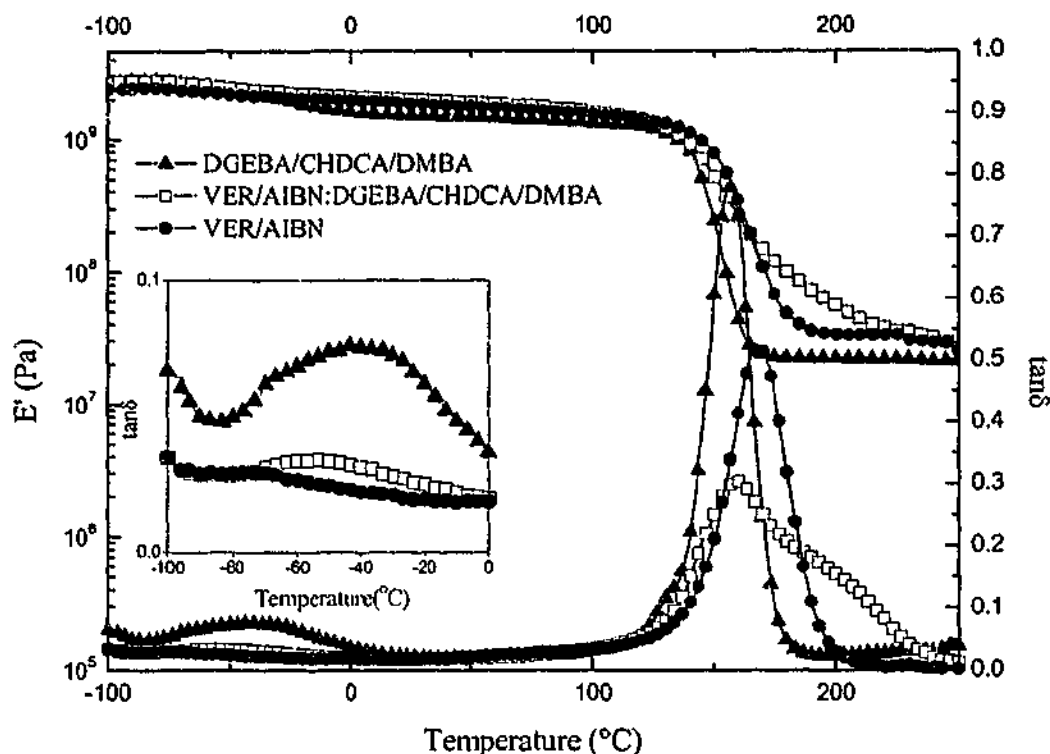


Figure 8.4 DMTA scans of DGEBA/CHDCA/DMBA, VER/AIBN and corresponding 50:50 IPN.

### DEBPADM-based IPNs

#### *The Glass Transition*

The neat DEBPADM cured with various azo initiators, the neat DGEBA and their corresponding IPNs all exhibited a single maximum in  $\tan\delta$  - see Figures 8.5 to 8.7. The DMTA results for these systems are listed in Table 8.2. The neat DEBPADM/AIBN64 polymer had a high  $T_g$  of 189°C followed by 163°C for DEBPADM/VR110 and 158°C for the DEBPADM/AZO168 resin. The difference in  $T_g$ s for the DEBPADM may be due to the competition between polymerization and degradation, as the VR110 and AZO168 initiated systems had to be cured at high temperatures (110 and 160°C respectively) to enable sufficient decomposition of the initiator, and these temperatures may cause depolymerization or degradation of the polymer<sup>21</sup>. The neat DGEBA/1-MeI polymer had a  $T_g$  of 186°C. The resulting 50:50 DEBPADM/AIBN64:DGEBA/1-MeI gave a  $T_g$  of 178°C, only slightly lower than the  $T_g$ s of the parent resins. The IPNs cured with the higher temperature azo initiators (VR110, AZO168) had  $T_g$ s that were significantly lower than the  $T_g$ s of the parent resins, due to plasticization with unpolymerized DEBPADM or small degradation

products as suggested by the incomplete cure observed by DSC (see Table 7.1) and FTIR (see Figures 7.7 and 7.8).

**Table 8.2. DMTA results for parent resins and their IPNs**

System	$\beta$ relaxation (°C)	$\alpha$ relaxation (tan $\delta$ maximum) (°C)	E' of rubbery plateau (10 <sup>7</sup> Pa)
DEBPADM/AIBN64	-80	189	6.4
DEBPADM/AIBN64: DGEBA/1-MeI	-72	178	5.4
DGEBA/1-MeI	-60	186	4.7
DEBPADM/VR110	-	163	5.7
VER/VR110: DGEBA/1-MeI	-65	120	3.9
DGEBA/1-MeI	-60	186	4.7
DEBPADM/VAZO168	-90	158	4.1
DEBPADM/VAZO168: DGEBA/1-MeI	-76	97	1.3
DGEBA/1-MeI	-60	186	4.7

\* using 2 wt% VAZO168; all other azo levels were 1 wt%

### *Rubbery Modulus*

The rubbery modulus of the 50:50 DEBPADM/AIBN:DGEBA/1-MeI IPN is  $5.4 \times 10^7$  Pa which is between the rubbery modulus of the DGEBA/1-MeI ( $4.7 \times 10^7$  Pa) and the DEBPADM/AIBN ( $6.4 \times 10^7$  Pa). However, the modulus values for the 50:50 DEBPADM/VR110:DGEBA/1-MeI IPN ( $3.9 \times 10^7$  Pa) and 50:50 DEBPADM/VAZO168:DGEBA/1-MeI IPN ( $1.3 \times 10^7$  Pa) both exhibit values of rubbery modulus which are lower than both the parent resins which may be due to under-curing.

### *Relaxational Behaviour*

Similar to the  $\beta$  relaxation in the neat VER, the  $\beta$  relaxation in the DEBPADM systems may also be associated with localized molecular motion of the methacrylate group<sup>239</sup>. In the neat DEBPADM systems some variation in the  $\beta$  relaxation is observed and this may be attributed to varying levels of cure in these systems: the undercured DEBPADM/VAZO168 has a lower  $\beta$  relaxation at -90°C compared to the more fully

cured DEBPADM/AIBN64 with a  $\beta$  relaxation at  $-80^\circ\text{C}$ . The  $\beta$  relaxations of the IPNs were close to the average of the parent resins.

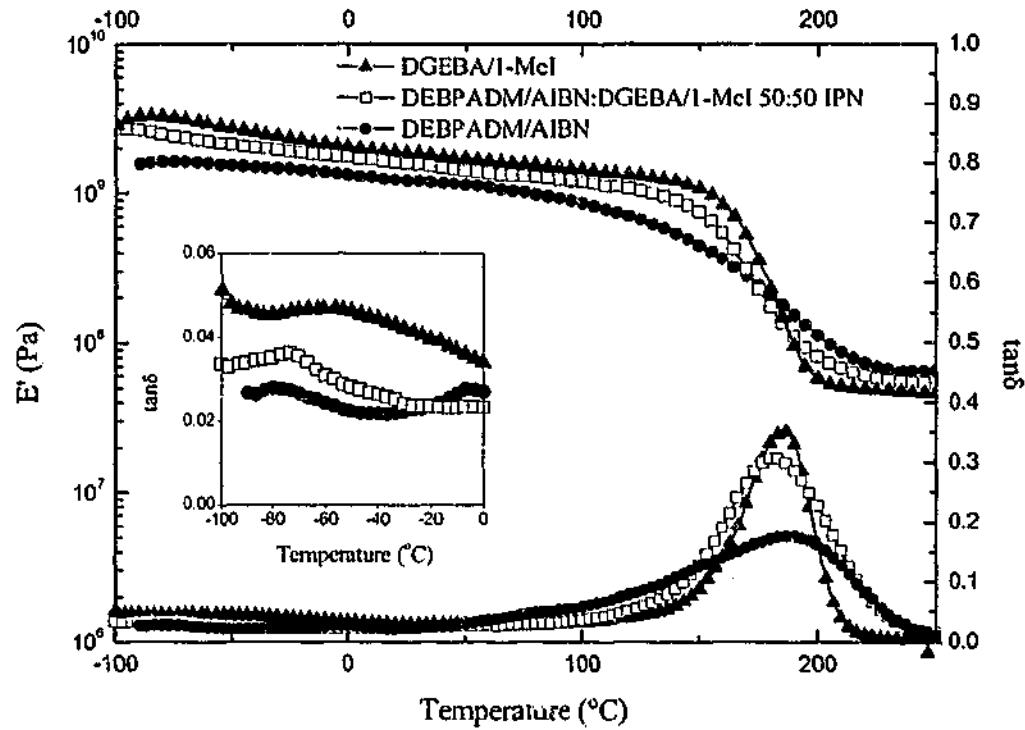


Figure 8.5 DMTA scans of DEBPADM/AIBN64, DGEBA/2wt% 1-MeI and the corresponding 50:50 IPN

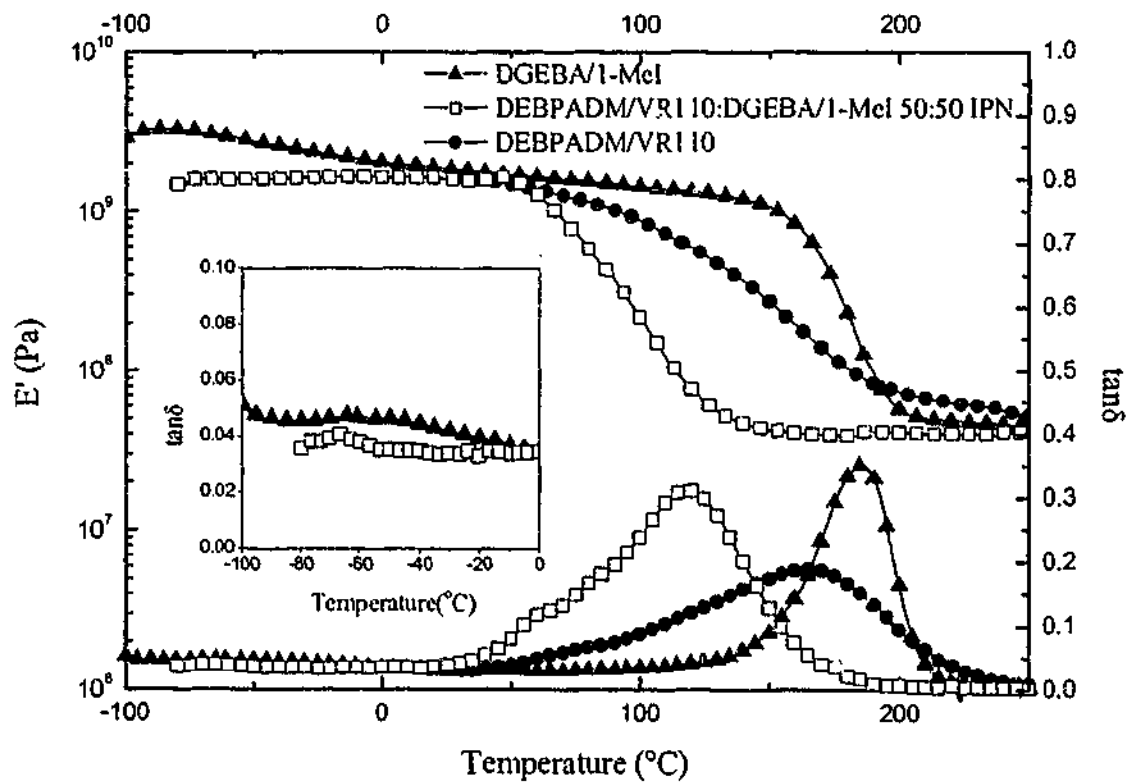
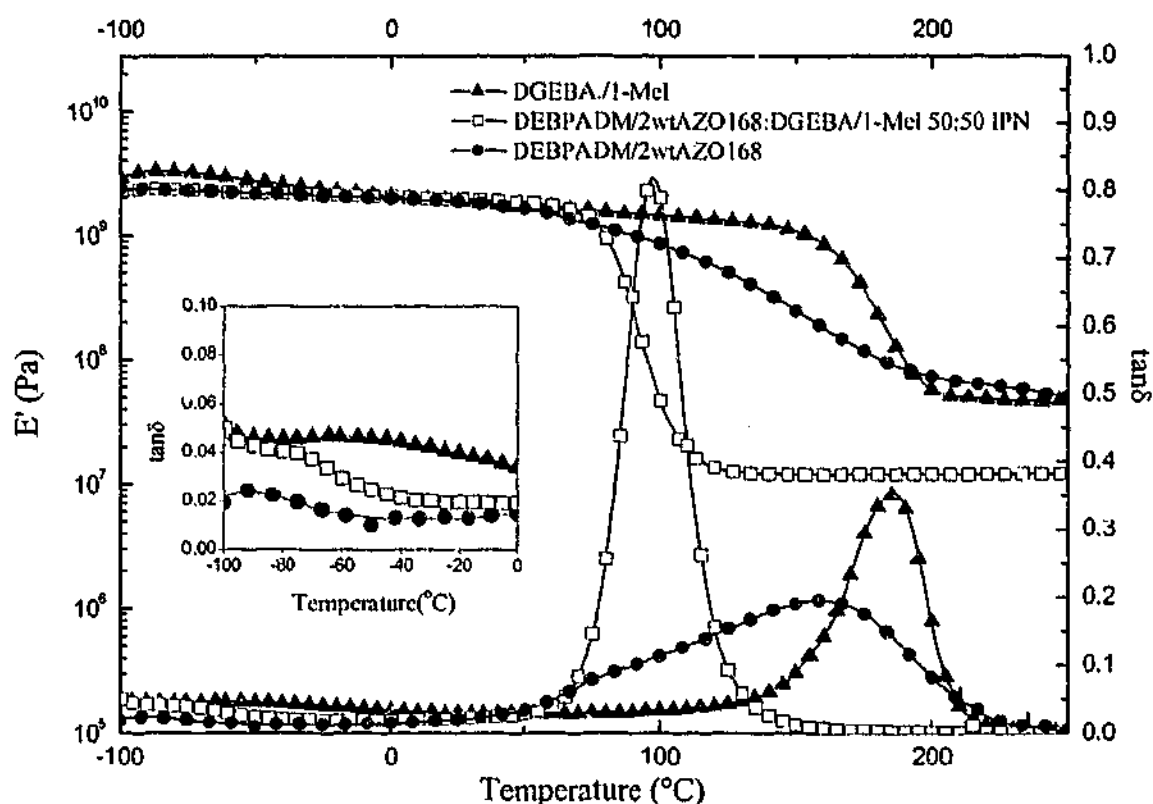


Figure 8.6 DMTA scans of DEBPADM/VR110, DGEBA/2wt% 1-MeI and the corresponding 50:50 IPN



**Figure 8.7** DMTA scans of DEBPADM/VAZO168AIBN, DGEBA/2wt% 1-Mel and the corresponding 50:50 IPN

### Variations of semi- and full-IPNs

#### *The Glass Transition*

A series of DMTA scans of semi- and full-IPNs based on the linear PGEMA or its crosslinking counterpart bisGMA with PGE or its crosslinking counterpart DGEBA are shown in Figures 8.8 and 8.9. The neat PGEMA/AIBN and neat bisGMA/AIBN have  $T_g$ s of 45°C (from DSC) and 173°C (from DMTA) respectively (see Table 8.3). The neat PGE/1-Mel and neat DGEBA/1-Mel have  $T_g$ s of 5°C (from DSC) and 185°C (from DMTA) respectively (see Table 8.3). The corresponding IPNs exhibit a range of dynamical mechanical behaviours. The 50:50 PGEMA/AIBN:DGEBA/1-Mel semi-IPN exhibits a single  $T_g$  at 100°C midway between the  $T_g$ s (45°C and 185°C) of the parent resins suggesting a single phase. The 50:50 bisGMA/AIBN:DGEBA/1-Mel IPN also exhibits a single  $T_g$  at 177°C which is midway between the  $T_g$ s of the parent resins but in this case the superposition of the  $T_g$ s is too small to lead to any conclusions about phase separation. In contrast, the 50:50 bisGMA/AIBN:PGE/1-Mel IPN exhibits a broad  $T_g$  at 83°C between the PGE/1-Mel ( $T_g$  of 5°C) and the bisGMA/AIBN ( $T_g$  of

173°C) suggesting a wide variation in phase mixing.

**Table 8.3 DMTA results for parent resins and their IPNs with PGE and PGEM.**

System	$\beta$ relaxation (°C)	$\alpha$ relaxations ( $\tan\delta$ maximum) (°C)	$E'$ of rubbery plateau ( $10^7$ Pa)
PGEMA/AIBN	-	45*	liquid
bisGMA/AIBN	-70	173	4.6
50:50 PGEMA/AIBN: DGEBA/1-MeI (5 wt%)	-75	100	2.9
50:50 bisGMA/AIBN: DGEBA/1-MeI (5 wt%)	-60	177	4.7
50:50 bisGMA/AIBN: PGE/1-MeI (5 wt%)	-	Broad peak at 83°C with a small shoulder at 18°C.	1.7
PGE/1-MeI (5 wt%)	-	5*	liquid
DGEBA/1-MeI (2 wt%)	-60	185	4.7

\* $T_g$ s from scanning DSC at 5°/min (DMTA measurements could not be made due to the low  $T_g$ s of these materials)

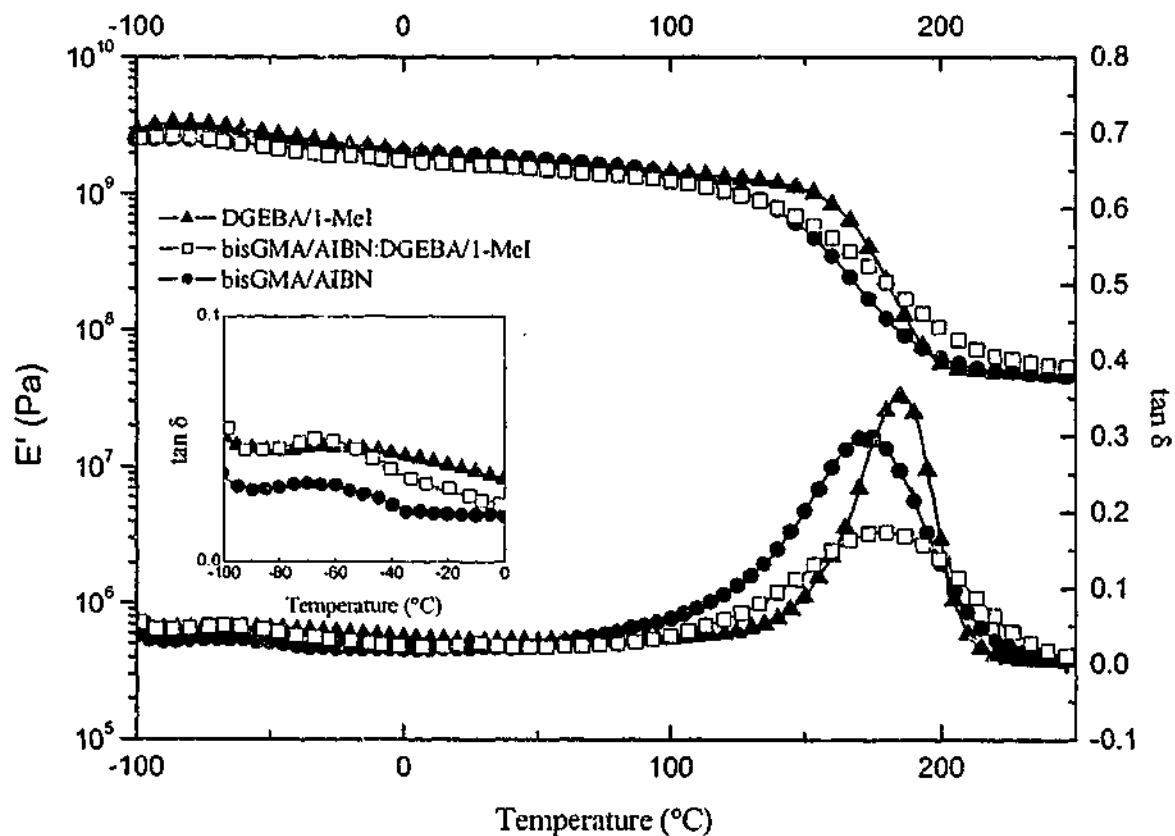


**Figure 8.8 DMTA scans of DGEBA/Me-I (2 wt%), bisGMA/AIBN, and corresponding 50:50 IPN.**

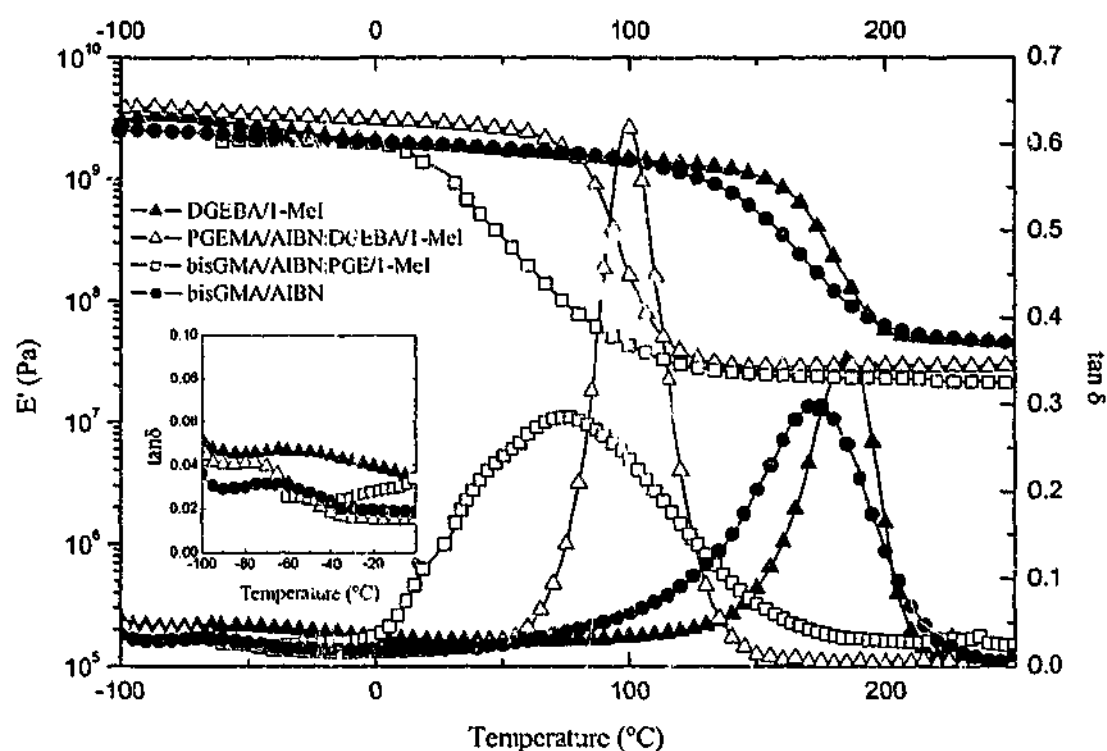


Figure 8.9 DMTA scans of DGEBA/1-MeI (2 wt%), bisGMA/AIBN, and the 50:50 semi-IPNs of PGEMA/AIBN:DGEBA/1-MeI (5 wt%) semi-IPN and bisGMA/AIBN:PGE/1-MeI (5 wt%).

#### Rubbery Modulus

The rubbery modulus of the 50:50 bisGMA/AIBN:DGEBA/1-MeI IPN is  $4.7 \times 10^7$  Pa which is between the rubbery modulus of the DGEBA/1-MeI ( $4.7 \times 10^7$  Pa) and the bisGMA/AIBN ( $4.6 \times 10^7$  Pa). The values of rubbery modulus for the 50:50 PGEMA/AIBN:DGEBA/1-MeI ( $2.9 \times 10^7$  Pa) and 50:50 bisGMA/AIBN:PGE/1-MeI ( $1.7 \times 10^7$  Pa) are low (as expected) due to the uncrosslinked nature of the PGEMA/AIBN and PGE/1-MeI of which they consist.

#### Relaxational Behaviour

As noted above, the  $\beta$  relaxation in the neat DGEBA/1-MeI ( $-60^\circ\text{C}$ ) may also be due to the localized motion of the bisphenol-A group<sup>240</sup>. Similar to the  $\beta$  relaxation in the neat VER, the  $\beta$  relaxation in the neat bisGMA ( $-70^\circ\text{C}$ ) may be associated with localized molecular motion of the methacrylate group<sup>239</sup>. The broad  $\beta$  relaxations of the 50:50 bisGMA/AIBN:DGEBA/1-MeI ( $-60^\circ\text{C}$ ) is close to the average of its parent resins

and the 50:50 PGEMA/AIBN:DGEBA/1-MeI IPN also exhibited a broad  $\beta$  relaxation in this region.

### 8.3 Small Angle Neutron Scattering (SANS).

An exploratory SANS study was undertaken on a series of IPNs and their parent resins and the spectra of the scattering intensity  $I(Q)$  in  $\text{cm}^{-1}$  versus the scattering vector  $Q$  in  $\text{\AA}^{-1}$  are shown in Figures 8.10 to 8.15\*. The atomic weight and scattering length due to individual atoms is listed in Table 8.4. A summation of the scattering due to each particular atom within each particular component of the IPN has been calculated to produce a scattering length per repeat unit for each component sub-unit (listed in Table 8.5). The scattering length ( $b_i$ ) for each component (see Section 2.4.3), the molecular weight (MW) of the repeat unit and density of the neat resin (see Table 8.6) were used to calculate the scattering length density for the neat resins:

$$\text{scattering length density} = \left( \frac{\rho \times \text{Avogadro's number}}{\text{MW of repeat unit}} \right) \times \left( \sum b_i \right)_{\text{component}} \quad \text{Equation 8.1}$$

In some cases the difference in scattering length density of components is close to the threshold of observable scattering; for example the scattering length density for the VER/AIBN is  $148 \times 10^8 \text{ cm}^{-2}$  which is very close to DGEBA/CHDCA/DMBA ( $155 \times 10^8 \text{ cm}^{-2}$ ), hence even if the system was phase separated, the difference in scattering length density may be too small for scattering to be observed.

Table 8.4 Scattering length and atomic weight associated with particular atoms<sup>163</sup>.

Atoms	Hydrogen	Deuterium	Carbon	Oxygen	Nitrogen
Scattering length (cm) ( $\times 10^{-12}$ )	-0.374	0.667	0.665	0.58	0.937
Atomic weight (g/mol)	1.001	2.014	12.011	16.00	14.007

\* SANS measurements were kindly performed at NIST, Gaithersburg by Dr Min Lin on samples formulated and prepared by the author.

Table 8.5 Composition and scattering length associated with the repeat unit.

	Hydrogen	Carbon	Oxygen	Nitrogen	Scattering Length (cm) ( $\times 10^{-12}$ )
DGEBA/DAO	32	25	4	1	7.2
DGEBA/BA	35	25	4	1	6.8
DGEBA/DDM	31	27.5	4	1	10.0
DGEBA/An	31	27	4	1	9.6
DGEBA/CHDCA/DMBA	34	29	7	0	10.6
DGEBA	24	21	4	0	7.3
model VER	17	14.7	2.6	0	4.9
DAO	20	8	0	2	-0.3
BA	11	4	0	1	-0.5
DDM	14	13	0	2	5.3
An	7	6	0	1	2.3
CHDCA	10	8	3	0	3.3
Me-I	6	4	0	2	2.3
bisGMA	36	29	8	0	10.5
Styrene	8	8	0	0	2.3

**Table 8.6 Summary of scattering length, MW of repeat unit, density and scattering length density for all the neat resins**

	Scattering length cm ( $\times 10^{-12}$ cm)	$M_w$ of repeat unit g/mol	Density <sup>+</sup> g/cm <sup>3</sup>	Scattering length density cm <sup>2</sup> ( $\times 10^9$ )
DGEBA	7.3	340.2	1	129
DGEBA/DAO	7.2	412.3	1.2	126
DGEBA/BA	6.8	413.3	1.18	117
DGEBA/DDM	10.0	429.3	1.19	162
DGEBA/An	9.6	433.3	1.18	158
DGEBA/CHDCA/DMBA	10.6	494.3	1.2	155
model VER	4.9	234.7	1.17	148
DAO	-0.3	144.1	1	-12
BA	-0.5	73.1	1	-43
DDM	5.3	198.2	1	160
An	2.3	93.1	1	149
CHDCAN	3.3	154.1	1.19	154
1-MeI	2.3	82.1	1	168
bisGMA	10.5	512.3	1	123
Styrene	2.3	104.1	1	135

Figures 8.10 to 8.15 show that the neat resins, the 50:50 VER/AIBN:DGEBA/1-MeI IPN and the 50:50 VER/AIBN:DGEBA/CHDCA/DMBA IPN showed weak scattering patterns indicating either a single phase system or the scattering density difference between phases was too small to produce any significant scattering. The 50:50 VER/AIBN:DGEBA/An semi-IPN, the 50:50 VER/AIBN:DGEBA/DDM IPN, the 50:50 VER/AIBN:DGEBA/BA semi-IPN and to a lesser extent the 50:50 VER/AIBN:DGEBA/DAO IPN all produced scattering indicative of a two phase system (see Figures 8.14 and 8.15). The DMTA data confirms evidence of a two phase structure for the semi-IPNs of 50:50 VER/AIBN:DGEBA/BA and 50:50 VER/AIBN:DGEBA/An (see Figures 8.2 and 8.3) and the 50:50

<sup>+</sup> density measurements taken from fully cured parent resins described in Section 4.5

VER/AIBN:DGEBA/DAO IPN (see Figure 8.2). The 50:50 VER/AIBN:DGEBA/DDM IPN only produced a single  $T_g$ , (see Figure 8.3) however the difference in  $T_g$  of the parent resins in the DDM based IPN (VER/AIBN - 169°C and DGEBA/DDM - 189°C) was not as significant as the DAO based IPN and thus a two phase system may be difficult to identify by DMTA alone.

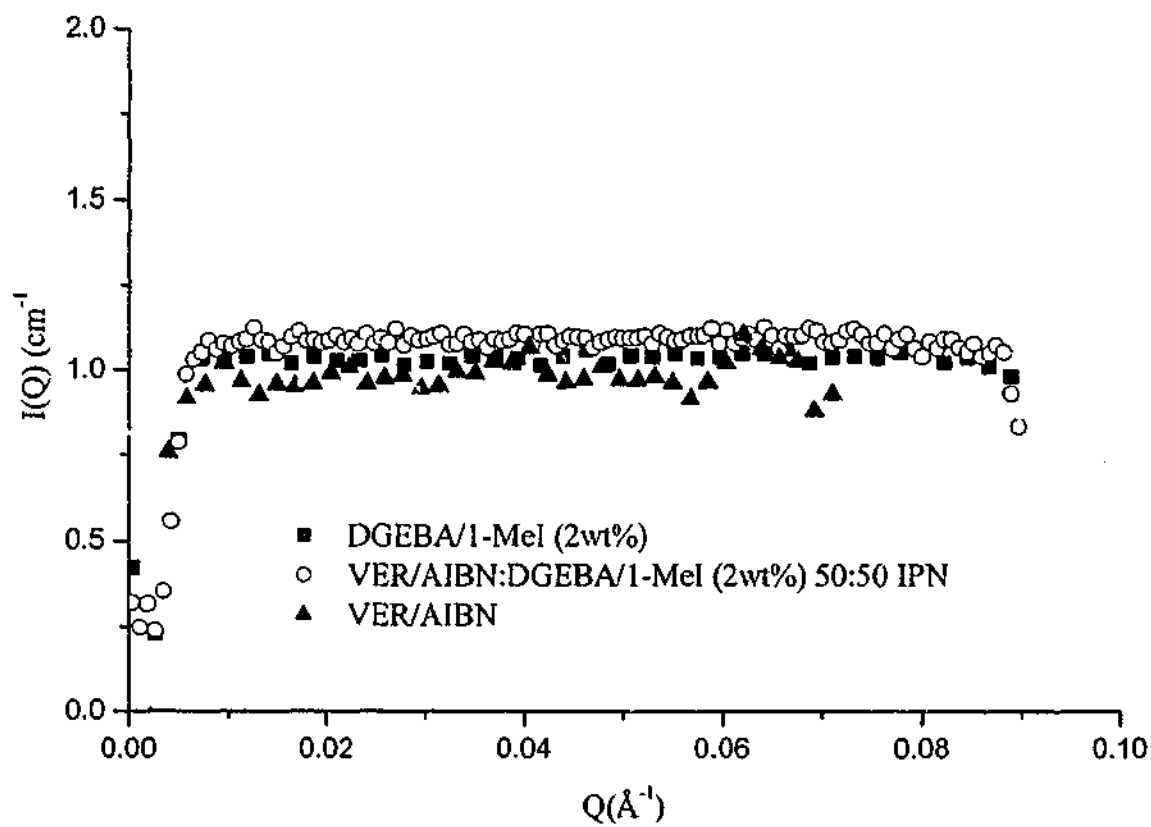


Figure 8.10 Scattering intensity  $I(Q)$  versus scattering vector  $Q$  for DGEBA/1-MeI, VER/AIBN and the 50:50 IPN.

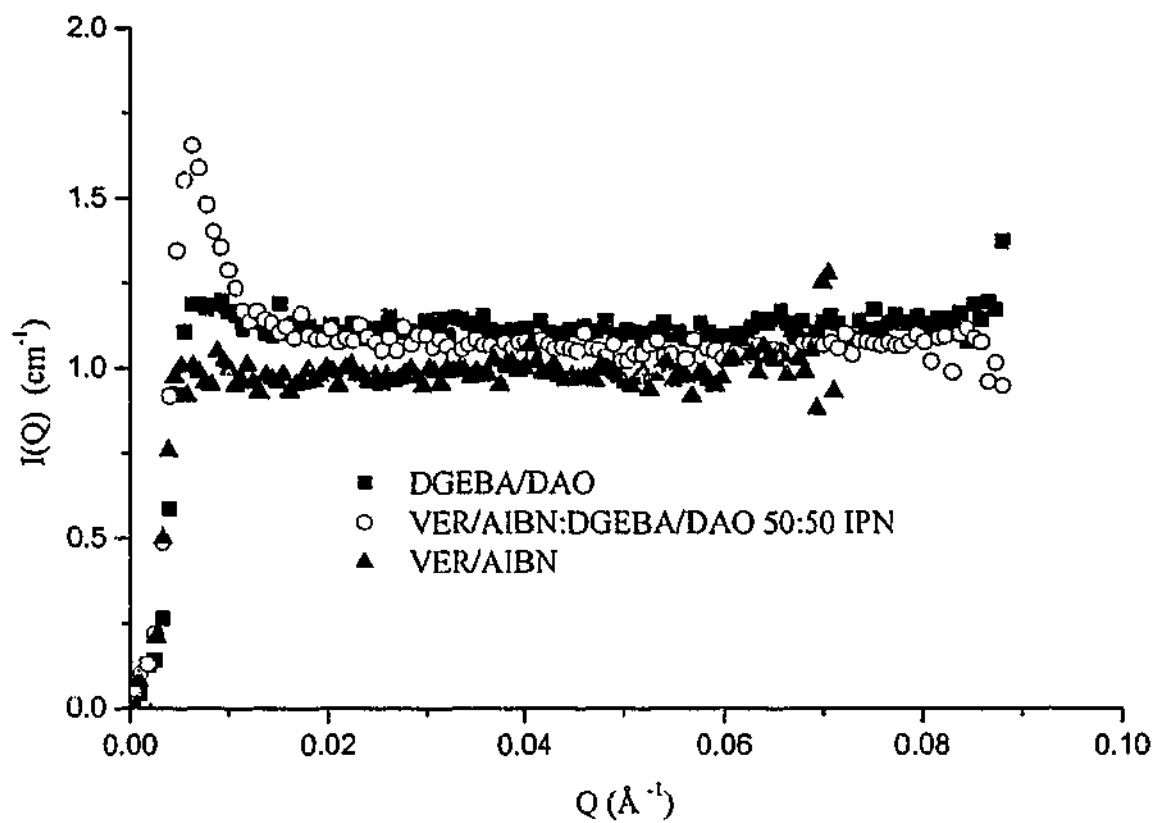


Figure 8.11 Scattering intensity  $I(Q)$  versus scattering vector  $Q$  for DGEBA/DAO, VER/AIBN and the 50:50 IPN.

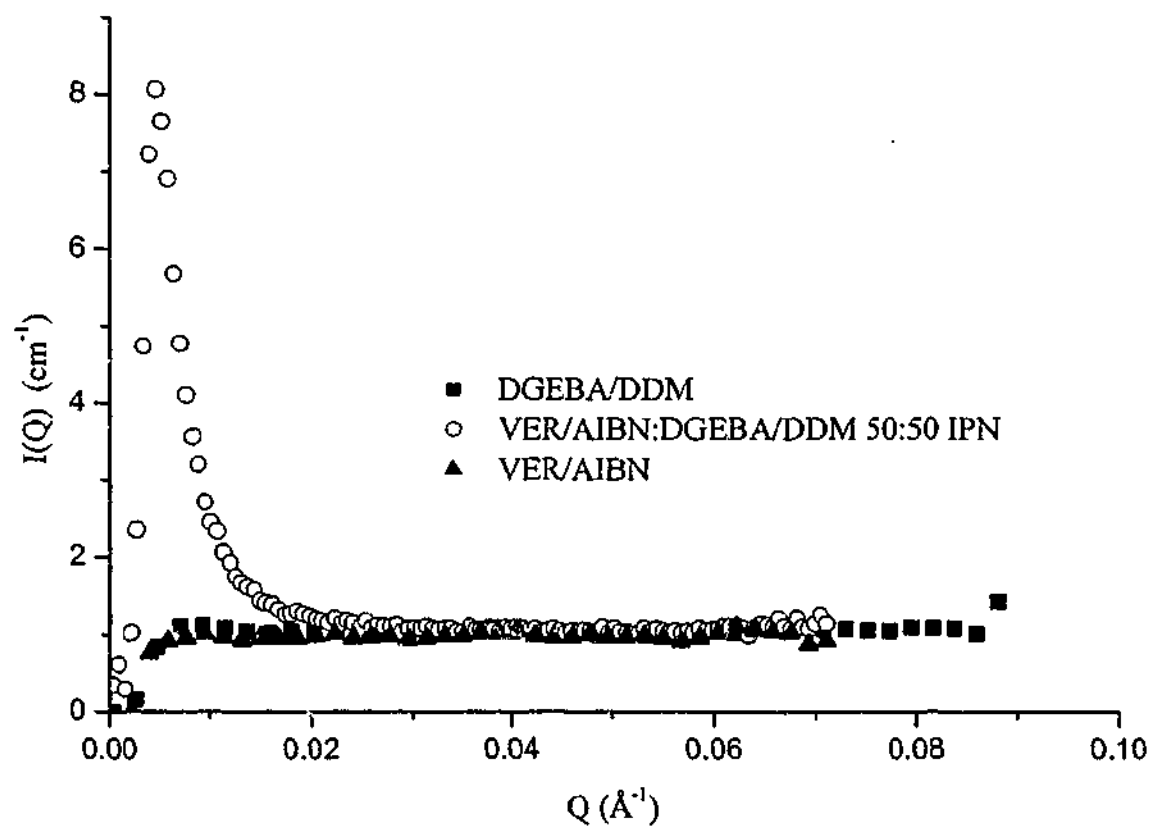


Figure 8.12 Scattering intensity  $I(Q)$  versus scattering vector  $Q$  for DGEBA/DDM, VER/AIBN and the 50:50 IPN.

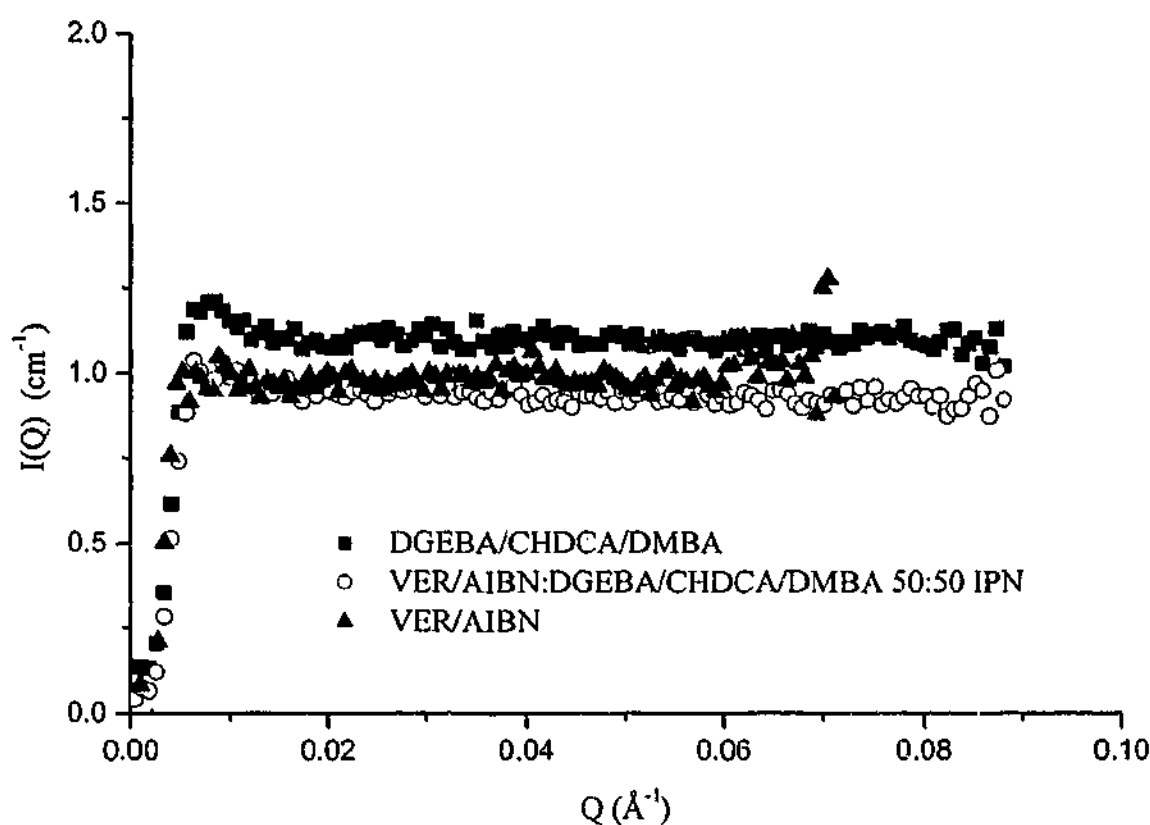


Figure 8.13 Scattering intensity  $I(Q)$  versus scattering vector  $Q$  for DGEBA/CHDCA/DMBA, VER/AIBN and the 50:50 IPN.

The scattering of the VER/AIBN:DGEBA:BA, VER/AIBN:DGEBA:DAO, VER/AIBN:DGEBA:An, VER/AIBN:DGEBA:DDM IPNs was fitted to the Deybe-Bueche model (see Section 2.4.3) as shown in Figures 8.14 and 8.15 and values of the correlation length in each IPN are listed in Tables 8.7 and 8.8.

At low  $Q$ , a simplified version of the Deybe-Bueche equation is given by<sup>164,166</sup>:

$$I(Q) = \left( \frac{A}{(1 + \xi^2 Q^2)^2} \right) + B \quad \text{Equation 8.2}$$

where  $A$  is a constant for the system,  $\xi$  is the correlation length and  $B$  is the background scattering. Equation 8.2 was fitted to the SANS data using a least square iteration over the  $Q$  range from 0.006 to 0.03  $\text{\AA}^{-1}$  (see Figure 8.14 and Figure 8.15)

The scattering data from the 50:50 VER/AIBN:DGEBA/BA IPN fits the Deybe-Bueche reasonably well (but deviates at  $0.010\text{\AA} < Q < 0.014\text{\AA}$ ), giving a  $\xi$  of  $181 \pm 4\text{\AA}$ . The scattering from the 50:50 VER/AIBN:DGEBA/DAO IPN fits the Deybe-Bueche equation well giving a  $\xi$  of  $151 \pm 12\text{\AA}$ . The scattering data from the 50:50 VER/AIBN:DGEBA/An IPN and 50:50 VER/AIBN:DGEBA/DDM IPN produced good

fits to the Deybe-Bueche equation with no observable deviation over the whole range of fitting from  $0.007\text{\AA} < Q < 0.03\text{\AA}$ . From this fit, the correlation lengths for VER/AIBN:DGEBA/An and VER/AIBN:DGEBA/DDM were  $186 \pm 8\text{\AA}$  and  $184 \pm 6\text{\AA}$  respectively. The sizes of the domains, however, are very small and, being far smaller than the wavelength of light, are not visually opaque.

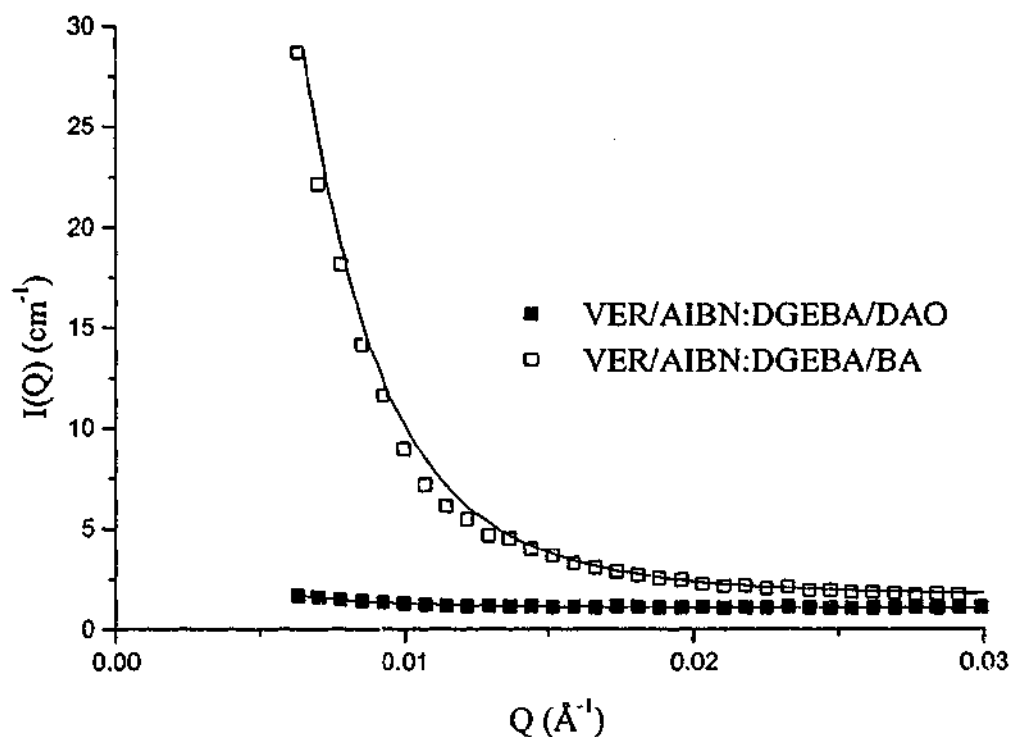


Figure 8.14 Deybe-Bueche fitting of 50:50 VER/AIBN:DGEBA:BA and 50:50 VER/AIBN:DGEBA:DAO scattering data

Table 8.7 Deybe-Bueche fitting results for 50:50 VER/AIBN:DGEBA:BA and 50:50 VER/AIBN:DGEBA:DAO

Deybe-Bueche Model VER/AIBN:DGEBA:BA		
$\chi^2 = 0.05$		
Variables	Fitted values	Error
A	155	$\pm 8$
$\xi$ ( $\text{\AA}$ )	181	$\pm 4$
B ( $\text{cm}^{-1}$ )	1.6	$\pm 0.1$
Deybe-Bueche Model VER/AIBN:DGEBA:DAO		
$\chi^2 = 0.006$		
Variables	Fitted values	Error
A	2.2	$\pm 0.4$
$\xi$ ( $\text{\AA}$ )	151	$\pm 12$
B ( $\text{cm}^{-1}$ )	1.10	$\pm 0.01$

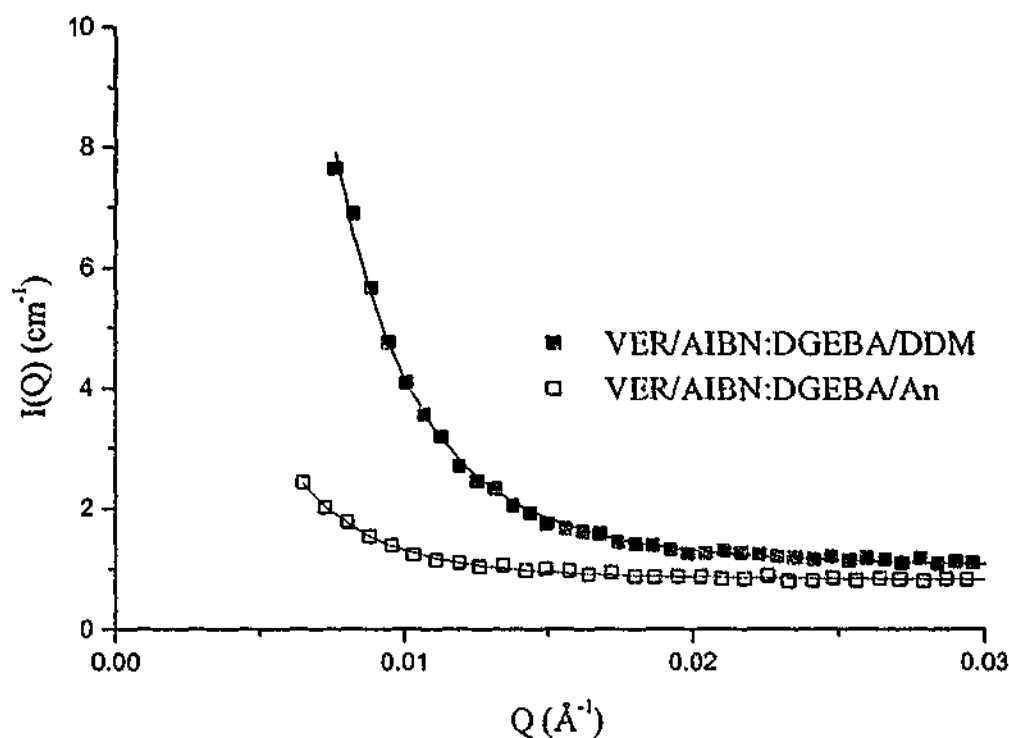


Figure 8.15 Deybe-Bueche fitting of 50:50 VER/AIBN:DGEBA:An and 50:50 VER/AIBN:DGEBA:DDM scattering data

Table 8.8 Deybe-Bueche fitting results for 50:50 VER/AIBN:DGEBA:An and 50:50 VER/AIBN:DGEBA:DDM

Deybe-Bueche Model VER/AIBN:DGEBA:An $\chi^2 = 0.0007$		
Variables	Fitted values	Error
A	10	$\pm 1$
$\xi$ (Å)	186	$\pm 8$
B (cm <sup>-1</sup> )	0.80	$\pm 0.01$
Deybe-Bueche Model VER/AIBN:DGEBA:DDM $\chi^2 = 0.0006$		
Variables	Fitted values	Error
A	61	$\pm 6$
$\xi$ (Å)	184	$\pm 6$
B (cm <sup>-1</sup> )	1.02	$\pm 0.02$

## 8.4 Conclusions

A range of 50:50 IPNs with differing morphologies have been produced. These comprise the clearly phase separated IPNs which showed two  $T_g$ s by DMTA and excess small angle neutron scattering: 50:50 VER/AIBN:DGEBA/An, 50:50

VER/AIBN:DGEBA/BA and the 50:50 VER/AIBN:DGEBA/DAO IPNs. Others whose phase structure can not be determined by DMTA analysis (showing a single  $T_g$  by DMTA) but which show obvious small angle neutron scattering such as the 50:50 VER/AIBN:DGEBA/DDM IPN; and those which are not obviously phase separated by DMTA (showing a peak with a shoulder in the DMTA spectrum) or SANS analysis (no small angle neutron scattering) such as the 50:50 VER/AIBN:DGEBA/CHDCA/DMBA IPN. The last groups of IPNs are those that appear to be single phase materials (showing a single  $T_g$  by DMTA and no small angle neutron scattering) such as the 50:50 VER/AIBN:DGEBA/1-MeI IPN. The phase morphology as observed by DMTA and SANS and the cure order and presence of grafting is summarized in Table 8.9.

**Table 8.9 Summary of phase morphology and curing order of IPNs**

System	VER cured first (V) epoxy cured first (E)	Grafting (Michael addition)	$\Delta T_g$ (parent resins) ( $^{\circ}\text{C}$ )	Two $T_g$ s by DMTA	Scattering density difference	Observed SANS
VER/AIBN: DGEBA/1-MeI	V	no	16	no	19	no
VER/AIBN: DGEBA/BA	E	yes	102	yes	31	yes
VER/AIBN: DGEBA/DAO	E	yes	40	yes	22	yes
VER/AIBN: DGEBA/An	V	yes	50	yes	10	yes
VER/AIBN: DGEBA/DDM	V	yes	20	no	14	yes
VER/AIBN: DGEBA/CHDCA/ DMBA	V	no	10	yes (a peak with a shoulder)	7	yes (borderline)

The four systems that showed significant small angle neutron scattering were fitted well to the Deybe-Bueche model which assumes a random distribution of phases with different sizes and shapes throughout a scattering volume (V). The correlation

length  $\xi$ , calculated from the Debye-Bueche equation was  $181 \pm 4 \text{ \AA}$ ,  $151 \pm 12 \text{ \AA}$ ,  $186 \pm 8 \text{ \AA}$  and  $184 \pm 6 \text{ \AA}$  for the 50:50 VER/AIBN:DGEBA/BA IPN, 50:50 VER/AIBN:DGEBA/DAO IPN, 50:50 VER/AIBN:DGEBA/An IPN and 50:50 VER/AIBN:DGEBA/DDM IPN respectively. The lower correlation length for the VER/AIBN:DGEBA/DAO IPN may be due to a reduction in phase separation due to the near simultaneous interlocking of the two networks during cure. This is not observed for the VER/AIBN:DGEBA/DDM IPN in which the correlation length is similar to that of the VER/AIBN:DGEBA/An semi-IPN perhaps because the slower cure of the epoxy component and the reduction in enthalpy during the cure of the DGEBA/DDM component causes phase separation before the interlocking of the two networks can occur.

# *Chapter 9*

## *Dual Photopolymerization and thermal curing kinetics of dimethacrylate-epoxy IPNs*

---

### **9.1 Introduction**

In Chapter 7, it was demonstrated that the cure order in IPNs could be reversed depending on the initiator systems used, although the effect of cure order on resulting morphology was difficult to interpret due to incomplete methacrylate cure. In Chapter 8, DMTA investigations also indicated that the cure order affected the resulting IPN phase morphology. In the present chapter, the isothermal photopolymerization kinetics of a dimethacrylate and the thermal cure of an epoxy/anhydride mixture have been investigated separately and within a 50:50 dimethacrylate/epoxy IPN using DSC and NIR. This combination of crosslinkable resins permits the partial or complete cure of each component independently of each other. The miscibility of the resulting IPNs is also presented here.

## 9.2 Cure kinetics and DMTA

### Thermal cure kinetics

Figure 9.1 shows the thermal polymerization behaviour of the dimethacrylate (using AIBN as initiator) and of the epoxy/anhydride system. Based on the heat of polymerization for methyl methacrylate of 56.2 kJ/mol<sup>222</sup>, the theoretical heat of polymerization of DEBPADM was calculated as 239 J/g (based on a molecular weight of 470 g/mol obtained by titration – see Section 3.2). The observed heat of polymerization of the dimethacrylate was 220 J/g, suggesting 90% cure. The heat of polymerization of the epoxy system was 300 J/g corresponding to 112 kJ/mol, which is similar to that found in Sections 5.1.2, 5.2.2 and 5.3.2 and in the literature<sup>16, 231, 234</sup>. The DSC behaviour of the 50:50 IPN (Figure 9.1) shows two distinct exotherms for which the lower and upper exotherms can be attributed to the DEBPADM/AIBN and DGEBA/anhydride cure, respectively. In agreement with this, the resolved contributions to the DSC exotherm (see Figure 9.1) are approximately equal to that expected from the weight fractions of DEBPADM and epoxy components in the IPN. The peak exotherm temperature for the methacrylate cure appears to be shifted to higher temperatures than in the parent resins, as observed in earlier DSC cure studies of related IPN systems (see Chapter 5), due to the effect of dilution of the system by the epoxy component. The peak exotherm temperature for the epoxy does not shift to a higher temperature as one might expect due to dilutional effects, but occurs at a similar temperature as that in the neat system. A similar behaviour was found for the VER/AIBN:DGEBA/DDM and VER/AIBN:DGEBA/An IPNs in Section 5.1.2 and this was attributed to the combined result of the decelerating dilution effect and an accelerating catalytic effect. This explanation is not applicable here because DEBPADM has no potentially accelerating hydroxyl groups. As shown later in Figure 9.15, the DMTA of the fully cured sample of the 50:50 DEBPADM/AIBN:DGEBA/DDSA/CHDCA/DMBA IPN exhibits two  $T_g$ s. Thus it is possible that phase separation occurs during the cure of the dimethacrylate component so that the subsequent polymerization of the epoxy occurs in its own phase. If this is the case, then a smaller dilution effect would be observed for the epoxy exotherm in the IPN.

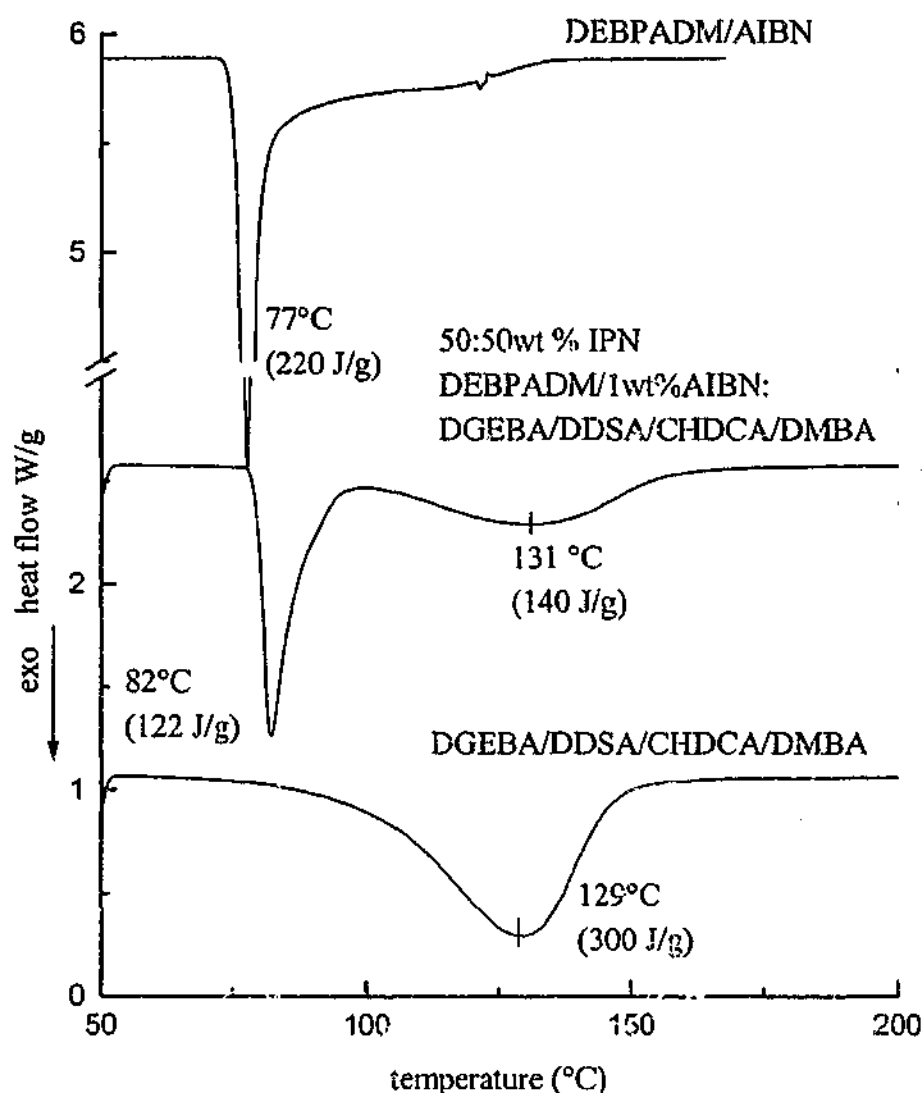


Figure 9.1 Scanning cure of DEBPADM/AIBN:DGEBA/DDSA/CHDCA/DMBA

### Photochemical cure kinetics

Two photo-polymerization systems were used in this work. The photo-redox mechanism of CQ/TMA - see Figure 2.16 and the iniferter XDT - see Figure 2.17. Figure 9.2 shows the dependence of the photocuring behaviour of the DEBPADM/CQ/TMA system at 50°C on the radiation intensity varied by using different neutral density filters. The rate of photo-polymerization depends strongly on the radiation intensity and approximately follows the theoretical square root dependency<sup>22</sup> but the total heat of polymerization at 50°C is approximately constant at 115 kJ/mol, suggesting that the final structure is independent of the rate of cure. The heat of polymerization of 115 J/g corresponds to 48% conversion and this low conversion is due to vitrification during cure which prevents complete polymerization<sup>14,19,20,56</sup> because the glass transition temperature ( $T_g$ ) of the fully cured DEBPADM (189°C, from DMTA at 1 Hz - see Section 8.2) is well above the

isothermal cure temperature.

Because the photocure reaction proceeds very rapidly during exposure to the unattenuated visible light source, a filter with an optical density of 1.3 (light transmission of 5%) was employed as the standard condition for the CQ/TMA photocuring to ensure that the reaction could be easily monitored. Figure 9.3 illustrates the effect of different exposure times on the DSC traces for the DEBPADM/CQ/TMA system at 50°C. Analogous, but slower photocuring behaviour was observed for DEBPADM/XDT (see Figure 9.4), however after 20 min of UV irradiation at 50°C, the heat of polymerization was 108 J/g (45% conversion) which is comparable to that found for the CQ/TMA initiation system after 10 min of irradiation (see Figure 9.3). Comparison of Figures 9.3 and 9.4 also show that when the irradiation is stopped, the polymerization drops off much more rapidly for the DEBPADM/XDT system as expected of a photo-iniferter. The advantage of the XDT over the CQ/TMA system is that the former results in less thermal dark reaction because the small dithiocarbamate radical (produced during irradiation of XDT) terminates growing radical chains in the absence of UV radiation<sup>105</sup>.

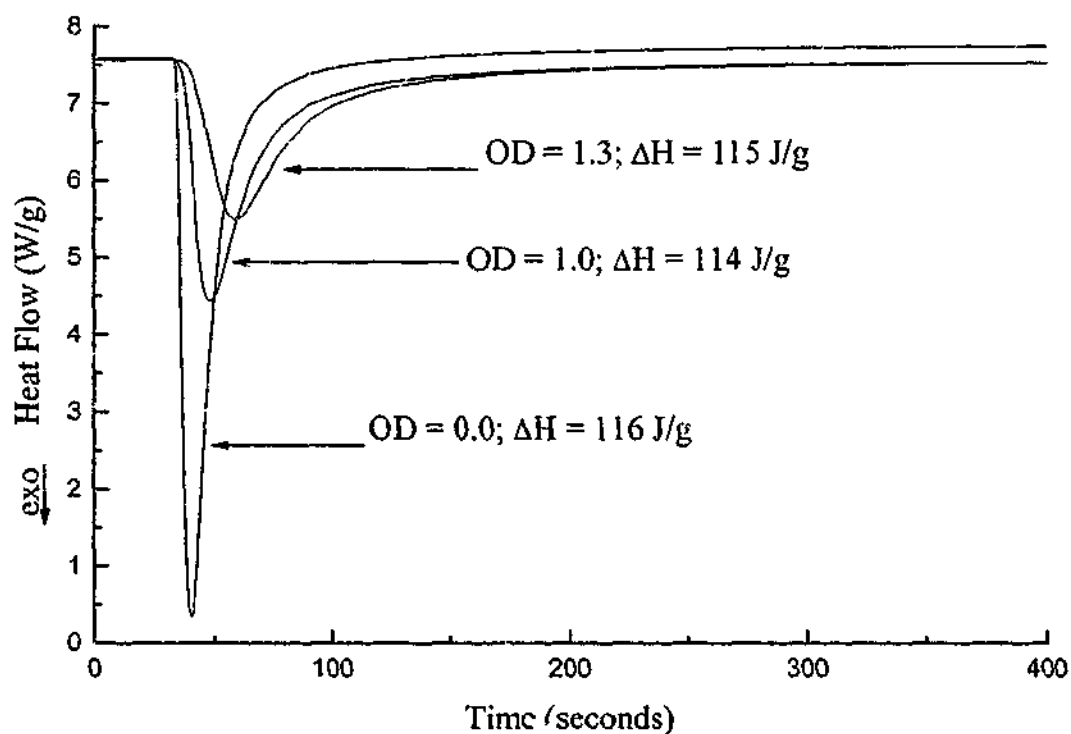


Figure 9.2 Photocuring of DEBPADM/CQ/TMA at 50°C with visible light using neutral density filters of differing optical densities (ODs); all systems exposed for 10 min.

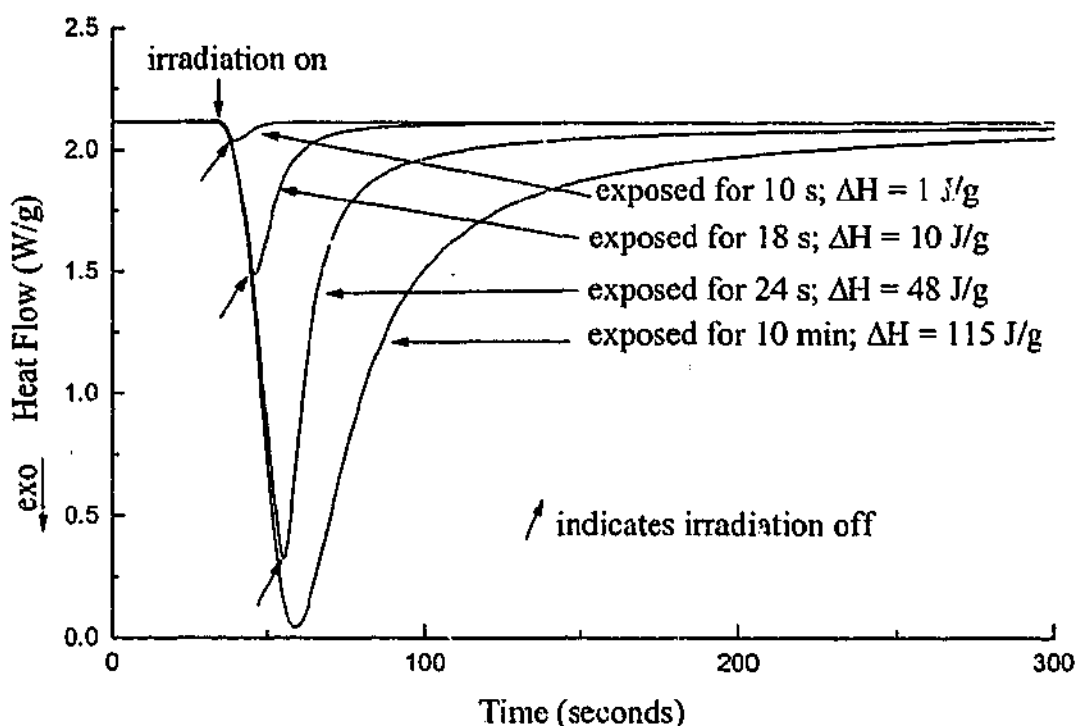


Figure 9.3 Photocuring of DEBPADM/CQ/TMA at 50°C with visible light for varying exposure times using the standard neutral density filter with an optical density of 1.3.

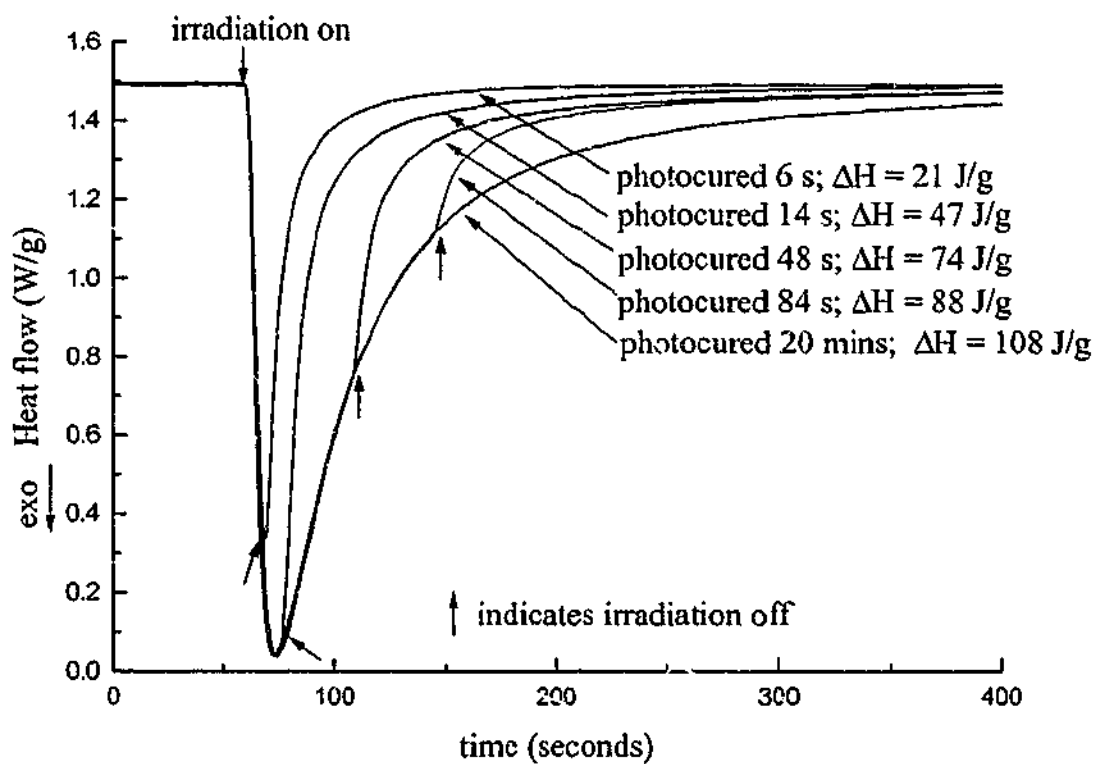


Figure 9.4 Photocuring of DEBPADM/XDT at 50 °C with UV radiation (with no neutral density filter) for varying exposure times.

To investigate the possible interactions between the initiator components, studies of the effects of components from each curing system on the other were undertaken.

The effects of the dimethacrylate components on the epoxy cure were first investigated. Scanning DSC of the DGEBA/DDSA/CHDCA/DMBA system containing 0.15 wt% TMA revealed that the DSC peak shifted from 129 to 122°C but the heat of polymerization was unaffected (see Figures 9.5a and 9.5b). This shows that the TMA, like DMBA, has an accelerating effect on the epoxy/anhydride cure. The scanning DSC of DGEBA/CQ/TMA (Figure 9.5c) and DGEBA/XDT (Figure 9.5d) also reveals a very high temperature exotherm close to 300°C, presumably due to thermal cure or degradation of the epoxy. Compared with the neat DGEBA/DDSA/CHDCA/DMBA curing behaviour, which gives a DSC exotherm peak at 129°C (see Figure 9.5a), ramping DSC of the 50:50 DEBPADM:DGEBA/DDSA/CHDCA/DMBA (see Figure 9.5e) shows an exotherm peak at 149°C (146 J/g), due to the dilution of the epoxy/anhydride reactants by the dimethacrylate resin which reduces the rate of epoxy cure, however close to full cure is achieved. From these studies it can be concluded that the cure of the epoxy is accelerated but otherwise not greatly changed when it is blended with the dimethacrylate component.

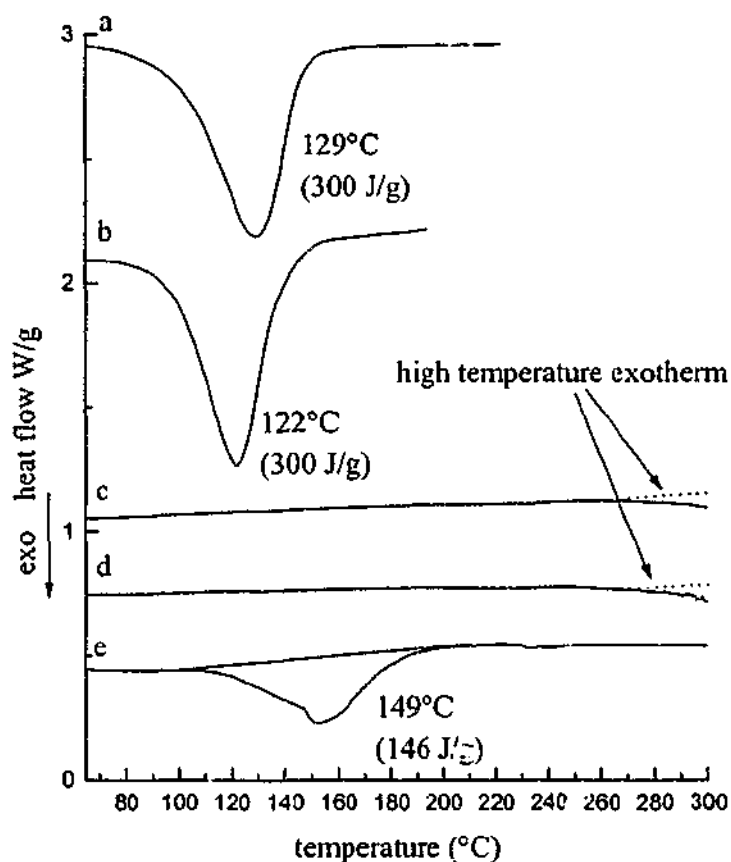


Figure 9.5 Effect of initiator components on the cure of DGEBA: a) temperature ramping DSC of DGEBA/DDSA/CHDCA/DMBA; b) temperature ramping DSC of DGEBA/DDSA/CHDCA/DMBA/TMA; c) temperature ramping DSC of DGEBA/CQ/TMA; d) temperature ramping DSC of DGEBA/XDT; e) temperature ramping DSC of the 50:50 DEBPADM:DGEBA/DDSA/CHDCA/DMBA

The effect of IPN components on the dimethacrylate cure was also investigated. Figure 9.6a illustrates the behaviour of uninitiated DEBPADM when scanned from 50 to 300°C - an exotherm peak appears at 178°C (42 J/g or 17% conversion), followed by an even higher temperature exotherm with a peak temperature at approximately 290°C, both apparently due to thermal cure of the dimethacrylate groups or degradation. The temperature ramping DSC of the DEBPADM/CQ/TMA system is also shown (see Figure 9.6b), and reveals three exothermic peaks - an onset to the polymerization occurs at 110°C and two overlapping peaks occur at 137°C and 195°C (having a total exotherm of 61 J/g or 25% conversion), and these peaks are followed by a broad, high temperature exotherm with a peak temperature close to 310°C. The peak at 137°C may result from thermally induced radicals from the CQ/TMA pair, while the peaks at 195°C and 310°C may be due to thermal cure of DEBPADM or degradation. To further investigate the effect of temperature on the CQ/TMA pair, the DEBPADM/CQ/TMA system was initially scanned from 50 to 170°C giving an exotherm of 32 J/g. When this sample was then photocured at 50°C, the resin produced an exotherm of 72 J/g. Although this exotherm is 43 J/g less than that for the virgin system (115 J/g) summation of partial polymerization of the DEBPADM during the prior thermal cure and the subsequent isothermal photopolymerization shows that the thermal scan does not impair the photo-initiating capacity of the CQ/TMA pair. When a mixture of DEBPADM/CQ/TMA:DGEBA was temperature ramped from 50°C to 300°C (see Figure 9.6c), a small exotherm (10 J/g, equivalent to 6% methacrylate conversion) at 186°C was observed. This small peak was superimposed over a broader exotherm, which is difficult to analyze in the higher temperature range of this scan (see Figure 9.6c) due to baseline instability, perhaps due to volatiles. These results suggest that the CQ/TMA system is more thermally stable in the IPN mixture than in the dimethacrylate monomer. Figure 9.6d also shows that if DEBPADM/CQ/TMA is partially photocured for 24 s at 50°C (giving a heat of polymerization of 48 J/g, equivalent to 20% conversion of methacrylate groups) and is then thermally scanned from 50 to 300°C, a broad exotherm of 55 J/g occurs with an onset at 75°C and a peak at 143°C. This peak may be due to the 'dark reaction' due to polymerization by the residual trapped radicals in the matrix (see Section 2.3.2) and also may be partially due to thermal cure of the system as was observed in the thermal scan of DEBPADM/CQ/TMA (see Figure 9.6b). This suggests that the CQ/TMA photo-initiating system may not be ideal for studies of sequential curing in the fully formulated IPN.

Similar investigations were undertaken on the DEBPADM/XDT system (Figure 9.7). Temperature-ramping DSC of the DEBPADM/XDT mixture (Figure 9.7b) over the range of 50-300°C shows an exotherm of 46 J/g (19% conversion) with an onset at 127°C and a peak at 184°C due to thermal cure. When the DEBPADM/XDT system was only scanned up to 170°C, an exotherm of 11 J/g was observed and subsequent photocuring of this sample at 50°C produced an additional exotherm of 95 J/g. The summation of these two exotherms (106 J/g) is very close to that found for the isothermal photocure of the virgin system (108 J/g) and shows that the thermal scan has little effect on the photo-initiating capacity of the XDT. When the neat DEBPADM/XDT system was partially irradiated with UV light for 14 s at 50°C, giving a heat of polymerization of 47 J/g (20% conversion), and was then temperature scanned from 50 to 300°C (Figure 9.7c), it produced a peak at 193°C and an exotherm of approximately of 17 J/g (7% conversion) which is smaller and at a higher temperature than that found with CQ/TMA as initiator (Figure 9.6d). Unlike the partially cured DEBPADM/CQ/TMA system (Figure 9.6d), the peak in the XDT system (Figure 9.7c) is unlikely to be due to residual radicals because the dithiocarbamate radical terminates other radicals in the absence of radiation<sup>104-109</sup> (see Section 2.3.2). The exotherm is most likely due to the thermal cure of the unreacted DEBPADM and the similarities of the peaks in these systems (Figures 9.7a-c) support this conclusion. In a similar temperature ramping DSC study of the partially photo-cured DEBPADM/XDT:DGEBA (Figure 9.7d), a more complicated exotherm profile is observed. There is a small exotherm (10J/g or 4 % conversion) at 146°C, which may be thermal cure of the DEBPADM/XDT, followed by a larger exotherm at 240°C possibly due to the higher temperature thermal cure of the DGEBA or DEBPADM. Temperature ramping DSC of a blend of DEBPADM/XDT and the anhydride mixture (Figure 9.7e) produces a small exotherm (12 J/g or 5 % conversion) at 144°C possibly due to thermal cure of the dimethacrylate.

In summary, the studies shown in Figures 9.5 to 9.7 reveal a number of interactions between the components in the IPN. The thermal cure of the DEBPADM is enhanced with the addition of the CQ/TMA producing a series of broad peaks with an onset at 110°C and an exotherm of 61 J/g (see Figure 9.6b). More significantly a dark reaction occurs during thermal ramping of the partially photocured DEBPADM/CQ/TMA system due to polymerization by radicals trapped in the matrix (see Figure 9.6d). In contrast, the DEBPADM/XDT (see Figure 9.7) is a cleaner system

because the dithiocarbamate radical terminates chain radicals in the absence of radiation. Thus XDT appears to be more suitable for sequential studies of cure in the IPN.

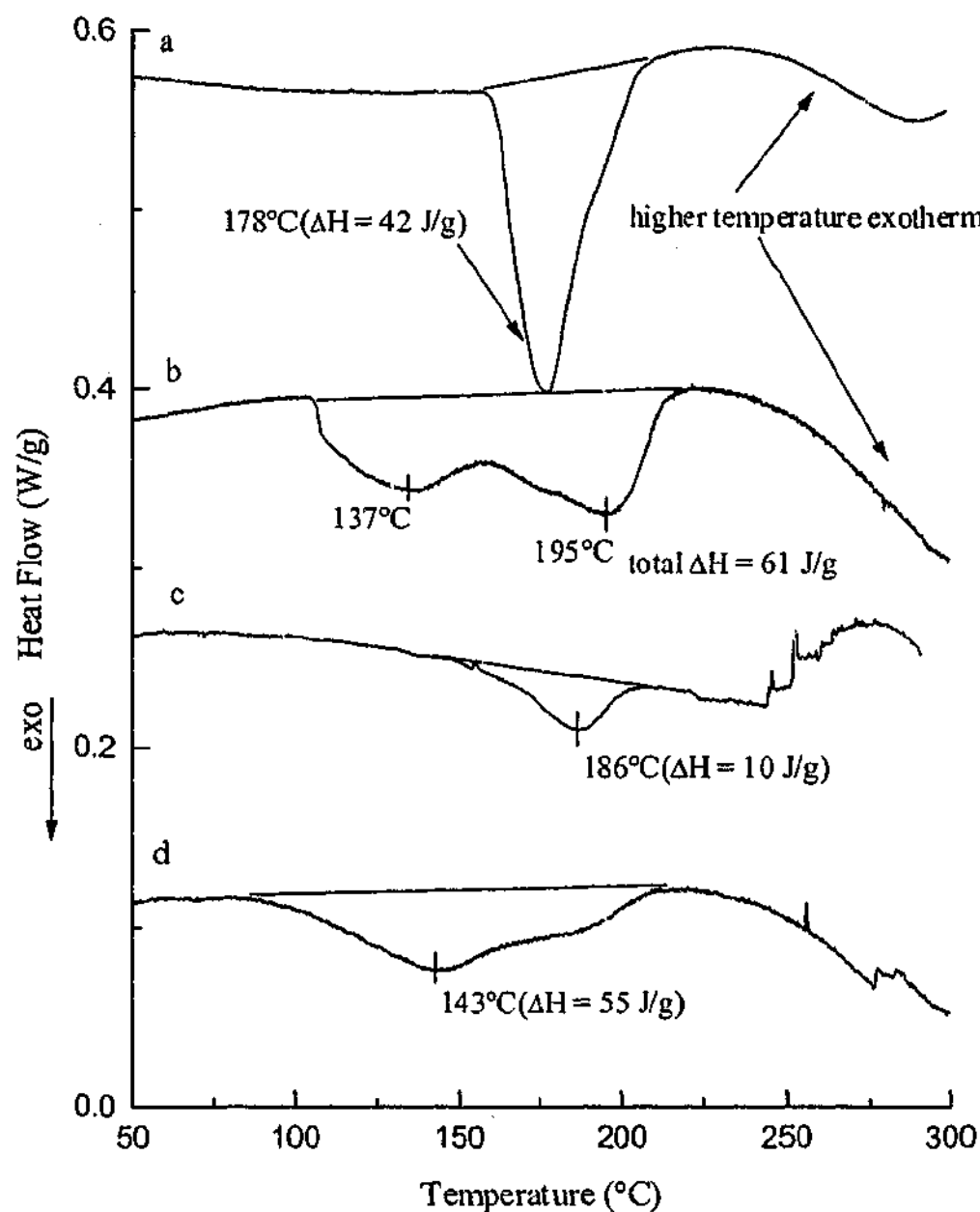
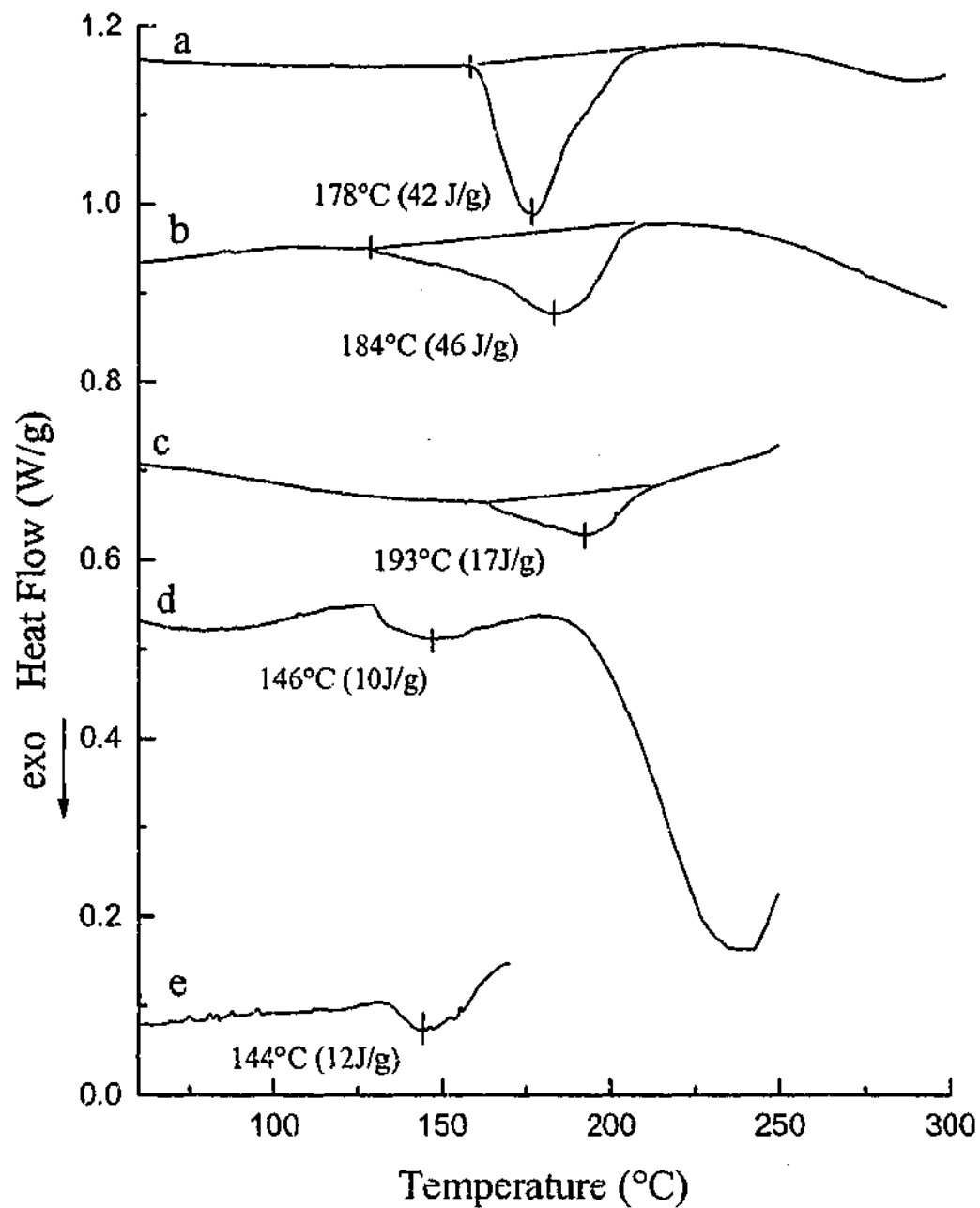
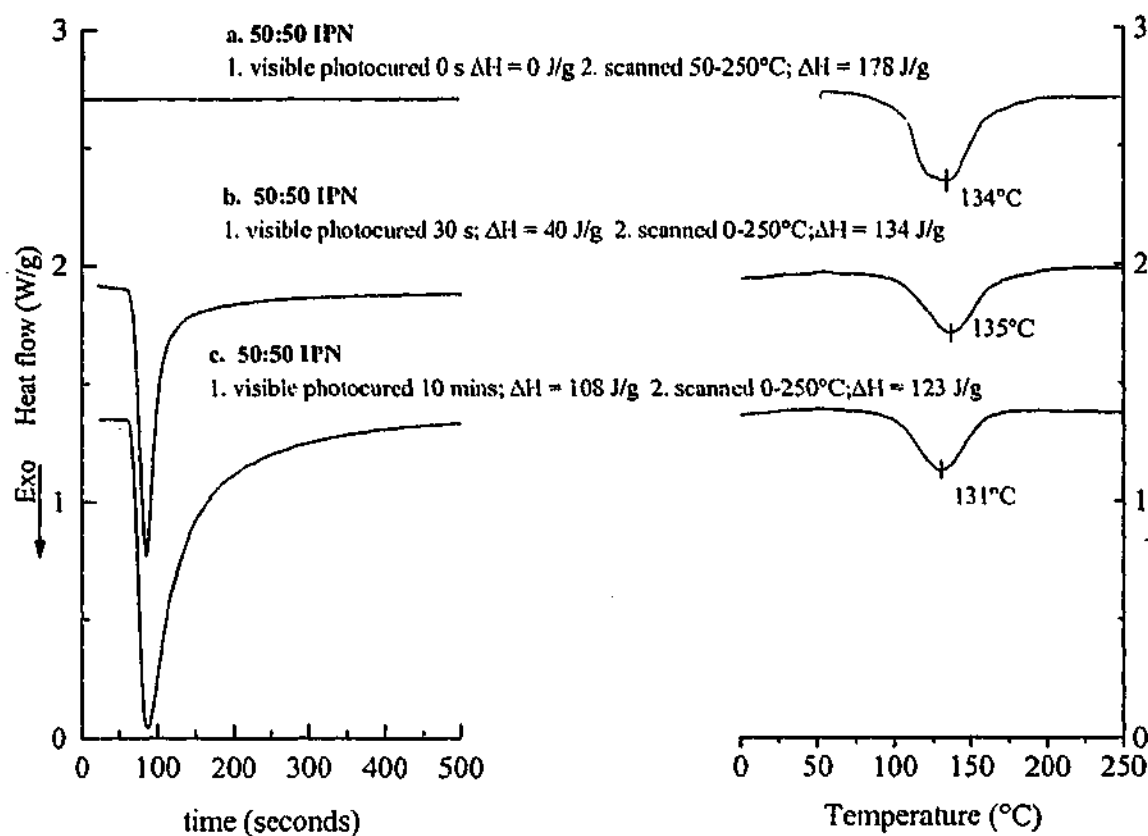


Figure 9.6 Effect of initiator components on the thermal cure of DEBPADM/CQ/TMA: a) temperature ramping DSC of DEBPADM alone; b) temperature ramping DSC of DEBPADM/CQ/TMA; c) temperature ramping DSC of DEBPADM/CQ/TMA:DGEBA; d) temperature ramping DSC of DEBPADM/CQ/TMA after photocuring for 24s to 20% conversion



**Figure 9.7** Effect of initiator components on the thermal cure of DEBPADM/XDT: a) temperature ramping DSC of DEBPADM alone; b) temperature ramping DSC of DEBPADM/XDT; c) temperature ramping DSC of DEBPADM/XDT (after photocuring for 14s to 20% conversion of methacrylate); d) temperature ramping DSC of DEBPADM/XDT:DGEBA (after photocuring for 25s to 27% conversion of methacrylate); e) DEBPADM/XDT: DDSA/CHDCA (containing the normal amount of ingredients – see Chapter 3)



**Figure 9.8** Photocuring behaviour of the 50:50 IPN DEBPADM/CQ/TMA:DGEBA/DDSA/CHDCA/DMBA at 50°C for varying irradiation times with visible light and the effect on the subsequent temperature-ramping exotherm behaviour.

Figure 9.8a shows the effect of temperature ramping on the DEBPADM/CQ/TMA:DGEBA/DDSA/CHDCA/DMBA IPN system without prior photocuring. The DSC peak occurs at 134°C which is a little greater than that found for the pure epoxy system (129°C – see Figure 9.1). This peak shift is partly due to the dilution of the epoxy/anhydride reactants by the dimethacrylate resin which reduces the rate of epoxy cure, as has been observed in Chapter 5 for VER based IPNs. However, opposing this dilution effect is an acceleration effect of TMA on the epoxy/anhydride cure (as noted above) so that the shift in the peak is not as much as expected. The temperature-ramping DSC peak in Figure 9.8a also appears to have a shoulder which differs from that of the pure epoxy/anhydride system (see Figure 9.1) and this may suggest that an additional process is occurring, such as was found in the thermal scans of the DEBPADM/CQ/TMA system (Figure 9.6b). Furthermore, we would expect an exotherm of 150 J/g due to the epoxy cure, but in the IPN system the exotherm is 178 J/g – the additional 28 J/g of energy evolved is consistent with partial thermal cure of

the DEBPADM component. When the dimethacrylate was partially photo-cured at 50°C (Figure 9.8b and Figure 9.8c), the temperature-ramped thermal epoxy cure peak became more symmetric but the heat of polymerization was reduced further and further below that expected for the full cure of the epoxy (theoretically 150 J/g for epoxy cure in the 50:50 IPN). This latter behaviour is very unusual – it should be noted that the second stage of the experiment depicted in Figure 9.8 involves a temperature ramp and so limitation in the extent of cure by vitrification cannot occur here. One possibility is that the formation of the dimethacrylate network topologically restricts the development of the epoxy network and this explanation may be similar to the ill-defined “interlock effect” suggested by Lin and co-workers<sup>133,137,230</sup> – see Section 2.4. Another explanation is that phase separation may occur during the IPN cure and evidence for this is discussed below. This may cause an imbalance in the partitioning of the DGEBA and anhydride species between the two phases so that full cure of the epoxy groups would not be attained.

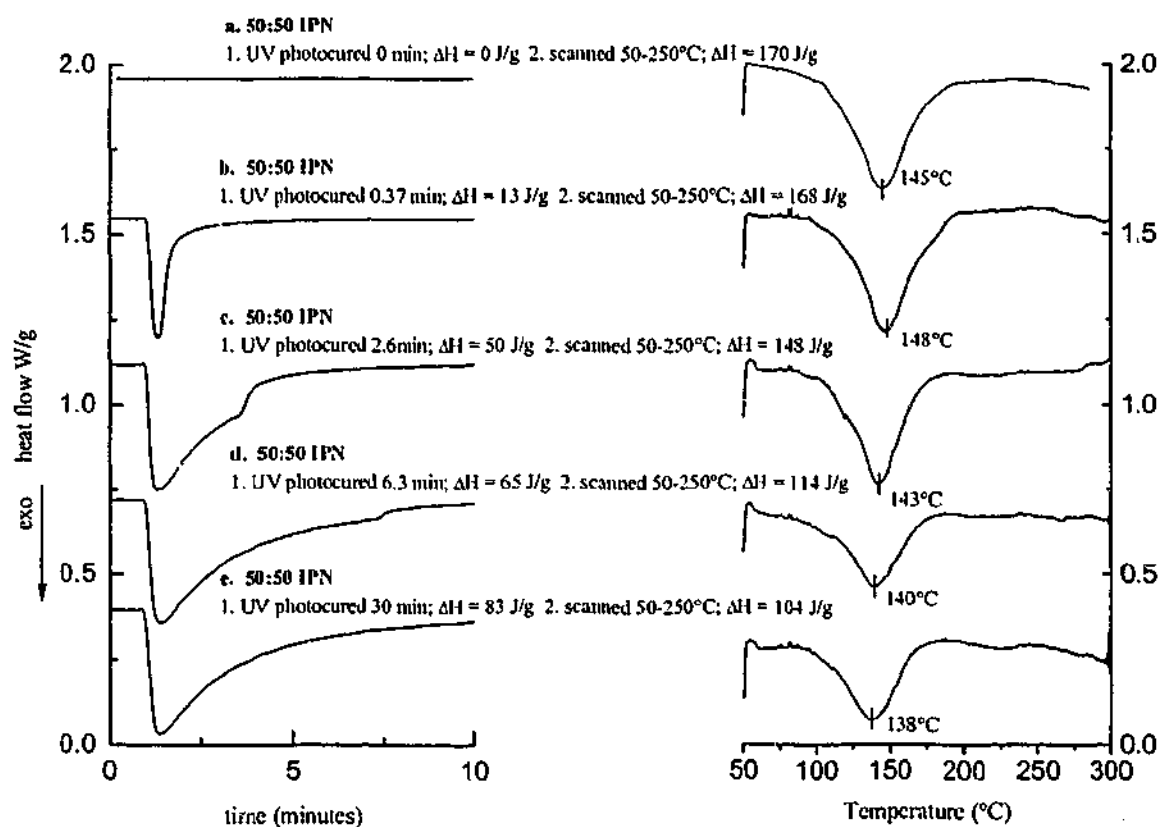


**Figure 9.9** Photocure behaviour of 50:50 DEBPADM/XDT: DGEBA/DDSA/CHDCA/DMBA at 50°C for varying times, followed by scanning DSC cure from 50-300°C.

Figure 9.9 illustrates the isothermal photocuring behaviour at 50°C of the dimethacrylate component in the 50:50 DEBPADM/XDT:DGEBA/DDSA/CHDCA/DMBA IPN and also shows the subsequent scanning cure behaviour of the epoxy component. For the un-irradiated sample (Figure 9.9a), the temperature-ramping DSC curing peak occurs at 145°C which is a considerably higher than that found for the pure epoxy (129°C – see Figure 9.1) due to the dilution of the epoxy/anhydride reactants by the dimethacrylate resin which reduces the rate of epoxy cure, as observed in Chapter 5. The epoxy curing peak is also higher than that in the 50:50 DEBPADM/CQ/TMA:DGEBA/DDSA/CHDCA/DMBA IPN (134°C – see Figure 9.8). This difference is due to the absence of TMA in the XDT-based IPN formulation so that no additional acceleration of the cure of the epoxy component occurs. The DSC peak in Figure 9.9a appears to be relatively symmetric in contrast to the DEBPADM/CQ/TMA:DGEBA/DDSA/CHDCA/DMBA IPN peak (see Figure 9.8a) perhaps due to the lack of any significant thermally-activated cure of the dimethacrylate. This is partly supported by the exotherm of 170J/g which is only slightly more than would be expected for the epoxy cure *per se*. Increasing the level of partial photo-curing of the DEBPADM/XDT component within the IPN (Figures 9.9b-e) reduces the amount of epoxy cure and this may be due to topological restrictions to the epoxy cure or may be due to an imbalance in epoxy/anhydride stoichiometry due to phase separation, as was suggested for the CQ/TMA initiating system (Figure 9.8).

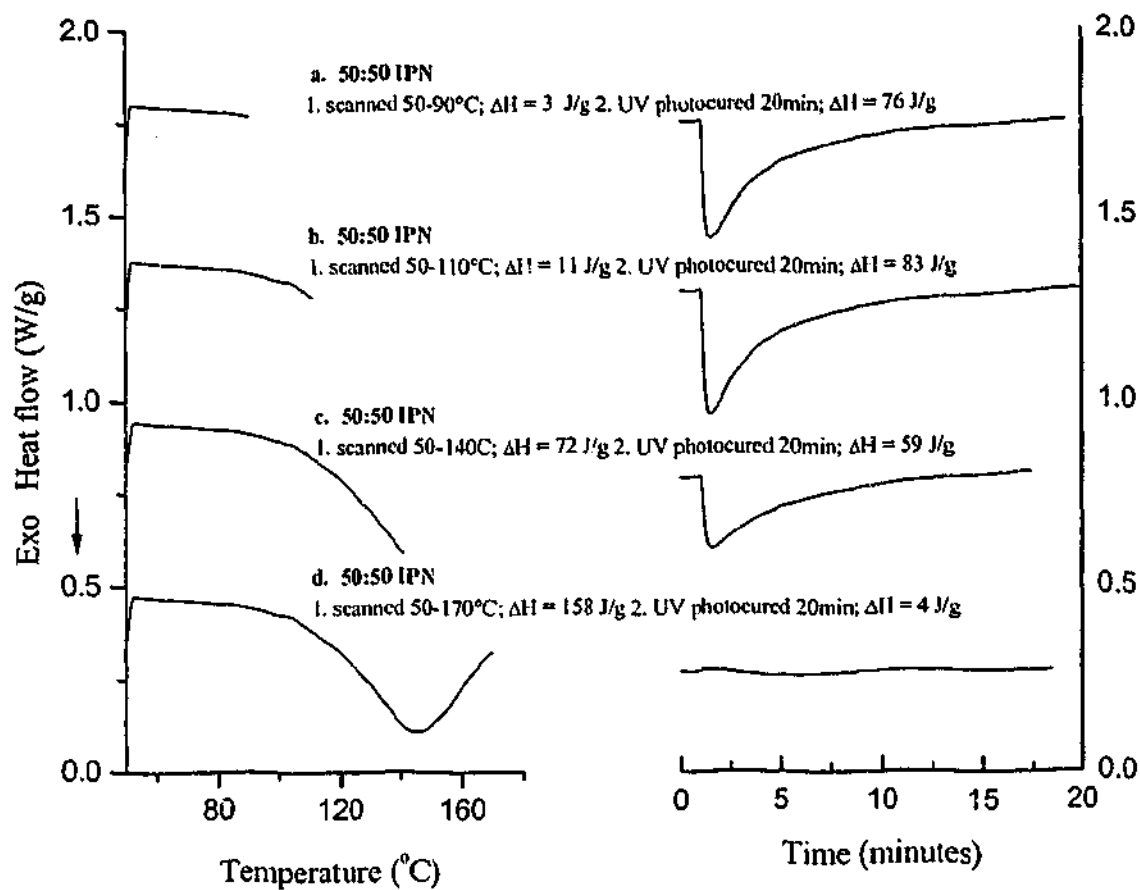


**Figure 9.10** Partial scan-cure of the epoxy component followed by photocuring of the dimethacrylate in DEBPADM/XDT:DGEBA/DDSA/CHDCA/DMBA at 50°C

Figures 9.10 and 9.11 show the effect of partial cure of the epoxy component on the isothermal photocuring behaviour of the dimethacrylate component in the 50:50 IPN of DEBPADM/XDT:DGEBA/DDSA/CHDCA/DMBA. As the upper temperature is raised in the temperature ramping part of the experiment, the amount of heat evolved rises due to an increase in the extent of epoxy cure. However the temperature ramping DSC stage may also involve some thermal cure of the dimethacrylate when ramped to the highest temperature (170°C) because the heat of polymerization evolved during the scan up to 170°C (158 J/g – see Figure 9.10d) is slightly more than the 150J/g expected from the epoxy cure and because Figure 9.7 shows that the DEBPADM/XDT system undergoes thermal cure at 184°C. Figure 9.10 and 9.11 also show that an increase in the extent of thermal cure of the epoxy component resulted in a reduction in the exotherm during the subsequent isothermal photopolymerization of the dimethacrylate component. This behaviour may have two causes. If the IPN is considered to be miscible, an increase of the epoxy conversion in the IPN would raise the  $T_g$  and this would reduce the mobility of the dimethacrylate groups and thus cause incomplete methacrylate polymerization due to IPN vitrification (as discussed in Chapter 5). This is further supported when one considers the effect of the isothermal photopolymerization

temperature - contrasting with the photocure behaviour in Figure 9.10 at 50°C, Figure 9.11, shows that much higher dimethacrylate conversions were obtained when the photopolymerization was performed at 100°C because the IPN can react further before vitrification occurs.

The effect of cure order on the cure behaviour and final conversion of each IPN component can be determined from a comparison of Figures 9.9e and 9.10d. If the dimethacrylate is photocured at 50°C before the subsequent thermal ramp (Figure 9.9e), the dimethacrylate is cured to 69% but less than its maximally attainable value (ca 90%), while the epoxy cure is limited to 69% by topological restrictions or by stoichiometry imbalance caused by phase separation. In contrast, if the curing sequence is reversed (see Figure 9.10d), the cure of the epoxy groups (158 J/g) is complete, while due to vitrification or topological restraint the dimethacrylate only cures to 3% conversion (4 J/g).

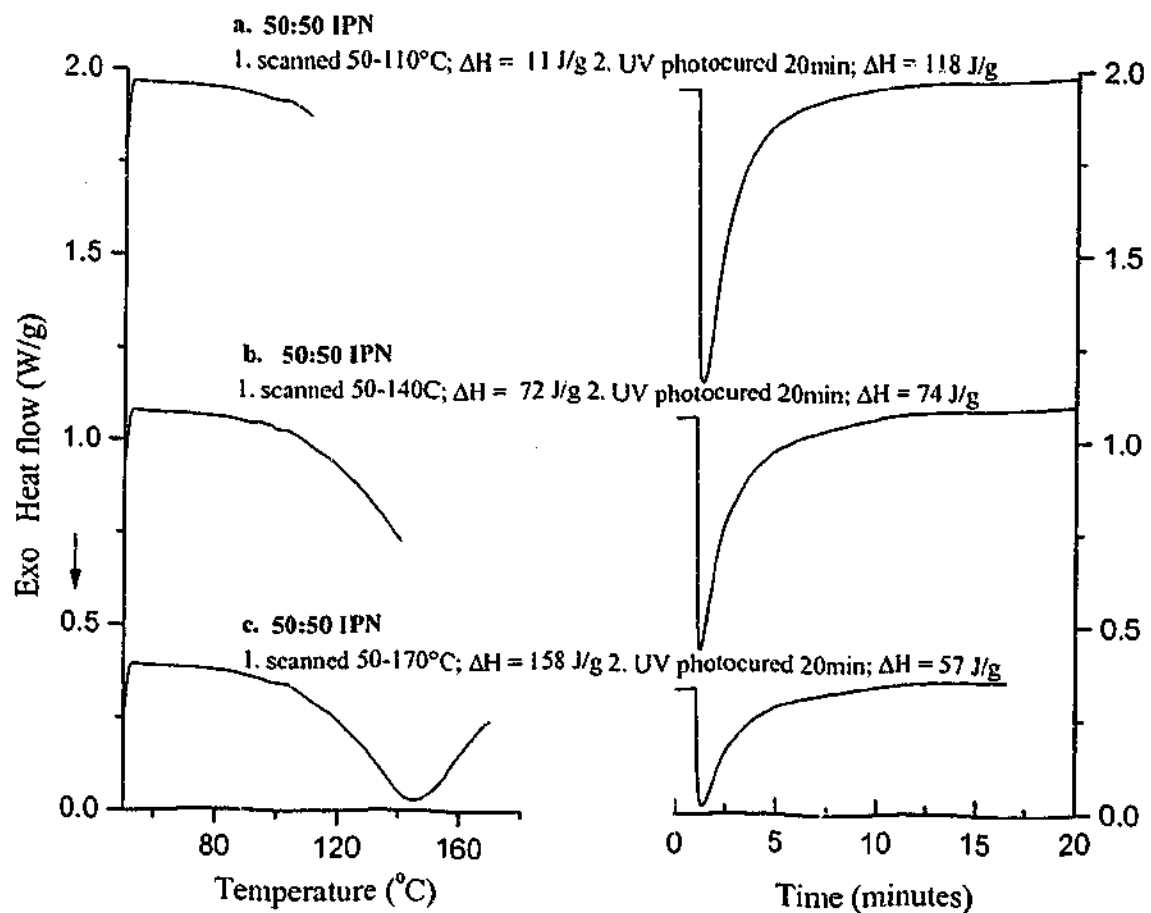


Figure 9.11 Partial scan-cure of the epoxy component followed by photocuring of dimethacrylate component in DEBPADM/XDT:DGEBA/DDS/CHDCA/DMBA at 100°C

Figure 9.12 shows the NIR spectra of the uncured IPN mixture and of IPNs after various sequences of photochemical and thermal cure - the conversion results are listed in Table 9.1. As suggested by the DSC studies (Figure 9.9), UV irradiation of the IPN mixture at 100°C for 30 min primarily causes methacrylate cure while the epoxy groups do not react significantly. Only after thermal cure of the IPN at 100°C for approximately 12 h do the epoxy groups undergo significant polymerization (see Table 9.1). Similarly, isothermal cure of the IPN at 100°C for 12 h only results in the polymerization of the epoxy-anhydride network and UV irradiation is required for methacrylate polymerization. Table 9.1 reveals that the extent of conversion of each species after thermal and radiation cure is dependent on the curing order in qualitative agreement with the DSC data. The first species to be polymerized was found to cure to a higher conversion because the other IPN component had plasticized the system. If the second species to be polymerized was the dimethacrylate then its conversion after photo-irradiation at 100°C was limited by either vitrification or topological restraint by the interpenetrating epoxy network. On the other hand, if the epoxy component was polymerized at 100°C after dimethacrylate photo-curing, the epoxy conversion was limited, due to vitrification or topological restraint (as discussed above) or may be due to phase separation (as discussed above) that causes an imbalance in the epoxy-anhydride stoichiometry.

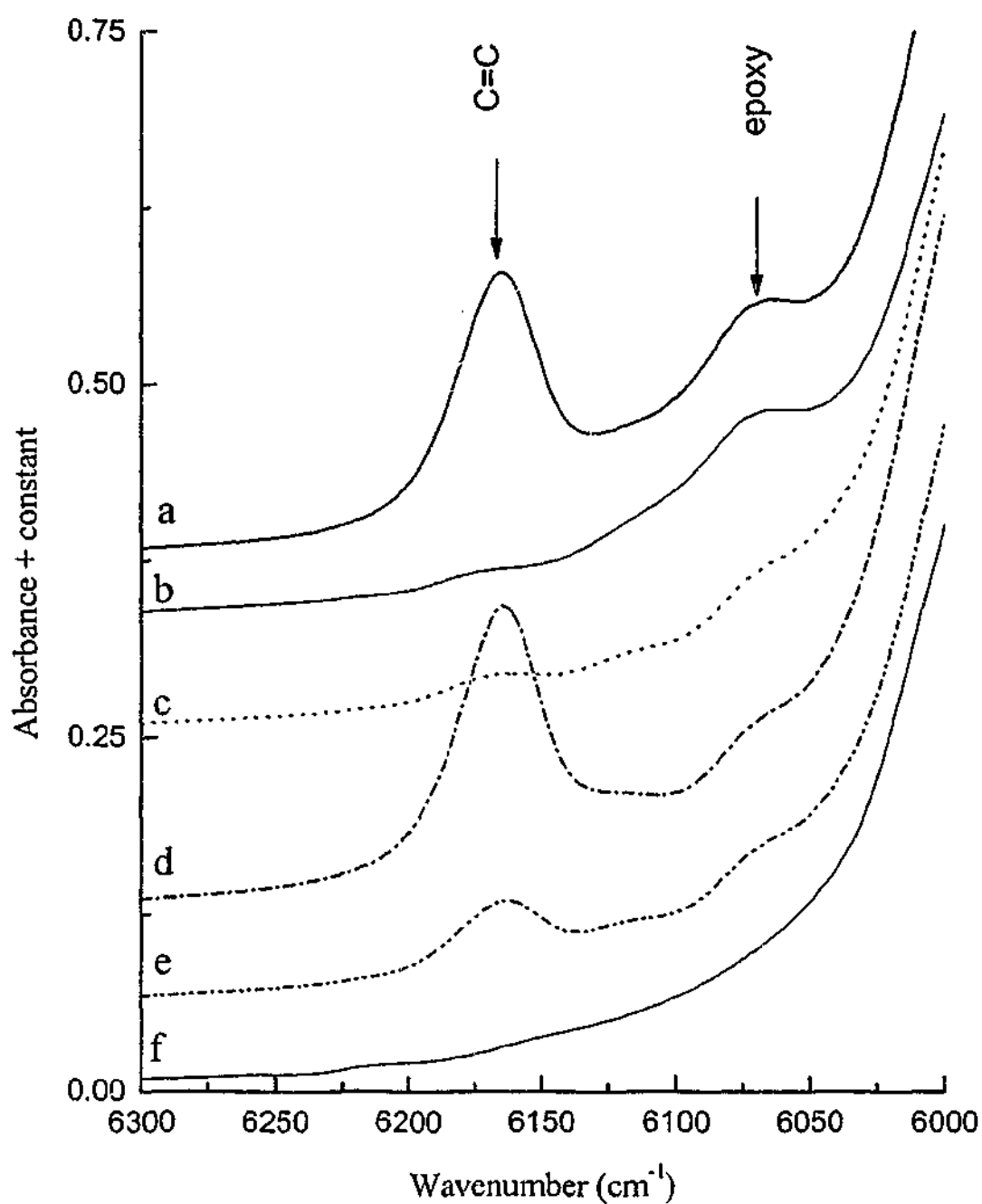


Figure 9.12 NIR spectra (path length 1mm) of the IPN based on the 50:50 DEBPADM/XDT: DGEBA/DDSA/CHDCA/DMBA components: a) uncured IPN; b) UV cure of IPN (without DMBA) at 100°C for 40 min; c) UV cure of IPN at 100°C/40 min and then isothermal cure at 100°C/12 h; d) isothermal cure of IPN at 100°C/12 h; e) isothermal cure of IPN at 100°C/12 h and then UV cure at 100°C/40 min; f) 4<sup>th</sup> order polynomial fit to spectra c to estimate the background spectra.

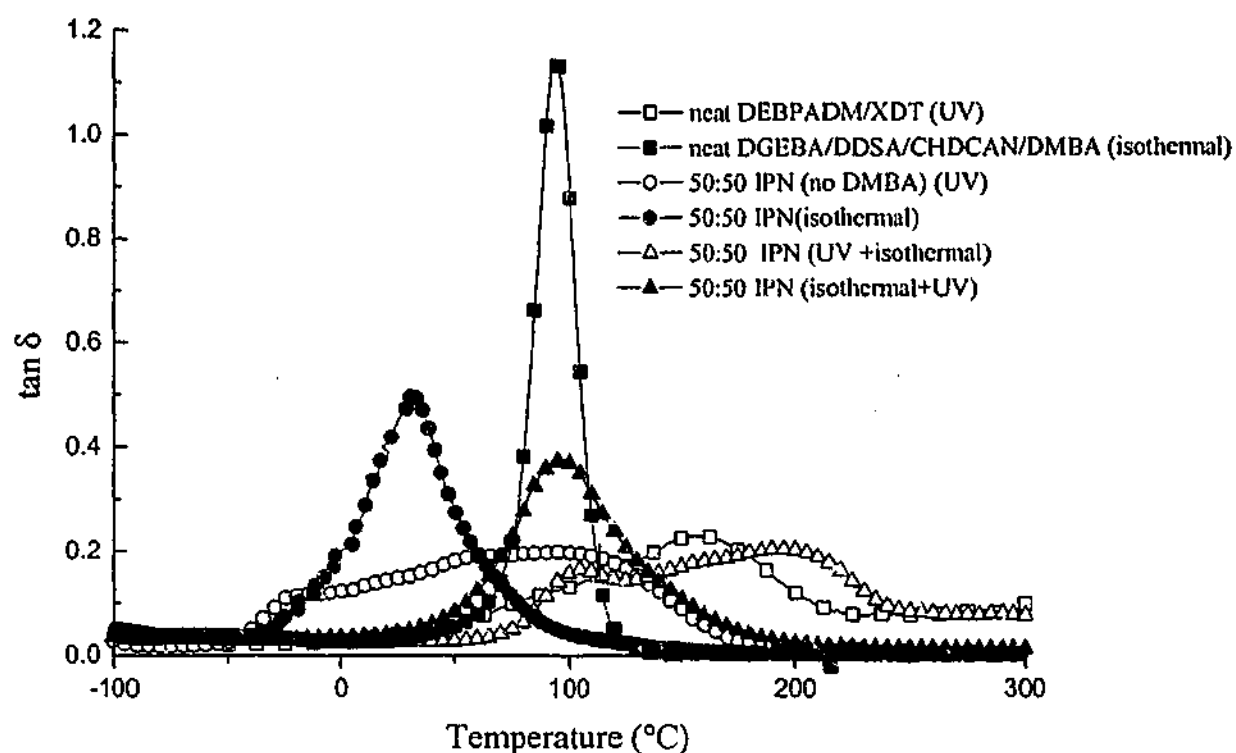


Figure 9.13  $\tan \delta$  versus temperature for the thermally cured DGEBA/DDSA/CHDCA/DMBA, photocured DEBPADM/XDT and 50:50 IPN after photocuring/thermally curing.

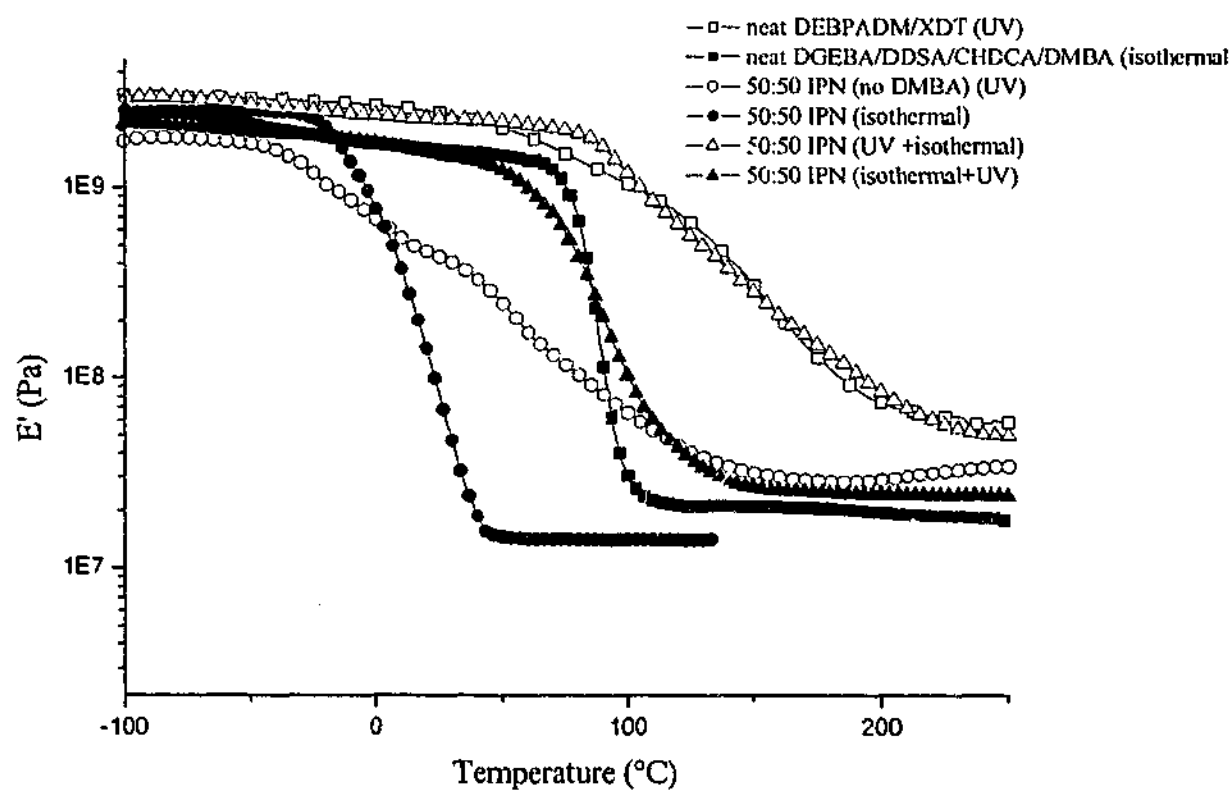


Figure 9.14 Real modulus ( $E'$ ) versus temperature for the thermally cured DGEBA/DDSA/CHDCA/DMBA, photocured DEBPADM/XDT and 50:50 IPN after photocuring/thermally curing.

**Table 9.1 Glass transition temperatures and conversions for the isothermally cured and photocured DEBPADM/XDT:DGEBA/DDSA/CHDCA/DMBA IPN and its parent resins using various cure schedules.**

Sample	$T_g$ (from $\tan\delta$ max in the DMTA trace)	Rubbery Modulus ( $10^7$ Pa)	Conversion from NIR*	
			methacrylate	epoxy
<i>Neat resins</i>				
Neat DEBPADM/XDT (UV cure at 100°C/40 min)	160 °C	5.5	75%	-
Neat DGEBA/DDSA/CHDCA/DMBA (isothermal cure at 100°C/12 h)	93 °C	1.7	-	85%
<i>IPNs-partially cured</i>				
IPN (UV cure at 100°C/40 min)	-20 °C and 75 °C	-	90%	20%
IPN but without DMBA catalyst for epoxy (UV cure at 100°C/40 min)	-20 °C and 80 °C	3 (but rising due to further curing of the epoxy)	90%	0%
IPN (isothermal cure at 100°C/12 hrs)	32 °C	1.5	0%	87%
<i>IPNs-full cure</i>				
IPN (UV cure at 100°C/40 min and then isothermal at 100°C/12 h)	103 °C and 196 °C	4.8	90%	75%
IPN (isothermal cure at 100°C/12 h and then UV cure at 100°C/40 min)	105°C	3.3	70%	87%

\* prior to the DMTA run

### Dynamical mechanical properties

Figure 9.13 and Figure 9.14 show the  $\tan\delta$  and storage modulus traces, respectively, for the parent network components and their blends while Table 9.1 lists the  $T_g$ s. The  $\tan\delta$  and  $E'$  curves show single glass transitions in the neat resins but the IPNs show a single or double transition, depending on the cure schedule. The  $T_g$  of the unreacted DGEBA/CHDCA/DDSA and DEBPADM components are -32°C and -28°C respectively (as measured by DSC). When cured, both single components networks have relatively high  $T_g$ s due to their high crosslink density but the epoxy has the lower  $T_g$  due to the flexibility introduced by the DDSA curing agent. When the uncured IPN resin is heated to 100°C and held for 12 hours, the  $T_g$  rises to 32°C, which lies between the  $T_g$  of the DEBPADM monomer (-28°C) and the cured epoxy resin (93°C). Subsequent photochemical cure of the dimethacrylate component resulted in a single glass transition at 105°C, suggesting a single-phase structure. The shape of the DMTA

trace was not significantly altered when this IPN was then post-cured at 180°C for 2 hours. To study the effect of the dimethacrylate cure on the DMTA behaviour of the IPN, DMBA was omitted from the formulation so that the thermal cure of the epoxy was delayed during the DMTA run. Thus, after photocuring the IPN at 100°C, two peaks were observed in the  $\tan\delta$  trace - at 80°C and at -20°C - which lie between the  $T_g$ s of the uncured epoxy/anhydride monomer mixture (-32°C) and the cured DEBPADM resin (160°C). Isothermal curing at 100°C of the epoxy component of this partially cured IPN resulted in two  $\tan\delta$  peaks in the DMTA spectrum at 103°C and 196°C (which was not significantly altered after post-curing at 180°C for 2 hours), confirming a two-phase structure.

The rubbery modulus of the neat DEBPADM/XDT (UV cured) ( $5.5 \times 10^7$  Pa) is slightly lower than observed for other thermally cured DEBPADM systems (see Section 8.2), possibly due to the reduced conversion of methacrylate groups (75%) which lowered the crosslink density (see Section 2.1.4). The rubbery modulus for the DGEBA/DDSA/CHDCA/DMBA ( $1.7 \times 10^7$  Pa) is lower than the observed in other DGEBA systems (see Section 8.2), primarily due to the lower crosslink density. In the thermally-cured 50:50 IPN (predominantly DGEBA cure) the rubbery modulus decreased by  $0.2 \times 10^7$  Pa compared with the neat DGEBA/DDSA/CHDCA/DMBA ( $1.7 \times 10^7$  Pa); this may have been due to unreacted DEBPADM swelling the system. This effect was also observed in the UV-cured 50:50 IPN (without DMBA and so predominantly DEBPADM cure) which exhibited a plateau in rubbery modulus which was lower than observed in the neat DEBPADM. Interestingly for the UV-cured 50:50 IPN (without DMBA) the modulus increases with temperature in the rubbery region and this was probably due to thermal cure of the epoxy component at this high temperature (see Figure 9.14). The fully-cured 50:50 IPN (UV cure of the DEBPADM component followed by isothermal cure of the DGEBA) gives a rubbery modulus at ( $4.8 \times 10^7$  Pa) which is close to the neat DEBPADM/XDT indicating the DEBPADM phase is continuous. In contrast the IPN (isothermal cure of the DGEBA component followed by UV cure of the DEBPADM component) has a rubbery modulus ( $3.3 \times 10^7$  Pa) which is close to the average of the two parent components ( $3.6 \times 10^7$  Pa) suggesting a co-continuous network.

From the above studies it is clear that the 50:50 IPN is one phase when the epoxy component is cured first and is followed by the photocure of the dimethacrylate

but not vice versa. In the case when the epoxy is cured first, the system may remain miscible because the decrease in the entropy of mixing and thus the increase in the free energy of mixing (Equation 2.29) as the epoxy approaches the gel point (theoretically 57%)<sup>32</sup> is counter-balanced by the large number of dimethacrylate molecules swelling the gel - hence one glass transition is observed. The subsequent photocuring of the dimethacrylate is a very rapid reaction and gelation is expected at ca. 1%<sup>33</sup> (see Section 2.1.3), which locks the two networks together and prevents phase separation. The situation is different when the order of curing is reversed. Here, during the photocuring step, the gelation of the dimethacrylate at low conversion causes a significant reduction in the entropy of mixing and this appears sufficient to cause some phase separation in the partly cured IPN. Once the epoxy begins to polymerize, the entropy of mixing decreases and the free energy of mixing is even further raised. Since the epoxy does not gel until high conversion<sup>32</sup>, the slow curing reaction allows diffusion of the growing epoxy-anhydride out of the dimethacrylate gel and results in further phase separation.

The fact that under the appropriate curing regime a two-phase structure can be formed in DEBPADM-based IPNs does not necessarily mean that the same occurs for the bisGMA-based IPNs previously investigated. For example, the 50:50 DEBPADM/AIBN:DGEBA/DDSA/CHDCA/DMBA IPN (where the DEBPADM cures first) has shown two  $T_g$ s at 100°C and 156°C (see Figure 9.15) corresponding to a DGEBA/DDSA/CHDCA/DMBA rich phase (c/f neat resin  $T_g$  of 93°C) and a DEBPADM/AIBN rich phase (c/f neat resin  $T_g$  of 189°C). The rubbery modulus of the thermally cured 50:50 DEBPADM/AIBN:DGEBA/DDSA/CHDCA/DMBA IPN ( $5.9 \times 10^7$  Pa) is close to the neat DEBPADM/AIBN ( $6.4 \times 10^7$  Pa) indicating the DEBPADM phase is continuous. In contrast the 50:50 bisGMA/styrene/AIBN:DGEBA/DDSA/CHDCA/DMBA IPN (where the VER cures first) shows a single  $T_g$  at 120°C (see Figure 9.16), which is located between the  $T_g$  of the neat DGEBA/DDSA/CHDCA/DMBA (93°C) and the bisGMA/styrene/AIBN (169°C) confirming a single phase structure for this type of IPN. This IPN also exhibits a rubbery modulus ( $2.3 \times 10^7$  Pa) which is close to the average of the two parent components ( $3.4 \times 10^7$  Pa) suggesting a miscible network blend. This single phase structure of the 50:50 bisGMA/styrene/AIBN:DGEBA/DDSA/CHDCA/DMBA IPN appears to result from the H-bonding between the epoxy component and the hydroxyl groups of the bisGMA unit which should enhance miscibility.

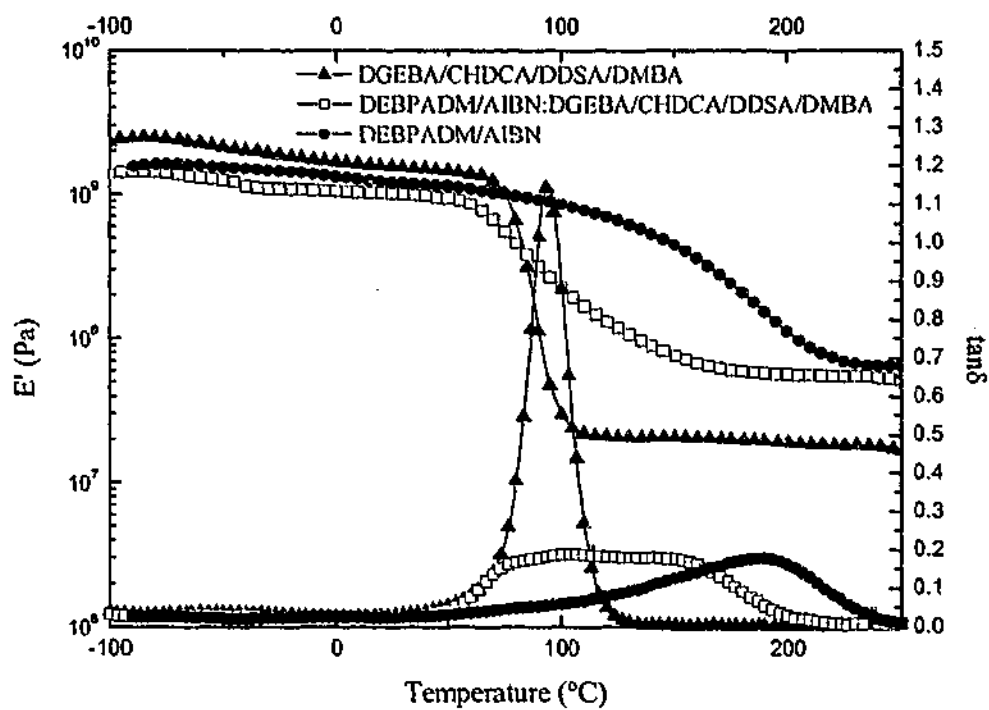


Figure 9.15 DMTA scans of DGEBA/CHDCA/DDSA/DMBA, DEBPADM/AIBN and the corresponding 50:50 wt% IPN.

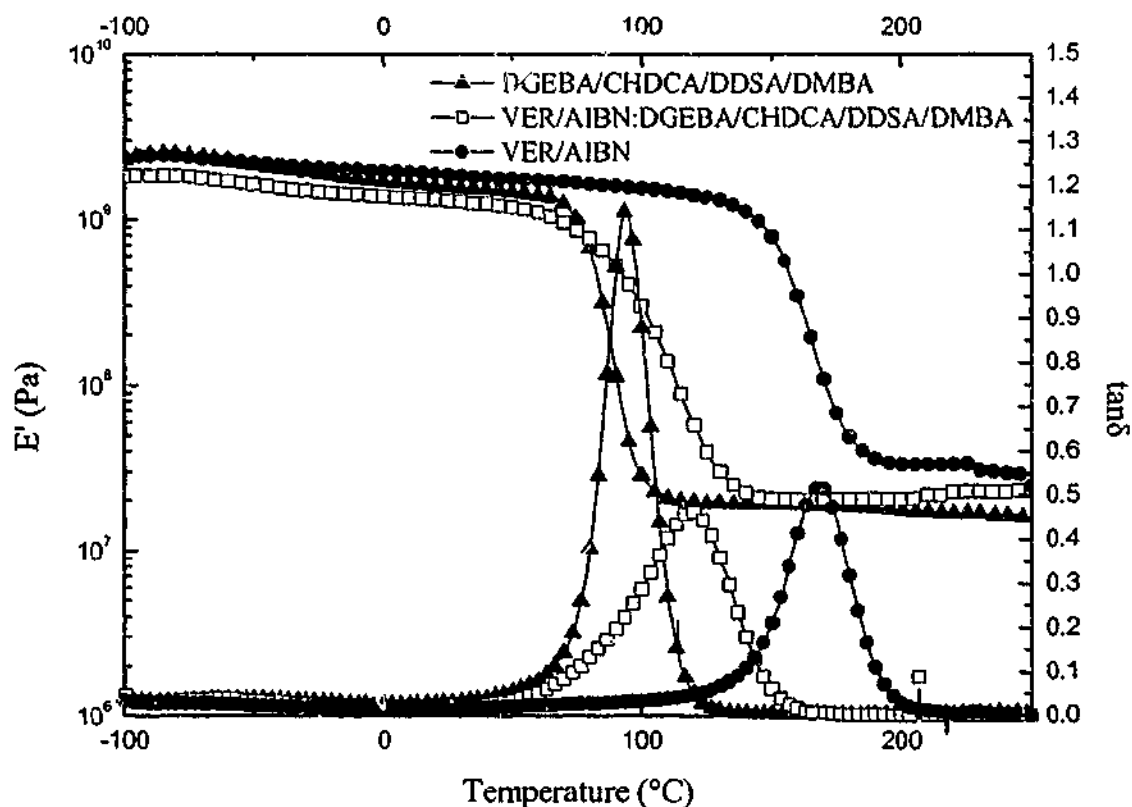


Figure 9.16 DMTA scans of DGEBA/CHDCA/DDSA/DMBA, VER/AIBN and the corresponding 50:50 wt% IPN.

## 9.3 Conclusion

IPNs were prepared from an anhydride-cured epoxy resin and a dimethacrylate photocured by two initiator systems. The combination of thermal and photo-chemical initiation has facilitated studies of the effect of either photocuring the dimethacrylate followed by thermal cure of the epoxy or by thermally curing the epoxy first followed by photocuring of the dimethacrylate. Some chemical interactions were observed between the IPN components and these were more serious in the IPNs containing the CQ/TMA photo-initiator. The dark reaction was also found to be more significant in the CQ/TMA than in the XDT-photoinitiated system and so the latter is more suitable for studies of the effect of cure sequence on the morphology of the resulting IPNs. The polymerization kinetics of the epoxy-methacrylate IPNs were studied by combinations of isothermal and temperature ramping DSC. When the epoxy component was thermally-cured before isothermal photopolymerization of the dimethacrylate, the final conversion of the dimethacrylate was limited by vitrification or topological restraint of the IPN. When the order of cure was reversed, the thermal cure of the epoxy was reduced, possibly due to vitrification or topological restraint or due to partitioning of the reactive components into separate phases. NIR studies of the cure of the dimethacrylate and epoxy components confirmed that the cure order affected the final conversion. DMTA studies of the NIR samples revealed a single glass transition when the epoxy component was cured first, but two glass transitions were observed when the dimethacrylate component was photocured prior to the epoxy/anhydride cure, confirming that phase separation had occurred.

In Chapters 5 and 6 we selected the epoxy (DGEBA) and dimethacrylate (bisphenol-A diglycidylether dimethacrylate, bisGMA) components of the IPN to have the same backbone (bisphenol-A attached to either a flexible glycidyl or ethylene oxide links) so as to maximize the enthalpic interactions and thus the miscibility of the two networks. In Chapter 5, we interpreted the curing kinetics and gelation behaviour of the epoxy-bisGMA based IPNs in terms of a single-phase structure even when the dimethacrylate component cured first. Unfortunately, due to the similar glass transition temperatures of the two components, we were unable to establish whether some phase separation had in fact occurred. In this Chapter, we observed that the backbone flexibility offered by the DDSA curing agent shifted the  $T_g$  of the parent epoxy

component below that of the dimethacrylate network which has enabled DMTA to be a useful miscibility probe. This revealed that rapid gelation of the first IPN component followed by slow polymerization of the second component can lead to a two phase structure whereas if the second curing component polymerizes rapidly and gels at an early stage then a single phase structure is more probable. The fact that under the appropriate curing regime a two-phase structure can be formed in DEBPADM-based IPNs does not necessarily mean that the same occurs for the bisGMA-based IPNs previously investigated. This conclusion derives from the observation that bisGMA differs from DEBPADM by the presence of a hydrogen-bonding hydroxyl group and this difference may make the epoxy-bisGMA IPN system more miscible. In fact, the 50:50 bisGMA/styrene/AIBN:DGEBA/DDSA/CHDCA/DMBA IPN has shown a single  $T_g$  at  $120^\circ\text{C}$ , which is located between the  $T_g$  of the neat DGEBA/DDSA/CHDCA/DMBA ( $93^\circ\text{C}$ ) and the bisGMA/styrene/AIBN ( $169^\circ\text{C}$ ) confirming a single-phase structure for this type of IPN.

# *Chapter 10*

## *Properties of cured IPNs*

---

### **10.1 Introduction**

To identify potential applications for IPNs it is essential to have an understanding of their properties. Both vinyl ester resins and epoxy resins are used in corrosive environments and their ability to resist degradation is dependent on a number of factors including the structures of the vinyl ester resin and epoxy used, the curing agents used and the cure schedule and their solvent (and particularly water) uptake. Therefore, in this Chapter, the water absorption characteristics of the 50:50 VER/AIBN:DGEBA/1-MeI IPN, 50:50 VER/AIBN:DGEBA/An IPN, 50:50 VER/AIBN:DGEBA/DDM IPN and their parent resins have been investigated. This range of systems investigated enabled a comparison between curing agents for the epoxy resins, semi-IPNs versus full-IPNs and neat resins versus IPNs to be made. In addition, since the epoxy/VER IPNs are likely to have applications in adhesive systems and composites, their mechanical properties are important. Therefore, mechanical property testing of the 50:50 VER/AIBN:DGEBA/1-MeI IPN and its parent resins are represented. This particular IPN was chosen as it exhibited good cure kinetics (showing little interaction between components and close to full cure being achieved - see Section 5.2).

## 10.2 Water Absorption

The water absorption characteristics VER/AIBN, DGEBA/DDM, DGEBA/An DGEBA/1-MeI and their corresponding 50:50 IPNs were studied over the temperature range of 50 to 100°C\*. A typical series of water sorption curves at differing temperatures is shown in Figure 10.1.

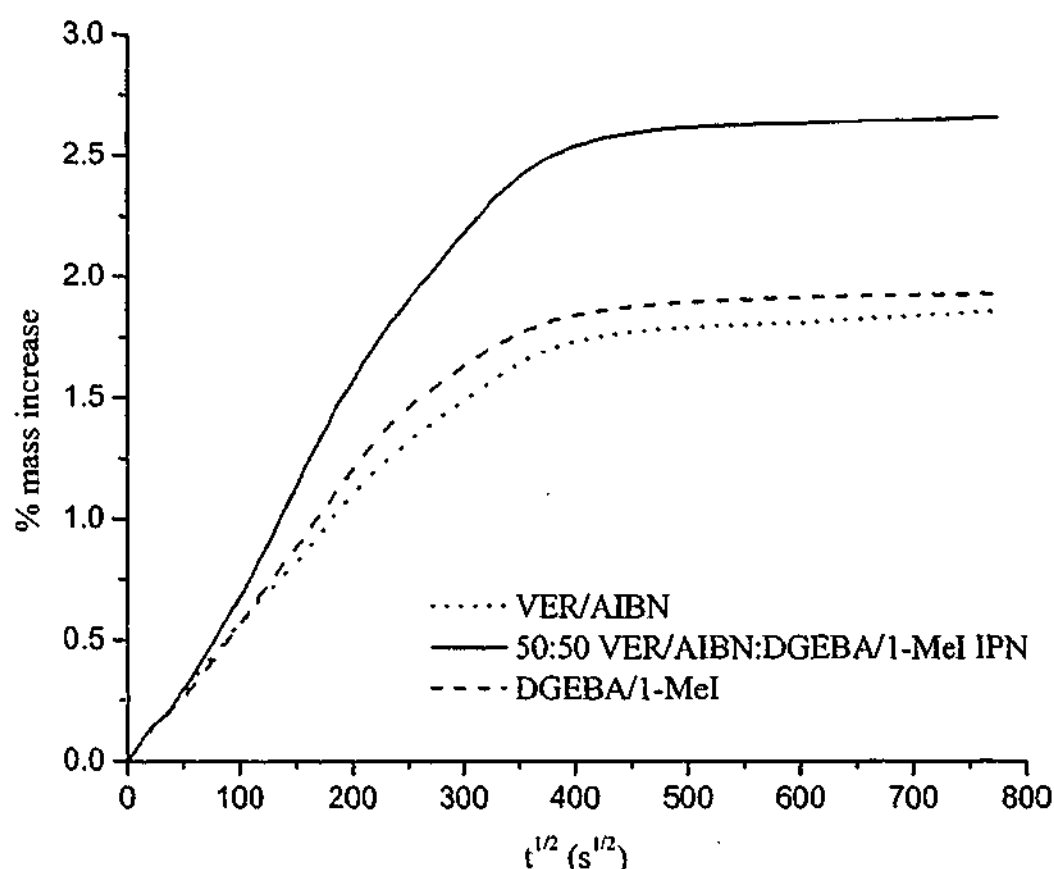


Figure 10.1 Typical water sorption curves for VER/AIBN, DGEBA/1-MeI and the corresponding 50:50 IPN at 90°C.

The equilibrium mass fraction of water ( $m_\infty$  - see Section 2.5.3) absorbed by the polymer in a water-saturated atmosphere at several temperatures for the neat resins and their IPNs are listed in Table 10.1. Two groups with different behaviours can be identified from the  $m_\infty$  data:

**Group A:** Polymers characterized by a relatively low hydrophilicity (low  $m_\infty$ ) which increases noticeably with temperature.

\* Water uptake measurements were kindly performed at ENSAM, Paris by Ilhame Merdas as part of a DIST-funded collaboration, on samples formulated and prepared by the author.

**Group B:** Polymers of intermediate hydrophilicity (intermediate  $m_{\infty}$ ), where the hydrophilicity depends only slightly on temperature.

**Table 10.1** Values of equilibrium mass fraction of water,  $m_{\infty}$ , at various temperatures for the systems under study.

	$m_{\infty}$ (50°C) (%)	$m_{\infty}$ (70°C) (%)	$m_{\infty}$ (90°C) (%)
DGEBA/1-MeI	1.7	1.9	1.93
50:50 VER/AIBN:DGEBA/1-MeI	2.34	2.65	2.66
VER/AIBN	0.92	1.39	1.86
DGEBA/An	1.5	1.7	1.88
50:50 VER/AIBN:DGEBA/An	1.93	2.3	2.5
VER/AIBN	0.92	1.39	1.86
DGEBA/DDM	1.97	1.98	2.35
50:50 VER/AIBN:DGEBA/DDM	1.08	-	1.95
VER/AIBN	0.92	1.39	1.86

The neat VER/AIBN system and to a lesser extent the 50:50 VER/AIBN:DGEBA/DDM belong to Group A, as they have a relatively low hydrophilicity (observed as a low  $m_{\infty}$ ), however the  $m_{\infty}$  increases significantly with temperature. In all the other systems the hydrophilicity depends only slightly on temperature (Group B), although within this group there was some variation, from systems that hardly varied with temperature (for example DGEBA/1-MeI and VER/AIBN:DGEBA/1-MeI) to systems which show a more significant change in  $m_{\infty}$  with temperature (for example DGEBA/An, DGEBA/DDM and 50:50 VER/AIBN:DGEBA/An IPN).

For the 50:50 VER/AIBN:DGEBA/1-MeI and 50:50 VER/AIBN:DGEBA/An IPNs, the hydrophilicity (as measured by  $m_{\infty}$ ) is significantly higher than for each of the

parent resins. This can be interpreted in terms of the heat of dissolution ( $H_s$ ) and the solubility pre-exponential factor ( $S_0$ ) as discussed in Section 2.5.3

The values  $H_s$  and  $\ln S_0$  are listed in Table 10.2 and were obtained from an Arrhenius plot of  $S$  versus  $1/T$ . The differing trends shown in the temperature dependence of the equilibrium concentration can be described in terms of Equation 2.35, such that the groups outlined above correspond to distinct ranges for the values of  $H_s$ , for instance:

$$\text{Group A : } |H_s| \leq H_w - \delta H \quad (\text{weak water-polymer interaction})$$

$$\text{Group B : } H_w - \delta H \leq |H_s| \leq H_w \quad (\text{intermediate water-polymer interaction})$$

where  $H_w$  (the enthalpy of water evaporation) is  $42 \text{ kJ.mol}^{-1}$  (see Section 2.5.3) and  $\delta H$  (approximately  $8 \pm 1 \text{ kJ.mol}^{-1}$ ) is the difference between  $H_w$  and  $|H_s|$ .

**Table 10.2 Values of heat of dissolution,  $H_s$ , and pre-exponential factor,  $S_0$ , for the systems under study.**

	$H_s$ ( $\text{kJ.mol}^{-1}$ )	$\ln S_0$ ( $\text{mol.m}^{-3}$ )
DGEBA/1-MeI	-39	-16.9
50:50 VER/AIBN:DGEBA/Mel	-39	-16.6
VER/AIBN	-25	-12.4
DGEBA/An	-37	-16.3
50:50 VER/AIBN:DGEBA/An	-37	-15.9
VER/AIBN	-25	-12.4
DGEBA/DDM	-38	-16.5
50:50 VER/AIBN:DGEBA/DDM	-34	-15.2
VER/AIBN	-25.1	-12.4

The IPNs were generally more hydrophilic than their parent resins and this may be explained by the pre-exponential factor varying smoothly with composition but the enthalpy of dissolution  $H_s$  remaining close to the value of the most hydrophilic component. This might be expected since the frequency factors for water binding and de-binding to absorption sites which determines  $S_0$  might be expected to be a monotonic function of composition, but the binding energy ( $H_s$ ) would be dominated by the more

strongly binding sites i.e. the epoxy resin components. The VER is much less hydrophilic than the epoxy resins, despite the similarity in the structure – although the reacted bisGMA molecule contains the bisphenol-A structure and two hydroxyl groups as is found in the amine-cured DGEBA resins it also contains the non-polar styrene units. Thus, it appears that the presence of the styrene bridge between the reacted methacrylate units of the bisGMA changes the spacing between polar sites or sterically restricts the binding of the water molecules and that the incorporation of the non-polar styrene units in the dimethacrylate reduces the hydrophilicity of the VER.

### 10.3 Compressive modulus and Yield

In this section the compressive yield strength and modulus for the VER/AIBN, DGEBA/1-MeI and the 50:50 wt% IPN of VER/AIBN:DGEBA/1-MeI were investigated over a range of different strain rates at ambient temperature. Figure 10.2 illustrates the stress-strain behaviour for the DGEBA/1-MeI system at three different strain rates - a clear maximum in compressive stress is not observed and as a result the knee of each stress-strain plot is used as a reproducible estimation of the yield stress, as discussed in Section 4.8.1. Figure 10.3 illustrates the stress-strain behaviour for the VER/AIBN system at three different strain rates; here we observe a clear maximum in stress or yield point. The corresponding compressive stress-strain curves over different strain rates for the 50:50 IPN of VER/AIBN:DGEBA/1-MeI are shown in Figure 10.4. The yield stress, yield strain, modulus and activation volumes are listed in Table 10.3. The modulus of these systems is relatively insensitive to changes in strain rate as the ambient test temperature is well below the  $T_g$  of the polymers and IPN and hence the molecular mobility is low (the material is vitrified). In contrast, there is quite a variation in the yield stress, percentage strain to yield and the overall shape of the stress-strain curves. The neat VER/AIBN shows a high yield stress (shown as a maximum in Figure 10.3) but the lowest strain to yield (9.4 % strain), the neat DGEBA/1-MeI shows the lowest yield stress (shown as an inflection point or knee in Figure 10.2) and the highest percentage strain to yield (10.6 % strain). The 50:50 VER/AIBN:DGEBA/1-MeI IPN exhibits properties which close to the average from the parent resins; the average yield stress for the neat VER and DGEBA is 119 MPa, the measured value of yield stress from the IPN is a little lower at 116 MPa. The percentage

strain at yield in the IPN (11.4 %) however is higher than the average expected from the neat resins (10.0 % strain).

For each system the yield strength rises with increasing strain rate and the yield strength is proportional to the logarithm of strain rate over three decades, as seen by other authors in similar studies of epoxy/amine systems<sup>219</sup>. A typical Eyring plot of yield stress versus strain rate (see Figure 10.5) enables the calculation of the activation volume for each system (see Table 10.3) from Equation 2.30. The activation volume in the systems varies with the VER having the highest activation volume of 2.6 nm<sup>3</sup>, the neat DGEBA/1-MeI having the lower at 1.8 nm<sup>3</sup> and the 50:50 VER/AIBN:DGEBA/1-MeI IPN having an activation volume of 2.5 nm<sup>3</sup> close to that of the neat VER/AIBN

**Table 10.3 Summary of results from compression experiments**

System	Yield Stress (MPa) at strain rate of $1.67 \times 10^{-5} \text{ s}^{-1}$	% Strain at yield at strain rate of $1.67 \times 10^{-5} \text{ s}^{-1}$	Modulus (GPa) at strain rate of $1.67 \times 10^{-5} \text{ s}^{-1}$	Activation volume $V_{\text{now}} \text{ (nm}^3\text{)}$
VER/AIBN	137±8	9.4 ±0.5	1.8±0.2	2.6±0.3
50:50 VER/AIBN: DGEBA/1-MeI IPN	116±6	11.4 ±0.5	1.6±0.2	2.5±0.2
DGEBA/1-MeI	102±9	10.6±0.7	1.7±0.2	1.8±0.2

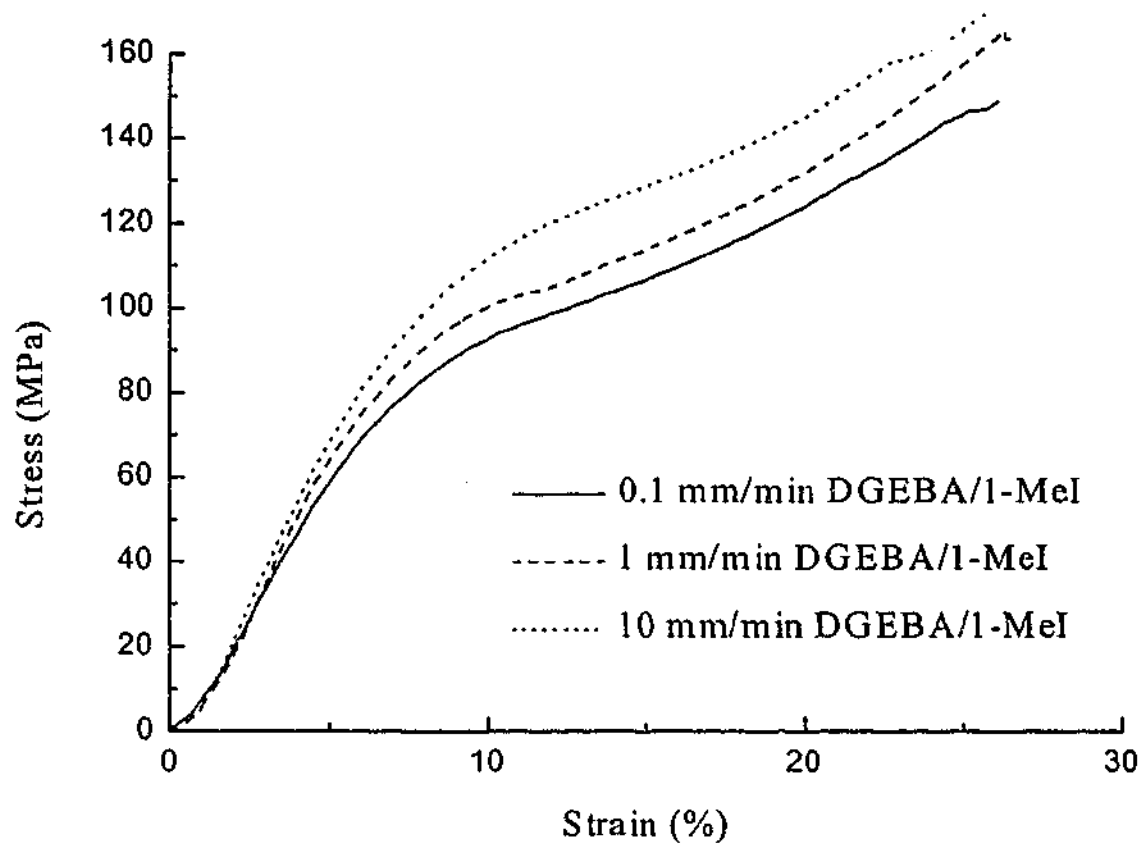


Figure 10.2 Compressive stress-strain curves for DGEBA/1-MeI at 0.1, 1.0 and 10 mm/min.

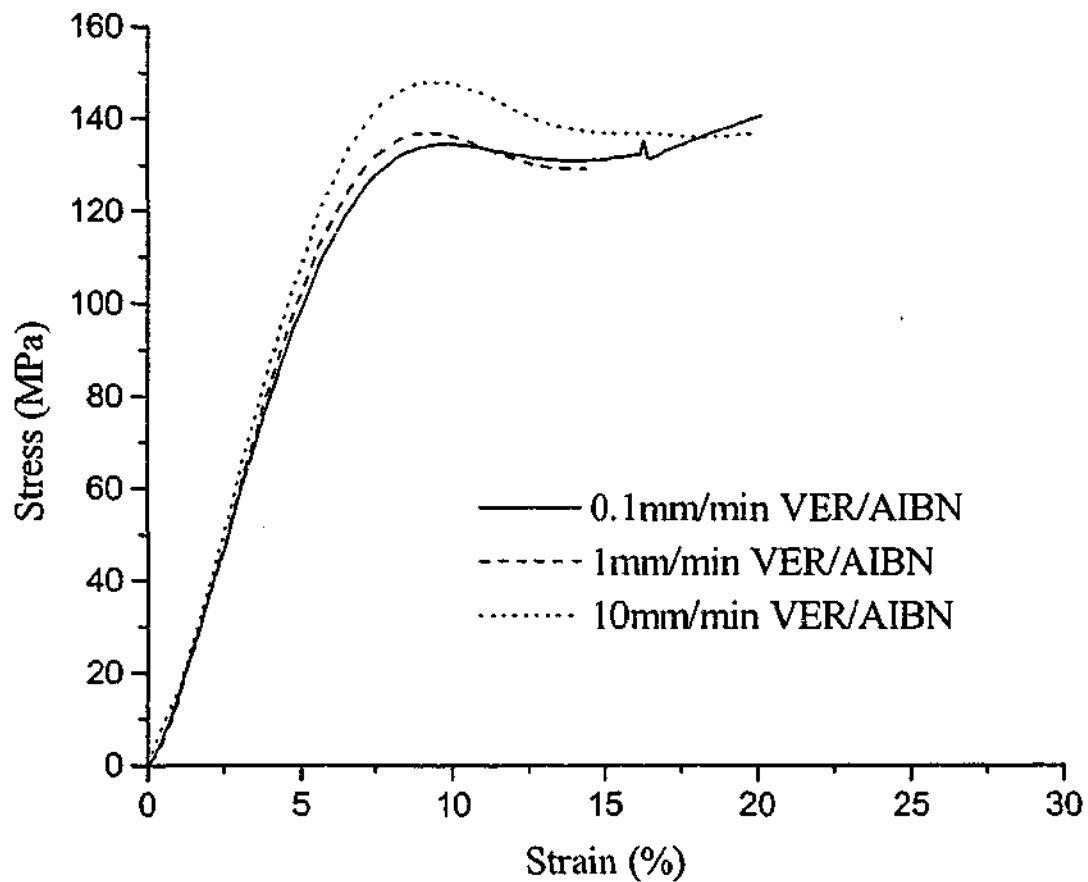


Figure 10.3 Compressive stress-strain curves for VER/AIBN at 0.1, 1.0 and 10 mm/min.

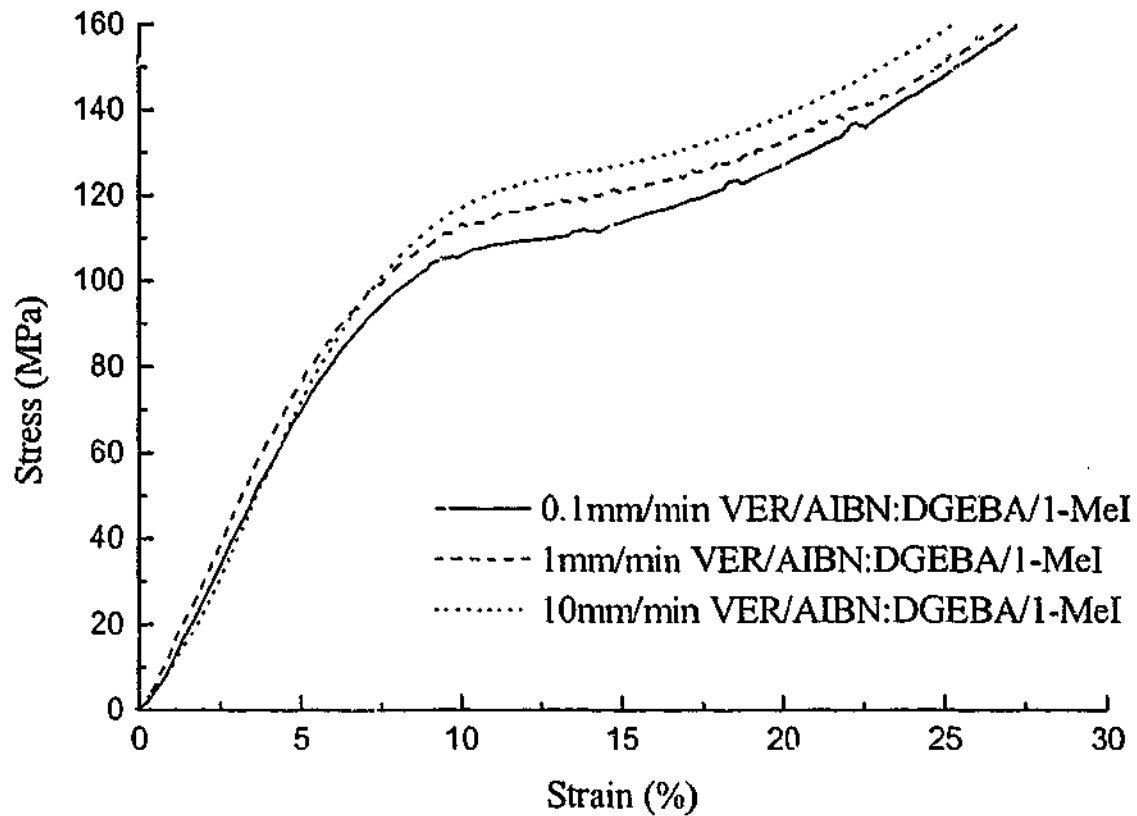


Figure 10.4 Compressive stress-strain curves for the 50:50 IPN of VER/AIBN:DGEBA/1-MeI at 0.1, 1.0 and 10 mm/min.

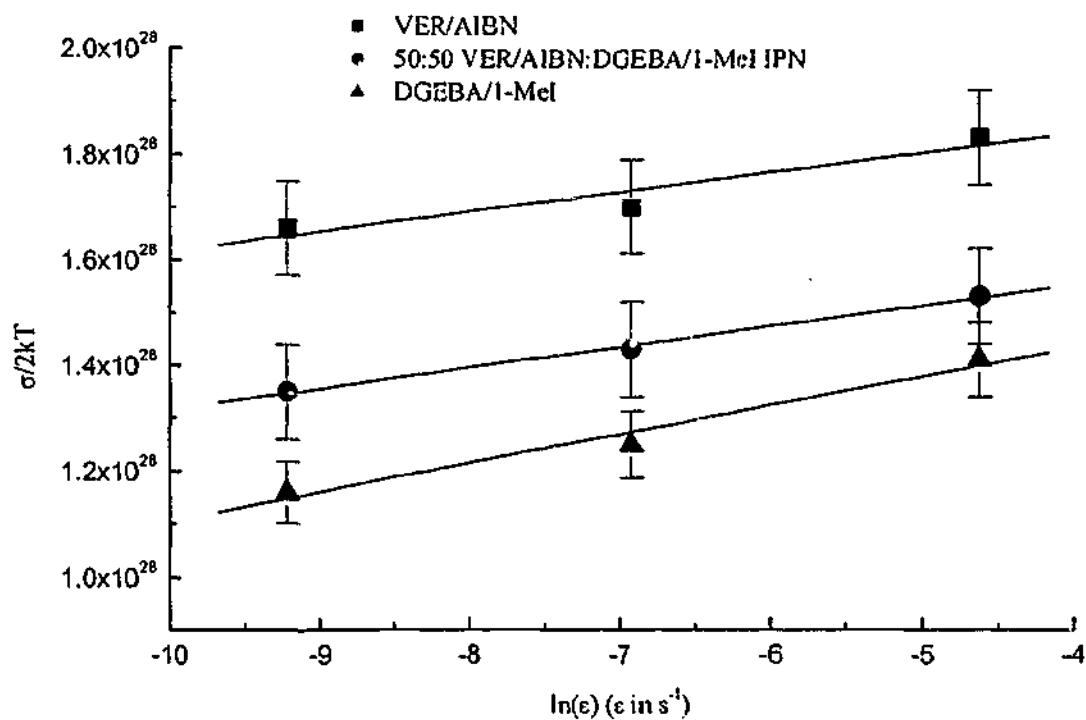


Figure 10.5 Compressive yield (MPa)/2kT versus logarithmic strain rate for VER/AIBN, DGEBA/1-MeI and the 50:50 IPN of VER/AIBN:DGEBA/1-MeI

## 10.4 Flexural Testing

The flexural stress-strain behaviour for VER/AIBN, DGEBA/1-MeI and IPN are illustrated in Figure 10.6. The flexural strength and modulus of elasticity in bending are listed in Table 10.4. In agreement with the compression experiments (Table 10.3), the VER/AIBN system has the highest flexural strength and modulus. The percentage strain to break of the VER was low, but was similar to values found in the literature<sup>2,43</sup>. The neat DGEBA/1-MeI exhibited the lowest flexural strength and modulus as found in the compression tests. The IPN exhibited flexural strength and modulus values which were approximately the average of its two components.

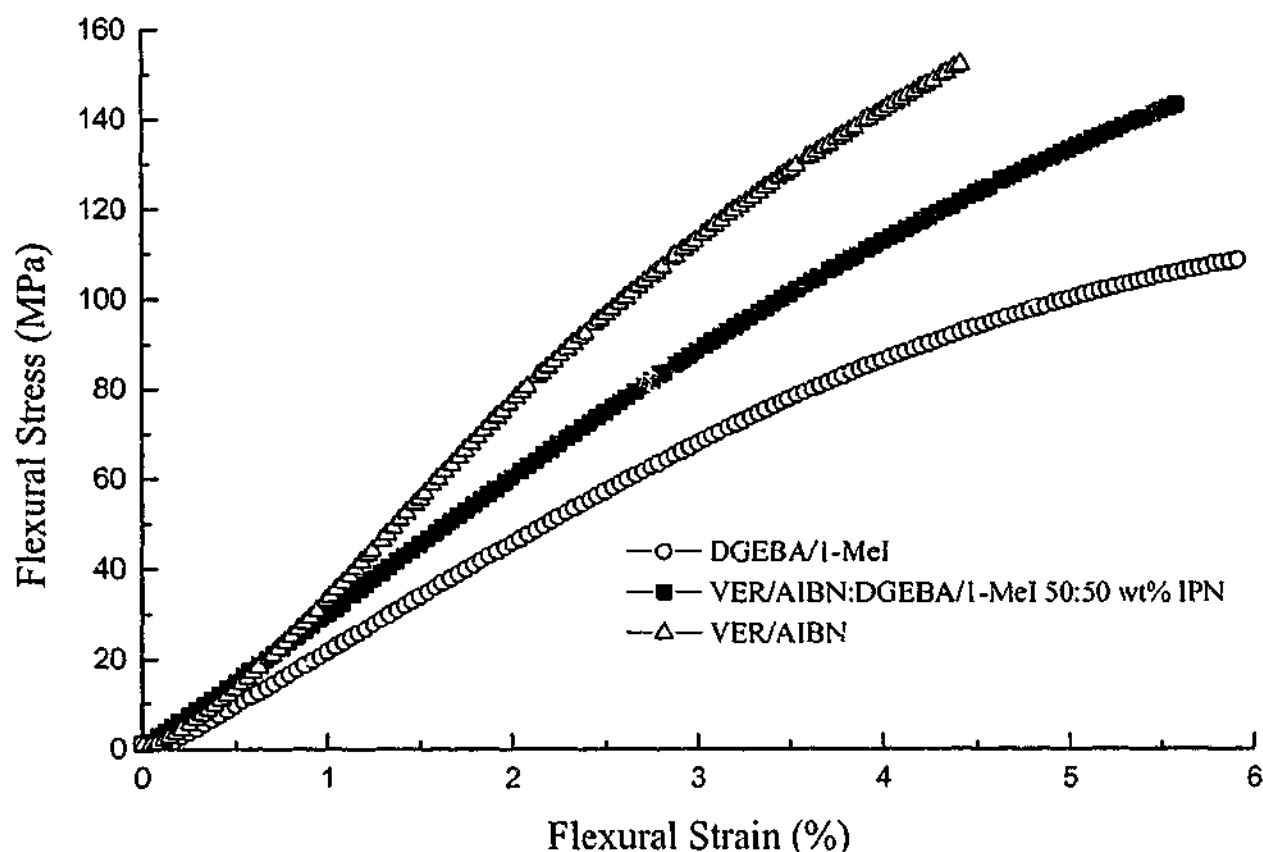


Figure 10.6 Typical stress-strain results for the DGEBA/1-MeI, VER/AIBN and resulting 50:50 IPN in 3 point bend.

Table 10.4 Summary of results from flexural experiments

System	Flexural Strength (MPa)	Strain at break (%)	Flexural Modulus (GPa)
VER/AIBN	153± 9	4.4	2.7± 0.3
50:50 VER/AIBN:DGEBA/1-MeI IPN	144± 8	5.6	2.6± 0.3
DGEBA/1-MeI	110± 10	5.9	2.1± 0.3

## 10.5 Conclusions

The water solubility characteristics of VER/AIBN, DGEBA/1-MeI, DGEBA/An, DGEBA/DDM and the corresponding 50:50 IPNs were studied. VER was less hydrophilic than the epoxy due to the presence of the non-polar styrene. The water equilibrium mass fraction increased with temperature if  $|H_s| < 42 \text{ kJ.mol}^{-1}$  as found for the VER/AIBN. In medium polarity polymers (all systems studied with the exception of VER/AIBN),  $H_s$  is close to  $-42 \text{ kJ.mol}^{-1}$ , and thus hydrophilicity is not significantly influenced by temperature. The IPNs were generally more hydrophilic than their parent resins and this may be explained by the pre-exponential factor varying smoothly with composition but the enthalpy of dissolution  $H_s$  remaining close to the value of the most hydrophilic component.

The compressive and flexural properties of VER/AIBN, DGEBA/1-MeI and the 50:50 VER/AIBN:DGEBA/1-MeI IPN have been investigated. The 50:50 VER/AIBN:DGEBA/1-MeI IPN exhibits modulus, yield stresses and activation volumes which are close to the average from the parent resins but the percentage strain at yield in the IPN is higher than the average expected from the neat resins.

# *Chapter 11*

## *Conclusions and*

### *Suggestions for Further*

#### *Studies*

---

### **11.1 Conclusions**

The polymerization behaviour of a series of IPNs formed from radically-initiated dimethacrylates in combination with either 1° amine-cured, 3° amine-cured or anhydride-cured epoxy resins has been investigated by temperature-ramping and isothermal DSC and by isothermal mid-FTIR, NIR and rheology. Detailed studies have been undertaken of the effect of using different combinations of curing components, the interactions that occur within these IPNs and the curing order of components on the overall cure kinetics and resulting miscibility. The mechanical and water absorption properties of a selection of these IPNs has also been reported.

The curing behaviours of IPNs formed from a model VER and an aliphatic or aromatic 1°-amine cured epoxy resin were extensively investigated and showed that IPNs formed with AIBN-initiated VER exhibited the most independent cure behaviour. In contrast, initiation of the VER component by BPO, CHP and MEKP all showed a redox reaction between the peroxide and the amine, particularly for aliphatic amine curatives, which caused acceleration of the peroxide decomposition in the early stages of the reaction and also resulted in premature depletion of the initiator system. The cure of the DGEBA resin was less affected by the radical initiator, however the hydroxy groups of bisGMA or from the peroxide diluent caused acceleration of the amine-epoxy

cure by H-bonding catalysis<sup>66,73</sup>. IPNs containing primary amine-cured epoxy component also showed that the cure rate of each component affected the degree of cure of the other component. In several cases, the presence of unreacted components (such as DEGBA or amines) of the epoxy system plasticized the IPN and enabled a higher level of reaction in the VER component before vitrification occurred. In addition, if one of the components (such as the VER component) attained a high level of cure early in the formation of the IPN, the high level of crosslinking contributed to premature vitrification, which limited the extent of cure of the other component. None of the curing behaviour could be attributed to the "network interlock" process suggested by Lin and co-workers<sup>133,137,230</sup> for the early stages of the cure. In most cases, near complete cure of the IPN components could be attained by postcuring above the  $T_g$  of the component networks. The Michael addition between the amine groups of the epoxy-amine system and the methacrylate groups of the VER were demonstrated by mid-FTIR and the amount of grafting due to the Michael addition was quantified by extraction studies of the semi-IPNs of VER/AIBN:DGEBA/BA and VER/AIBN:DGEBA/An, which revealed that a larger proportion of the DGEBA/BA linear polymer had grafted to the network forming VER compared to the DGEBA/An linear polymer as expected on nucleophilicity grounds.

IPNs were also prepared from 3° amine (imidazole)-cured DGEBA and radical-cured VER. Similar to that observed in the primary amine-cured IPNs, the imidazole-based IPNs also indicated that for the AIBN and CHP initiated VERs, the IPNs did not show significant chemical interaction effects between the VER and epoxy resin components and full cure of the VER was achieved at moderate temperatures. However, all of the peroxide-initiated IPN systems exhibited a redox reaction between the 1-MeI amine and the peroxide, causing accelerated decomposition of the peroxides and hence the rate of cure of the vinyl ester component was accelerated. In the case of the BPO (and possibly the MEKP), the cure of the vinyl species was incomplete due to loss of initiator activity, perhaps by non-radical redox reactions - full cure was not achieved even at very high temperatures by thermal cure for the BPO-based IPN. The extent of epoxy cure was nearly complete at moderate temperatures for all IPN systems containing the 1-MeI cured DGEBA. This suggested that even if interactions occurred between the initiator systems, there was sufficient residual imidazole to allow full cure of the DGEBA. In general, dilution effects of the reacting DGEBA system by the VER components were observed for the IPNs containing 1-MeI in the early stages of the

cure. In addition, during isothermal cure at 70°C, unreacted DGEBA monomer plasticized the IPN allowing a higher plateau conversion of the vinyl groups in the IPN, provided there were no strong interactions between the 1-MeI and the radical initiators. In contrast, when the conversion of the VER component was near complete, the subsequent reaction of the epoxy was limited by vitrification of the IPN associated with the high level of crosslinking in the VER component.

In the chemorheology section of this work, the cure kinetics of the 50:50 IPNs of VER/AIBN:DGEBA/1-MeI, VER/AIBN:DGEBA/DDM and their parent resins were monitored via NIR and rheometry at 70°C. The VER/AIBN:DGEBA/1-MeI IPN was selected as it exhibited minimal interactions between components and close to full cure could be achieved while the VER/AIBN:DGEBA/DDM IPN was chosen as a more complicated system with a number of interactions occurring (which had been identified in the initial curing study). For both of these systems, NIR spectroscopy showed that the rate of consumption of epoxy groups was slower than that found for the vinyl groups. The rate of vinyl (total styrene and methacrylate) conversion in the 50:50 VER/AIBN:DGEBA/DDM was found to be slower than in the 50:50 VER/AIBN:DGEBA/1-MeI, and the rates of vinyl conversion in both IPNs were slower than in the neat VER/AIBN resin. This decrease in rate in the IPNs was partly due to the dilution of the VER reactants by the other components as previously observed by DSC and mid-FTIR studies of IPNs containing the amine-cured and imidazole-cured epoxy component. In addition, for the VER/AIBN:DGEBA/DDM IPN, the DDM amino groups interacted with the radicals and retarded the cure rate. The rate of epoxy conversion in VER/AIBN:DGEBA/1-MeI was slower than in the neat DGEBA/1-MeI, which is also consistent with dilutional effects. In contrast, for the 50:50 VER/AIBN:DGEBA/DDM IPN, the epoxy group reaction was faster compared with the epoxy conversion in the neat system, due to the presence of the hydroxy groups in the bisGMA molecule acting as a catalyst of the epoxy-amine reaction, which offset any dilutional effect by the VER components. The similarity between the gel point for the VER/AIBN system and the IPNs indicated it was the gelation of the VER component rather than the gelation of the epoxy component that had the dominant effect on the overall gel point of the IPN. The gelation was fastest in the neat VER/AIBN system and was slowest in the VER/AIBN:DGEBA/DDM IPN; this correlated well with the NIR vinyl conversion data for VER/AIBN, VER/AIBN:DGEBA/1-MeI and VER/AIBN:DGEBA/DDM systems. The delayed gelation of the IPNs was due, in part,

to a dilutional effect (confirmed by the study of a xylene diluted VER/AIBN resin) and in part due to amine-radical interactions.

Both the VER/AIBN:DGEBA/1-MeI and VER/AIBN:DGEBA/DDM IPNs and their corresponding parent resins vitrified in the latter stages of the reaction because the isothermal cure temperature was well below the glass transition temperature of the resin components. Compared with the parent resins, the real modulus for both these IPNs rose more slowly to the glassy region and was consistent with the NIR results. The degree of conversion of the vinyl and epoxy groups when the parent resins and their IPNs vitrified was interpreted in terms of the plasticization of the VER component by DGEBA and the vitrification of the IPN prior to full cure of the epoxy component caused by the high level of crosslinking contributed by the VER component.

The initial investigations of the cure kinetics of these IPN systems indicated the VER/AIBN:DGEBA/1-MeI IPN was a system in which little interaction between components occurred. As a consequence, further DSC and FTIR studies were undertaken to study the effect of curing order on a range of IPNs prepared from a 1-MeI-cured epoxy resin and a dimethacrylate resin initiated by a number of azo-initiators (of differing reactivities). In the neat DGEBA/1-MeI, DEBPADM/AIBN, DEBPADM/VAZO88 and DEBPADM/VR110 resins, close to full cure was achieved. For the neat, high temperature DEBPADM/AZO168 resin, full cure was not attained, possibly due to the compromise between using a high enough temperature for azo decomposition while avoiding depolymerization or decomposition of the methacrylate polymer. By appropriate initiator selection, it was possible to interchange the order of cure of the components within the IPN so that either the dimethacrylate or epoxy cured first, without the complications due to interactions between components that had been observed in the IPNs that contained primary amine curatives and peroxides. In the isothermal cure of 50:50 DEBPADM/AIBN:DGEBA/1-MeI, the dimethacrylate polymerized first. As a result, the final conversion of the dimethacrylate in the IPN was enhanced by plasticization and the epoxy conversion was reduced by premature vitrification. After postcure, however, both groups reacted nearly completely and so the fully cured IPN exhibited a single high temperature  $T_g$  close to the  $T_g$  of the parent resins (see Table 11.2). For the 50:50 IPN of DEBPADM/VR110:DGEBA/1-MeI the methacrylate and epoxy groups cured at a similar rate and the final isothermal conversions were less than 100%. Postcuring caused almost 100% reaction of the epoxy

but the methacrylate groups were not fully cured due to the competition between polymerization and degradation and as a result the plasticization by residual methacrylate monomer and degradative products lowered the  $T_g$  of the IPN below that of the parent resins (see Table 11.2). In the 50:50 IPN of DEBPADM/AZO168:DGEBA/1-MeI, the epoxy cured first, but due to the high isothermal temperature required to initiate the polymerization of the methacrylate which caused degradation of the methacrylate component, an incompletely cured system with an even lower single glass transition temperature was produced (see Table 11.2).

The miscibility of the IPNs was investigated by DMTA and SANS. Some IPNs that were clearly phase separated - including the 50:50 VER/AIBN:DGEBA/An, VER/AIBN:DGEBA/BA and VER/AIBN:DGEBA/DAO IPNs, showing two  $T_g$ s by DMTA and excess small angle neutron scattering. The 50:50 VER/AIBN:DGEBA/DDM IPN showed obvious small angle neutron scattering and the absence of two glass transitions was due to close proximity of the glass transitions of the parent resins. The 50:50 VER/AIBN:DGEBA/CHDCA/DMBA IPN appeared to be partially phase separated, as suggested by DMTA (showing a single  $T_g$  with a shoulder) but no small angle neutron scattering was observed. The 50:50 VER/AIBN:DGEBA/1-MeI IPN appeared to be a single-phase material (showing no small angle neutron scattering and a single  $T_g$  by DMTA, but the presence of a single transition could not confirm this assignment due to the similarity of the  $T_g$ s of the parent resins). The correlation lengths,  $\xi$ , calculated from the Debye-Bueche equation (which assumes a random distribution of phases) were  $181 \pm 4 \text{ \AA}$ ,  $151 \pm 12 \text{ \AA}$ ,  $186 \pm 8 \text{ \AA}$  and  $184 \pm 6 \text{ \AA}$  for the 50:50 VER/AIBN:DGEBA/BA, VER/AIBN:DGEBA/DAO, VER/AIBN:DGEBA/An and VER/AIBN:DGEBA/DDM IPNs respectively.

To further probe the effect of crosslinking or non-crosslinking components within IPNs on their miscibility, a series of semi and full IPNs based on the monomer PGEMA or its crosslinking counterpart (bisGMA) and with PGE or its crosslinking counterpart (DGEBA) were also investigated. The 50:50 PGEMA/AIBN:DGEBA/1-MeI semi-IPN exhibited a single glass transition midway between the  $T_g$ s of their parent resins, however the 50:50 bisGMA/AIBN:PGE/1-MeI semi-IPN produced a broad glass transition region due to a range of PGE/1-MeI rich and bisGMA/AIBN rich phases.

The studies discussed above led to a final curing study in which a combination of thermal and photochemical initiation was used to study the effect of either photocuring the dimethacrylate followed by thermal cure of the epoxy/anhydride or by thermally curing the epoxy/anhydride first followed by photocuring of the dimethacrylate. When the epoxy component was thermally-cured before isothermal photopolymerization of the dimethacrylate, the final conversion of the dimethacrylate was limited by vitrification or topological restraint of the IPN. When the order of cure was reversed, the thermal cure of the epoxy was reduced, possibly due to vitrification or topological restraint or due to partitioning of the reactive components into separate phases. NIR studies of the cure of the dimethacrylate and epoxy components confirmed that the cure order affected the final conversion. DMTA studies of the NIR samples revealed a single glass transition when the epoxy component was cured first, but two glass transitions were observed when the dimethacrylate component was photocured prior to the epoxy/anhydride cure, confirming that phase separation had occurred.

The curing order, interactions that occur between components, and the DMTA and SANS results are listed in Tables 11.1 and 11.2 for all the semi-IPNs and full-IPNs. These results indicate the phase composition of IPNs is strongly dependent on the miscibility of the components constituting the IPN and also the polymerization kinetics of those components. The backbone monomers chosen in this work (DEBPADM, bisGMA and DGEBA) were chosen to be similar in structure to reduce the thermodynamic binary interaction parameter and thus increase the miscibility of the polymers, however it may be noted that small changes in structure had a significant effect on the resulting IPN morphology. The fact that, under the appropriate curing regime, a two-phase structure could be formed in DEBPADM-based IPNs did not necessarily mean that the same occurred for the bisGMA-based IPNs. This derives from the presence of a hydrogen-bonding hydroxyl group in the bisGMA molecule and this difference appears to make the epoxy-bisGMA IPN system more miscible. Thus the 50:50 DEBPADM/AIBN:DGEBA/CHDCA/DDSA/DMBA IPN showed two  $T_g$ s, whereas the 50:50 bisGMA/styrene/AIBN:DGEBA/DDSA/CHDCA/DMBA IPN showed a single  $T_g$  located between the  $T_g$  of the neat DGEBA/DDSA/CHDCA/DMBA and the bisGMA/styrene/AIBN (see Table 11.1). Although the base resins (DGEBA, VER and DEBPADM) were similar in these IPNs, there was quite a variation in the curatives used for the cure of the DGEBA component. In IPNs containing BA, DAO, An and DDM curing agents for the epoxy and styrene as a co-monomer for the

bisGMA, these additives appear to be responsible for an increase in the thermodynamic binary interaction parameter resulting in a two-phase morphology and changes in the curing orders of the IPN component had little effect on their lack of miscibility. However, in other systems where there was perhaps more miscibility between components, changing the curing order resulted in either a one or two phase IPN. For example, in the 50:50 DEBPADM/XDT:DGEBA/CHDCA/DDSA/DMBA IPN, the absence of the non-polar styrene component increased the systems miscibility so that the selective photocuring of the dimethacrylate component of a dimethacrylate/epoxy IPN clearly indicated that by changing the cure order the phase morphology could be controlled.

Although the H-bonding between the crosslinking bisGMA (and linear PGEMA) and epoxy components appeared to promote the formation of single phase IPNs, the grafting reaction by Michael addition between components had a minimal effect - all IPNs in which the Michael addition was present were clearly phase separated. It may be concluded that grafting between components within an IPN does not necessarily encourage the formation of a single phase system; in fact it is possible that the IPN could phase separate prior to any grafting between components and thus grafting in the IPN would have no effect on the formation of a single phase material.

Due to importance of the physical properties of the IPNs on potential applications, the water absorption characteristics and mechanical properties of some cured IPNs were examined. The water absorption characteristics of VER/AIBN, DGEBA/1-MeI, DGEBA/An, DGEBA/DDM and the corresponding 50:50 IPNs were studied. The VER was much less hydrophilic than the epoxy resins, despite the similarity in the structure - it appeared that the presence of the styrene bridge between the reacted methacrylate units of the bisGMA changed the spacing between polar sites or sterically restricted the binding of the water molecules and that the incorporation of the non-polar styrene units in the dimethacrylate reduces the hydrophilicity of the VER. The IPNs were generally more hydrophilic than their parent resins and may be explained by the pre-exponential factor varying smoothly with composition but the enthalpy of dissolution  $H_s$  remaining close to the value of the most hydrophilic component.

**Table 11.1 Summary of the effect of curing order and component miscibility, and a comparison of semi- and full- amine type IPNs.**

System	Initial component to cure (vinyl=V; epoxy=E)	H-bonding	Grafting (Michael addition)	T <sub>g</sub> from DMTA (°C)	Observe SANS (b, ×10 <sup>3</sup> cm <sup>3</sup> )	Evidence for a two phase structure*
VER/AIBN				169		N
VER/AIBN: DGEBA/1-Mel	V	Y	N	189	N (19)	N
DGEBA/1-Mel				185		N
VER/AIBN				169		N
VER/AIBN: DGEBA/BA	E	Y	Y	Peak 1. 71 Peak 2. 141	Y (31)	Y
VER/AIBN: DGEBA/DAO	E	Y	Y	Peak 1. 120 Peak 2. 146	Y (22)	Y
DGEBA/BA				67		N
DGEBA/DAO				119		N
VER/AIBN				169		N
VER/AIBN: DGEBA/An	V	Y	Y	Peak 1. 111 Peak 2. 161	Y (10)	Y
VER/AIBN: DGEBA/DDM	V	Y	Y	171	Y (14)	Y
DGEBA/An				109		N
DGEBA/DDM				189		N
VER/AIBN				169		N
VER/AIBN: DGEBA/CHDCA/ DMBA	V	Y	N	157 with a shoulder	N (7)	Y
DGEBA/CHDCA/ DMBA				159		N
VER/AIBN				169		
VER/AIBN: DGEBA/CHDCA/ DDSA/DMBA	V	Y	N	120	N/A	N
DGEBA/CHDCA/ DDSA/DMBA				93		N
DEBPADM/AIBN				189°C		N
DEBPADM/AIBN: DGEBA/CHDCA/ DDSA/DMBA	V	N	N	Peak 1. 100 Peak 2. 156	N/A	Y
DGEBA/CHDCA/ DDSA/DMBA				93		N

\*(Y= yes, N=no)

**Table 11.2** A summary of the effect of curing order and comparison of semi- and full-IPN formation on the component miscibility.

System	Initial component to cure (vinyl=V; epoxy=E)	H-bonding	Grafting (Michael addition)	T <sub>g</sub> from DMTA (°C)	Evidence for a two-phase structure
DEBPADM/AIBN				189	N
DEBPADM/AIBN: DGEBA/1-MeI	V	N	N	178	I
DGEBA/1-MeI				185	N
DEBPADM/VR110				163	N
DEBPADM/VR110: DGEBA/1-MeI	E	N	N	120	I
DGEBA/1-MeI				185	N
DEBPADM/VAZO168				158	N
DEBPADM/VAZO168: DGEBA/1-MeI	E	N	N	97	I
DGEBA/1-MeI				185	N
DEBPADM/XDT				160	N
DEBPADM/XDT: DGEBA/CHDCA/DDSA/ DMBA (initially photocured)	V	N	N	Peak 1. 103 Peak 2. 196	Y
DGEBA/CHDCA/DDSA/ DMBA				93	N
DEBPADM/XDT				160	N
DEBPADM/XDT: DGEBA/CHDCA/DDSA/ DMBA (initially thermal cured)	E	N	N	105	N
DGEBA/CHDCA/DDSA/ DMBA				93	N
bisGMA/AIBN				172	N
bisGMA/AIBN: DGEBA/1-MeI	V	Y	N	178	I
DGEBA/1-MeI				185	N
PGEMA/AIBN				45	N
PGEMA/AIBN: DGEBA/1-MeI	V	Y	N	100	N
DGEBA/1-MeI				185	N
bisGMA/AIBN				172	N
bisGMA/AIBN: PGE/1-MeI	V	Y	N	peak at 83, shoulder at 18	Y
PGE/1-MeI				5	N

\*(Y = yes, N = no and I = inconclusive)

The compressive and flexural properties of VER/AIBN, DGEBA/1-MeI and the 50:50 VER/AIBN:DGEBA/1-MeI IPN were investigated. The 50:50 VER/AIBN:DGEBA/1-MeI IPN exhibited modulus and yield strength properties that were close to the average from the parent resins but the IPN exhibited higher strain at yield.

In conclusion to this study of epoxy-dimethacrylate based IPNs, numerous interactions (both chemical and physical) have been systematically defined and interpreted. A range of miscibility levels were produced with the different IPN combinations and these structures have been explained in terms of chemical and physical interactions and the cure kinetics of the IPN components. The combination of thermal and photoinitiation for the cure of the 50:50 DEBPADM/XDT:DGEBA/CHDCA/DDSA/DMBA IPN was one of the most exciting aspects of this work. This combination produced a single glass transition when the epoxy component was cured first, but two glass transitions were observed when the dimethacrylate component was photocured prior to the epoxy/anhydride cure. This work gave an indication of the variety of phase morphologies (and thus properties) which may be possible in these IPN systems.

## 11.2 Suggestions for Future Work

The experiments undertaken in this study have contributed to a more comprehensive understanding of the cure kinetics, rheology, phase structure and properties of epoxy/dimethacrylate based IPNs. However there are a number of aspects that should be further investigated.

Since the increase in molecular weight of each of the components is a driving force for phase separation in IPNs and phase separation can only occur for an ungelled system, further investigations on the effect of curing order on resulting miscibility and morphology should be undertaken on IPN combinations. To aid analysis, the  $T_g$ s of the components in these combinations should differ significantly. In particular, it is possible that complex nano-structures could be developed by appropriate curing programs. This area has great potential for the development of new materials with unique properties.

The chemorheology study undertaken in Chapter 6 consisted of separate dynamic rheology and NIR spectroscopy experiments on IPN samples at 70°C. In situ NIR analysis of samples in the rheometer could have given more accurate conversion at the gel point, and combining this with a photocuring setup could have enabled the photocuring kinetics and rheology to be monitored simultaneously.

In Chapter 9 the combination of partial photocuring and partial thermal cure of IPNs enabled a relatively high degree of control and separation of the polymerization of each component. This polymerization of each IPN component could be further controlled if the dual photocuring of IPN components was undertaken. Also, in this work IPNs were either fully photocured followed by thermal cure or vice versa, however, intermittent photocuring could potentially produce an array of different phase structures with unique properties.

The SANS studies in this work were performed on un-deuterated samples and as a result, in some cases, the difference in scattering length density of individual components was close to the observable limits. Deuteration of one of the components within the IPN would produce a greater difference in scattering length density of

individual components and would ensure scattering was observed if the IPN was heterogeneous.

Transmission Electron Microscopy could also be utilized to investigate the miscibility and phase separation of systems where the  $T_g$ s of the parent resins were close together and when the scattering length density was small.

The systems investigated here were predominantly 50:50 w/w IPNs; further investigations should vary the ratio of components within the IPN and study its effect on the phase structure and morphology of the IPN and thus the effect on the properties of the fully cured material. Although no synergistic effects were observed in mechanical properties with the 50:50 VER/AIBN:DGEBA/1-MeI IPN it is possible that other ratios of components may have resulted in an improvement in properties.

As this study was predominantly a study of the cure kinetics and miscibility of epoxy/dimethacrylate IPNs, only limited mechanical property testing was undertaken. A more complete study of the mechanical properties of all the IPN systems studied – in particular IPNs of the same chemical nature differing only in cure order and thus phase morphology - would assist in developing structure-property relationships which would open avenues for industrial applications for these materials.

## Appendix I

The  $\chi^2$  (chi-squared) test can be described by:

$$\chi^2 = \sum_{i=1}^k \frac{(x_i - \mu)^2}{\sigma^2}$$

where  $k$  is the number of data points,  $x_i$  is the variable,  $\mu$  is the mean and  $\sigma$  is the standard deviation.

The test is designed to convert the deviations between the experimental data and theoretical values into the probability of the experimental data occurring at the value expected theoretically, taking into account both the size of the sample and the number of variables (degrees of freedom)<sup>244</sup>.

**References:**

1. Sperling, L.H. and Mishra, V., in *IPNs Around the World-Science and Engineering* Kim, S.C. and Sperling, L.H., Eds. (John Wiley and Sons, New York, 1997) pp. 1-26.
2. Chou, Y.C. and Lee, L.J., in *Interpenetrating Polymer Networks* Klemperer, D.K., Sperling, L. H. and Utracki, L.A., Ed. (1994), vol. ACS 239, pp. 305-331.
3. Subramaniam, R. and McGarry, F.J., *J. Adv. Mat.*, 26-35 (1996).
4. Subramaniam, R. and McGarry, F.J., Toughened Polyester: A Novel System, "49th Annual Conference, Composites Institute, The Society of the Plastics Industry Inc Feb 1994" (1994).
5. Lin, M.S. and Chang, R.J., *J. Appl. Polym. Sci.* 46, 815-827 (1992).
6. Sperling, L.H. and Mishra, V., *Polymers for Advanced Technologies* 7, 197-208 (1995).
7. Verchere, D., Sautereau, H., Pascault, J.P., Moschiar, S.M., Riccardi, C.C., and Williams, R.J.J., in *Toughened Plastics I Science and Engineering* Keith Riew, C. and Kinloch, A.J., Eds. (American Chemical Society, Washington D.C., 1993), vol. 233, pp. 336-363.
8. Utracki, L.A., in *Interpenetrating Polymer Networks* Klemperer, D., Sperling, L.H., and Utracki, L.A., Eds. (American Chemical Society, New York, 1994) pp. 77-123.
9. Dusek, K., *Collect. Czech. Chem. Commun.* 58, 2245-2265 (1993).
10. Dusek, K., *Makromol. Chemie.* 240, 1-15 (1996).
11. Stauffer, D., Coniglio, A., and Adam, M., *Adv. Polym. Sci.* 44, 103-155 (1982).
12. Cook, W.D., *Euro. Polym. J.* 14, 715-720 (1978).
13. Loshaek, S., *J. Polym. Sci.* 15, 391-404 (1955).
14. Aronhime, M.T. and Gillham, J.K., *Adv. Polym. Sci.* 78, 83-112 (1986).
15. Chompff, A.J., *Polymer Networks-Structures and Mechanical properties* (Plenum Press, New York, 1971), 145-190.
16. Wise, C.W., Cook, W.D., and Goodwin, A.A., *Polymer* 38, 3251-3261 (1997).
17. Cook, W.D., Simon, G.P., Burchill, P., Lau, M., and Fitch, T.J., *J. Appl. Polym. Sci.* 64, 769-781 (1997).
18. Kloosterboer, J.G. and Lijten, G.F.C.M., *Polymer* 31, 95-101 (1990).
19. Gillham, J.K., in *Developments in Polymer Characterisation-3* Dawkins, J.V., Ed.

- (Applied Science Publishers, London, 1982), vol. 3, pp. 159-227.
20. Gillham, J.K., *Polym. Eng. Sci.* **26**, 1429-1433 (1986).
  21. Cook, W.D., *Polymer* **33**, 2152-2161 (1992).
  22. Jellinek, H.H.G., *Degradation of Vinyl Polymers*. Hutchinson, E., Ed., Physical Chemistry (Academic Press, New York, 1955),
  23. Flory, P.J., *Principles of Polymer Chemistry* (Cornell University Press, New York, 1967)
  24. de Gennes, P.G., *Scaling Concepts in Polymer Physics* (Cornell University Press, New York, 1979)
  25. Dusek, K., *Adv. Polym. Sci.* **78**, 1-58 (1986).
  26. Flory, P.J., *J. Amer. Chem. Soc.* **63**, 3083-3090 (1941).
  27. Stockmayer, W.H., *J. Polym. Sci.* **9**, 69-71 (1952).
  28. Stockmayer, W.H., *J. Polym. Sci.* **11**, 424-428 (1953).
  29. Flory, P.J., *J. Amer. Chem. Soc.* **63**, 3091-3096 (1941).
  30. Flory, P.J., *J. Amer. Chem. Soc.* **63**, 3096-3101 (1941).
  31. Macosko, C.W. and Miller, D.R., *Macromolecules.* **9**, 206-211 (1976).
  32. Macosko, C.W. and Miller, D.R., *Macromolecules.* **9**, 529-534 (1976).
  33. Walling, C., *J. Amer. Chem. Soc.* **67**, 441-447 (1945).
  34. Odian, G., *Principles of Polymerization* (John Wiley and Sons, Toronto, ed. 2nd, 1981), Chapter 3.
  35. Kloosterboer, J.G., *Adv. Polym. Sci.* **84**, 1-61 (1988).
  36. O'Driscoll, K.F., in *Comprehensive Polymer Science. The synthesis, characterisation, reactions and applications of polymers-chain polymerization* Eastmond, G.C., et al., Eds. (Pergamon Press, Oxford, 1989), vol. 3, pp. 161-170.
  37. Moad, G. and Solomon, D.H., *The Chemistry of Free Radical Polymerization* (Elsevier Science Inc, Oxford, 1995), Chapter 5.
  38. Soh, S.K. and Sundberg, D.C., *J. Polym. Sci: Polym. Chem. Ed.* **20**, 1299-1313 (1982).
  39. Soh, S.K. and Sundberg, D.C., *J. Polym. Sci: Polym. Chem. Ed.* **20**, 1315-1329 (1982).
  40. Rizzardo, E., in *Polymer Update: Science and Engineering* Cook, W.D. and Guise, G.B., Eds. (Polymer Division, RACI, Australia, 1989) pp. 27-28.
  41. Anderson, T.F. and Messick, V.B., in *Developments in Reinforced Plastics-I* Pritchard, G., Ed. (Applied Science Publishers, London, 1980) pp. 29-58.
  42. Pastorino, R.L., in *Unsaturated Polyester Technology* Bruins, P.F., Ed. (Gordon

- and Breach, New York, 1976) pp. 63-84.
43. Gallagher, R.B. and Kamath, V.R., in *Sheet Molding Compounds Science and Technology*. (Hanser/Gardner Publishers, Munich, 1993) pp. 29-48.
  44. Macosko, C.W., *Brit. Polym. J.* **17**, 239-245 (1985).
  45. Winter, H.H., *Adv. Polym. Sci.* **134**, 167-230 (1997).
  46. Winter, H.H. and Chambon, F., *J. Rheo.* **30**, 367-382 (1986).
  47. Chambon, F. and Winter, H.H., *J. Rheo.* **31**, 683-697 (1987).
  48. Venkataraman, S.K. and Winter, H.H., *Rheo. Act.* **29**, 423-432 (1990).
  49. Winter, H.H., *Polym. Eng. Sci.* **27**, 1698-1701 (1987).
  50. Hess, W., Vilgis, T.A., and Winter, H.H., *Macromolecules.* **21**, 2536-2542 (1988).
  51. Lairez, D., Adam, M., Emery, J.R., and Durand, D., *Macromolecules.* **25**, 286-289 (1992).
  52. Eloundou, J.P., Feve, M., Gerard, J.F., Harran, D., and Pascault, J.P., *Macromolecules.* **29**, 6907-6916 (1996).
  53. Eloundou, J.P., Gerard, J.F., Harran, D., and Pascault, J.P., *Macromolecules.* **29**, 6917-6927 (1996).
  54. Scanlan, J.C. and Winter, H.H., *Macromolecules.* **24**, 47-54 (1991).
  55. Winter, H.H., *Prog. Coll. Polym. Sci.* **75**, 104-110 (1987).
  56. Wisanrakkit, G. and Gillham, J.K., *J. Appl. Polym. Sci.* **41**, 2885-2929 (1990).
  57. Graessley, W.W., *Macromolecules.* **8**, 186-190 (1975).
  58. Garnish, E.W., in *Structural Adhesives: Developments in Resins and Primers* Kinloch, A.J., Ed. (Elsevier Applied Science Publishers, London, 1986), vol. 57.
  59. Chandra, R., Rajabi, L., and Soni, R.K., *J. Appl. Polym. Sci.* **62**, 661-671 (1996).
  60. Noordam, A., Wintraecken, J.J.M.H., and Walton, G., in *Crosslinked Epoxies* Sedlacek, B. and Kahovec, J., Eds. (W.Gruyter & Co., Berlin, 1987) pp. 373-389.
  61. Ashcroft, W.R., in *Chemistry and Technology of Epoxy resins* Ellis, B., Ed. (Blackie Academic and Professional, London, 1993) pp. 37-70.
  62. Ellis, B., in *Chemistry and Technology of Epoxy resins* Ellis, B., Ed. (Blackie Academic and Professional, London, 1993) pp. 1-35.
  63. Tacca, J.M., Bechara, I.S., and Bye, M.L., *SPI Technical Conference*, (1984).
  64. Shanks, R.A., in *Polymer Update: Science and Engineering* Cook, W.D. and Guise, G.B., Eds. (Polymer Division RACI, Melbourne, 1989) pp. 69-101.
  65. Shechter, L. and Wynstra, J., *Ind. Eng. Chem.* **48**, 86-93 (1956).
  66. Smith, I.T., *Polymer* **2**, 95-108 (1961).
  67. Eloundou, J.P., Feve, M., Harran, D., and Pascault, J.P., *Makromol. Chemie.* **230**,

- 13-46 (1995).
68. Wisanrakkit, G. and Gillham, J.K., *J. Appl. Polym. Sci.* **42**, 2453-2463 (1991).
69. Bidstrup, S.A. and Macosko, C.W., *J. Polym. Sci. B: Polym. Phys.* **28**, 691-709 (1990).
70. Matejka, L. and Dusek, K., in *Crosslinked Epoxies* Sedlacek, B. and Kahovec, J., Eds. (W.Gruyter & Co., Berlin, 1987) pp. 231-239.
71. Charlesworth, J., *J. Polym. Sci. Polym. Chem. Ed.* **18**, 621-628 (1980).
72. Matejka, L., *Macromolecules.* **33**, 3611-3619 (2000).
73. Horie, K., Hiura, H., Sawada, M., Mita, I., and Kambe, H., *J. Polym. Sci. A-1.* **8**, 1357-1372 (1970).
74. Lee, H. and Neville, K., *Handbook of Epoxy Resins* (McGraw-Hill, USA, 1967).
75. Brydson, J.A., *Plastic Materials* (Butterworth-Heinemann Ltd, London, ed. 5th, 1993), 697.
76. Hodd, K.A., *Epoxy Resins* (Pergamon Press, London, 1990), 11.
77. Woo, E.M. and Seferis, J.C., *J. Appl. Polym. Sci.* **40**, 1237-1256 (1990).
78. Dusek, K., Lunak, S., and Matejka, L., *Polym. Bull.* **7**, 145-152 (1982).
79. Ochi, M., Iesako, H., and Shimbo, M., *J. Polym. Sci. B: Polym. Phys.* **24**, 251-261 (1986).
80. Park, W.H. and Lee, J.K., *J. Appl. Polym. Sci.* **67**, 1101-1108 (1998).
81. Farkas, A. and Strohm, P.F., *J. Appl. Polym. Sci.* **12**, 159-168 (1968).
82. Heise, M.S. and Martin, G.C., *J. Appl. Polym. Sci.* **39**, 721-738 (1990).
83. Barton, H. and Shepard, P.M., *Makromol. Chem.* **176**, 919 (1975).
84. Dearlove, T.J., *J. Appl. Polym. Sci.* **14**, 1615-1626 (1970).
85. Potter, W.G., *Uses of Epoxy Resins* (Butterworth & Co, London, 1975), p 217.
86. O'Hearn, T.P., in *Engineered Materials Handbook - Engineering Plastics.* (Metals Park Ohio ASM International, Ohio, 1988), vol. 2, pp. 272-275.
87. Sandner, B., Kammer, S., and Wartwig, S., *Polymer* **37**, 4705-4712 (1996).
88. Kamath, V.R. and Gallagher, R.B., in *Developments in Reinforced Plastics-1* Pritchard, G., Ed. (Applied Science Publishers, London, 1980) pp. 121-144.
89. Sheppard, C. and Kamath, V.R., *Polym. Eng. Sci.* **19**, 597-606 (1979).
90. Imoto, M., Otsu, T., Ota, T., Takasugi, H., and Matsuda, M., *J. Polym. Sci.* **22**, 137-147 (1956).
91. Brinkman, W.H., Damen, L.W.J., and Maira, S., Accelerators for the organic peroxide curing of polyesters and factors influencing their behaviour, 23rd ANTEC 1968 Reinforced Plastics/Composites division (The Society of the

- Plastics Industry, 1968).
92. Walling, C. and Indictor, N., *J. Amer. Chem. Soc.* **80**, 5814-5818 (1958).
  93. Andrzejewska, E., *Prog. Polym. Sci.* **26**, 605-665 (2001).
  94. Lecamp, L., Youssef, B., Bunel, C., and Lebaudy, P., *Polymer* **40**, 1403-1409 (1999).
  95. Decker, C., Zahouily, K., Decker, D., Nguyen, T., and Viet, T., *Polymer* **42**, 7551-7560 (2001).
  96. Scherzer, T. and Decker, U., *Polymer* **41**, 7681-7690 (2000).
  97. Cook, W.D., *Polymer* **33**, 600-609 (1992).
  98. Cook, W.D., *J. Polym. Sci. A: Polym. Chem.* **31**, 1053-1067 (1993).
  99. Cook, W.D. and Rizzardo, E., *Chem. Aust.*, 437-440 (1988).
  100. Anseth, K.S., Newman, S.M., and Bowman, C.N., *Adv. Polym. Sci.* **122**, 177-217 (1995).
  101. Vollenbroek, F.A. and Spiertz, E.J., *Adv. Polym. Sci.* **84**, 85-109 (1988).
  102. Moad, G. and Solomon, D.H., *The Chemistry of Free Radical Polymerization* (Elsevier Science Inc, Oxford, 1995), pp 336-339.
  103. Moad, G. and Solomon, D.H., *The Chemistry of Free Radical Polymerization* (Elsevier Science Inc, Oxford, 1995), 26-27.
  104. Kannurpatti, A.R., Lu, S., Bunker, G.M., and Bowman, C., *Macromolecules.* **29**, 7310-7315 (1996).
  105. Kannurpatti, A.R., Anderson, K.J., Anseth, J.W., and Bowman, C., *J. Polym. Sci. B: Polym. Phys.* **35**, 2297-2307 (1997).
  106. Otsu, T. and Kuriyama, A., *J. Macromol. Sci., Chem.* **A21**, 961-977 (1984).
  107. Otsu, T. and Yoshida, M., *Makromol. Chem.* **3**, 127-132 (1982).
  108. Otsu, T., Yoshida, M., and Tazaki, T., *Makromol. Chem.* **3**, 133-140 (1982).
  109. Otsu, T. and Matsumoto, A., *Adv. Polym. Sci.* **136**, 75-129 (1998).
  110. Lem, K.W. and Han, C.D., *Polym. Eng. Sci.* **24**, 175-184 (1984).
  111. Stone, M.A., Fink, B.K., Bogetti, T.A., and Gillespie, J., J.W., *Polym. Eng. Sci.* **40**, 2489-2497 (2000).
  112. Mousa, A. and Karger-Kocsis, J., *Polym. & Polym. Comp.* **8**, 455-460 (2000).
  113. Auad, M., Aranguren, M., and Borrajo, J., *Polymer* **41**, 3317-3329 (2000).
  114. Auad, M., Aranguren, M., and Borrajo, J., *J. Appl. Polym. Sci.* **66**, 1059-1066 (1997).
  115. Dua, S., McCullough, R.L., and Palmese, G.R., *Polym. Comp.* **20**, 379-391 (1999).
  116. Ganem, M., Mortaigne, B., Bellenger, V., and Verdu, J., *J. Macromol. Sci., P.*

- Appl. Chem.* A30, 829-848 (1993).
117. Brill, R.P. and Palmese, G.R., *J. Appl. Polym. Sci.* 76, 1572-1582 (2000).
  118. Kamal, M.R. and Sourour, S., *Polym. Eng. Sci.* 13, 59-64 (1973).
  119. Varma, I.K., Rao, B.S., Choudhary, M.S., Choudhary, V., and D.S. Varma, *Makromol. Chemie.* 130, 191-199 (1985).
  120. Herzog, D. and Brown, T.B., *Mat. Performance* 33, 30-33 (1994).
  121. Hag, N. and Harrison, P., *Brit. Plast. Rub.*, 25-26 (1996).
  122. Rao, B.S., *Popular Plastics* 33, 33-37 (1988).
  123. Harrison, P., *Corr. Prev. & Cont.* April, 43-44 (1994).
  124. Utracki, L.A. and Bata, G.L., in *Polymer Alloys III* Klemperer, D. and Frisch, K.C., Eds. (Plenum Press, New York, 1983) pp. 91-104.
  125. Sperling, L.H. and Friedman, D.W., *J. Polym. Sci. B: Polym. Phys.* 7, 425-427 (1969).
  126. Yang, Y.S. and Lee, L.J., *Macromolecules.* 20, 1490-1495 (1987).
  127. Dusek, K., *Polym. Gel. Net.* 4, 383-404 (1996).
  128. Jin, S.R., Widmaier, J.M., and Meyer, G.C., *Polymer* 29, 346-350 (1988).
  129. Oleinik, E.F., *Adv. Polym. Sci.* 80, 49-99 (1986).
  130. Fasce, D.P. and Williams, R.J.J., *Polym. Bull.* 34, 515-522 (1995).
  131. Tanzi, M.C., Pornaro, F., Muccio, A., Grassi, L., and Danusso, F., *J. Appl. Polym. Sci.* 31, 1083-1091 (1986).
  132. Tanzi, M.C., Levi, M., and Danusso, F., *J. Appl. Polym. Sci.* 42, 1371-1376 (1991).
  133. Lin, M.T., Jeng, K.T., Huang, K.Y., and Shih, Y.F., *J. Appl. Polym. Sci.* 31, 3317-3325 (1993).
  134. Lin, M.S., Chang, Yang, T., and Shih, Y.F., *J. Appl. Polym. Sci.* 55, 1607-1617 (1995).
  135. Lin, M.S., Liu, C.C., and Lee, C.T., *J. Appl. Polym. Sci.* 72, 585-592 (1999).
  136. Lin, M.S. and Jeng, K.T., *J. Polym. Sci. A: Polym. Chem.* 30, 1941-1951 (1992).
  137. Lin, M.S. and Lee, S.T., *Polymer* 36, 4567-4572 (1995).
  138. Fan, L.H., Hu, C.P., Zhang, and Ying, S.K., *J. Appl. Polym. Sci.* 59, 1417-1426 (1996).
  139. Fan, L.H., Hu, C.P., and Ying, S.K., *Polymer* 37, 975-981 (1996).
  140. Hsu, T.J. and Lee, L.J., *Polym. Eng. Sci.* 25, 951-958 (1985).
  141. Chou, Y.C. and Lee, L.J., *Polym. Eng. Sci.* 34, 1239-1249 (1994).
  142. Zhou, P. and Frisch, H.L., *Macromolecules.* 27, 1788-1794 (1994).

143. Zhou, P., Xu, Q., and Frisch, H.L., *Macromolecules*. **27**, 938-946 (1994).
144. Widmaier, J.M. and Drillieres, S., *J. Appl. Polym. Sci.* **63**, 951-958 (1997).
145. Frounchi, M., Burford, R.P., and Chaplin, R.P., *Polymer* **35**, 5073-5078 (1994).
146. Udagawa, A., Sakurai, F., and Takahashi, T., *J. Appl. Polym. Sci.* **42**, 1861-1867 (1991).
147. Decker, C., Viet, T.N.T., Decker, D., and Weber-Koehl, E., *Polymer* **42**, 5531-5541 (2001).
148. Chou, Y.C. and Lee, L.J., *Polym. Eng. Sci.* **35**, 976-988 (1995).
149. Yang, J., Winnik, M.A., Ylitalo, D., and Devoe, R.J., *Macromolecules*. **29**, 7047-7054 (1996).
150. Zhou, P., Frisch, H.L., Rogovina, L., Makarova, L., Zhdanov, A., and Sergeienko, N., *J. Polym. Sci. A: Polym. Chem.* **31**, 2481-2491 (1993).
151. Dubuisson, A., Ades, D., and Fontanille, M., *Polym. Bull.* **3**, 391-398 (1980).
152. Frisch, H.L., Frisch, K.C., and Klempner, D., *Polym. Eng. Sci.* **14**, 646-650 (1974).
153. Lipatov, Y.S., in *Interpenetrating Polymer Networks* Klempner, D., Sperling, L.H., and Utracki, L.A., Eds. (American Chemical Society, New York, 1994) pp. 125-139.
154. King, S., in *Modern Techniques for Polymer Characterization* Penthrick, R.A. and Dawkins, J.V., Eds. (John Wiley and Sons, New York, 1999) pp. 171-232.
155. Junker, M., Alig, I., Frisch, H.L., Fleischer, G., and Schulz, M., *Macromolecules*. **30**, 2085-2091 (1997).
156. Abetz, V., Meyer, G.C., Mathis, A., Picot, C., and Widmaier, J.M., in *IPNs around the world* Kim, S.C. and Sperling, L.H., Eds. (John Wiley and Sons, New York, 1997) pp. 203-217.
157. Elliniadis, S., Higgins, J.S., Choudhary, R.A., and Jenkins, S.D., *Macro. Symp.* **112**, 55-61 (1996).
158. Tan, S., Zhang, D., and Zhou, E., *Polym. Inter.* **42**, 90-94 (1997).
159. Tan, S., Zhang, D., and Zhou, D., *Polymer* **38**, 4571-4575 (1997).
160. Aa, J.H., Fernandez, A.M., and Sperling, L.H., *Polym. Mat. Sci. Eng.* **56**, 541-545 (1986).
161. Lal, J., Widmaier, J.M., Bastide, J., and Boue, F., *Macromolecules*. **27**, 6443-6451 (1994).
162. Richards, R.W., *Makromol. Chem.* **40**, 209-222 (1990).
163. Higgins, J.S. and Benoit, H.C., *Polymers and Neutron Scattering*. Lovesey, S.W.

- and Mitchell, E.W.J., Eds., *Oxford Series on Neutron Scattering in Condensed matter* (Oxford University Press, New York, 1996), Chapter 1.
164. Paul, D.R. and Bucknall, C.B., *Polymer Blends* (Wiley, New York, 2000).
165. Deybe, P. and Bueche, A.M., *J. Appl. Phys.* **20**, 518-526 (1949).
166. Higgins, J.S. and Benoit, H.C., *Polymers and Neutron Scattering*. Lovesey, S.W. and Mitchell, E.W.J., Eds., *Oxford Series on Neutron Scattering in Condensed matter* (Oxford University Press, New York, 1996), p 239 & 286.
167. Widmaier, J.M., *Macro. Symp.* **93**, 179-186 (1995).
168. Suther, B., Xiao, H.X., Klempner, D., and Frisch, K.C., in *IPNs around the world: Science and Engineering* Kim, S.C. and Sperling, L.H., Eds. (John Wiley and Sons, New York, 1997) pp. 49-73.
169. Flory, P.J., *J. Chem. Phys.* **9**, 660-661 (1941).
170. Huggins, M.L., *J. Chem. Phys.* **9**, 440-443 (1941).
171. Ali, S.A.M. and Hourston, D.J., in *Advances in Interpenetrating Polymer Networks* Klempner, D. and Frisch, K.C., Eds. (Technomic Publishing Company, Lancaster, 1994) pp. 17-44.
172. Suther, B., Xiao, H.X., Klempner, D., and Frisch, K.C., *Polym. Adv. Tech.* **7**, 221-233 (1996).
173. Du Prez, F.E., Tan, P., and Goethals, E.J., in *IPNs around the world* Kim, S.C. and Sperling, L.H., Eds. (John Wiley and Sons, New York, 1997) pp. 123-138.
174. Frisch, H.L. and Zhou, P., in *Interpenetrating Polymer Networks* Klempner, D., Sperling, L.H., and Utracki, L.A., Eds. (American Chemical Society, Washington, 1994) pp. 269-283.
175. Burford, R.P., Jones, J.J., and Mai, Y.-W., in *Interpenetrating Polymer Networks* Klempner, D., Sperling, L.H., and Utracki, L.A., Eds. (American Chemical Society, Washington, 1994) pp. 285-303.
176. Lipatov, Y.S., *J. Macromol. Sci., Rev. Macromol. Chem. Phys.* **C30**, 209-232 (1990).
177. Wang, M.W., Lee, C.T., and Lin, M.S., *Polym. Inter.* **44**, 503-509 (1997).
178. McCrum, N.G., Buckley, C.P., and Bucknall, C.B., *Principles of Polymer Engineering* (Oxford University Press, New York, 1991), pp 172-177.
179. Ward, I.M., *Mechanical properties of Solid Polymers* (John Wiley and Sons, Chichester, ed. 2nd, 1983), 377-380.
180. Ward, I.M. and Hadley, D.W., *An Introduction to the Mechanical Properties of Solid Polymers* (John Wiley and Sons, Chichester, 1996), p 207.

181. Mayr, A.E., Cook, W.D., and Edward, G.H., *Polymer* **39**, 3719-3724 (1998).
182. Rodriguez, E.L., *Polym. Eng. Sci.* **58**, 1083-1086 (1998).
183. Park, S.J., Park, W.B., and Lee, J.R., *Polym. J.* **31**, 28-31 (1999).
184. Lin, M.S. and Lee, S.T., *Polymer* **38**, 53-58 (1997).
185. Hawkins, W.L., *Polymer Degradation and Stabilization* (Springer-Verlag, Berlin, 1984),
186. Mallinson, J.H., *Corrosion-Resistant Plastic Composites in Chemical Plant Design* (Marcel Dekker Inc, New York, 1988),
187. Rabek, J.F., *Polymer Photodegradation* (Chapman and Hall, Cambridge, 1995), Chapter 2.
188. Tcharkhtchi, A., Bronnec, P.Y., and Verdu, J., *Polymer* **41**, 5777-5785 (2000).
189. Moy, P. and Karasz, F.E., in *Water in Polymers* Rowland, S.P., Ed. (American Chemical Society, Washington, 1980) pp. 505-513.
190. Crank, J. and Park, G.S., in *Diffusion in Polymers* Crank, J. and Park, G.S., Eds. (Academic Press, London, 1979) pp. 1-37.
191. Merdas, I., ThomINETTE, F., and Verdu, J., *J. Appl. Polym. Sci.* **77**, 1439-1444 (2000).
192. Pascault, J.P., Sautereau, H., Verdu, J., and Williams, R.J.J., *Thermosetting Polymers* (Marcel Dekker, Basel, 2002), 422-467.
193. Plecnik, J.M., Berg, R.L., and Curcio, J.V., *International Encyclopedia of Composites*. Lee, S.M., Ed. (VCH Publishers, London, 1991), vol. 4, 205.
194. Morel, E., Bellenger, V., and Verdu, J., *Polymer* **26**, 1719-1724 (1985).
195. McMaster, M.G. and Soane, D.S., *IEEE Transactions on Components, Hybrids and Manufacturing Technology* **12**, 373-385 (1989).
196. Young, R.E., in *Unsaturated Polyester Technology* Bruins, P.F., Ed. (Gordon and Breach, New York, 1976) pp. 315-342.
197. Ghorbel, I. and Valentin, D., *Polym. Comp.* **14**, 324-334 (1993).
198. Sonwala, S.P. and Spontak, R.J., *J. Mat. Sci.* **31**, 4757-4765 (1996).
199. Gutierrez, C., Martinez-Ruvalcaba, A., Michel-Valdivia, E., and Gonzalez-Romero, V.M., Effects of the exposure of an epoxy resin to chemicals on its mechanical properties, 54th Annu. Tech. Conf. - Soc. Plast. Eng., Mexico (1996).
200. Ranney, T.A. and Parker, L.V., *Ground Water Monitoring and Remediation* **17**, 97-103 (1997).
201. Cook, W.D., Dean, K., and Forsythe, J.S., *Mat. Forum* **25**, 30-59 (2001).
202. Jarboe, R., *Reinforced Plastics*, 48-52 (1995).

203. Cook, W.D., *J. Appl. Polym. Sci.* **42**, 1259-1261 (1991).
204. Brandrup, J. and Immergut, E.H., eds., *Polymer Handbook.*, 3rd edition ed., John Wiley and Sons: New York., 1989, p.II/1-II/34.
205. Sigma-Aldrich, *Applications: Free radical Initiators [online]*, available at <http://www.sigma-aldrich.com/aldrich/brochure/> [03/01/2002].
206. Dupont-Chemicals, *Vazo free radical initiators [online]*, available at <http://www.dupont.com/vazo/overview.html> [03/01/2002].
207. Wako-Chemicals, *Product details [online]*, available at <http://www.wako-chem.co.jp/specialty/index.htm> [03/01/2002].
208. Otsu, T. and Kuriyama, A., *Polym. Bull.* **11**, 135-142 (1984).
209. Critchfield, F.E., Funk, G.L., and Johnson, J.B., *Anal. Chem.* **28**, 76-79 (1956).
210. Dell'Erba, R., Martuscelli, E., Musto, P., and Ragosta, G., *Polym. Net. Blends.* **7**, 1-11 (1997).
211. Skoog, D.A. and Leary, J.J., *Principles of Instrumental Analysis* (Saunders College Publishing, Orlando, ed. 4, 1992), 123-136.
212. Rey, L., Galy, J., Sautereau, H., Lachenal, G., Henry, D., and Vial, J., *Appl. Spect.* **54**, 39-43 (2000).
213. Poisson, N., Lachenal, G., and Sautereau, H., *Vib. Spect.* **12**, 237-247 (1996).
214. Dean, K., Cook, W.D., Zipper, M.D., and Burchill, P., *Polymer* **42**, 1345-1359 (2001).
215. Dean, K., Cook, W.D., Zipper, M.D., and Burchill, P., *Polymer* **42**, 3589-3601 (2001).
216. Cook, W.D., *J. Appl. Polym. Sci.* **42**, 2209-2222 (1991).
217. Ferry, J.D., *Viscoelastic properties of polymers*, (John Wiley and Sons, New York, 1961), p 252.
218. *Annual Book of ASTM Standards, Standard Test Designation D790* (1992).
219. Cook, W.D., Mayr, A.E., and Edward, G.H., *Polymer* **39**, 3725-3733 (1998).
220. *Annual book of ASTM standards, Standard test designation D695* (1992).
221. Barton, J.M., *Macromol. Sci. Chem.* **A8**, 25-32 (1979).
222. Sawada, H.J., *J. Macromol. Sci., Chem.* **c3**, 313- (1991).
223. Tong, L.K.J. and Kenyon, W.O., *J. Amer. Chem. Soc.* **69**, 1402-1405 (1947).
224. Ravve, A., *Principles of Polymer Chemistry* (Plenum Press, New York, 1995), p 42.
225. Rozenberg, B.A., *Adv. Polym. Sci.* **75**, 113 (1985).
226. Ginsburg, D., *Concerning Amines* (Pergamon Press, Oxford, 1967).

227. O'Driscoll, K.F. and McArdle, S.A., *J. Polym. Sci.* **XL**, 557-561 (1959).
228. Hill, D.J.T. and O'Donnell, J.H., *J. Polym. Sci: Polym. Chem. Ed.* **20**, 241-244 (1982).
229. Tobolsky, A.V., *J. Amer. Chem. Soc.* **80**, 5927-5929 (1958).
230. Lin, M.S., Yang, T., and Huang, K.Y., *Polymer* **35**, 594-601 (1994).
231. Ooi, S.K., Cook, W.D., Simon, G.P., and Such, C.H., *Polymer* **41**, 3639-3649 (2000).
232. Vogt, J., *J. Adhes.* **22**, 139-151 (1987).
233. Gillham, J.K., *The role of polymer matrix in processing and structural properties of composites*. Seferis, J.C. and Nicclais, L., Eds. (Plenim Press, New York, 1983), vol. 127,
234. Corcuera, M.A., Mondragon, I., Riccardi, C.C., and Williams, R.J.J., *J. Appl. Polym. Sci.* **64**, 157-166 (1996).
235. Yates, W.R. and Ihrig, J.L., *J. Amer. Chem. Soc.* **87**, 710-715 (1965).
236. Dean, K., Cook, W.D., Rey, L., Galy, J., and Sautereau, H., *Macromolecules.* **34**, 6623-6630 (2001).
237. Heise, M.S., Martin, G.C., and Gotro, J.T., *Polym. Eng. Sci.* **32**, 529-534 (1992).
238. Cook, W.D., *Euro. Polym. J.* **14**, 721-727 (1977).
239. Shan, L., Robertson, C.G., Verghese, K.N.E., Burts, E., Riffle, J.S., Ward, T.C., and Reifsnider, K.L., *J. Appl. Polym. Sci.* **80**, 917-927 (2001).
240. Ochi, M., Okazaki, M., and Shimbo, M., *J. Polym. Sci.: Poly. Phys. Ed.* **20**, 689-699 (1982).
241. Sanz, G., Garmendia, J., Andres, M.A., and Mondragon, I., *J. Appl. Polym. Sci.* **55**, 75-87 (1995).
242. Occhi, M., Iesako, H., and Shimbo, M., *J. Polym. Sci: B: Polym. Phys.* **24**, 1271-1282 (1986).
243. Ziaee, S. and Palmese, G.R., *J. Polym. Sci: B: Polym. Phys.* **37**, 725-744 (1999).
244. Kreyszig, E., *Advanced Engineering Mathematics* (John Wiley and Sons, New York, 1988), p 1280.